Design and Optimisation of a Spring Particle Sizer

A thesis submitted to the University College London for the degree of Doctor of Philosophy

2012

by

AISHA SALIHU

Supervisor:
Prof Haroun Mahgerefteh

Department of Chemical Engineering
University College London
Torrington Place
London WC1E 7JE

I, Aisha Salihu verify that the work presented in this thesis is my own. Where information has been derived from other sources, I confirm that this has been indicated in the thesis.

Aisha Salihu

ABSTRACT

This thesis describes the results of a series of investigations examining the operational performance followed by the fundamental re-development of two analytical instruments, namely a Pneumatic Spring Particle Sizer (PSPS) and handheld Spring Particle Sizer (handheld SPS) for size distribution analysis of dry powders in the 100 – 2000 μm size range. Each instrument shares the same basic principle of operation involving the use of a closed coil helical extension spring, which is partly filled with the test powder. Particle size distribution data is obtained by stretching the spring to known lengths and measuring the mass of the discharged particles from the spring's coils. In the case of the Handheld SPS, aimed at on the spot quality control applications, the test particles are discharged from the spring using manual shaking. In the case of the PSPS on the other hand, the particles are discharged using pulsating pressurised air.

The design, development and evaluation of two methods for the in-situ measurement of the sample mass within the PSPS are discussed. These include a full-bridge strain gauge assembly and the investigation of the correlation between the minimum fluidisation velocity and the mass of the test sample within the spring. The strain gauge proved to be a successful method producing a mass resolution of ± 1 % for a total sample mass of 280 g. The second method was unsuccessful as it was found that the minimum fluidisation velocity, in most cases did not follow a clear trend with mass.

Detailed investigations are conducted aimed at understanding the processes governing the mass discharge rate from the PSPS and hence the sample analysis time by studying the particle migration behaviour. A pulsating fluidised bed of similar dimensions to the spring is used to mimic the behaviour in the spring. Tests involved pulsating fluidisation followed by particle size distribution analysis at equal distances along the length of the bed containing poly-dispersed and mono-dispersed particles. It was observed that any operating or design parameter that promoted the degree of mixing, for example, increasing the fluidising air pulse frequency would reduce the test analysis time. The analysis time also increased with the sample poly-dispersity.

In an attempt to reduce the sampling time, the handheld SPS was rotated using a variable speed tumbler as an alternative to manual shaking. Despite the marked reduction in the sampling time, this method resulted in the discharge of particles larger than spring coil openings thereby producing erroneous results.

Calibration experiments for the same types of powders revealed a linear relationship between the discharge sample volume and its mass, independent of the particle size in the range 212 – 1000 μm. This allows in-situ measurement of the discharge sample mass in the handheld unit by reading the sample volume collected in the integrated graduated collection cylinder and reference to a previously generated calibration line.

DEDICATION

This thesis is dedicated to my Father, Mother, and my siblings Othman, Fatima, Samira, Najib and Fa'iz who have always been there to give me support. I love you all.

ACKNOWLEDGEMENTS

In the name of Almighty Allah, the Most Gracious, the Most Merciful.

All praise and thanks are due to Almighty Allah, Who in His Infinite Mercy and Grace enabled me to complete this thesis. I bow my head with all submission and humility by way of gratitude due to Almighty Allah.

I would like to express my sincere gratitude to my supervisor, Professor Haroun Mahgerefteh, for giving me the opportunity to work on this project, for his inspiration, patience, invaluable support and guidance, and without whom this would not have been possible.

I would like to extend my gratitude to my fellow PhD students and colleagues, Shirin, Maria, Rashed, Solomon, Sergey, Peng, Navid, Garfield, Vikram and Alex, for their moral support, kindness and valuable discussions.

I must also acknowledge the kindness of the technical staff from the departmental chemical engineering and electronic workshops for their invaluable help and support during the construction of the various pieces of equipment for the development of Spring Particle Sizer.

The financial support I receive from the Petroleum Technology Development Fund (PTDF) is greatly acknowledged.

I would like to express my deepest and greatest gratitude to my Parents, Air Cdre A. and Mrs. B. Salihu for their sacrifice and love. They have always been there to share my joys and sorrows, and always stood by me. They have always encouraged and supported me to pursue all my dreams. Finally, to my siblings, Othman, Fatima, Samira, Najib and Fa'iz who have acted as my motivators and kept me going through the hard times. Words cannot express how much I love and appreciate you all.

TABLE OF CONTENTS

NOMENCLATURE

Symbol	Name	Units
A	Particle area	m^2
C_D	Drag Coefficient	-
d_{static}	Spring aperture size when static	m
$d_{dynamic}$	Spring aperture size when dynamic (transverse vibration)	m
F_D	Drag force	$Pa \cdot m^2$
g	Acceleration due to gravity	$m \cdot s^{-2}$
m	Mass of particles	kg
P	Particle perimeter	m
ΔP	Pressure drop	Pa
R	Unrolled particle radius (see figure 2.2)	m
Re	Reynolds number	Dimensionless
S	Particle surface area	m^2
u_{mf}	Minimum fluidisation velocity	$m \cdot s^{-1}$
V	Particle volume	m^3
x_v	Volume diameter	m
x_s	Surface diameter	m
x_{sv}	Surface volume diameter	m
x_d	Drag diameter	m
x_f	Free-falling diameter	m
x_{Stk}	Stokes' diameter	m
x_a	Projected area diameter	m
x_p	Projected area diameter	m
x_c	Perimeter diameter	m
x_A	Sieve diameter	m
x_F	Feret's diameter	m
x_M	Martin's diameter	m
x_R	Unrolled diameter (see figure 2.2)	m
x	Particle diameter	m

Greek Letters		
Symbol	**Name**	**Units**
ρ_f	Fluid density	$kg \cdot m^{-3}$
ρp	Solid density	$kg \cdot m^{-3}$
v	Settling velocity	$m \cdot s^{-1}$
μ	Fluid viscosity	Pa·s
ε	Voidage	-
θ_R	Unrolled diameter angle (see figure 2.2)	
$\subset$	Circularity	-
ϕ	Sphericity	-
ϕ_v	Volume shape coefficient	-
ϕ_s	Surface shape coefficient	-

Abbreviations	
A1 and A2	Airedale Springs 1 and 2 respectively
ca.	circa
handheld SPS	handheld Spring Particle Sizer
HP VEE	Hewlett Packard Visual Engineering Environment
PSD	Particle Size Distribution
PSPS	Pneumatic Spring Particle sizer
SPS	Spring Particle Sizer (general name for all models)

CHAPTER 1 INTRODUCTION

Materials that incorporate or, are produced from powders are all around us. The most commonly encountered powders include cement, limestone, fertilizer, cosmetic powders, salt/sugar, detergents, and many other household items. In fact, over 75 % of all materials processed in industry are in particulate form (Merkus, 2009).

Particle size and size distribution (PSD) determines many of the properties of particles such as its dissolution rate, reactivity, segregation and flowability (Merkus, 2009). Consequently, accurate measurement and classification of particles by size play an essential role in manufacturing as even small differences in size or shape can affect process performance and product attributes.

The determination of PSD is by no means limited or restricted to commercial products or any one area of technology, but actually cuts across various fields. For example, it has become increasingly important to characterise very small particles due to the effects of air pollution and emission control regulations in recent years (European Council, 2008). Within the agricultural industry, it is important to use the correct fertilizer particle size, to enable sufficient infusion into the soil at the appropriate rate. The use of particles that are too small run the risk of sub-standard crops, and particles too large may lead to damaged crops (Cooper, 2010).

Due to its significant importance within a wide variety of industries, particle size analysis has become the largest and fastest growing segment of the particle characterisation market. In 1993, the US Department of Commerce estimated the impact of particle science and technology to United States industrial output to be one trillion dollars annually (Allen, 2003).

The continual growth in the particle characterisation market has led to the development of numerous techniques to measure PSD. These techniques fall into two distinct categories, fractionating and non-fractionating methods. Fractionating methods classify the particles according to their size or density such as sieving or sedimentation. Examples of non-

fractionating methods on the other hand include laser diffraction and ultrasound spectroscopy (Bernhardt, 1994).

Increasing developments in technology has led to increasing advances in the level of sophistication of particle size analysis methods. Some instruments, such as laser diffraction particle sizers have been developed to operate in an on-line mode by integrating into the manufacturing process. This feature is essential during the manufacture of large quantities of powders as it enables the control of the particle size if and when required, thus resulting in considerable reduction in the production of 'off-spec' particles.

Some manufactures now provide accessories that enable off-line instruments to be adapted to on-line operations. For example both Mettler Toledo International Inc. (2012) and CSC Scientific Company Inc. (2012) offer sieving techniques with online capabilities.

A number of factors should be considered prior to selecting a particle size analyser. The most important factors include sample analysis time, particle size range, accuracy/sensitivity, sample mass, cost, maintenance and robustness as well as on-line or off-line capability (Bernhardt, 1994).

Despite the advances in particle size analysis techniques, a number of technological and operational problems exist that limits the scope and range of applicability of the available instruments. These include the robustness of the instruments, complicated operating procedures, sample representation problems due to small sample sizes and on-line particle size measurement at low cost.

In the light of the above shortcoming, Mahgerefteh and his co-workers at UCL (Mahgerefteh and Shaeri, 2000, Mahgerefteh and Kamugasha, 2004, Patel, 2001, Kerdvibulvech, 2008) developed a Spring Particle Sizer (SPS) aimed at overcoming a number of the problems associated with conventional techniques for particle sizing.

In its basic form, the SPS comprises a closed coil helical extension spring, which is partially filled with the test powder. When the spring is extended incrementally along its length and mechanically agitated, particles are discharged according to the opening distance between the spring coils. For a uniformly extending spring, the latter may be found from the spring total

extension and the number of coils. The measurements of the spring extension and the corresponding mass of the powder discharged are then used to construct the particle size distribution.

The Pneumatic Spring Particle Sizer (PSPS) and the Hand-held unit are two versions of this technique developed by Mahgerefteh et al. (2000, 2004). In the case of the PSPS, the test particles inside the vertically held spring are discharged using pulsating air. The hand-held unit on the other hand, as the name suggests is a portable version in which the particles from the spring are discharged by manual shaking or agitation. For both units, the PSD is determined by plotting the percentage mass of discharged powder at a particular spring extension against corresponding particle size.

The Spring Particle Sizer offers a number of advantages compared to conventional techniques available for particle sizing. These include robustness, large sample capacity (limited by the spring size), ease of operation and low capital and maintenance costs.

Despite all this, the SPS suffered from a number of fundamentally important design and operational limitations, which compromised their commercial success. Examples included non-uniform spring coil opening, sample loss during testing and long analysis time. In the case of the pneumatic sizer, the inability to measure the mass discharge from the spring in-situ limited its use to off-line applications.

This thesis describes the results of a series of investigations relating to the fundamental design and operational development of the spring particle sizers aimed at addressing the above limitations.

The thesis comprises nine chapters.

As most particles are irregular in shape, Chapter 2 reviews the different particle size definitions. The varying definitions of particle shape and size are described both qualitatively and quantitatively presented. Different methods of presenting particle size distribution data are also discussed.

Chapter 3 reviews the most commonly used particle size distribution techniques, operating principles followed by a discussion of their strengths and weaknesses. The review commences with a brief discussion of commonly used sampling techniques due to its importance in particle size analysis.

In chapter 4, the various modifications of Spring Particle Sizer (SPS) developed at UCL prior to the present work are presented and discussed. These include the two early versions (Mark I and Mark II) involving the mechanical agitation of the loaded spring using an electromagnet incorporating an automated mass measurement mechanism.

Being the focus of this thesis, the detailed design and operating features of the Pneumatic Spring Particle Sizer (PSPS) and the handheld SPS together with their merits and disadvantages are presented and discussed next.

The proceeding chapters, present work carried out in the present study as summarised below.

Chapter 5 presents the results of a series of investigations using image analysis for characterising two especially fabricated springs in terms of coil opening uniformity and reproducibility. The performance of the selected springs in terms of the aperture uniformity is next evaluated by comparing their standard deviation for a given aperture size against the corresponding data for sieves.

A major drawback of the PSPS is the requirement to measure the sample mass discharged from the spring independently using a balance. Apart from increasing capital cost and analysis time, the above relies on collecting all the particles discharged from the spring. In practice, this is extremely difficult to achieve due to sample loss. The development of various techniques aimed at addressing the above limitation by introducing in-situ mass measurement capability is presented in chapter 6. These rely on the use of in-built strain gauges (section 6.2) or correlating the powder mass within the spring to the minimum fluidisation velocity (section 6.6).

The study of the different factors affecting the sample discharge time and thereby developing operating methodologies for reducing the PSD analysis time is presented in chapter 7.

Central to the above are a series of experiments investigating particle migration behaviour within the spring. These involve using a pulsating fluidized of similar dimensions to the spring followed by careful extraction of representative samples from the static bed at different powder depths for PSD analysis. Various pulsating air frequencies and pressures are used in order to investigate their impact on particle size migration and the corresponding sample discharge time.

Chapter 8 presents a comparison of particle size measurement with standard sieve data to the performance characteristics of the handheld unit. This is presented in terms of its accuracy and reproducibility when using a variable speed tumbler as an alternative to manual shaking. The development of volume to mass calibration curves for direct mass measurement from the unit is also discussed.

Chapter 9 describes the general conclusions and main findings of this thesis and the recommendations for future improvements.

CHAPTER 2 PARTICLE CHARACTERISATION

This chapter deals with the various approaches used to express the size of a single particle. A number of definitions used in the thesis such as particle shape, particle size distribution are also presented.

2.1 Particle Size

The particle size is one or more linear dimensions defined to characterize an individual particle (Yang, 2003). An ideal particle like a sphere is uniquely defined by its diameter, or for a matchstick, its length, breadth and height. However, it becomes more complex for a grain of sand or other irregular particles (Yang, 2003).

For irregular shaped particles, the particle size is derived from certain reference properties, this however, depends mainly on the particle sizing method employed (Yang, 2003). Several diameters have been defined and used to characterize irregular particles, using geometry and a theoretical equivalent sphere with regard to some properties (e.g. volume, settling velocity, surface area, projected area). Commonly used diameters are defined in table 2.1 below. Figure 2.1 gives an illustration for some of these defined diameters.

Table 2.1: Equivalent Diameters for Irregular Particles (Allen, 1997; International Organisation for Standardisation, 2001; International Organisation for Standardisation, 2008; Webb & Orr, 1997; Yang, 2003; Arai, 1996).

Symbol	Name	Definition	Formula
x_v	Volume diameter	Diameter of a sphere having the same volume as the particle	$V = \frac{\pi}{6} x_v^3$ .....(2.1)
x_s	Surface diameter	Diameter of a sphere having the same surface as the particle	$S = \pi x_s^2$ .....(2.2)
x_{sv}	Surface volume diameter	Diameter of a sphere having the same external surface to volume ratio as the particle	$x_{sv} = \frac{x_v^3}{x_s^2}$ .....(2.3)

x_d	Drag diameter	Diameter of a sphere having the same resistance to motion as the particle in fluid of the same viscosity and velocity ($Re < 0.2$)	$F_D = C_D A \rho_f \frac{v^2}{2}$ .....(2.4) Where $C_D A = f(x_d)$ .....(2.5) $F_D A = 3\pi x_d \mu v$ .....(2.6) $\mathrm{Re} = \frac{\rho v x}{\mu}$ .....(2.7)
x_f	Free-falling diameter	Diameter of a sphere having the same terminal velocity as the particle in fluid of the same viscosity and density	
x_{Stk}	Stokes' diameter	The free-falling diameter of particle in laminar flow region ($Re < 0.2$)	$x_{Stk}^{\ 2} = \frac{x_v^3}{x_d}$ .....(2.8)
x_a	Projected area diameter	Diameter of circle with the same area as the projected area of the particle resting in stable position	$A = \frac{\pi}{4} x_a^2$ .....(2.9)
x_p	Projected area diameter	Diameter of circle with the same area as the projected area of the particle resting in random orientation	Mean value for all possible orientations $x_p = x_s$ for convex particles
x_c	Perimeter diameter	Diameter of circle with the same perimeter as the particle	$P = \pi x_c$ .....(2.10)
x_A	Sieve diameter	The width of the minimum square aperture that the particle will pass	
x_F	Feret's diameter	The mean value of the distance between pairs of parallel tangents to the projected outline of the particle, (see figure 2.1)	
x_M	Martin's diameter	The mean chord length of the projected outline of the particle,(see figure 2.1)	
	Krumbein	The maximum line that can be drawn on the projected area in a constant direction (Arai, 1996)	
x_R	Unrolled diameter	The mean chord length through the centre of gravity of the particle(see figure 2.2)	$E(x_R) = \frac{1}{\pi} \int_0^{2\pi} x_R d\theta_R$ ....(2.11)

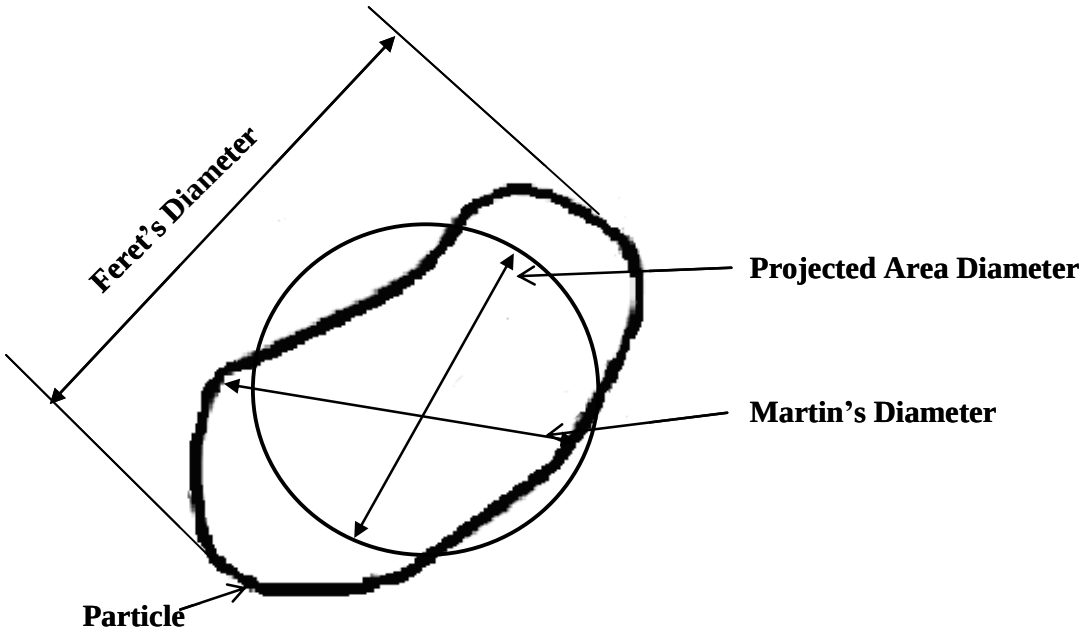

Figure 2.1: Three diameters used to estimate particle size of irregular particles (Yang, 2003).

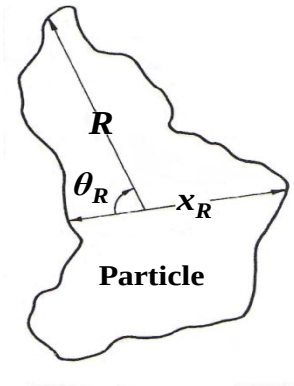

Figure 2.2: Definition of unrolled diameter x_R, radius R and angle θ_R (Allen, 2003)

2.2 Particle Shape

Particle shape is another fundamental particulate feature, which affects several powder properties. Examples of these include powder packing, bulk density, cohesion, flowability, caking behaviour (Heyd and Dhabbar, 1979), porosity, interaction with fluids and the covering power of pigments (Allen, 1997).

Some mathematical expressions have been developed to define the shape of an irregular particle (see examples in (Allen, 1997) and (Gotoh et al., 1997). However complexity prevents them from being used widely in powder technology (Shaeri, 1997).

Particle shape is often described by the particle's geometrical characteristics. These are used to establish shape parameters such as Circularity, Convexity and Aspect Ratio, which help to identify and quantify distinctions in particle shape. These parameters are standardized to a range between 0 and 1, in order to provide quick and easy comparability (Sysmex Corporation, 2009).

The common shape parameters used are as follows:

a) Circularity/Roundness $\propto$**:** Wadell (1933) introduced the ''degree of circularity'', defined as "the ratio of the perimeter of the particle to that of a sphere of the same projected area". This is given by:

$$\propto = \frac{\text{Circumference of circle having same cross sectional area as the particle}}{\text{Perimeter of projected particle image}} = \frac{2\sqrt{\pi A}}{P} \quad \text{.....(2.12)}$$

where,

A = Area of particle

P = Perimeter of particle

b) Sphericity: Wadell (1933) also proposed the ''degree of true sphericity'' defined as "The ratio of the surface area of a particle to that of a sphere of the same volume". According to the International Organisation for Standardisation (2008) the most widely used sphericity factor is given by equation 2.13:

$$\phi = \frac{\text{Surface area of volume of equivalent sphere}}{\text{Surface area of particle}} = \left(\frac{x_v}{x_s}\right)^2 = \pi\frac{x_v^2}{S} \quad \text{.....(2.13)}$$

where,

x_v = Diameter of a sphere having the same volume as the particle

d_s = Diameter of a sphere having the same surface as the particle

S = Surface area of the particle

c) Aspect ratio: The ratio of the length of a particle to its width at right angles. This signifies the elongation of the particle. It is defined by the ratio of the smallest and largest diameter (International Organisation for Standardisation, 2008; Sysmex Corporation, 2009).

***d) Flakiness index*:** The ratio of the mass of particles with thickness of less than 0.5-0.6 of their mean sieve size to the mass of tested particles (British Standards Institute, 1997).

e) Convexity: Convexity is the measure of surface roughness of a particle. It is obtained by dividing the object area by the area enclosed by an imaginary "rubber band" wrapped around the object. The convexity has values in the range 0 – 1. A convex or smooth shape has convexity 1.0 (e.g. sphere), while a concave or "spiky" shape has a lower value, close to 0 as shown in figure 2.3 (Huck, 2006; Sysmex Corporation, 2009).

***f) Volume shape coefficient*:** The ratio of the volume of a particle to that of a cube of the same diameter (Allen, 1997).

$$\phi_v = \frac{V}{x^3} \tag{2.14}$$

where,

ϕ_v = volume shape coefficient

V = particle volume

x = particle diameter

g) Surface shape coefficient: This is the coefficient of proportionality relating the surface area of the particle with the square of its measured diameter (Allen, 1997).

$$\phi_s = \frac{S}{x^2} \tag{2.15}$$

where,

ϕ_s = surface shape coefficient

S = surface area of a particle

h) Surface volume coefficient: This is the ratio of surface to volume shape factors combining the features of the two together (Allen, 1997).

i) Elongation shape factor: The ratio of the length of a rectangle with two sides parallel to the longest dimension of a particle to its width (Gotoh et al., 1997).

***j) Dynamic shape coefficient*:** The ratio of the resistance-to-motion of a particle to that of a spherical particle of the same volume (Gotoh et al., 1997).

Various definitions for expressing particle shape are defined in table 2.2. Diagrammatic examples are given in figure 2.4.

Table 2.2: Definitions of Particle Shape (Allen, 1997; United State of Pharmacopeia, 2000).

Term	Description
Acicular	Slender, needle-like particle of similar width and thickness
Angular	Sharp-edged or having approximately polyhedral shape
Crystalline	Having the geometric symmetry characteristic of a crystal
Dendritic	Having a branched crystalline shape
Fibrous	Threadlike, either regularly formed or not
Flaky	Thin, flat particle of similar length and width
Granular	Having an approximately equi-dimensional but irregular shape
Irregular	Having different measurements in the three dimensions
Nodular	Having a rounded irregular shape
Spherical	Global shape
Lath	Long, thin, and blade-like particle
Equant	Particles of similar length, width, and thickness; both cubical and spherical particles are included
Plate	Flat particles of similar length and width but with greater thickness than flakes
Columnar	Long, thin particle with a width and thickness that are greater than

those of an acicular particle

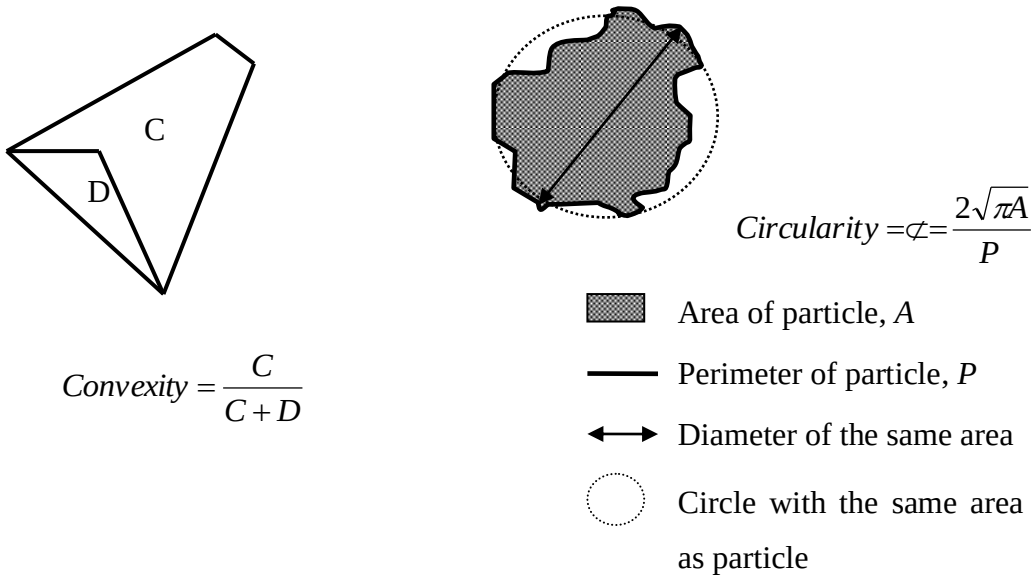

Figure 2.3: Particle Shape Parameters (Sysmex Corporation, 2009).

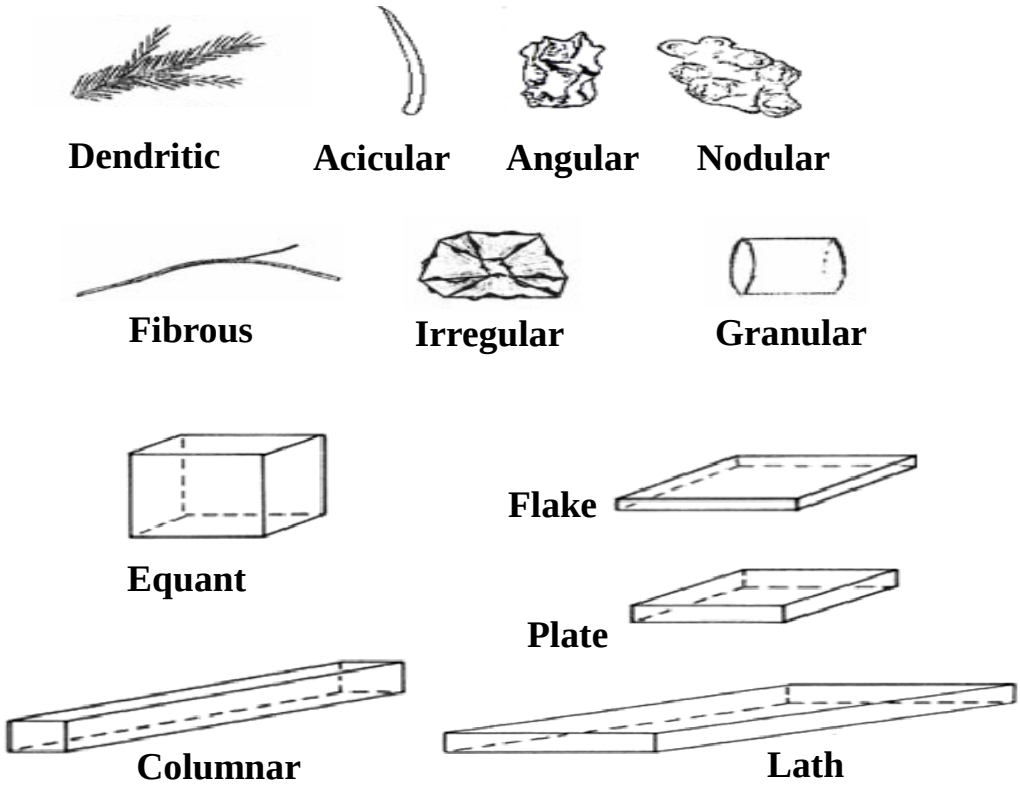

Figure 2.4: Diagrammatic examples of common particle shapes (Beehag, 2000; Merkus, 2009; United State of Pharmacopeia, 2000).

2.3 Particle Size Distribution (PSD)

Particulate systems are usually characterised by the existence of a wide range of shapes and sizes in them. They are evaluated to determine the particle size and distribution (PSD) from a sample representing the whole system. The PSD of a powder, a granular material, or particles dispersed in fluid, is a list of values or a mathematical function that defines the relative amounts of particles present, sorted according to size (Jillavenkatesa et al., 2001).

A PSD can be presented either as a frequency distribution, cumulative distribution or as a differential distribution, in a graphical or in a tabular form. The method used to determine a PSD is called particle size analysis, and the apparatus, a particle size analyser (Syvitski, 2007).

2.3.1 Frequency Distribution

A frequency distribution presents the ratio of particles in each size range to the total particles under test. This ratio can be in fractions, percentage by mass, volume or any other basis upon which the data may be acquired.

It is often of interest to evaluate and represent the so-called particle size distribution as a histogram, or frequency curve over a given range or a 'bin' distribution curve (Sommer, 2001). The data can be presented as a table as shown in Table 2.3 or interpreted pictorially as a histogram, where the frequency of the particle in each size range is plotted against the particle related size (International Organisation for Standardisation, 1998). Figure 2.5(a) shows a typical frequency distribution presented as a histogram.

Table 2.3: Typical particle size distribution data table by number of particles.

Diameter Range, (µm)	Frequency (number)	Percentage of Particles in Size Range (x %)
40-50	3	0.57
50-60	10	1.88
60-70	25	4.71
70-80	49	9.23
80-90	77	14.50
90-100	97	18.27
100-110	98	18.46
110-120	79	14.88
120-130	51	9.61
130-140	27	5.09
140-150	10	1.88
150-160	5	0.94

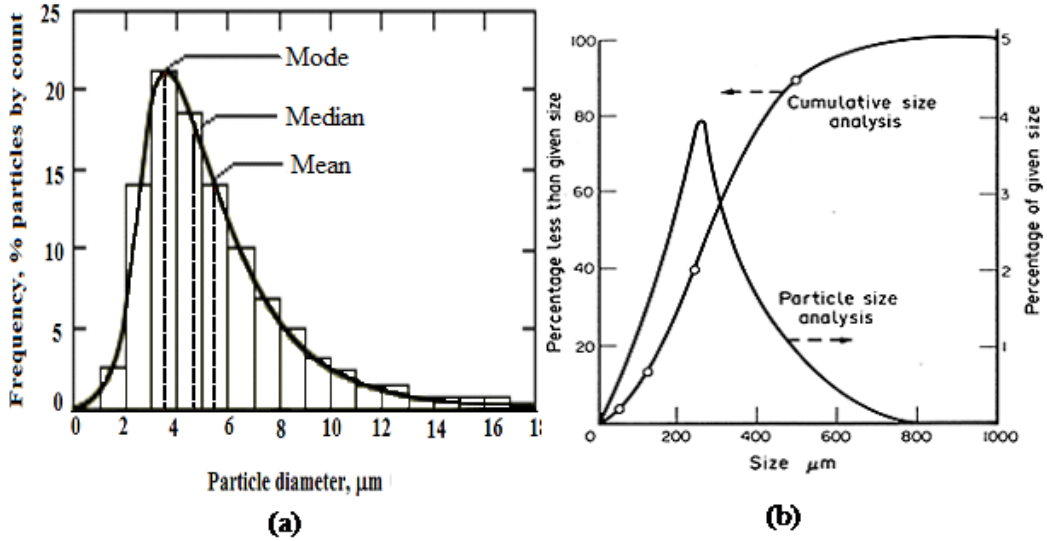

Figure 2.5: Typical frequency distribution presented as a histogram (a) (OriginLab, 2009) and a frequency distribution presented as a cumulative curve with the right ordinate on a linear scale (b) (Earle and Earle, 2004).

2.3.2 Cumulative Distribution

The particle size distribution may also be presented as a cumulative distribution. A cumulative distribution on a weight basis represents the weight fraction of the particles with diameters smaller or larger than a specific size. This is known as an undersize or oversize cumulative distribution respectively (International Organisation for Standardisation, 1998). The weight fraction is determined relative to the total weight of the sample. It is characteristically shaped as a logistic curve as illustrated by figure 2.5 (b).

When the particle size distribution is very broad it is difficult to represent it accurately on the linear scale. It is thus, often advantageous to plot the frequency against the logarithm of the size rather than the size itself (Colloidal Dynamics, 1999). A typical example is shown in figure 2.6.

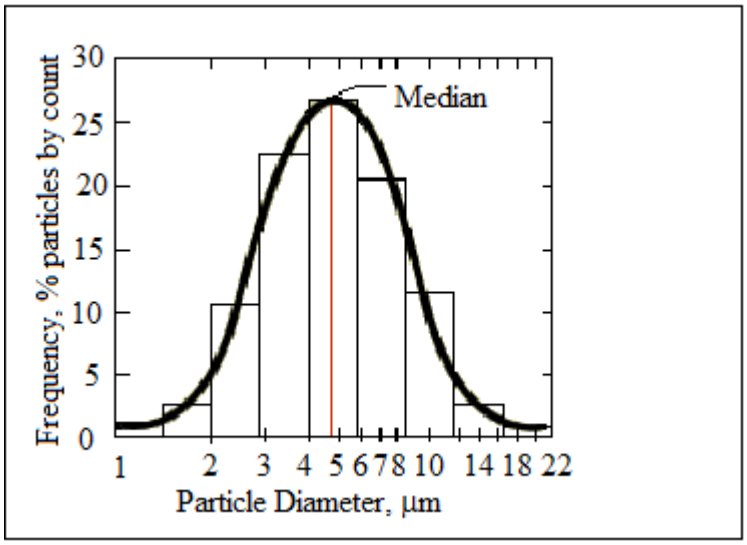

Figure 2.6: Histogram and frequency curve of a log-normal particle size distribution (OriginLab, 2009).

2.4 Conclusions

This chapter gave a number of definitions used to characterise particles. The knowledge of particulate characteristics is essential for the manufacturing, handling and application of all

particulate based materials. Most particulate materials consist of irregular shaped particles; it can therefore be complicated to classify individual particles into certain sizes. Thus, several methods are used to specify this equivalent diameter, based on volume, mass, surface or linear dimensions. The range of particle sizes within a test powder is represented in the form of a particle size distribution, which can either be a histogram, frequency distribution or a cumulative distribution.

CHAPTER 3 A REVIEW OF PARTICLE SIZING AND SAMPLING TECHNIQUES

In chapter 2, the physical characteristics of irregular and regular shaped particles measured by various PSD techniques were presented. In this chapter, a review of the current state of the art techniques used to determine PSD in academia and industry is presented. The advantages and disadvantages of each technique is also presented and discussed. A discussion of the various sampling techniques that can be used to prepare a representative sample prior PSD analysis is given first.

The PSD techniques reviewed include:

- Sieving
- Optical and Electron Microscopy
- Sedimentation Techniques
- Laser Diffraction/ Static Light Scattering
- Dynamic Light Scattering
- Electrical Sensing Zone (Coulter Principle)
- Impaction
- Acoustic Attenuation Spectroscopy
- Focused Beam Reflectance Measurement

3.1 Sample Preparation

An essential precursor to performing particle size analysis is the preparation of a representative sample which reflects the physical or chemical characteristics of the bulk powder. A non-representative/bias sample can lead to an over or under representation of the corresponding parameter in the bulk powder being analysed as well as segregation of particles according to size or density.

In order to reduce the impact of sample bias on the results of particle size analysis, two important rules of sampling need to be adhered to (Allen, 2003):

1. The powder should be in motion when sampled.
2. The whole of the powder stream should be taken for many short time increments of time in preference to part of the stream being taken for the whole duration.

There are two main branches of powder sampling:

Static: Techniques used on non-flowing or stored material. Examples include, scooping from the top, cone and quartering and sample thief methods.

Dynamic: Most powder systems are transported at some point during their manufacture as flowing streams. Examples of commonly used methods include conveyer belt sampling, table sampling, chute splitter, and a spinning riffler.

Table 3.1 gives a summary of the advantages and limitations of the various sampling techniques for static and dynamic systems.

Table 3.1: Sampling techniques comparison (Allen and Khan, 1970, Jillavenkatesa et al., 2001).

METHOD	ADVANTAGES	DISADVANTAGES
Cone & quarter	Good for powders with poor flow characteristics	Operator dependent
Scooping from the top	Reliable for homogenous and non-flowing powder	Particle segregation
Table sampling	Separates a large quantity of material	Initial feed dependant
Chute splitter	Reduce powder sample by half after one pass	Operator bias
Spinning riffler	Reliable for free flowing powder	Inability to handle large quantities efficiently

3.2 Particle Sizing Techniques

A wide range of manual and automated measuring techniques are available to determine the particle size distribution of a sample of powder. In practice, each method is applicable to a finite range of sizes and gives a particular equivalent size which is dependent on the technique's measurement principle. A number of factors need to be considered when selecting a particle sizing instrument. These include (Weiner, 2010):

1. Quantitative Specifications - size range capability, throughput, accuracy, precision, reproducibility and resolution.
2. Qualitative Specifications - ease-of-use, cost, versatility, support and life cycle.

Table 3.2 gives a general summary of the most commonly used particle size distribution techniques including the size range capability and the principle of operation. The following is their description.

Table 3.2: Comparison of Methods for particle size analysis based on various principles (Merkus, 2009).

Technique	Size range (µm)	Type of size	Type of quantification	Sample types	Sample size	Analysis time (mins)	Cost (≈ k£)	On-line capability
Sieving	$5\text{-}10^5$	Sieve opening	Mass	P, Su	Large	20	1-20	No
Microscopy		Length/Shape/Structure	Number		Very small	10		
- optical	0.3-500			E, Sp, Su			< 10	Yes
- SEM	0.01-500			E, Su			> 10	No
- TEM	0.001-5			E, Su			> 10	No
Sedimentation		Stokes' diameter		Su				
- gravitational	0.3-200	+diffusion	Mass		Small/ medium	≥ 30	3-50	No
- centrifugal	0.02-10		Mass/optical		Small/ medium	15	10-50	No
Laser diffraction	$0.1\text{-}10^4$	Scatter diameter	Volume	A, E, Pa, Sp, Su	Small/ medium	< 1	> 10	Yes
Dynamic Light Scattering	0.005-1	Hydro-dynamic	Scatter intensity	A, E, Pa, Sp, Su	Small	1	10-50	Yes
Electrical Sensing Zone	0.5-1000	Volume	Number	Su	Small	2	10-50	No
Impaction	0.01-50	Aero-dynamic	Mass	A, Pa	Small	10	1-25	No
Ultrasound attenuation	0.01-3,000	US-attenuation	Volume	E, Su	Medium/large	5	> 50	Yes
Focused Beam Reflectance Method	0.5-3,000	Chord length	Number	A, E, Pa, Su	Small	<1	10-50	Yes

Notes: Sample types: A = aerosol; E = emulsion; P = powder; Pa = powder dispersion in air; Sp = spray; Su = suspension.

3.2.1 Sieving

Sieving is perhaps the first method used to measure particle size in ancient Egypt over 4000 years ago. Archaeological evidence such as wall paintings, have shown ground foodstuff being sieved, possibly through a rough cloth of woven reeds to remove the large bits for further grinding. Sieving is commonly considered as one of the most simple, reproducible, and inexpensive particle sizing methods available. Recently sieve analysis has been described as the 'Cinderella' of particle metrology in that it does most of the work while getting little of the credit (Rideal, 2008).

There are two types of standard sieves used for obtaining particle size measurements, perforated sieves and woven-wire sieves. These are illustrated in figure 3.1.

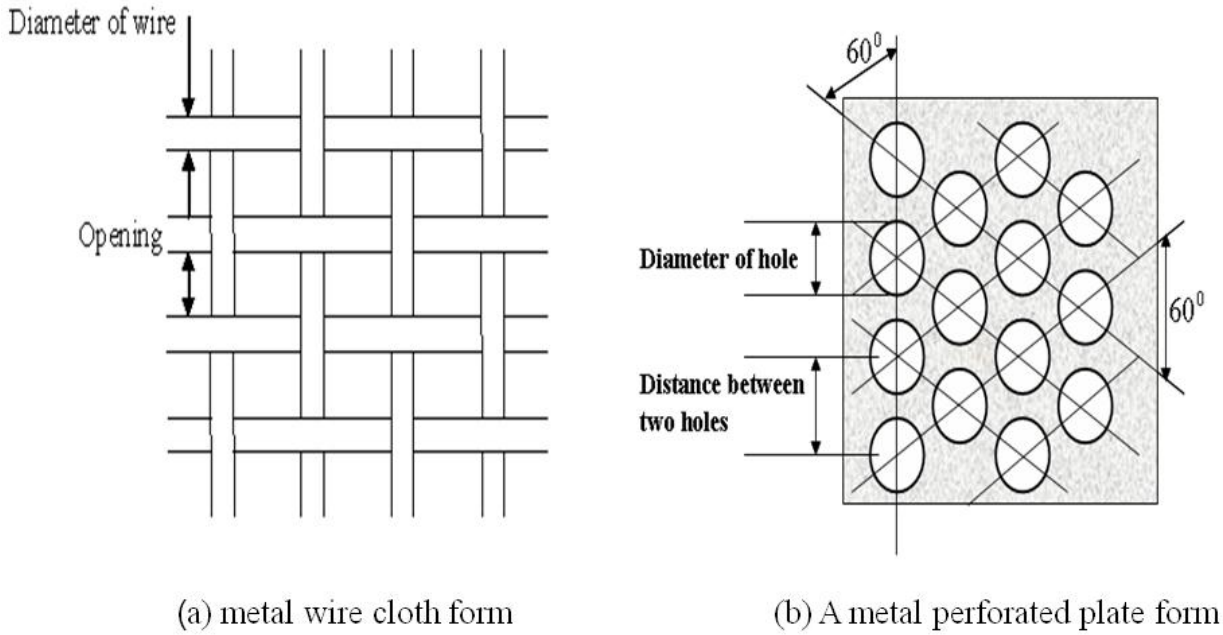

Figure 3.1: Types of Standard Sieve (Arai, 1996).

Sieving involves separating particulate material of various-sized particles, either dry or suspended in a liquid, into two or more fractions, by passing through screens of specified mesh sizes usually made from metal wire (Bernhardt, 1994). Typical sieve trays consist of a shallow pan with a wire mesh bottom or an electroformed grid. Aperture sizes of sieve trays are typically in the range 5 μm to 125 mm.

Prior to sieving the sample, the sieves are stacked up with the smallest aperture size at the bottom and the largest one at the top. The entire sample is placed on the top sieve (largest aperture size), covered, and the stack of sieves is then shaken for a specified time period, usually with a mechanical shaker. The particle size distribution of the sample is then determined using the mass or volume of the sample retained in each sieve.

Wet sieving is generally used to measure the PSD of materials originally suspended in a liquid or for powders that agglomerate during dry sieving. In this technique, a non-solvent liquid is added continuously to the sample in the top sieve. The solvent eliminates the electrostatic and surface forces which normally impede the flow of fine particles through the sieve apertures under dry conditions.

A major advantage of sieving is it allows a relatively broad particle size spectrum to be analysed quickly and reliably. Conversely, one of the main disadvantages of using sieving is the impact of particle shape on the efficacy of the PSD results. Since sieving measures the smallest diameter that can pass through the mesh opening, irregular-shaped particles tend to be more difficult to analyse resulting in inaccurate PSD measurements.

Other disadvantages associated with sieving include blinding, sieve cloth sagging, cohesion between particles, especially when powder consists of fine particles and the limited range of aperture sizes available.

3.2.2 Optical Microscopy

Optical microscopy is used to determine particle size by examining the morphological appearance and shape of individual particles either directly with the naked eye or by using a microscopic image.

Particles to be imaged in an optical microscope are usually dispersed in a drop of viscous fluid on a glass slide. Their images are then visually compared with a set of standard circles, geometric shapes, or linear grids to derive their actual sizes and shapes (Yang, 2003).

The microscope's eyepiece micrometer or graticule is calibrated against a stage micrometer (a microscope slide with a scale etched on the surface) for each magnification and length used. An example of an eyepiece graticule used in optical microscopy is shown in figure 3.2.

Optical microscopy is used to examine particles in the size range 0.3 µm – 500 µm. It is not recommended for particles below 3 µm due to the blurring of the edges of the images seen due to diffraction effects (Allen, 1997; Merkus, 2009).

The main limitations of optical microscopy are the resolution of the image, the size and height of the field of view and the large number of particles required to be measured to obtain a size distribution (Etzler and Sanderson, 1995).

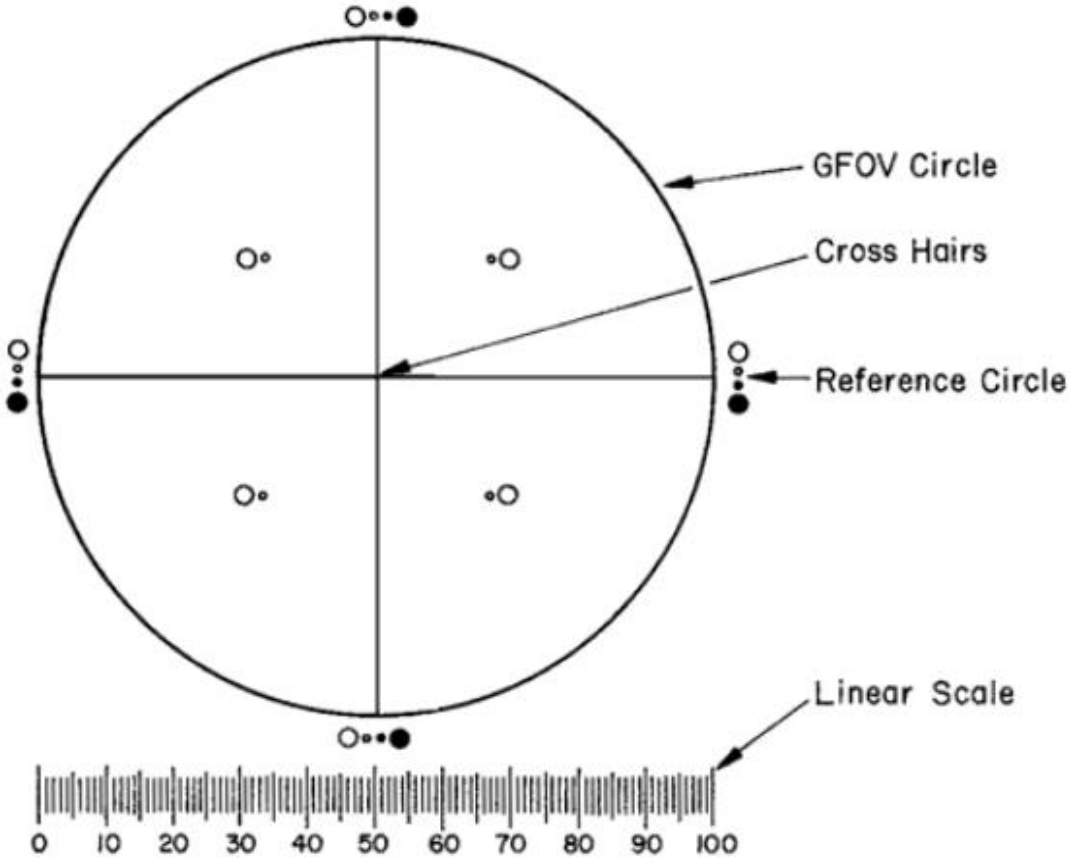

Figure 3.2: Examples of eyepiece graticules used in microscopy (United States Pharmacopeia, 2007).
GFOV = Graticule Field of View

3.2.3 Electron Microscopy

An electron microscope characterises particles by bombarding the particle(s) with high-energy electrons. It is capable of much higher magnifications and has a greater resolving power than an optical microscope, allowing it to see much smaller objects in finer detail. There are two types of electron microscopes commonly employed:

1. Transmission electron microscope (TEM).
2. Scanning electron microscope (SEM).

In TEM, a thin solid specimen (≤ 0.2 μm thick) is bombarded in vacuum with a focused electron beam (100 – 200 keV) of sufficient energy to penetrate through the specimen. The transmitted electrons form an image of the internal and external structure of the particles due to differences in interaction between the electrons and the atomic constituents of the sample. Thus, it yields information on particle size and shape as well as atomic structure and defects present in the material. TEM is often used for the direct examination of particles in the size range 0.001 – 5 μm (Allen, 1997; Merkus, 2009).

In SEM on the other hand, a focused beam of electrons (5 – 50 keV) is used to scan across a sample in a series of parallel tracks. The interaction between the electrons and the sample produce various secondary electron emissions (SEE) including back scattered electrons (BSE) and X-rays. A cathode ray tube is used to display the detected signals. The SEM is applicable for a size range of 0.01 – 500 μm with a resolution of 5 nm (Allen, 1997; Merkus, 2009).

The type of electron microscope used and the cost of analysis are dependent on the size range of the test particles, magnification and the particles resolution required.

The disadvantages associated with electron microscopy are that it can be time consuming, high cost and requires a high level of operator expertise and training. Another drawback is that the particles need to remain static at all times.

3.2.4 Sedimentation Techniques

Sedimentation is one of the oldest established techniques used to measure particle size distribution. Sedimentation techniques use the fact that a single solid (or nonporous) sphere settling in a fluid has a terminal settling velocity (under gravity) which is uniquely related to its diameter. The measured velocities are then converted to Stokes diameters by applying the Stokes equation, assuming that the particles are all spherical in shape. The resulting relationship between the frictional force given by Stokes' law and the gravitational force on the particle is given by (International Organisation for Standardisation, 2001):

$$x_{Stk} = \sqrt{\frac{18\mu h}{(\rho_p - \rho_s)gt}} \tag{3.1}$$

Where,

x_{Stk} = equivalent spherical diameter of particle (m)

μ = coefficient of viscosity of suspension medium (Pa s)

h = sedimentation distance (m)

ρ_p = density of particle (kg m^{-3})

ρ_s = density of suspension medium (kg m^{-3})

g = gravitational acceleration (m s^{-2})

t = time of settling (s)

Sedimentation techniques can be classified according to the various combinations of the suspension type (Homogeneous or Line Start), measurement principle (Incremental or Cumulative) and the type of force field applied (Gravitational or Centrifugal (Kerdvibulvech, 2008). Figure 3.3 shows some of the methods that can be used to determine the quantity of particles that have settled.

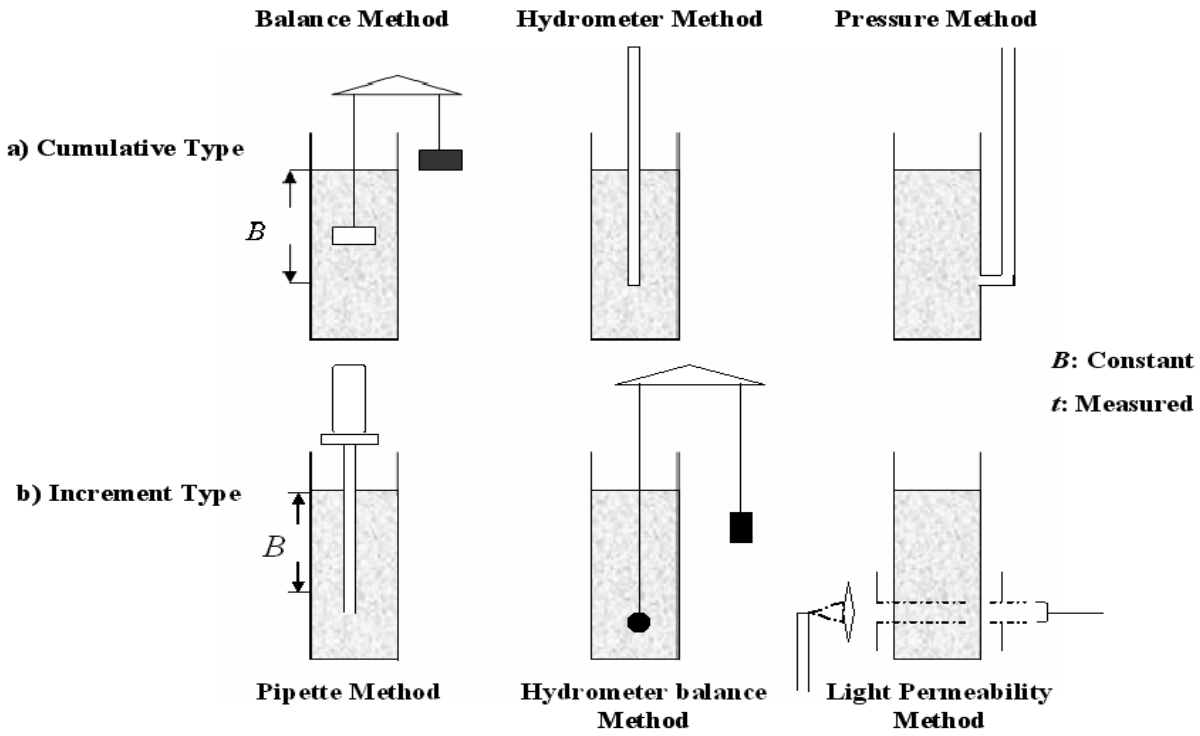

Figure 3.3: Types of Sedimentation Methods (Arai, 1996).

The cumulative type method determines the rate at which the particles settle is determined, typically, by weighing the mass of settled particles at a certain depth, *B*, over time. On the other hand the incremental method determines the change in the concentration of the particles with time is measured at known depths (Arai, 1996).

Gravitational sedimentation methods are capable of measuring particles in the size range 0.3 – 200 µm while centrifugal sedimentation methods can measure particles in the size range 0.02 – 10 µm (Merkus, 2009).

The limitations of sedimentation methods include:

- Aggregation of particles. However, this can be minimised by the addition of dispersant (Cornell and Hoveling, 1998)
- Not suitable for very fine particles due to the impact of Brownian motion.
- Not suitable for particles of different densities.
- Maximum settlement is required for best results; as a consequence the method is therefore slow (15 – 20 minutes in most cases).

3.2.5 Laser Diffraction/ Static Light Scattering

When a beam of light passes through a particulate system, the particles scatter some of the light in all directions. Some of the light is absorbed, some is reflected, some is refracted and some diffracted. This is illustrated in figure 3.4.

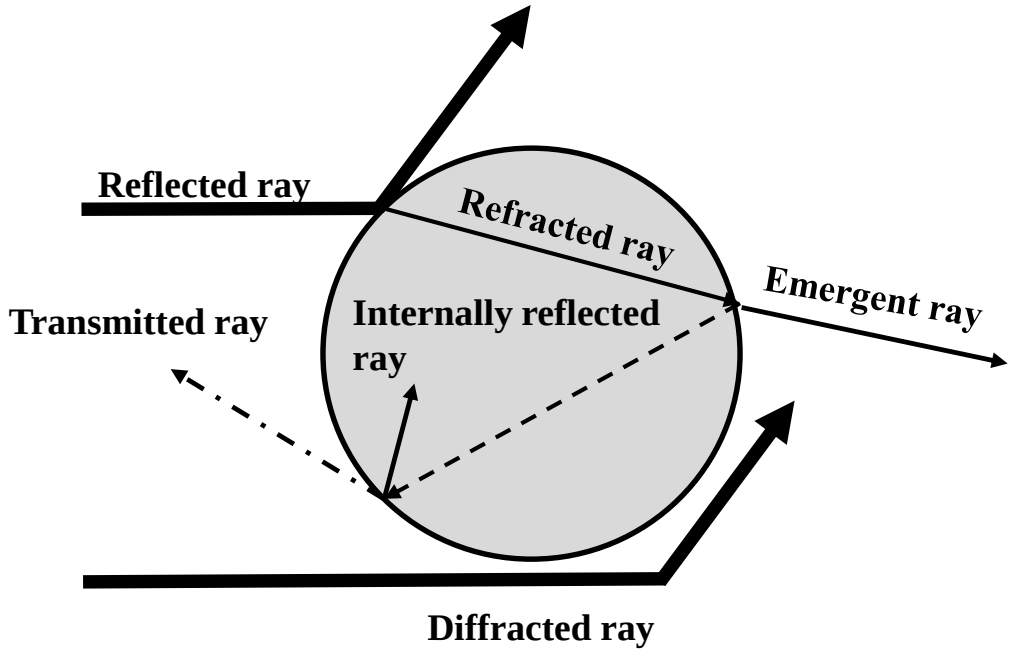

Figure 3.4: Interaction of a light ray with a particle (Allen, 2003).

Laser diffraction, also known as low angle light scattering, is a technique developed in the early 1970s, which depends on the above method to determine particle size. It relies on the fact that particles passing through a laser beam scatter distinct angular light patterns that is inversely proportional to their size.

Small particles scatter light at wide angles and low intensity whereas large particles scatter light at narrow angles and high intensity. Therefore, the particle size distribution is obtained by measuring the intensity of light scattered from a sample as a function of angle. This is compared with a scattering model based on Mie theory or the Fraunhofer theory, in order to calculate the size distribution. Figure 3.5 shows an example of the light scattering patterns observed for small and large particles.

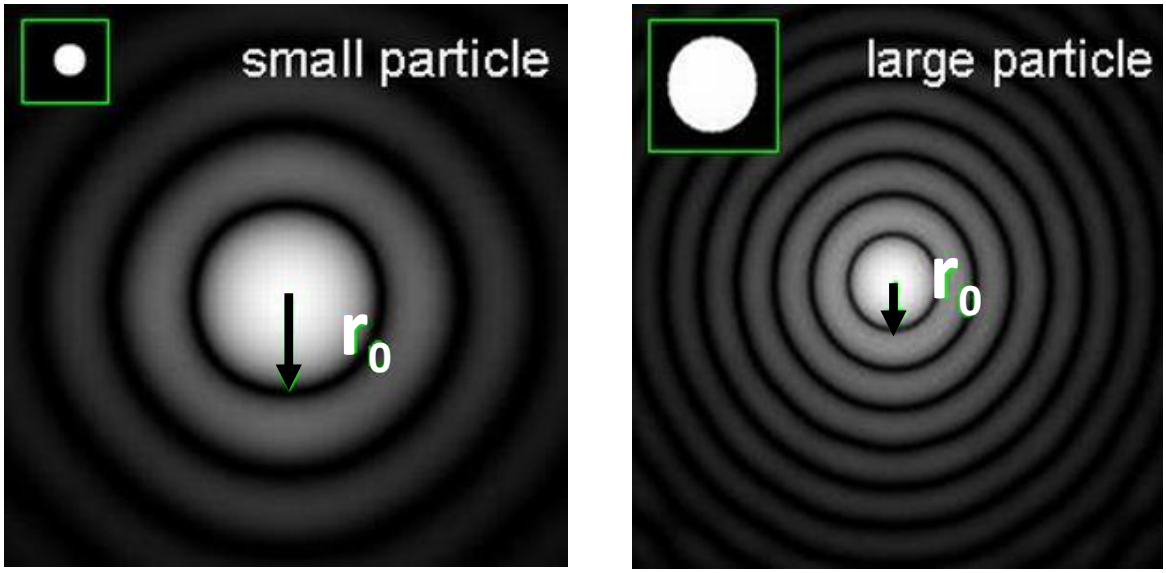

(a) **(b)**

Figure 3.5: Light scattering patterns observed for a small particle (a) and a large particle (b) [the distance r_0 of the first minimum to the centre is dependent on the particle size] (Sympatec GmbH, 2010) .

Mie theory assumes the particles are optically homogeneous and spherical. The model requires knowledge of both the real and imaginary (adsorption) parts of the refractive index. Fraunhofer theory on the other hand assumes that the particles being measured are opaque and scatter light at narrow angles. As a result, it is only applicable to large particles and will give an incorrect assessment of the fine particle fraction (Allen, 1997). According to ISO 13320:2009 (International Organisation for Standardisation, 2009), both theories give similar results for particles greater than 50 µm, while the Mie theory is recommended for particles smaller than 50 µm.

The benefits of laser diffraction are that it is a non-intrusive and flexible method that can be used for either dry or wet samples. It is also able to measure particle size in the range 0.02 – 2000 µm (Seville et al., 1998; Rumpf, 1990). Figure 3.6 shows an illustration of a typical laser diffraction instrument.

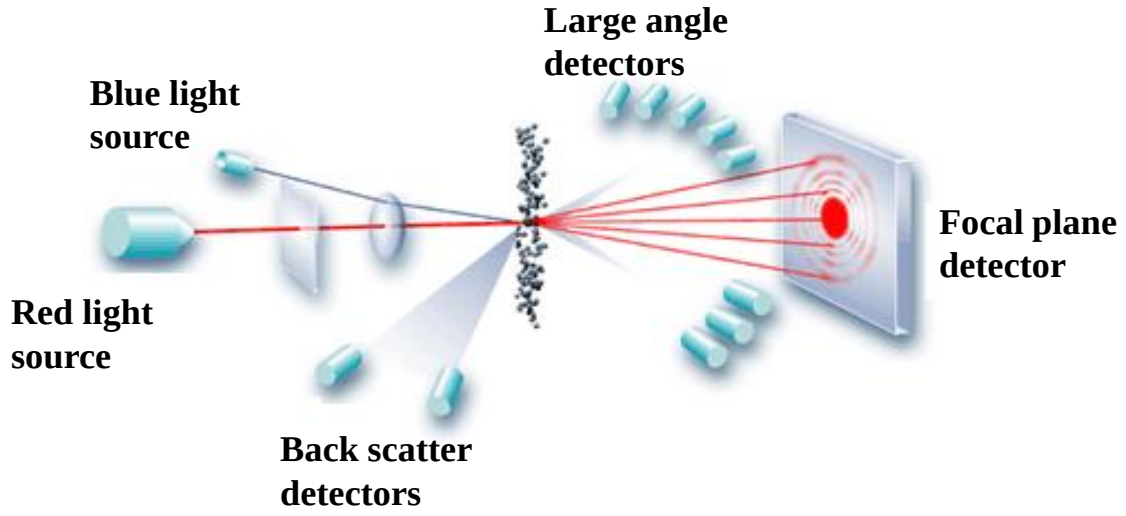

Figure 3.6: Schematic illustrating laser diffraction configuration with light diffracting off the particulate sample shown in the centre of the diagram (Malvern Instruments Ltd, 2009).

A disadvantage of laser diffraction is the occurrence of "multiple scattering" when the concentration of particles is high. At low particle concentrations, the laser diffraction instrument follows Beer-Lambert's law; i.e. the turbidity (a measure of the incident light lost due to scattering) varies linearly with the particle concentration. However, as the particle concentration increases Beer's law no longer holds due to the re-scattering of radiation by surrounding particles. This results in higher angles than predicted in theory and leads to an underestimation of the particle's size.

3.2.6 Dynamic Light Scattering

Dynamic Light Scattering (DLS) technique, also known as Quasi-elastic light scattering (QELS) and Photon correlation spectroscopy (PCS), measures the time-dependent fluctuations in the intensity of scattered light due to Brownian motion. Analysis of these intensity fluctuations enables the determination of the distribution of diffusion coefficients of the particles, which are converted into a size distribution using established theories.

Early particle size analysers using the DLS method placed the detector at 90 degrees to the incident light as shown in figure 3.7. This required a high powered laser and was sensitive to dust contamination of the fluid. The correlation technique limited the

resolution capabilities of the algorithm, so it was often not capable of independently determining the presence of multiple modes in a sample.

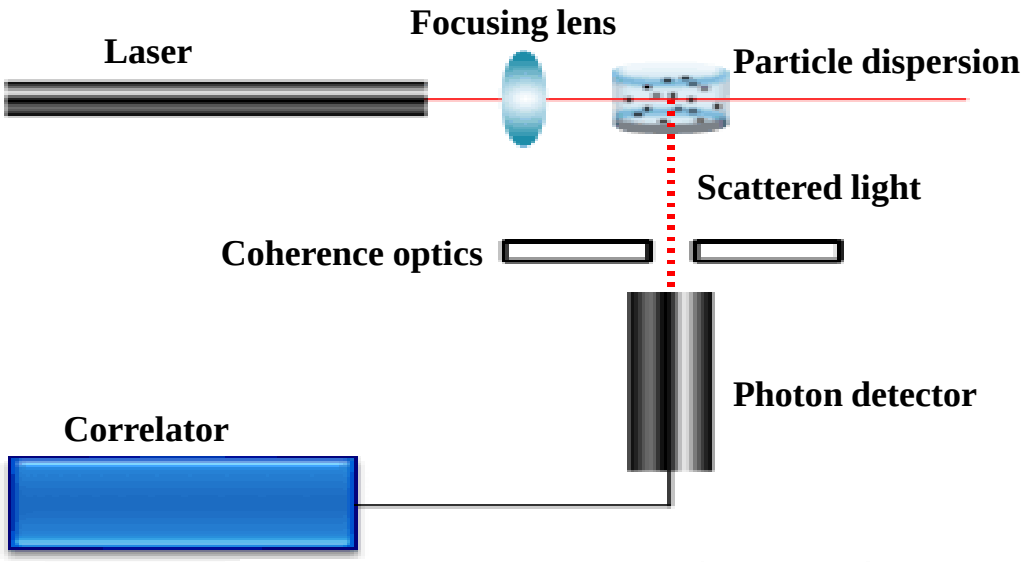

Figure 3.7: Schematic diagram of a conventional 90° dynamic light scattering instrument (Malvern Instruments Ltd, 2009).

In more recent DLS instruments, the detector is place at or near 180 degrees to the incident light beam. This allows the measurement of higher concentration suspensions and eliminates the need for dilution and the effect of dust contamination (Horiba Jobin Yvon, 1996).

The main advantages of DLS include the capability of measuring average size relatively rapidly (a few minutes) without calibration. However, there are some limitations to this technique. Samples must be highly dilute to avoid multiple scattering and over-attenuation of the light beam results in an underestimation of the particle size. Its ability to separate accurately multimodal distribution, and determine wide size distributions has also been questioned (Horiba Jobin Yvon, 1996).

3.2.7 Electrical Sensing Zone (Coulter Principle)

The Coulter method of sizing and counting particles is based on measurable changes in electrical resistance produced by non-conductive particles suspended in an electrolyte.

The instrument consists of two electrodes fixed at either side of a small orifice or aperture, with a dilute suspension of particles in an electrolyte as shown in figure 3.8. As the particle passes through the orifice, the particles displace their own volume of electrolyte causing a change in electrical resistance. This in turn gives rise to a change in the amplitude of the voltage pulse. Such pulses can then be counted and the number concentration of particles in the known volume of suspension can be estimated. The pulse heights are proportional to the particle volume, therefore the particle diameter derived from this method is the equivalent volume diameter (Wynn and Hounslow, 1997).

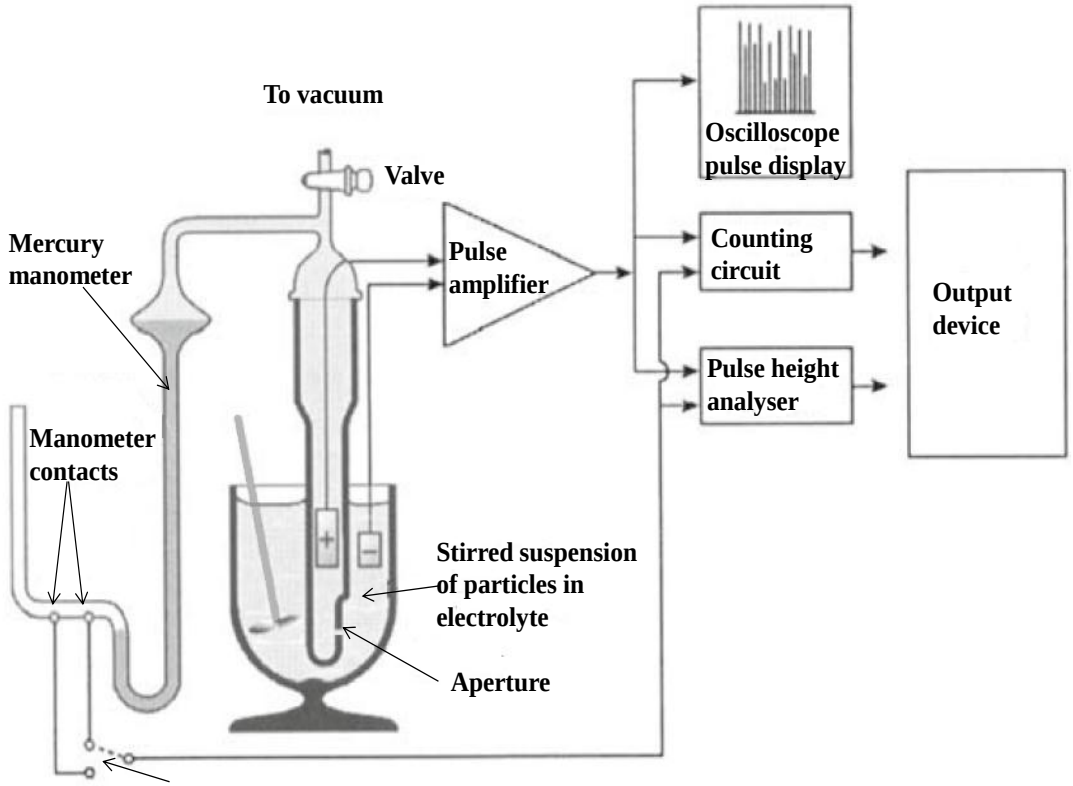

Figure 3.8: Schematic for a Standard Electrical Sensing Zone Method Instrument (Figueiredo, 2000).

According to the International Organisation for Standardisation (2007) an aperture should be chosen such that the diameter of the largest particles to be analysed is less than approximately 60 % of the diameter of the aperture. This is to reduce the possibility of blocking the aperture. Also for particles that are spherical or nearly spherical, the aperture chosen is such that the diameter of the largest particles is less than 80 % of the diameter of the aperture (International Organisation for Standardisation, 2007).

Measurements from this method are subject to errors especially at high concentrations of particles. The instrument relies on the assumption that particles pass through an orifice tube one at a time, so that each counted pulse corresponds to a single particle, and the magnitude of the pulse corresponds to a single particles size. However, if two or more particles pass through the orifice in close proximity, the resulting signal will be a single pulse and the magnitude of the single pulse will equal the sum of the magnitudes of each particle. Although this does not affect the total particulate volume observed, it does reduce the observed number of particles and increases the observed mean size (Wynn and Hounslow, 1997).

Another limitation of the Coulter method is the particle size determined is dependent on the shape of the particles. Flaky materials rotate as they pass through the orifice resulting in over-sizing; whilst extreme shapes like rods may cause a change in size distribution if the whole shape cannot be accommodated in the orifice. If the particles contain pores, these will be filled by the electrolyte solution leading to an untrue change in the voltage pulse (Allen, 1997). The material of the particle may also influence the size measurement, since the proportionality to the volume is different for conductive and non-conductive particles (Eckhoff, 1969). Care is required with powder of wide size range as any uncounted fraction may form a substantial part of the distribution (Van der Plaats et al., 1981).

3.2.8 Impaction

This technique is used for measuring aerosol particles. The principle is that particles have greater inertia than the gas and this prevents their following exactly the same streamlines of the gas flow around a surface. Some of the larger particles will impinge upon and be retained by the surface (Rumpf, 1990).

The most common form this technique applied consists of stages arranged in series, each stage consisting of one or more slits or holes facing a surface which may be a microscope slide coated to prevent re-entrainment of particles. The slits or holes are progressively smaller. The aerosol is drawn through the array with a pump. Each stage has a smaller mean ‘cut-off’ size than the previous stage, so the particles are classified according to

size. Some means must be provided for determining the amount of material collected at each stage if a size distribution is to be obtained (Rumpf, 1990).

3.2.9 Acoustic Attenuation Spectroscopy

Acoustic attenuation, also known as ultrasound attenuation spectroscopy, is technique whereby sound pulses are transmitted through a dispersed sample. Particles absorb and scatter ultrasound in the similar manner they do with light. The attenuation of the sound pulses is measured over a wide range of ultrasonic frequencies and at a range of detector spacing. Instead of measuring scattered energy versus angle, the transmitted energy versus frequency is measured. This attenuation depends on the particle size, which can then be calculated from the measured spectra (Dukhin et al., 1998).

3.2.10 Focused Beam Reflectance Measurement

The focused-beam reflectance measurement (FBRM) is among the most widely used in-process techniques (Barrett and Glennon, 2002). FBRM uses a focused beam of laser light that scans across particles passing in front of a probe window to measure a chord length distribution (CLD), which is a function of the true particle diameter distribution

The measurement principle of FBRM is based on backward light scattering. A laser beam is coupled to an immersible probe via an optical fibre. This laser beam is deviated from the probe's central axis in a rotational movement with a high constant velocity and focused into a disperse medium. When a particle passes this laser beam light scattering occurs. A certain fraction of the light is scattered back (back scatter) into the system and is conducted to a detector and converted into an electronic signal.

The time period of backscatter is multiplied by the scan speed and the result is a chord length of the particle. By knowing the chord lengths and the population of the particles, the chord-length distribution is produced.

Advantages of the technique include ease of use, little maintenance or calibration requirements and its capacity for on-line and in-situ measurements in systems with high

solid concentration. Compared with CLD information, the PSD is more useful because it is directly related to product quality and process productivity. However, it is not easy to convert a measured CLD into its corresponding PSD accurately due to the lack of a theoretical analysis (Mingzhong et al., 2006).

3.3 On-Line Techniques

Industrial plants that do not have continuous analysis are typically controlled using off-line measurements. Online analysis addresses the significant disadvantages of off-line systems.

With an online system, the analytical procedure is automated, eliminating operator-to-operator variability. Furthermore, the best systems give almost instantaneous measurement, allowing real-time tracking of the variable as different process parameters change. This is in sharp contrast to the delays that can accumulate with an off-line procedure involving sample procurement, transport to the lab, analysis and subsequent feedback of the results. The change is likened to switching from having snapshots of the process to having a video (Pugh, 2007).

Malvern Instrument Limited (2002) has developed several on-line particle size analysers based on a number of techniques, primarily using laser diffraction. However, acoustic techniques such as ultrasonic spectroscopy also show potential for on-line applications, particularly in regards to colloidal-based materials. According to the company, the instruments offer real-time repeatable particle size data regardless of the instantaneous process loading (i.e. sample concentration) resulting in instant feedback to allow a process engineer to adjust the process parameters, if required (Malvern Instruments Limited, 2002; Strategic Directions International Inc., 2001). However, they are very expensive (ca £65,000) and not robust to use in aggressive environments thus not suitable for in-line particle size measurement in typical powder production plants. In addition, the systems' response is subject to errors due to the variations in suspension conditions, solvent, temperature and focal point position (Patel, 2001).

3.4 Conclusions

The existence of the large number of particle sizing instruments operating based on different techniques is a verification of the importance of particle sizing in the particle production and processing industries. These techniques are extremely diverse, and although each has its benefits, there is no perfect instrument to cover all types of materials and for all size ranges. The most commonly used techniques include, sieving, laser diffraction, microscopy, light scattering and sedimentation. Certain qualitative and quantitative specifications must be taken into account when selecting a particle sizing instrument.

Several problems associated with conventional particle sizing techniques, including expense, complicated operating procedures, robustness, sample representation problems and on-line potential; limit the scope of their capabilities. This has continued the search for an instrument, which can address and overcome a range of these issues.

CHAPTER 4 SPRING PARTICLE SIZER (SPS)

In this chapter, the historical development of various prototypes of the Spring Particle Sizer (SPS) is reviewed. The Vibro-spring Particle Analyser initially developed by Mahgerefteh and Shaeri (2000) is presented first. This is followed by the design and improvement of the Pneumatic Spring Particle Sizer (PSPS) developed by Patel (2001). Finally, the Hand-held SPS, designed by Kerdvibulvech (2008) is discussed.

4.1 Vibro-Spring Particle Sizer (Mark I)

Mahgerefteh and Shaeri (2000) developed a novel technique for particle size analysis, which utilizes a vibrating extension spring. Figure 4.1 shows a schematic representation of the instrument. A test powder containing different sized particles is fed via an elbow feed into a horizontal extension spring. One end of the spring is extended by a screw thread, which is affixed to an adjustable plate. The spring extension is measured by the position of the screw head. The whole system is vibrated to enable particle discharge from the spring. A computer controlled stepper motor is used to control the system directly as shown in figure 4.2. Separated samples are collected at different extensions in containers attached to a carousel. Each collected sample is then weighed to produce a PSD. The mean particle size of each discharged sample is inferred from the spring extension and the number of active coils being used for the discharge. This information is used to plot the particle size distribution. A detailed description is given by Kerdvibulvech (2008)

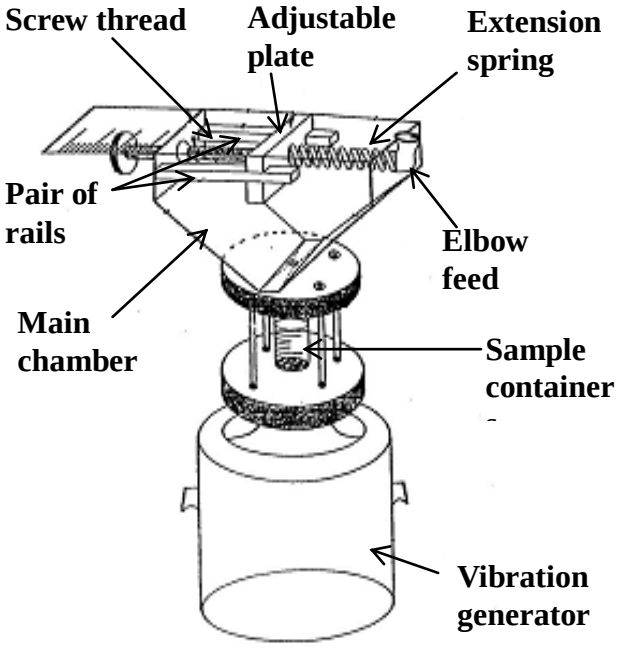

Figure 4.1: Schematic representation of Vibro-Spring Particle Size Analyser (Patel, 2001).

Figure 4.2: Photograph of Vibro-Spring Particle Size Analyser (Patel, 2001).

According to Shaeri (1997), this device is capable of measuring particles in the size range of 75-800 μm with a resolution of ca ± 20 μm. The ability of this device to separate a test powder into different size fractions allows it to be considered as a classifier.

The Vibro-spring particle size analyser offers several advantages over conventional techniques because it is robust, simple and has the potential to provide on-line measurements. Compared to sieving, this technique is in principle capable of producing an infinite number of size cuts while the alternative is restricted to the standard size cuts available. Another significant problem associated with sieving is blinding of the apertures which lead to "down time" to clean the wire meshes increasing the risk of sieve cloth deforming or breaking which will cause result inaccuracy. Neither of these problems is associated with the Vibro-spring particle sizing technique. If any particles are trapped between the spring openings, they are released as the spring is stretched to the next size cut (Kerdvibulvech, 2008).

The disadvantage of this technique was the lack of an in-situ mass measurement capability as the collectors filled with particles during tests (see figure 4.1) are manually removed from the carousel and weighed. In addition, the number of collectors attached on the carousel also restricts the number of size cuts.

4.2 Vibro-Spring Particle Sizer (Mark II)

Patel (2001) developed a fully automated Spring Particle Sizer, which overcame most of the problems associated with the earlier design by Mahgerefteh and Shaeri (2000). Full details of the system's design are given by Patel (2001); hence, a brief account is given here.

Figure 4.3 shows a schematic representation of the Vibro-Spring Particle Sizer (Mark II) developed by Patel (2001).

Approximately 10g of test powder is fed into the Vibro-Spring Particle Sizer via the feed funnel mounted at one end of the spring. The required spring extension is controlled using the two aluminium bars affixed to both ends of the spring.

The size and mass of the discharged particles are determined from the spring extension and a specially designed in-situ cantilever mechanism respectively. The cantilever mechanism is similar to a conventional pan balance and equilibrium, and relies on the use of a non-contacting capacitance transducer. The addition of test powder to the spring offsets the balance of the system resulting in a downward deflection of the spring. Its displacement is detected by the capacitance transducer, which outputs a stable analogue voltage signal that varies linearly with the mass of sample in the spring. However, the maximum output range of the capacitance transducer used was 5 mm, which limits the maximum mass of sample that can be analysed to 10 g (Kerdvibulvech, 2008).

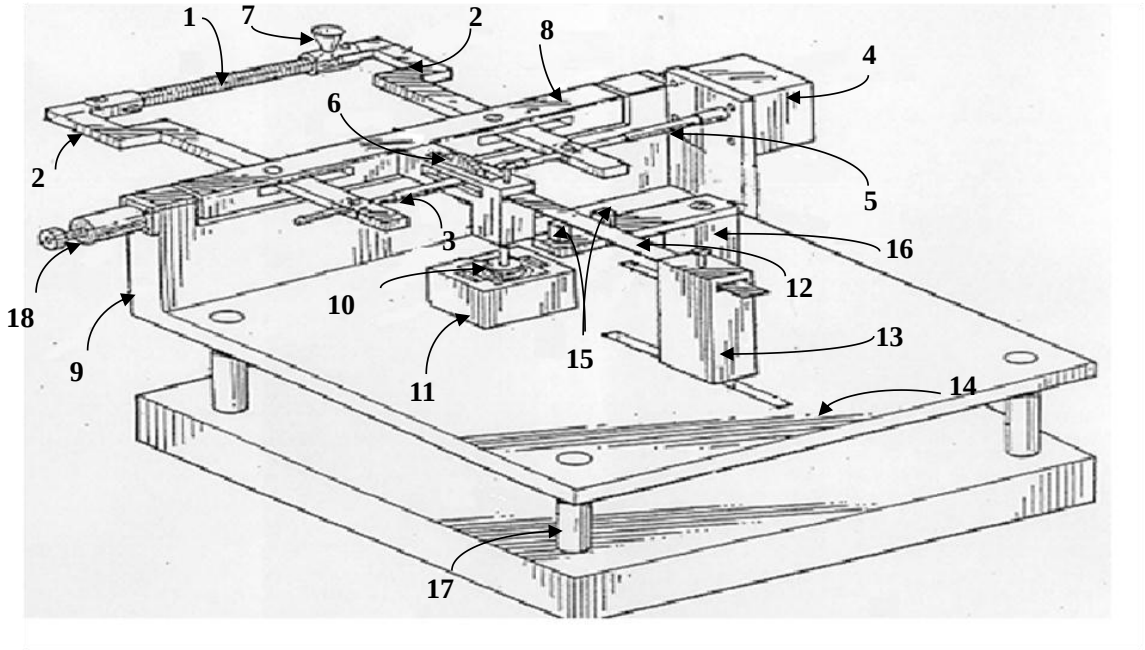

Figure 4.3: Perspective representation of the Vibro-Spring Particle Sizer (Mark II) (Patel, 2001).

1. Spring
2. Rectangular bars
3. Control screw
4. Stepper motor
5. Wire connection
6. Control disk
7. Funnel
8. T-piece
9. Support frame
10. Steel disk
11. Electro-magnet
12. Spring steel reed
13. Reed support block
14. Base plate
15. Infrared detector
16. Detector support legs
17. Base support legs
18. Ball bearings

The ability to automatically weigh the quantity of powder in the spring in-situ significantly reduces the testing time thus making the technique particularly suited for process control applications. In such circumstances, reproducibility is as important as absolute measurements since operators are frequently interested in knowing whether the size distribution of a product is different from the specification (Patel, 2001).

The system was validated by comparing the measured PSD against sieve measurements for a variety of dry powders in the size range 30 – 1200 μm. The PSD data exhibited very good reproducibility and excellent agreement with sieve measurements (Patel, 2001).

The Vibro-Spring Particle Sizer (Mark II) offered several advantages over conventional techniques due to its robustness, ease of use and the ability to provide on-line measurements due to its in-situ mass measurements and system automation.

Despite the improvements to the Vibro-Spring Particle Sizer (Mark II), Patel (2001) identified a number of possible improvements to translate the Vibro-Spring Particle Sizer for use in the real industrial environment. These include errors in spring length caused by slippage of the gear mechanism and extended analysis times for fine powders due to an angled funnel.

Another design limitation identified by Patel (2001) is the bending of the horizontal spring as it is vibrated vertically. The bending causes significant variations in the intercoil distance especially at its mid-length where the maximum deflection occurs, thereby leading to errors in size analysis. Figures 4.4 and 4.5 show schematic representations of the spring's static and dynamic intercoil distances respectively. Mahgerefteh and Shaeri (2001) developed a mathematical model predicting the spring's dynamic profile during vibration allowing the determination of the maximum intercoil distance, $d_{dynamic}$ (see figure 4.5).

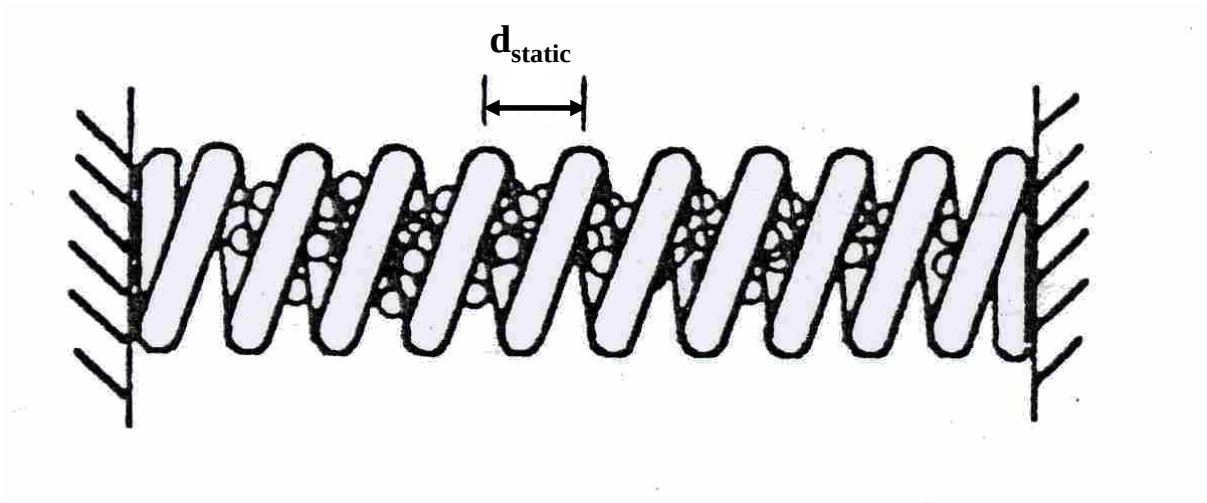

Figure 4.4: Schematic representation of the pitch length of a static spring (Patel, 2001).

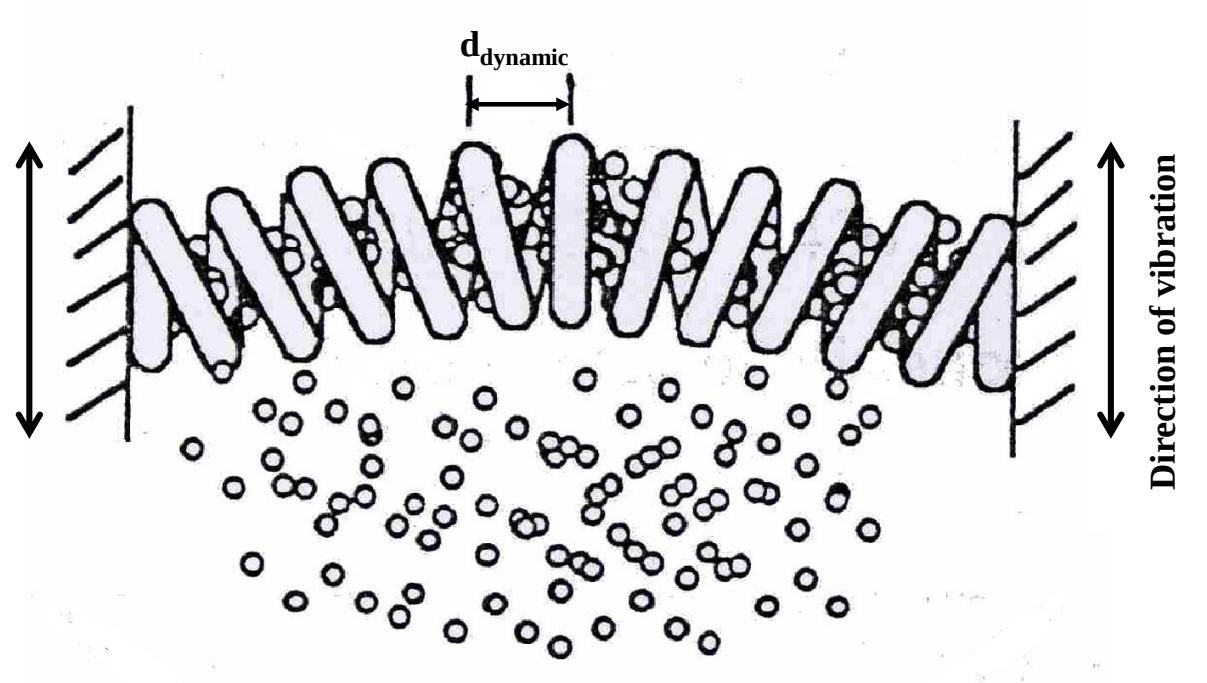

Figure 4.5: Schematic representation of the pitch length of a dynamic spring (Patel, 2001).

4.3 The Pneumatic Spring Particle Sizer (PSPS)

Mahgerefteh and Kamugasha (2004) developed the Pneumatic Spring Particle Sizer (PSPS), which is used in this study, to address the drawbacks associated with Patel's (2001) Vibro-Spring Particle Sizer (Mark II). Figure 4.6 shows a schematic representation of the PSPS.

The PSPS consists of a large capacity extension spring (23 mm i.d., 180 mm length, 3 mm wire dia.) which is stretched vertically along its length by a screw mechanism in conjunction with a stepper motor. The unit has a capacity of 75 cc, this translates to a maximum sample mass of approximately 190 g for Glass Ballotini with a bulk density of ca 2540 kg m^{-3}. The spring extension is monitored and controlled by an optical shaft encoder attached to the stepper motor.

The test powder is fed into the unit via a feed hopper, which is mounted on a feed plate. The top end of the extension spring used for particle size analysis is inserted into the base of the supporting plate via a spring connector. The bottom end of the extension spring is inserted into the top of a conical base holder, which also houses the compressed air inlet channel, and the 32 µm screen mesh used to support particles within the spring (Kerdvibulvech, 2008). Pulsed compressed air is used to agitate and discharge the particles from the spring chamber.

The above assembly (parts 1-13, figure 4.6) is mounted onto a supporting base via three aluminium rods. The base also supports the feed plate via three aluminium rods (16) mounted in a triangular formation.

The entire system is housed by a 1 mm thick Perspex cylindrical enclosure, which contains the powder discharged from the spring. The powder discharged from the spring is directed towards a machined outlet orifice (20 mm) located at the bottom of the base using gravity. The discharged powder can then be collected and weighed (Kerdvibulvech, 2008).

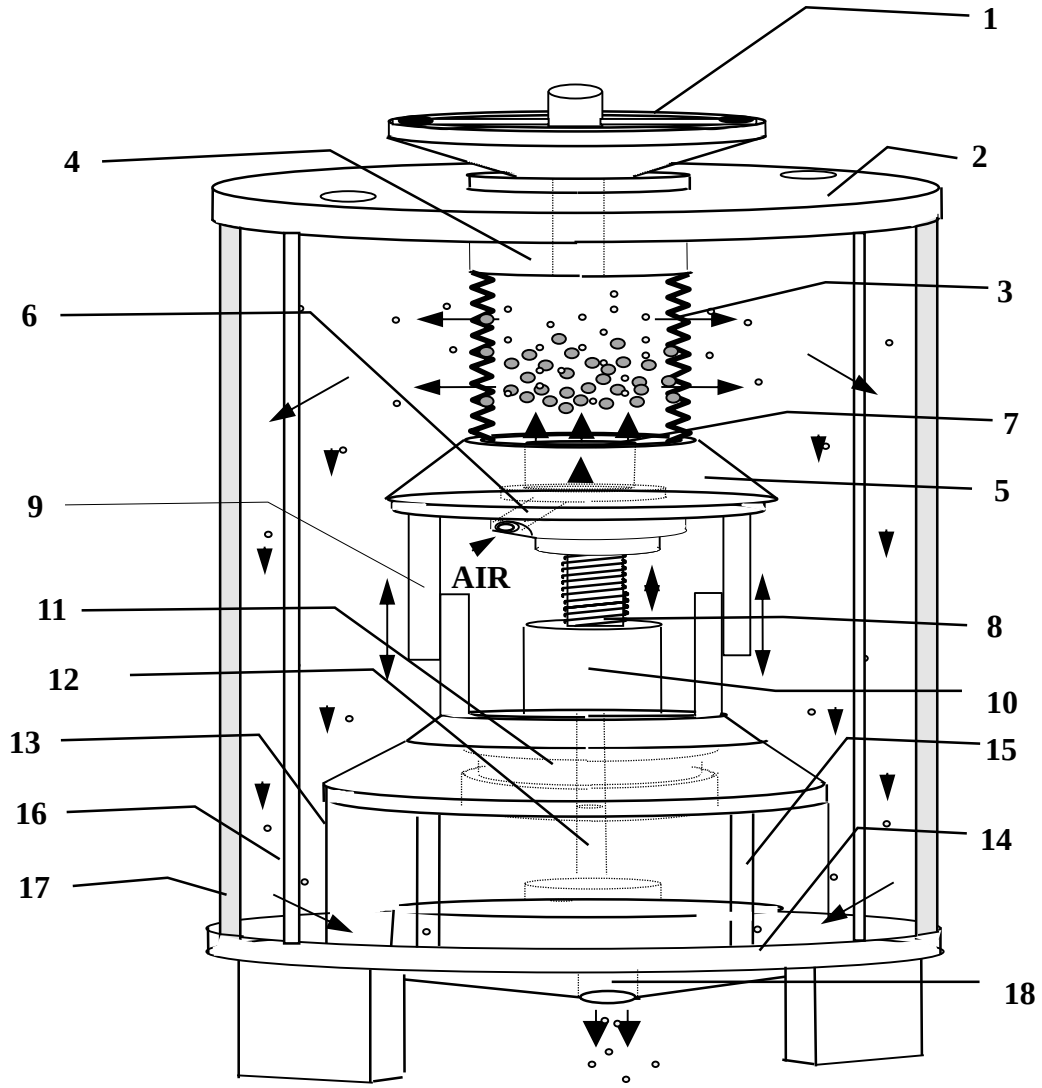

Figure 4.6: Schematic diagram of Pneumatic Spring Particle Sizer (Kerdvibulvech, 2008).

1. Feed hopper
2. Supporting plate
3. extension spring
4. Spring connector
5. Conical base holder
6. Compressed air inlet channel
7. Screen mesh
8. Spring extension screw
9. Telescopic enclosure
10. Hollow aluminium tube
11. Stepper motor
12. Optical shaft encoder
13. Cylindrical aluminium container
14. Supporting base
15. Aluminium rods
16. Aluminium support rods
17. Perspex cylindrical enclosure
18. Outlet orifice

The weighing mechanism situated at the bottom of the structure consists of an aluminium collection pan used to capture discharged powder from the spring. A 30 μm filter cloth attached to the pan, allows the release of compressed air from the system whilst simultaneously preventing the loss of discharged powder to atmosphere. The collection pan is mounted onto a weighing pan-balance for direct mass measurement. The weighing mechanism also includes a system of electro-magnets and solenoids specially designed to clamp the weighing pan up during particle size analysis. This action enables the weighing pan to be attached to the system, capturing the discharged powder whilst allowing the compressed air to escape to the atmosphere. Once the discharged powder has been collected, the weighing pan is unclamped and isolating it from the whole system. This in turn, stabilises the weighing pan before the monitoring of the mass of each discharged size cut.

The device was compared against sieves using measured PSD data for a selection of dry powders in the size range 100 – 2000 μm. The PSD data exhibited very good reproducibility and excellent agreement with sieve measurements (Kerdvibulvech, 2008).

4.3.1 Electronic Drive and Control Box

Kerdvibulvech (2008) gave a detailed description of the control software and the electronic configuration of the control box used to operate the PSPS. Therefore, only a brief summary of the PSPS controls is given in this section.

The Pneumatic Spring Particle Sizer is controlled using a 32-Bit computer interface bus. The computer interface is linked to the control box, which electronically operates the moving parts of the pneumatic SPS. Bits of data are sent to and from the control box to the computer via this network, which allows for control inputs and measurement outputs to be entered and interpreted by the operator

4.3.2 Control Software HP VEE

HP VEE (Hewlett Packard Visual Engineering Environment) is a visual programming language developed by Hewlett-Packard for programming tasks in instrument control,

measurement processing and test reporting. It produces dramatic improvements in test development time (Helsel, 1998). The software was used for programming the electronic transducers for the SPS system.

The software package provides a GUI (Graphic User Interface) for manipulating graphical objects and linking them into block diagrams to represent a program. The DT VPI Manual (Data Translation Visual Programming Interface) and Patel's PhD thesis (2001) also provide further details on the data acquisition interface and the control of the I/O (Input/Output) subsystems.

4.4 Handheld Spring Particle Sizer

The handheld version of the Spring Particle Sizer was developed by Kerdvibulvech (2008) using the same principle of spring extension for powder fractionation. Figure 4.7 shows a photograph of the handheld Spring Particle Sizer. The unit consists of an extension spring (24.5 mm i.d., 72 mm long and 3 mm wire dia.) housed within a Perspex tube and supported by three aluminium rods. A support base holds the other end of the spring through which test powder is fed, and contains openings where particles fall through and are collected from a sample bottle.

Extension of the spring to cause particle discharge is obtained by turning the screw cap of the unit, which houses the extension mechanism, in an anti-clockwise direction. The extension screw cap is machined with 26 TPI (teeth per inch) threads, stretches by ca. 0.98 mm for each full turn (Kerdvibulvech, 2008). The handheld SPS agitated is by shaking to enhance particulate discharge. As spring aperture size increases, particles are discharged into the Perspex tube. By holding the unit vertically and tapping on the tube gently, the particles fall into the sample container and mass measurement can be carried out manually to obtain the particle size distribution.

The device provides the same attractiveness and advantages as the pneumatic SPS over the conventional instruments currently available. The handheld SPS is relatively inexpensive, robust, simple to use, able to handle a good amount of sample (ca. 30 g). Other benefits

include a very low maintenance cost and most importantly, the unit can be used to monitor particle size distribution for quality assurance purposes. Its main advantage is that it is very easy to carry and can be used as a tool for checking and rechecking conformity with the prescribed standards of powders at various stages in any production process. For this device, the operating sequence, mass measurement and data acquisition have been designed to be completely manual (due to the purpose it was developed for).

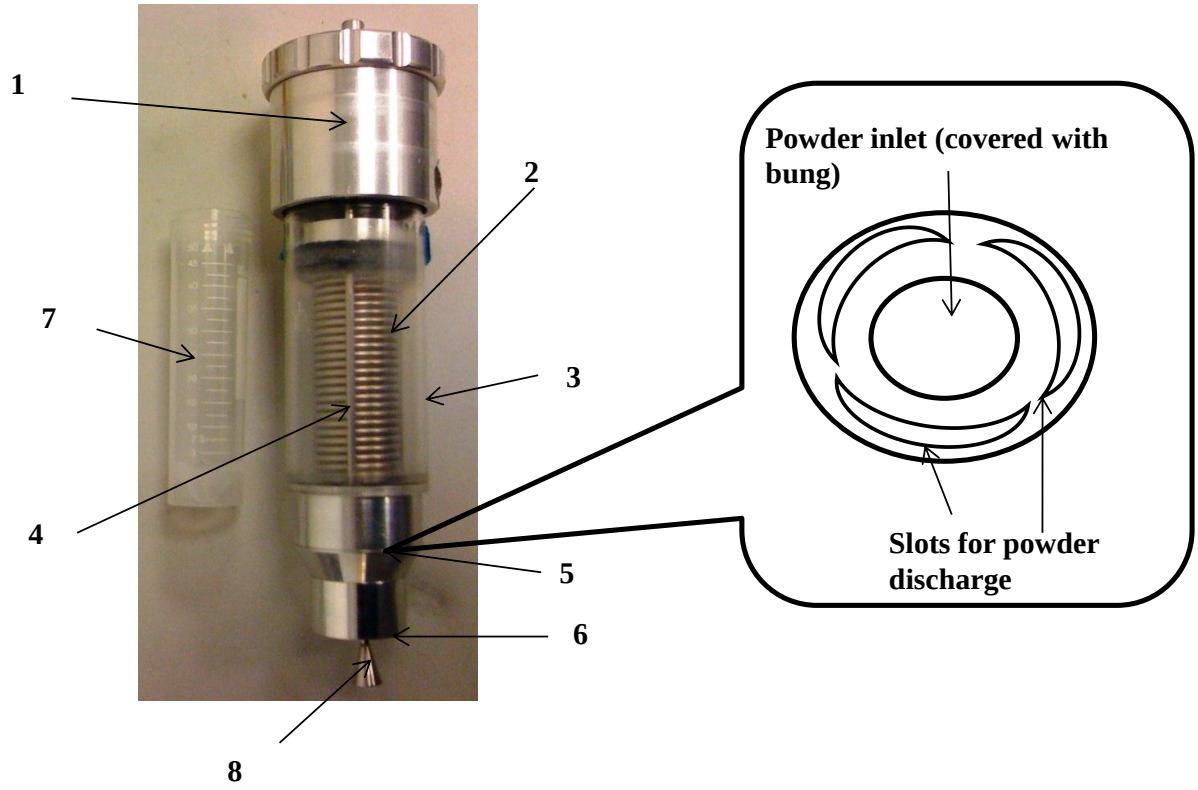

Figure 4.7: Photograph of the Handheld Spring Particle Sizer with calibrated Perspex sample collector.

1. Extension screw cap
2. Closed-coil extension spring
3. Perspex tube
4. Aluminium rods
5. Support base
6. Powder outlet
7. Sample collector
8. Rubber bung handle

4.5 Problems Associated with the Spring Particle Sizer

Despite various improvements in the SPS, it has encountered a number of fundamentally important design and operational limitations, which have hindered its commercial success. Major problems include sample retention in the PSPS system primarily through static charge build up by the fluidising air stream in addition to obstructions within the unit. This consequently leads to errors in the PSD due to sample loss. The lack of an in-situ mass measurement system, which may address the problem, has inhibited this and limited its use for on-line applications.

Other drawbacks included non-uniform spring coil openings, non-reproducibility of springs, and extended analysis time.

CHAPTER 5 SPRING COIL APERTURE ANALYSIS

5.1 Introduction

The efficacy and reproducibility of PSD measured using the PSPS critically depends on the uniformity of the spring coil apertures as the spring is extended. Also, from a commercial point of view when producing the PSPS, it is highly advantageous to utilise springs with very similar coil opening uniformity to avoid having to perform individual calibrations.

This chapter presents the results and discussion of a series of tests involving the measurements of the mean spring coil aperture and standard deviation at a given spring extension for two 'identically fabricated' springs, A1 and A2 supplied by Airedale Springs Limited (2008). Provided that the elastic limit of each spring is not exceeded and assuming all the spring's apertures open uniformly, the nominal spring coil aperture size can then be calculated by dividing the change in spring length following extension by the number of active coils in the spring.

The performance of the two springs is then evaluated by comparing their standard deviation for a given aperture size against the corresponding data given by the British Standards Institute (British Standards Institute, 2000) for sieves.

5.2 Experimental Arrangement

Khan (2009) conducted a series of tests using springs produced by various spring manufacturers, namely Airedale Springs Limited, Skegness Springs Limited and UCL Chemical Engineering Workshop to determine the spring with the most uniform coil apertures. The tests showed that springs produced by Airedale Springs Limited (Airedale Springs Limited, 2008) had the most uniform coil apertures. Consequently, Airedale Springs Limited springs are used throughout this study.

Figure 5.1 shows a schematic diagram of the experimental setup used to determine the uniformity of the spring coil apertures. Table 5.1 gives the dimensions of the two Airedale Springs Limited springs, A1 and A2 used in the experiments. The springs are made of stainless steel grade 316.

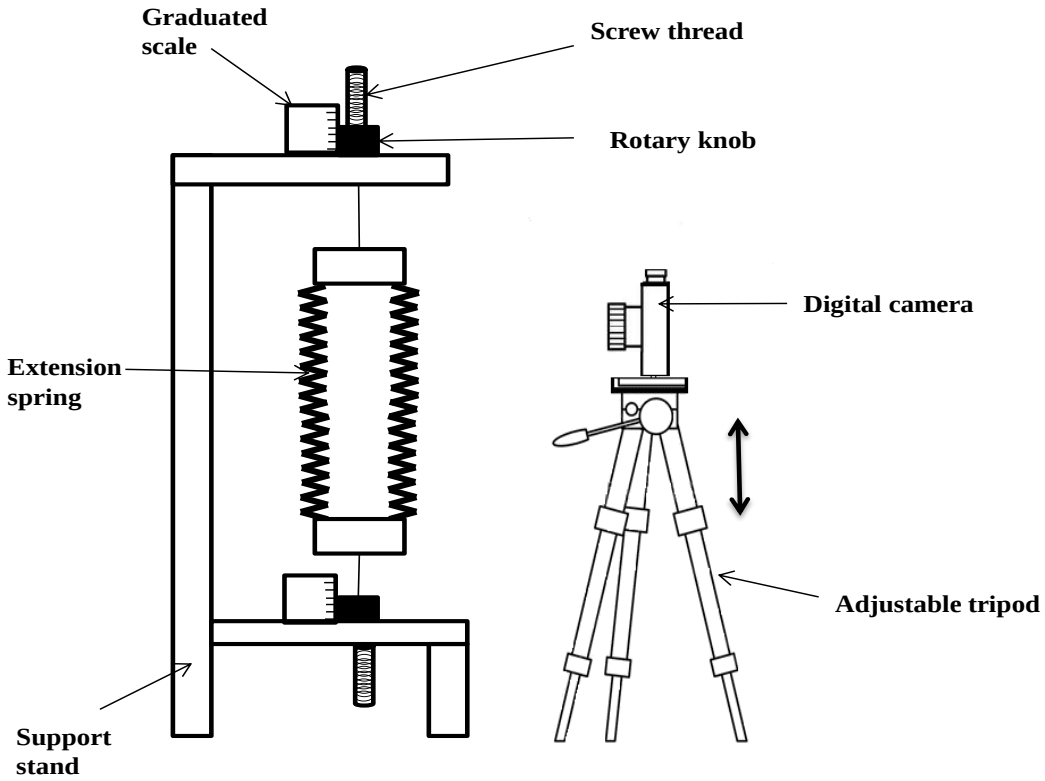

Figure 5.1: Schematic diagram of image analysis experimental set-up using digital photography for measuring spring coil aperture size.

Table 5.1: Dimensions of the two Airedale Springs Limited springs (A1 and A2) used in the experiments.

Number of active coils	32
Wire diameter	2.03 mm
Internal diameter	21.5 mm
External diameter	25.5 mm
Active Length	67 mm

Returning to figure 5.1, the test springs were held in position on both ends by metallic wires attached to 1 mm pitch screw threads. Each spring was extended by turning the rotary knobs and the total spring extension was determined using the graduated scales adjacent to the rotary knobs.

A preliminary visual check was conducted using the transmitted light from a fibre-optic light source to verify no presence of closed coils when the spring was extended. Following this test, a 5 megapixel camera (Sony Cyber-shot DSC-F707) was used to take six photographs along the length of the spring. The height of the camera was adjusted using a tripod to minimise optical errors associated with misalignment. The above procedure was performed with the spring extended from one side (unilateral extension) and then repeated with the spring extended from both sides (bilateral extension). Table 5.2 gives the total spring extension, the mode of spring extension (unilateral or bilateral) and the nominal spring opening aperture for each test performed. As mentioned in section 5.2, the nominal spring coil aperture size is calculated by dividing the total spring extension by the number of active coils in the spring.

The photo editing software Irfanview (Škiljan, 2008) was used to perform the image analysis in this study. Each photograph was magnified by 400 % and the number of pixels between each coil was converted to an aperture size using the known size of the spring wire (2.03 mm) as the reference calibration. Figure 5.2 shows an example of the analysis performed on a photograph taken from Test 5 (see table 5.2). To reduce the errors due to image resolution, all the pixel measurements were taking along an imaginary line drawn through the centre of the spring.

Table 5.2: Summary of extensions tests carried out on springs A1 and A2.

Test Number	Spring	Extension Type	Total Spring Extension (mm)	Nominal Spring Coil Aperture (µm)
1	A1	Unilateral	2	62.5
2	A1	Bilateral	2	62.5
3	A1	Unilateral	4	125
4	A1	Bilateral	4	125
5	A1	Unilateral	6	187.5
6	A1	Bilateral	6	187.5
7	A1	Unilateral	8	250
8	A1	Bilateral	8	250
9	A1	Unilateral	10	312.5
10	A1	Bilateral	10	312.5
11	A2	Unilateral	2	62.5
12	A2	Bilateral	2	62.5
13	A2	Unilateral	4	125
14	A2	Bilateral	4	125
15	A2	Unilateral	6	187.5
16	A2	Bilateral	6	187.5
17	A2	Unilateral	8	250
18	A2	Bilateral	8	250
19	A2	Unilateral	10	312.5
20	A2	Bilateral	10	312.5

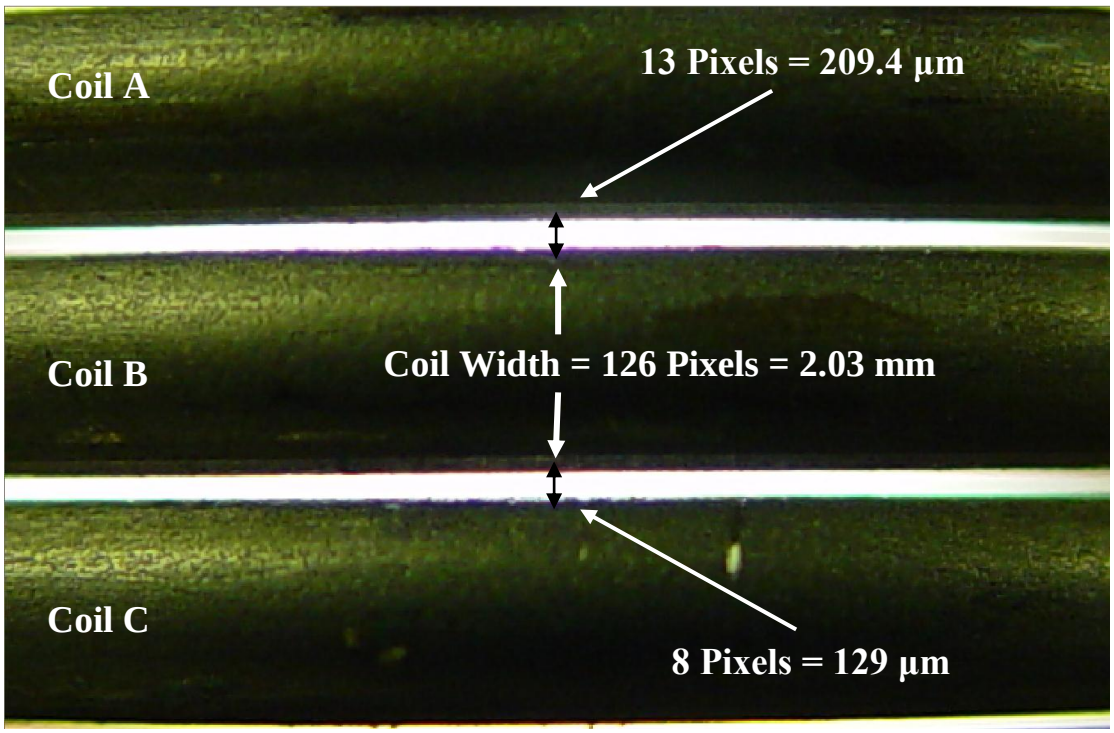

Figure 5.2: An example of the image analysis technique used on a magnified digital photograph from Test 5 (unilateral extension of spring A1 to 6 mm) to determine the spring coil apertures.

5.3 Results and Discussion

The following presents the results of the image analysis performed to determine the uniformity of the spring coil apertures for the two Airedale springs.

Figure 5.3 shows the variation of the spring coil aperture size with aperture number for spring A1 following a 2 mm extension (Tests 1 and 2). Curves A and B are the measured coil aperture sizes following unilateral and bilateral extensions respectively. The nominal spring coil aperture size based on the total spring extension is also indicated in the figure.

The large variations observed in the measured coil apertures in figure 5.3 highlights the non-uniformity of spring A1. The figure also shows that extending the spring unilaterally or bilaterally had no impact on the results. In contrast to the nominal spring coil aperture size of 62.5 μm, the measured aperture sizes varied between 18 μm to 126 μm for unilateral extension (curve A) and 16 μm to 138 μm for bilateral extension (curve B).

Figures 5.4 to 5.12 show the variation in coil aperture size with aperture number for springs A1 and A2 at various spring extensions (Tests 3 to 20). The nominal spring coil aperture for each extension is given in each figure. The figures show the same large variations in the measured coil aperture size irrespective of the spring being extended unilaterally or bilaterally.

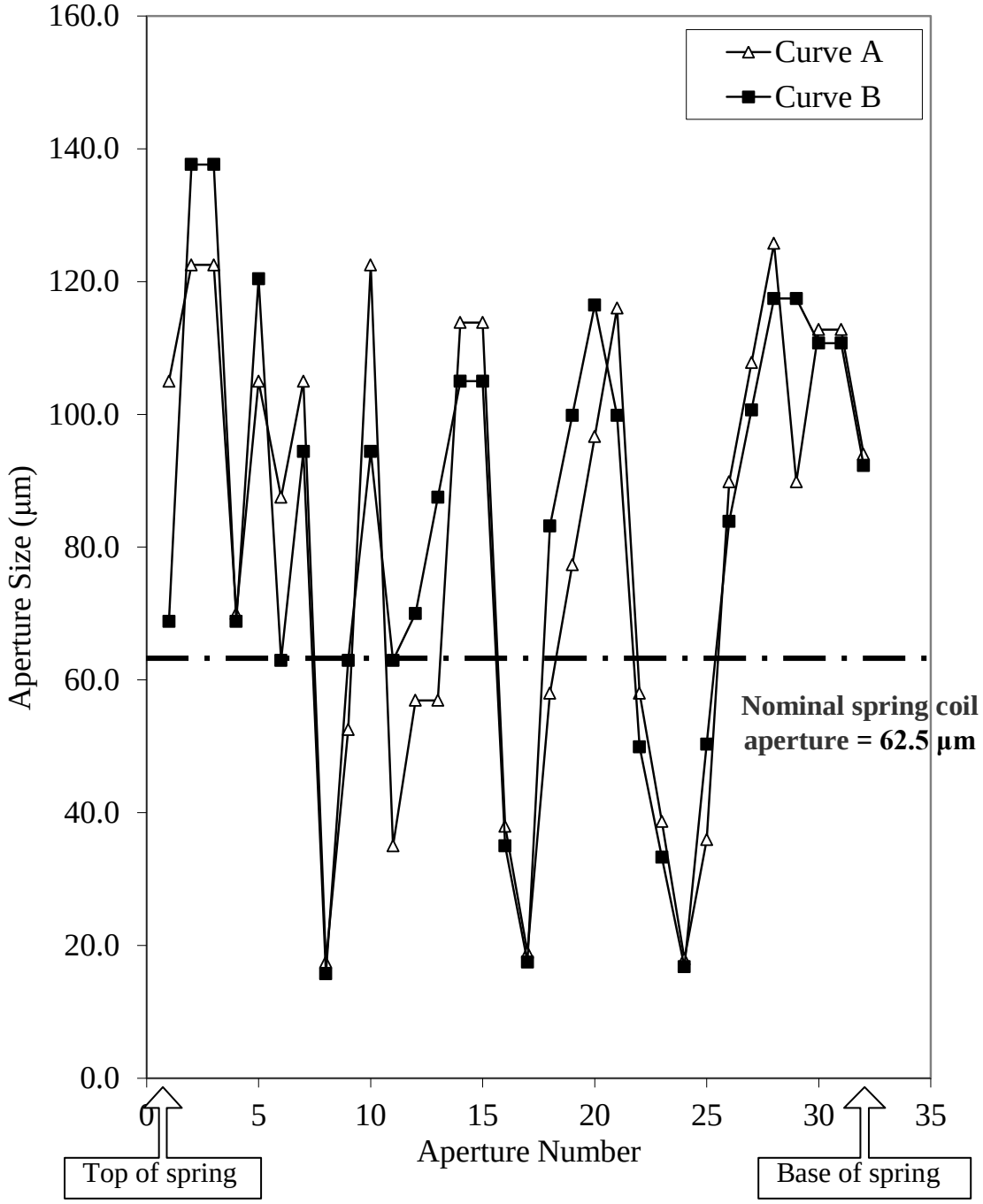

Figure 5.3: Variation of individual aperture size along the length for spring A1 when extended to 2 mm.

Curve A: A1 unilateral extension

Curve B: A1 bilateral extension

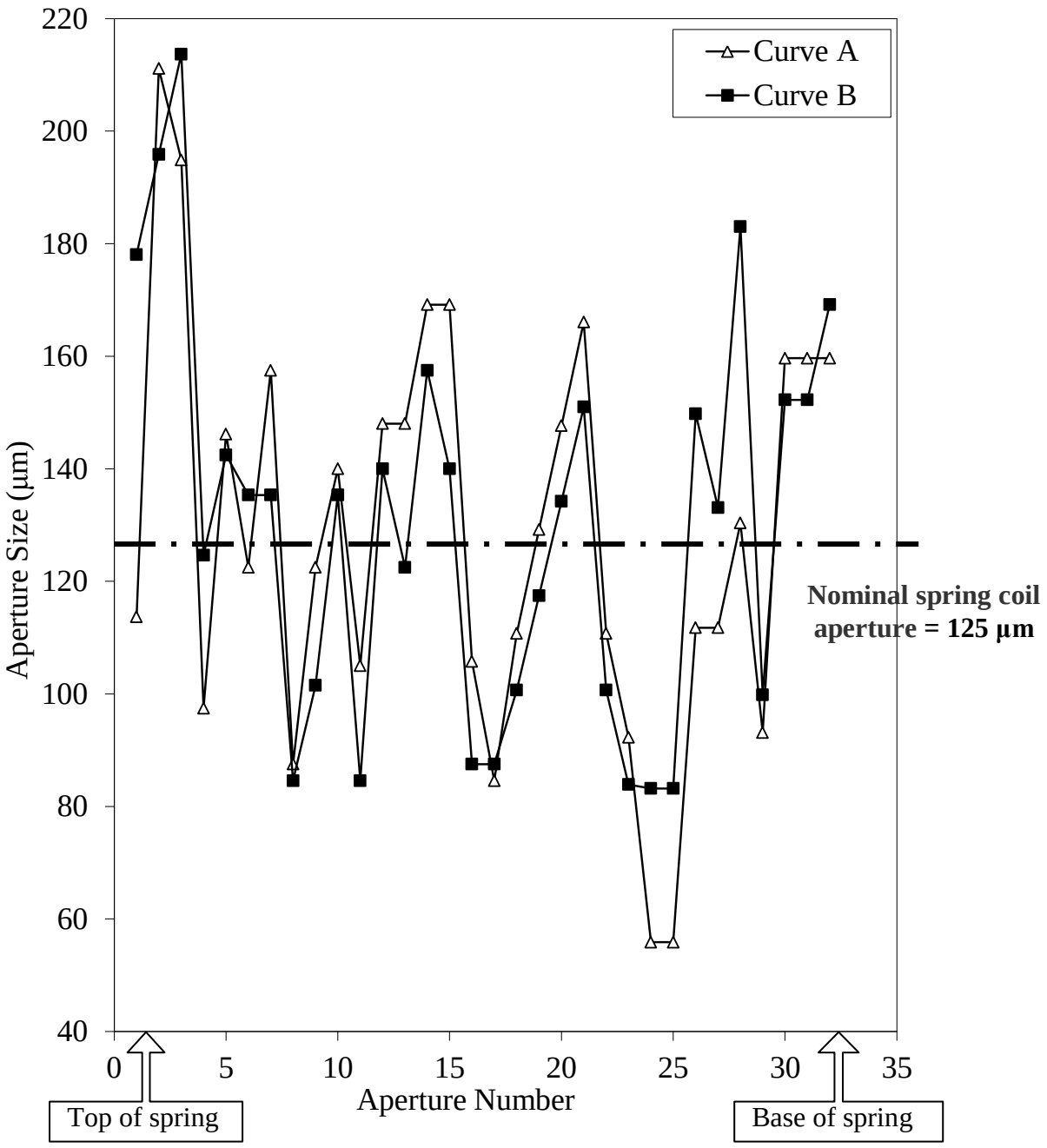

Figure 5.4: Variation of individual aperture size along the length of A1 when extended to 4 mm.

Curve A: A1 unilateral extension

Curve B: A1 bilateral extension

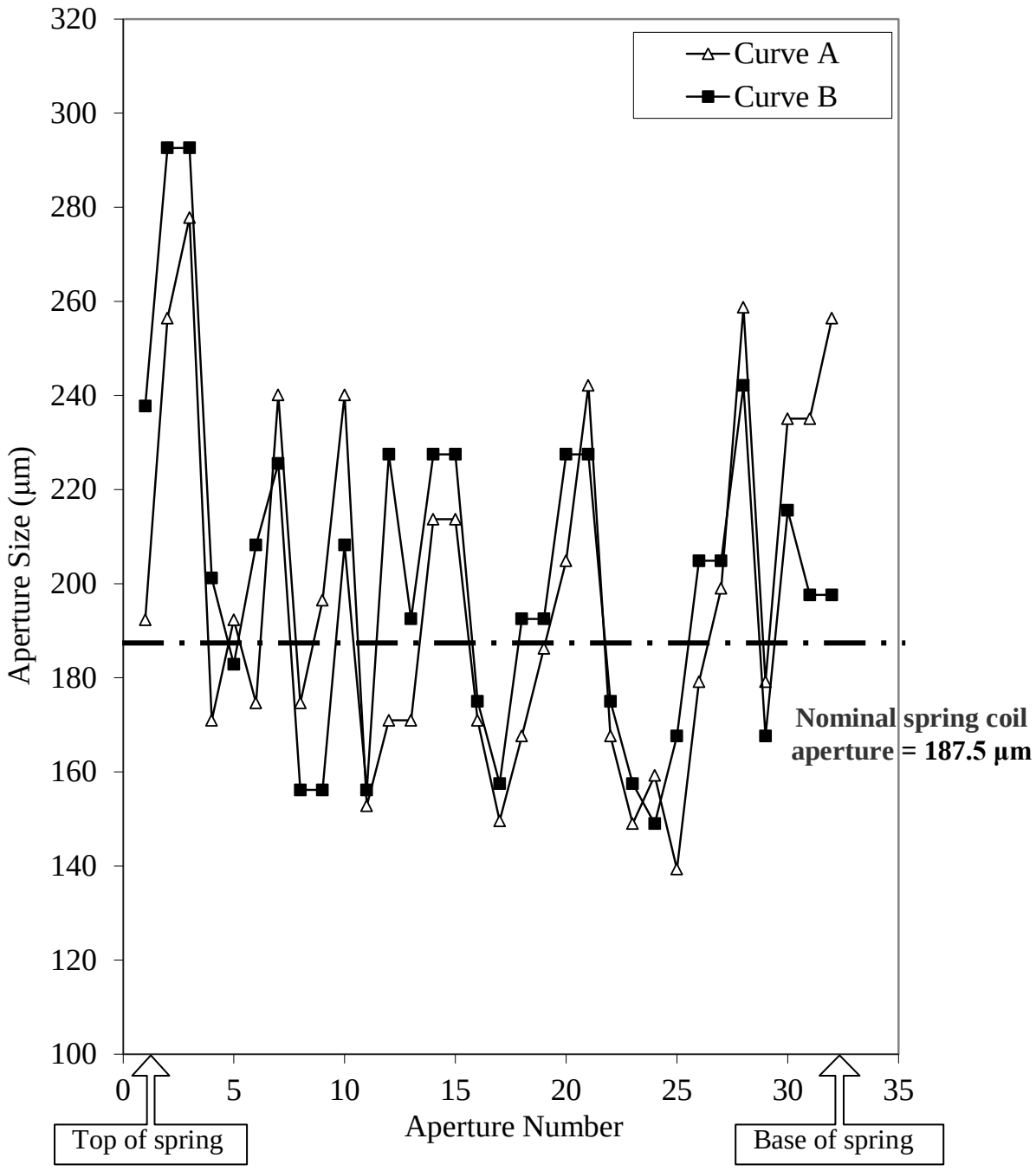

Figure 5.5: Variation of individual aperture size along the length of A1 when extended to 6 mm.

Curve A: A1 unilateral extension

Curve B: A1 bilateral extension

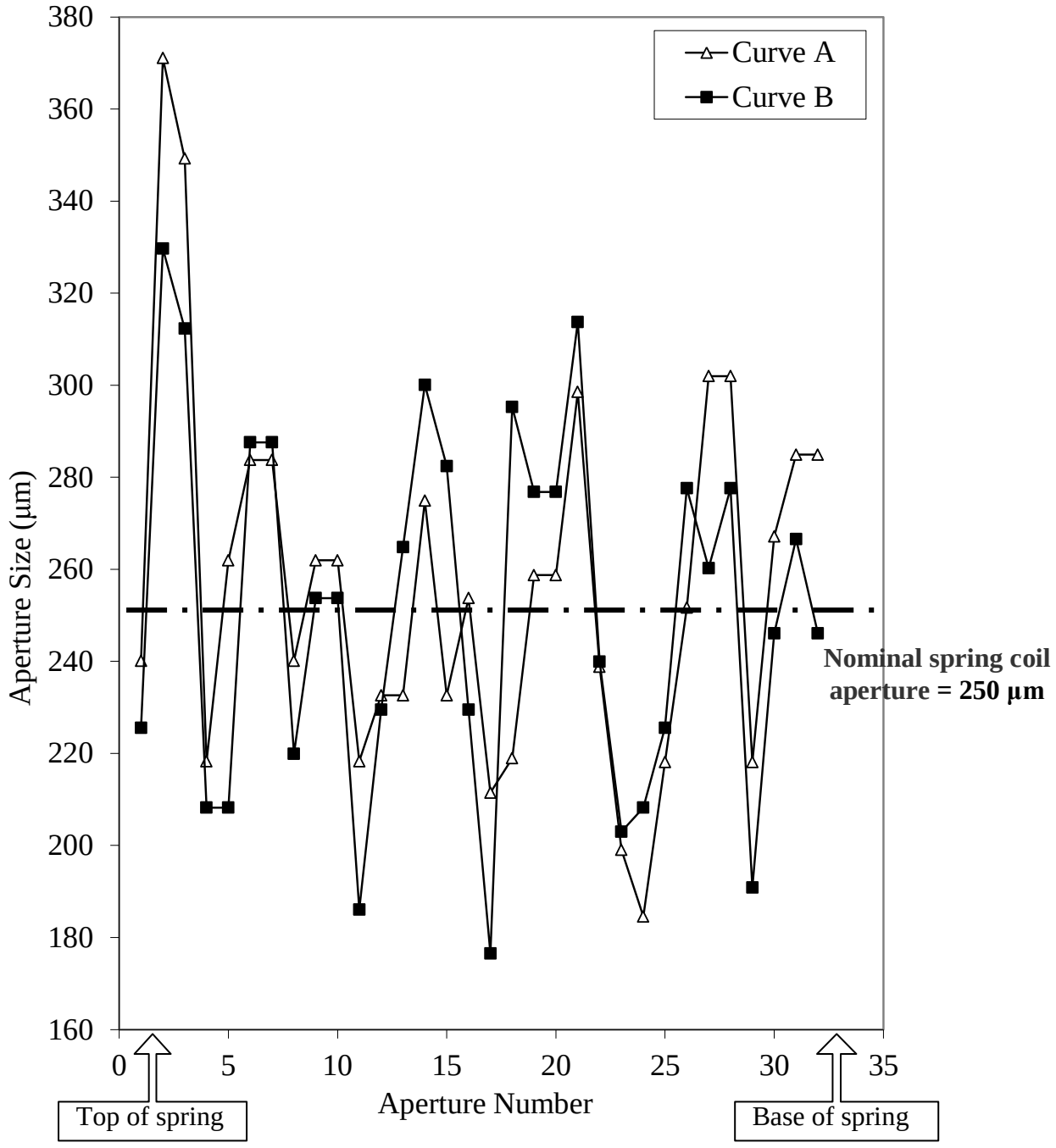

Figure 5.6: Variation of individual aperture size along the length of A1 when extended to 8 mm.

Curve A: A1 unilateral extension

Curve B: A1 bilateral extension

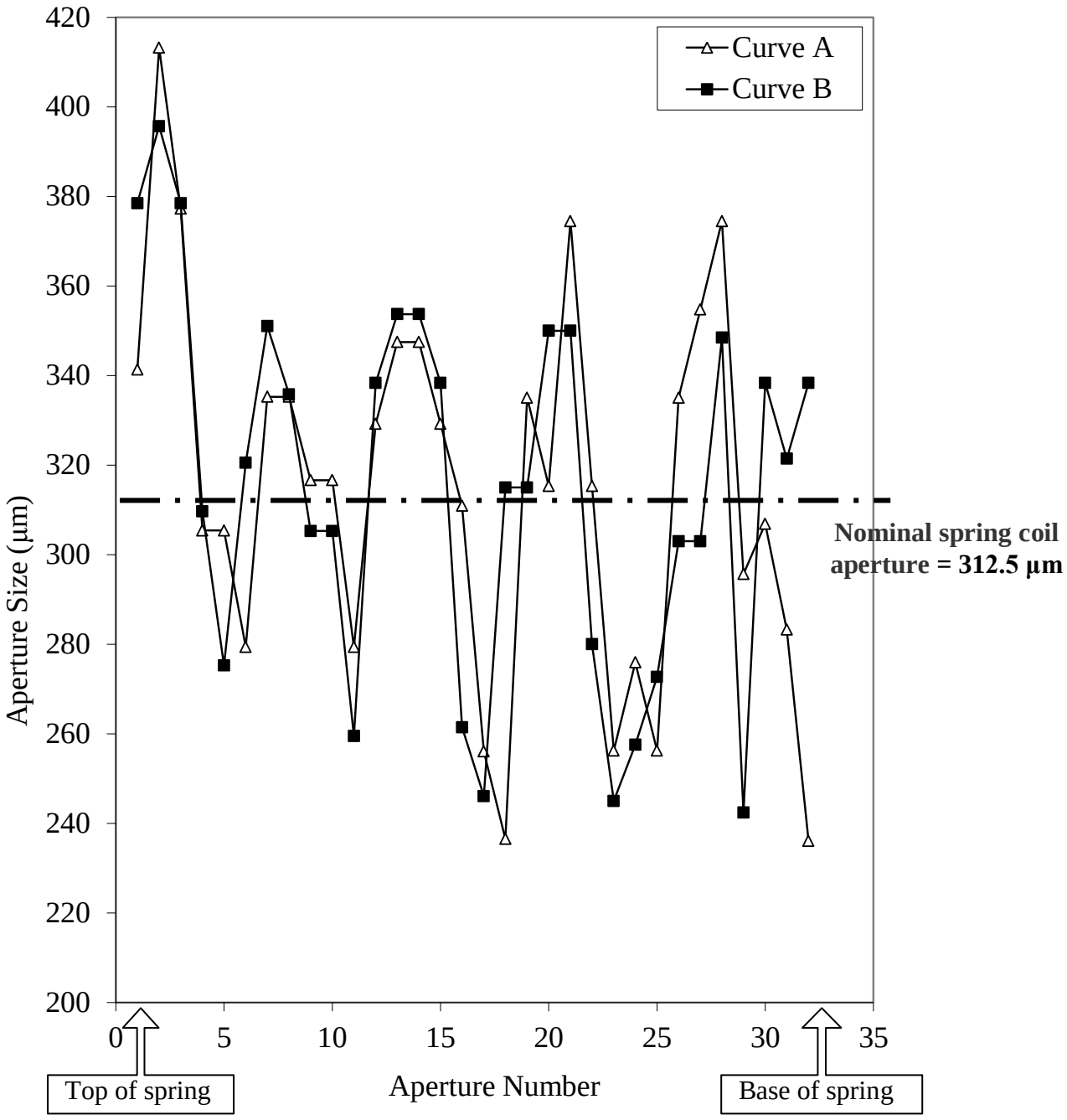

Figure 5.7: Variation of individual aperture size along the length of A1 when extended to 10 mm.

Curve A: A1 unilateral extension

Curve B: A1 bilateral extension

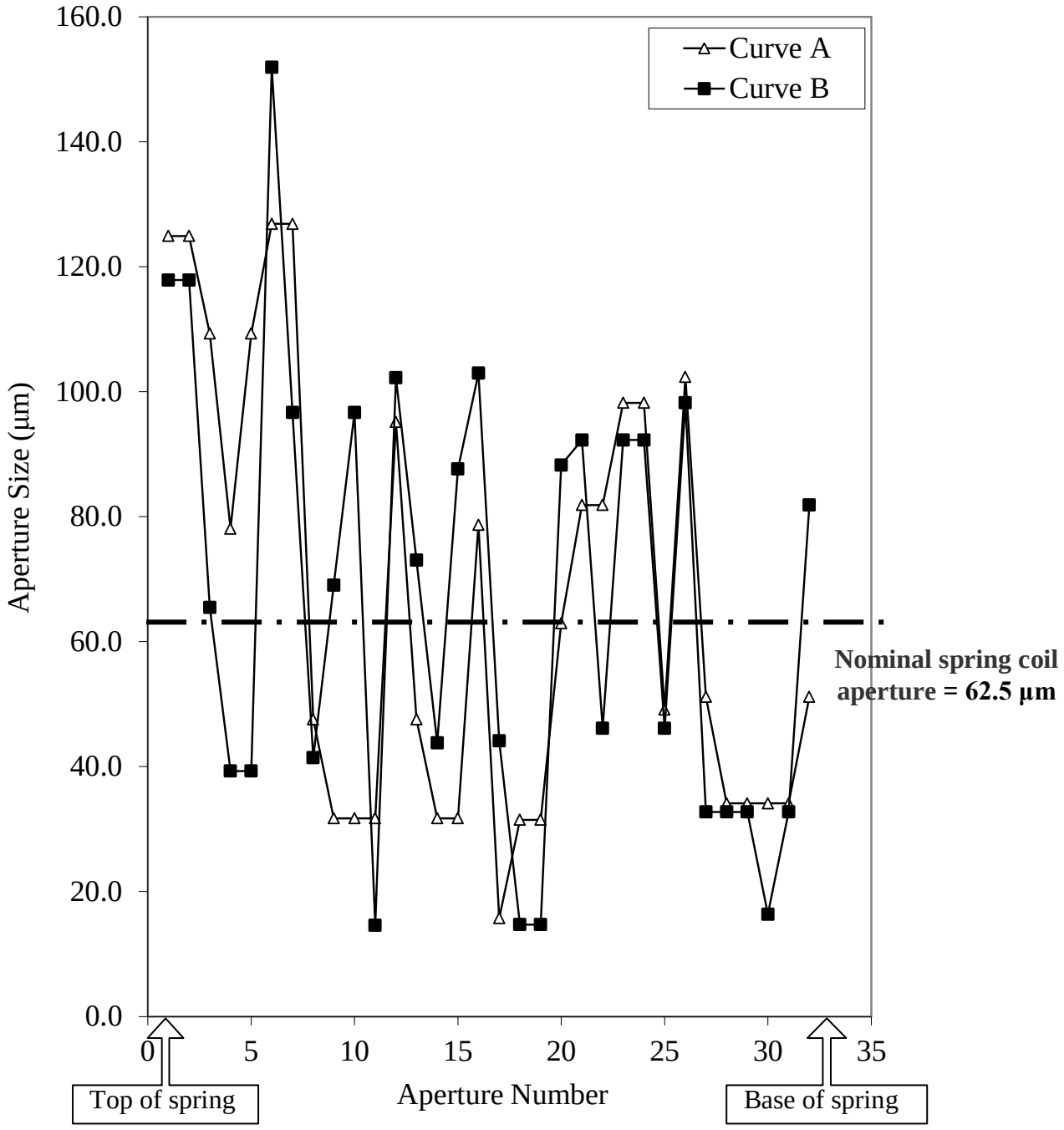

Figure 5.8: Variation of individual aperture size along the length of A2 when extended to 2 mm.

Curve A: A2 unilateral extension

Curve B: A2 bilateral extension

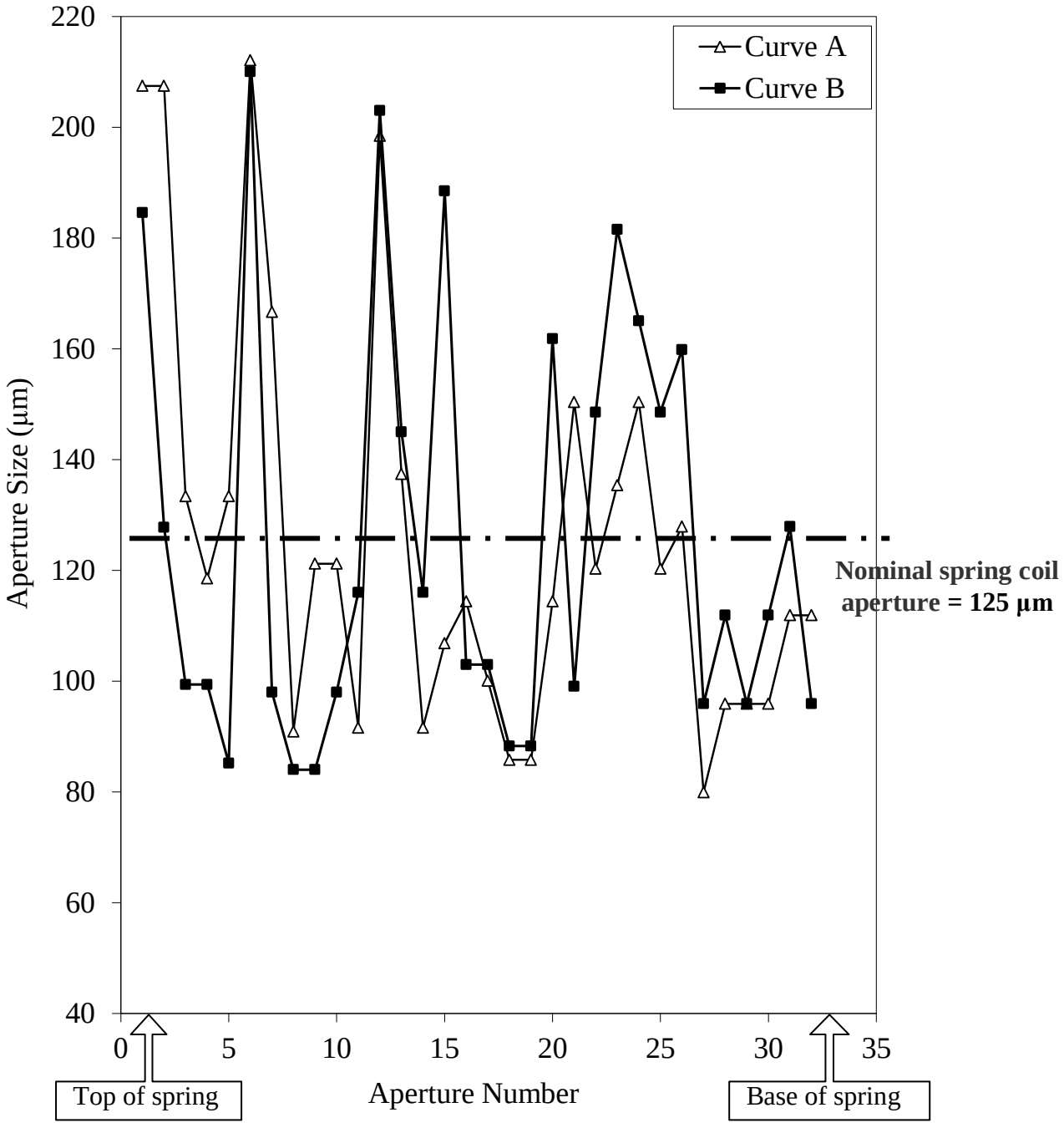

Figure 5.9: Variation of individual aperture size along the length of A2 when extended to 4 mm.

Curve A: A2 unilateral extension

Curve B: A2 bilateral extension

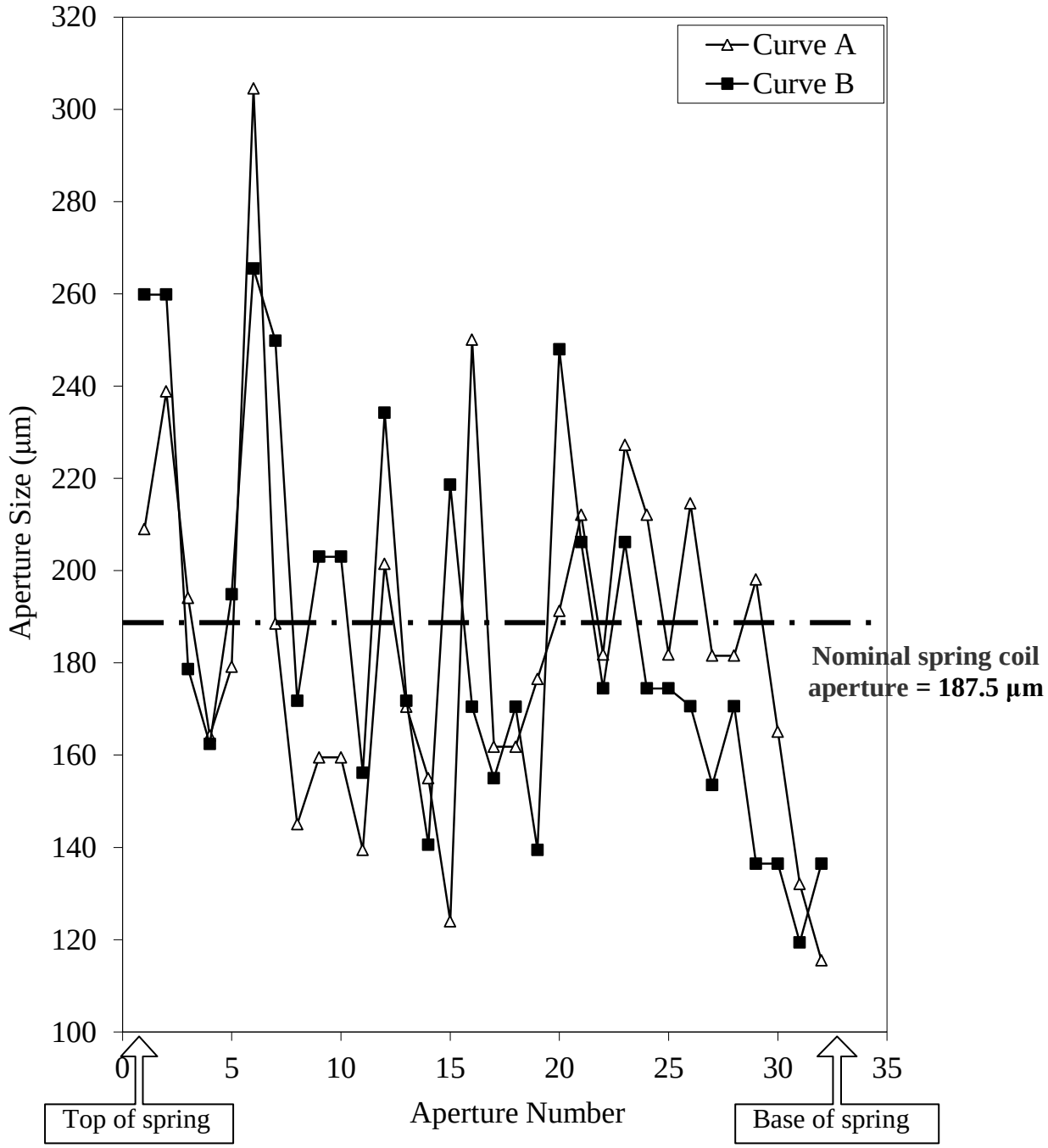

Figure 5.10: Variation of individual aperture size along the length of A2 when extended to 6 mm.

Curve A: A2 unilateral extension

Curve B: A2 bilateral extension

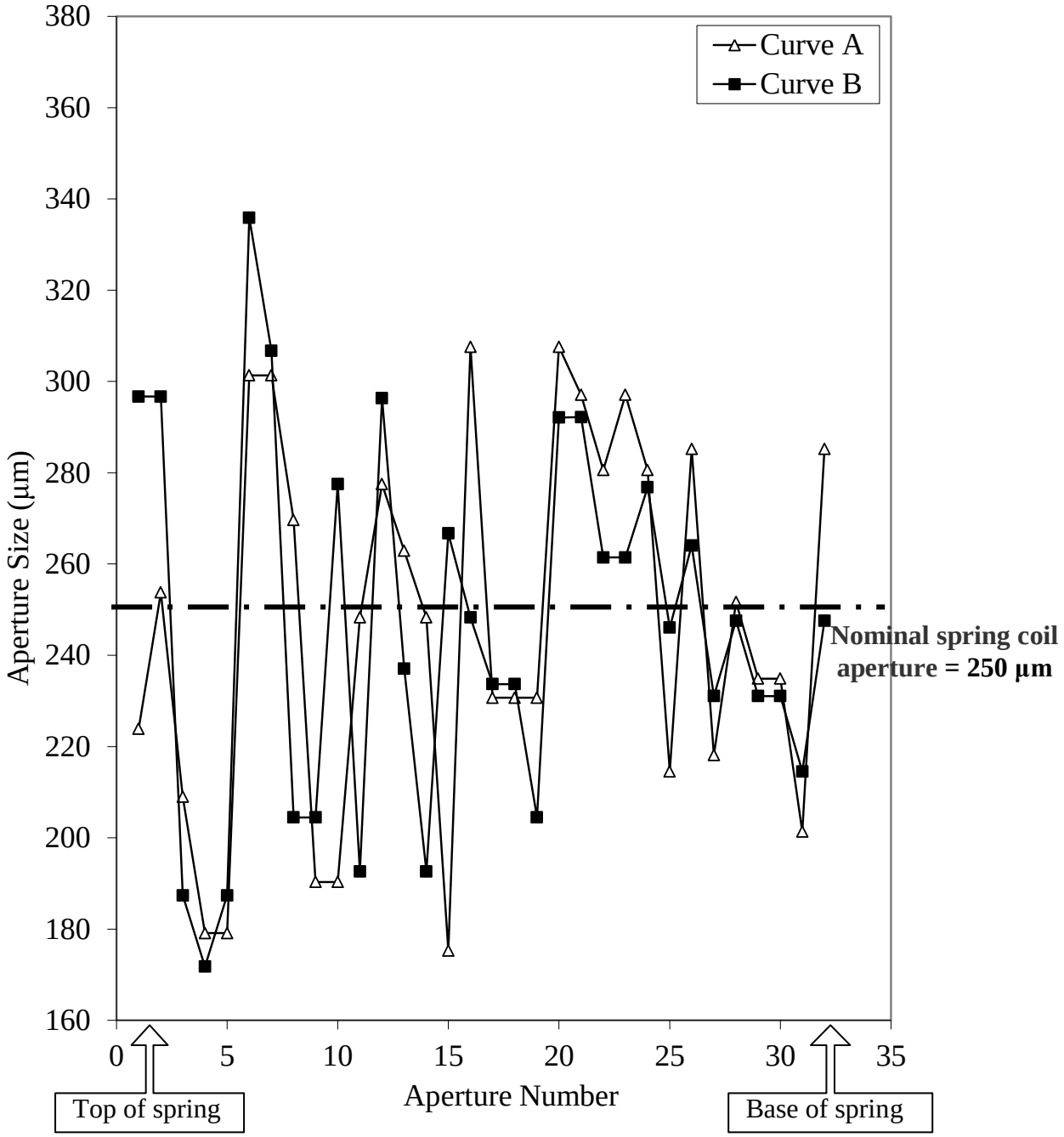

Figure 5.11: Variation of individual aperture size along the length of A2 when extended to 8 mm.

Curve A: A2 unilateral extension

Curve B: A2 bilateral extension

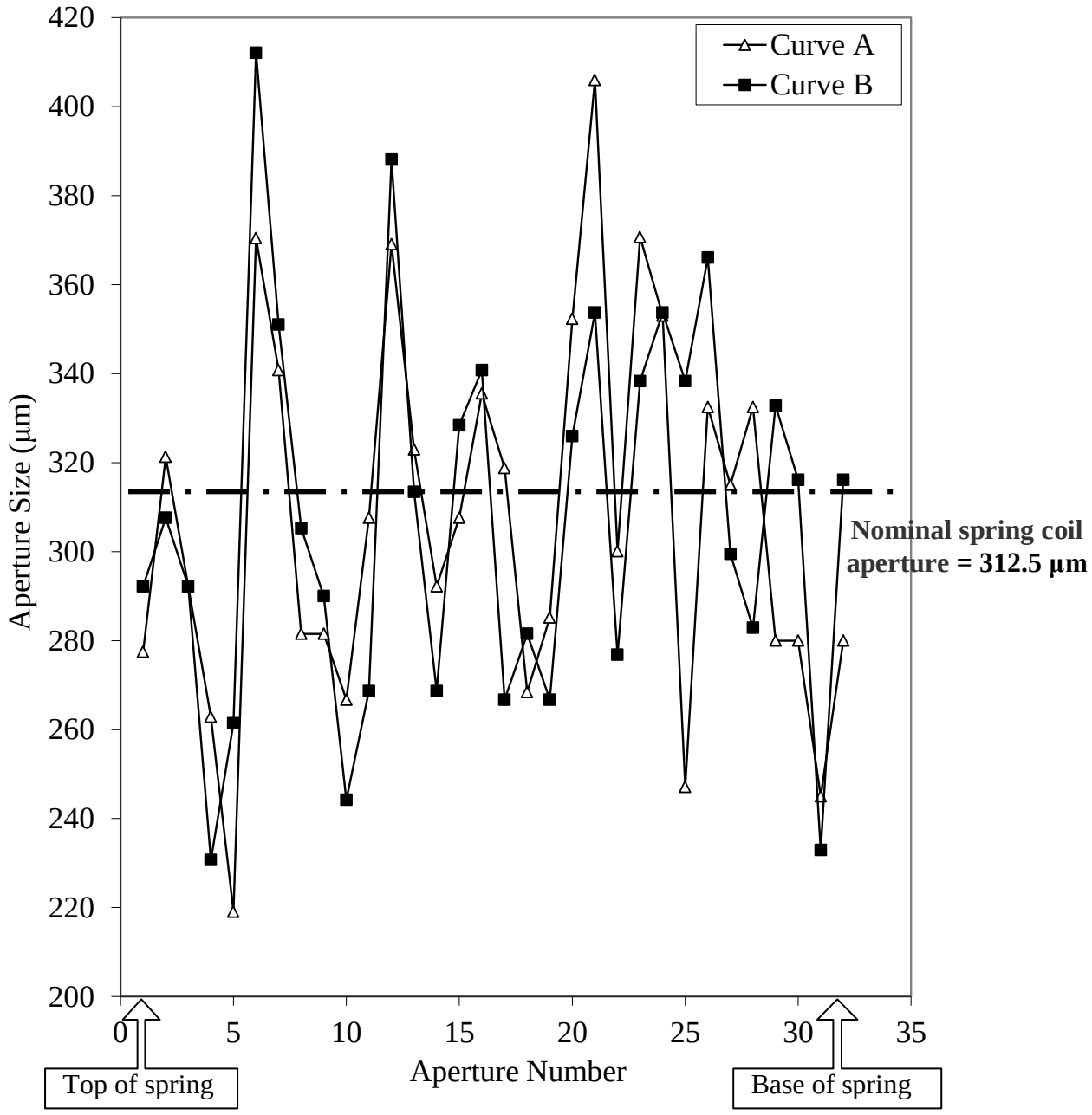

Figure 5.12: Variation of individual aperture size along the length of A2 when extended to 10 mm.

Curve A: A2 unilateral extension

Curve B: A2 bilateral extension

Table 5.3 gives the % difference between the mean and nominal spring coil aperture sizes for tests 1 to 20. The table shows that with the exception of tests 1 and 2 which had a difference of ca. 20%, the absolute difference between the nominal and mean spring coil aperture size for springs A1 and A2 is < 7%. The large differences seen in tests 1 and 2 may be attributed to the initial tension in the spring, which becomes more significant at small spring extensions.

Table 5.3: Percentage difference between the mean and nominal spring coil aperture sizes for tests 1 to 20 using springs A1 and A2.

Test Number	Spring	Mean Coil Aperture Size (μm)	Nominal Coil Aperture size (μm)	% Difference
1	A1	80.5	62.5	22.3
2	A1	82.2	62.5	23.9
3	A1	128.7	125	2.8
4	A1	130.0	125	3.8
5	A1	197.4	187.5	5.0
6	A1	201.4	187.5	6.9
7	A1	256.7	250	2.6
8	A1	251.9	250	0.7
9	A1	314.9	312.5	0.8
10	A1	315.2	312.5	0.9
11	A2	64.8	62.5	3.5
12	A2	64.7	62.5	3.4
13	A2	124.7	125	-0.3
14	A2	124.4	125	-0.5
15	A2	182.6	187.5	-2.7
16	A2	184.3	187.5	-1.7
17	A2	245.9	250	-1.6
18	A2	244.5	250	-2.2
19	A2	305.4	312.5	-2.3
20	A2	306.8	312.5	-1.8

Table 5.4 gives a comparison of the standard deviations for sieves and springs A1 and A2 for various sieve aperture sizes. The large standard deviations observed for springs

A1 and A2's clearly demonstrates the level of non-uniformity of the springs. The table also shows that regardless of how springs A1 and A2 were extended (unilateral or bilateral) the standard deviation for a given aperture size is consistently greater than that for a sieve. However, it should be noted that the standard deviation for sieves normally increases with time due to deformation of the apertures caused by regular cleaning of the sieves (Kerdvibulvech, 2008).

Table 5.4: Comparison of standard deviations for sieves and springs A1 and A2 for various aperture sizes.

Nominal Aperture Size (µm)	Sieve		A1				A2			
			Unilateral		Bilateral		Unilateral		Bilateral	
	Mean Size (µm)	Standard Deviation	Mean Size (µm)	Standard Deviation	Mean Size (µm)	Standard Deviation	Mean Size (µm)	Standard Deviation	Mean Size (µm)	Standard Deviation
62.5	63.0	9.9	80.5	35.2	82.2	34.3	64.8	36.1	64.7	36.5
125.0	125.0	14.4	128.7	36.6	130.0	35.5	124.7	37.4	124.4	38.3
187.5	180.0	18.0	197.4	37.7	201.4	36.3	182.6	38.5	184.3	40.1
250.0	250.0	22.4	256.7	40.8	251.9	40.0	245.9	41.0	244.5	41.2
312.5	315.0	26.1	314.9	42.3	315.2	41.9	305.4	42.3	306.8	43.0

5.4 Conclusions

The efficacy and reproducibility of PSD measured using the PSPS critically depends on the uniformity of the spring coil apertures as the spring is extended. Also, from a commercial point of view when producing the PSPS, it is highly advantageous to utilise springs with very similar coil opening uniformity to avoid having to perform individual calibrations.

In this chapter the uniformity of two 'identical' Airedale Springs Limited (A1 and A2) springs was evaluated by comparing the mean and the standard deviation of the spring coil apertures as the springs are extended for any given load. The study was carried out using digital photography, and involved extending the springs unilaterally and bilaterally. A comparative study of the results produced by both springs against standard sieve data (British Standards Institute, 2000) was also presented and discussed.

For tests for extensions ranging from 2 mm to 10 mm, both springs exhibited a non-uniform trend. This was demonstrated by the observed wide range of spring coils aperture sizes for all extensions evaluated. The results also show that the extension method (unilateral or bilateral) has no significant impact on the uniformity of the coil aperture sizes.

With the exception of tests carried out for A1 at a 2 mm extension which had a difference of > 20%, the observed mean sizes for both springs showed an absolute difference of < 7% as opposed to the expected mean.

Comparisons of A1 and A2 at various extensions against sieve data show that both springs exhibit standard deviations considerably greater than that for a sieve of the same aperture size. However, when both springs are compared, the greatest difference is 17.5 μm. A smaller difference is observed at aperture sizes above 250 μm, where the standard deviations for both springs converge. Thus, the results indicate that the springs are reproducible; however, their precision is lower compared to sieves (British Standards Institute, 2000).

CHAPTER 6 MASS MEASUREMENT

6.1 Introduction

An important practical limitation of the Pneumatic Spring Particle Sizer (PSPS) is the loss of sample during analysis, resulting in errors in the measured Particle Size Distribution (PSD). The loss of sample is due to two main factors:

1) Static charge induced adhesion of the test particles to the cylindrical Perspex container wall (see figure 4.6, chapter 4).
2) Accumulation of test particles in crevices and joints along the structure of the PSPS.

In this chapter, the design, development and evaluation of two methods for the in-situ measurement of the sample mass within the spring with the aim of addressing the above problems is presented. These include a full-bridge strain gauge assembly and measuring the minimum fluidisation velocity of the test sample within the spring.

6.2 Strain Gauge Principle

A strain gauge is a sensor whose electrical resistance varies with the applied load following the application of an electric current.

In applications that require a strain gauge to be bonded to a larger structure under stress, a strain gauge bridge circuit is used to measure strain from the degree of imbalance. The degree of imbalance can be accurately measured using a precision voltmeter located in the centre of the bridge (Strain gauges, 2011). Figure 6.1 shows a typical full-bridge strain gauge circuit containing four strain gauges bonded to a test member.

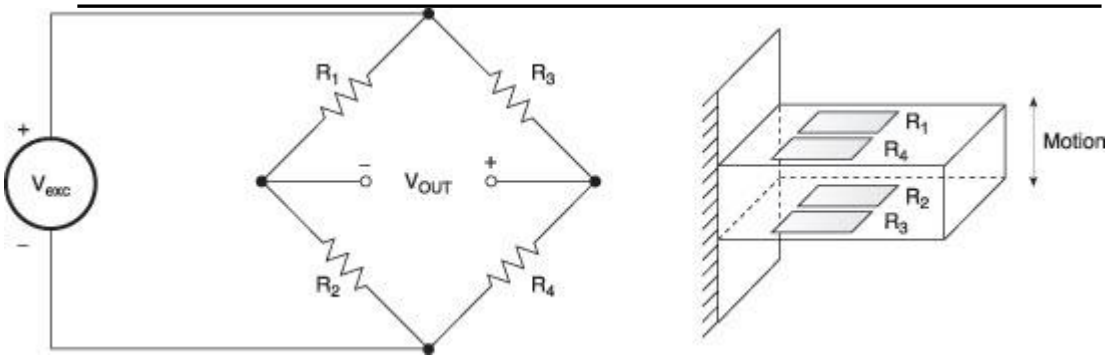

Figure 6.1: Schematic representation of a typical full-bridge strain gauge circuit (Radecky, 2009).

Two strain gauges are mounted on the top surface, and the other two are mounted on the opposite surface of the test member. When the beam is forced downward the top two gauges under tension increase in resistance while the bottom two decrease, unbalancing the bridge and producing an output proportional to the displacement. Upward motion reverses the roles of the strain gauges.

As the output signal from the strain gauge bridge circuit is small, (typically a few millivolts) the signal is amplified to increase the signal level to 5 to 10 volts, a suitable level for application to external data collection systems such as recorders or PC Data Acquisition and Analysis Systems (Strain gauges, 2011).

The bridge nulls out potential errors due to temperature changes because all four strain gauges have the same temperature coefficient and are located in close proximity to the specimen. The resistance of the lead wire does not affect the accuracy of the measurement provided that the input amplifier has high input impedance and the bridge excitation is remotely sensed (Radecky, 2009).

6.3 Strain Gauge Experimental Arrangement

Figures 6.2 shows a schematic of the experimental setup constructed to evaluate the suitability of using a full-bridge strain gauge circuit to measure the mass of the test powder in the spring.

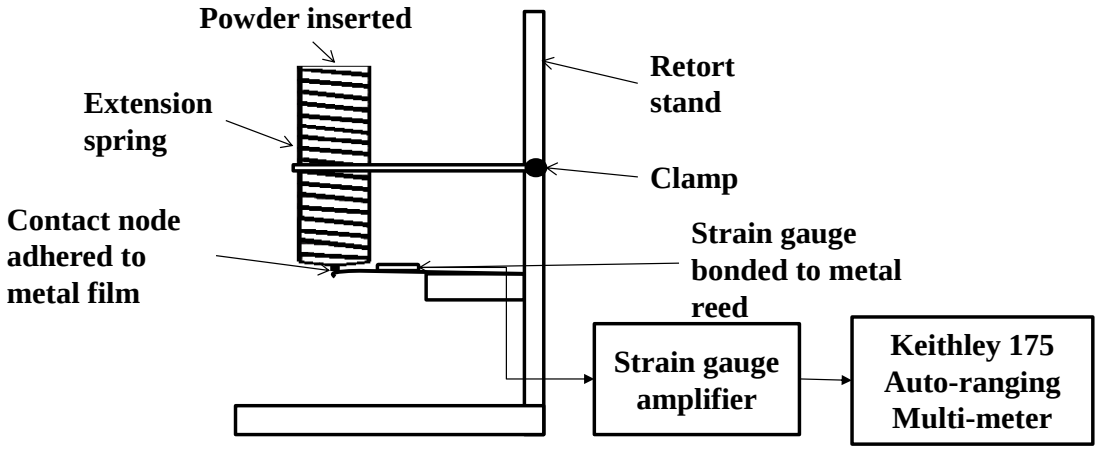

Figure 6.2: Schematic diagram of strain gauge experimental set-up for in-situ mass measurement in PSPS.

The close-coiled extension spring (24.5 mm i.d, 123.5 mm length, 3 mm wire diameter) used in this investigation is clamped vertically along its length using a retort stand. A thin stainless steel film (30 μm) with a contact node located in the centre is welded to the base of the spring to act as a seal for the test powder.

An Omega Engineering strain gauge (model SGT-2/350-FB43) (Omega Engineering, 2009) is bonded onto a 250 μm thick stainless steel reed using methyl cyanoacrylate. The reed is positioned directly below the contact node to mirror the displacement of the steel film as test sample is added to the spring. The magnitude of the steel reed's deflection is then recorded as a voltage, using the full-bridge strain gauge circuit. To increase the measurement resolution and improve the signal-to-noise ratios from the strain gauge circuit, a strain gauge amplifier connected to a Keithley 175 auto-ranging multi-meter (converts the signal into a voltage) is used.

The system is calibrated using 280 g of bronze shot powder added to the extension spring in 10 g, 5 g and 2 g increments. The output voltage from the Keithley 175 auto-ranging multi-meter is recorded after each increment in mass. The data obtained is then used to determine a mathematical correlation between the mass of sample in the spring as a function of the measured strain gauge output voltage for calibration. Each test is performed twice to establish reproducibility.

6.4 Strain Gauge Results and Discussion

Figure 6.3 shows the variation of the strain gauge output voltage with mass following the addition of 10 g incremental samples into the spring. The measurements are taken twice, labelled Test 1 (curve A) and Test 2 (curve B) to determine reproducibility.
Curve C shows the calibration line based on regression analysis of the data from curves A and B.

The equation for the calibration line is given by

$$y = 0.3832x \qquad (6.1)$$

Where, y is the strain gauge output voltage and x is the mass of sample in the spring. The correlation coefficient is 0.9917.

A statistical t-test (Bland and Altman, 2009) was carried out to determine the reproducibility based on Tests 1 and 2 data. Table 6.1 gives the results obtained. It can be observed that with 95 % confidence, the difference between the upper and lower confidence intervals from data is 0.0096 mV/g (= upper limit – lower limit), indicating good reproducibility.

The minimum and maximum deviation between Tests 1 and 2 are ± 0.7 mV and ± 5 mV respectively (translating to ± 1.83 g and ± 13.05 g respectively). However, the larger deviation is experienced at higher masses, i.e. above 200 g. This may be due to hysteresis experienced on the strain gauge.

Table 6.1: Reproducibility results of tests 1 and 2 for a 10 g incremental increase in mass using t-test.

	Coefficients (mV/g)	Standard Error	Lower limit (mV/g)	Upper limit (mV/g)
X Variable 1	0.3832	0.0026	0.3784	0.3880

To test the validity of equation 6.1 as the calibration line for in-situ mass measurement using the strain gauge, further tests were conducted for 2 g and 5 g increments in mass.

Figure 6.4 shows the same data as in figure 6.3 but performed using smaller mass intervals of 2 g (curve A) , 5 g (curve B) and 10 g (curve C). Curve D shows the calibration line generated using equation 6.1.

The mass sensitivity of the instrument inferred from the slope of the correlated data in figure 6.4 was 0.3832 mV/g and precision of the multimeter, ± 1 mV. Using this data, the resolution of the strain gauge was determined as ± 2.6 g. For the typical 280 g test sample the above translates into a mass resolution of ± 0.93 %.

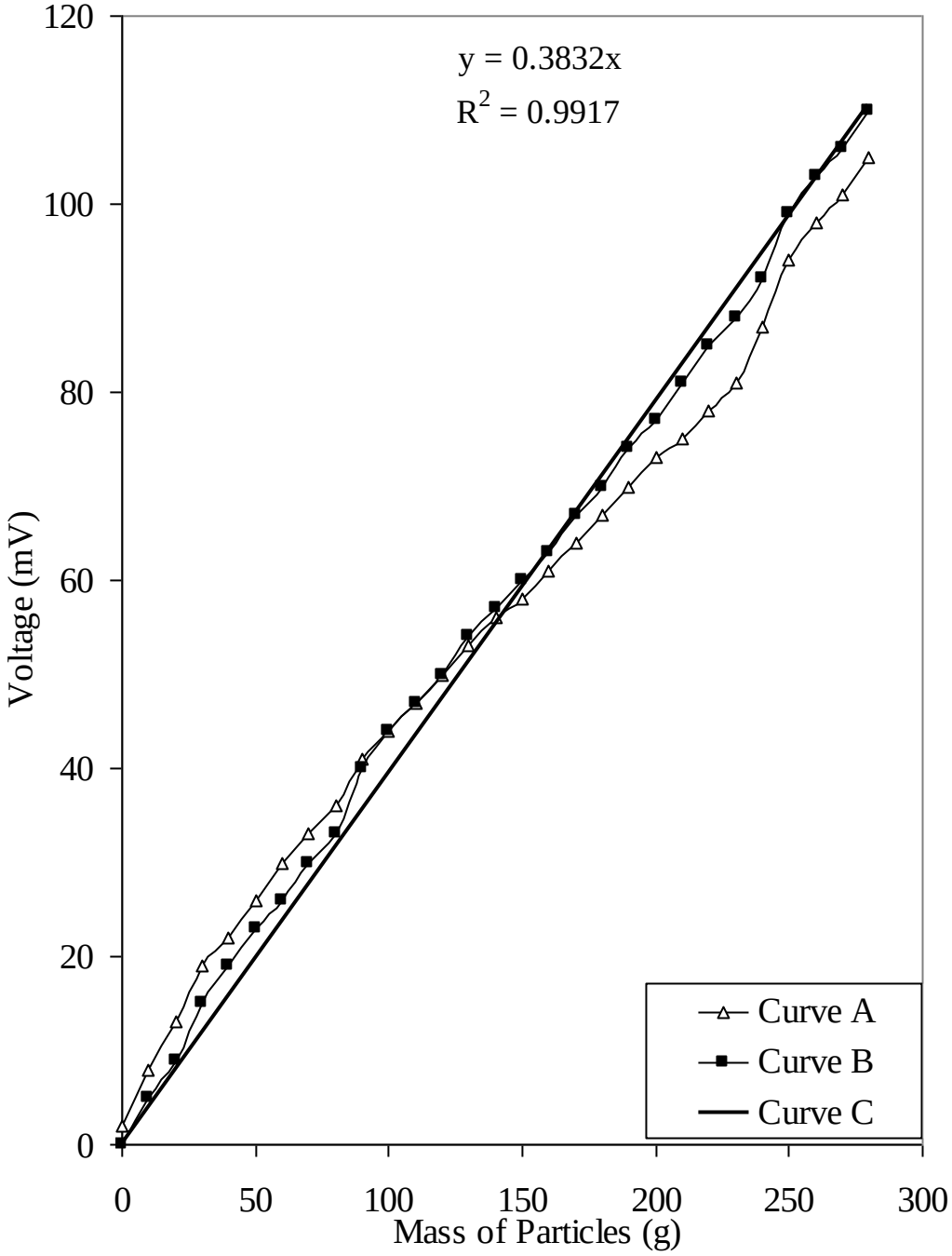

Figure 6.3: Variation of the strain gauge output voltage with 10 g incremental mass of sample in the spring.

Curve A: Test 1

Curve B: Test 2

Curve C: Correlated data obtained from the average of tests 1 and 2

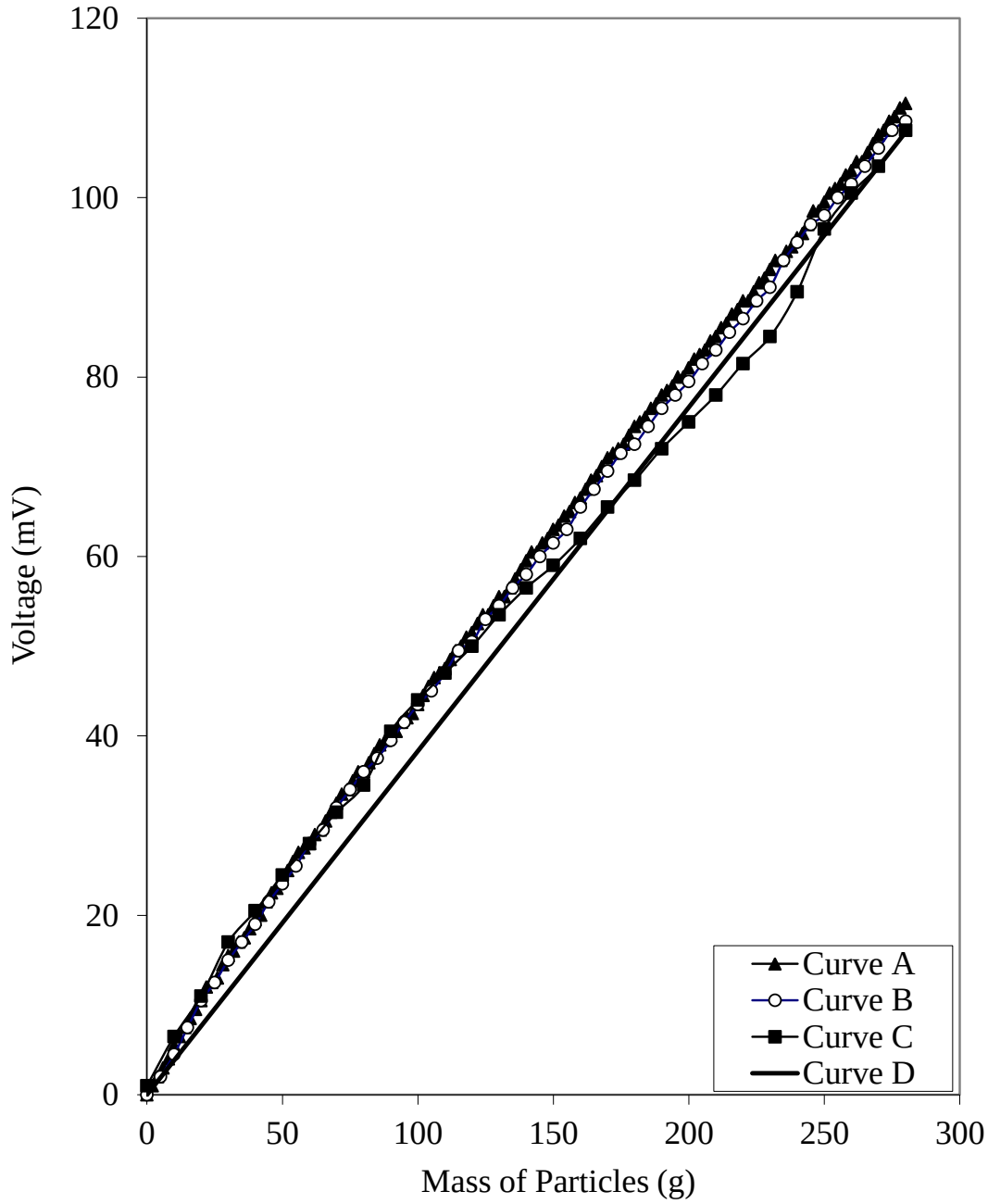

Figure 6.4: Variation of the strain gauge output voltage with mass of sample in the spring for various incremental masses compared to calibration curve developed using linear regression.

Curve A: 2 g increments

Curve B: 5 g increments

Curve C: 10 g increments

Curve D: Predicted data

6.5 Application of Strain Gauge In-Situ Mass Measurement Technique to the PSPS

The results of the evaluation study showed that a strain gauge assembly is in principle capable of measuring with relative accuracy (± 2.6 g for a typical 280 g test sample) the mass of sample in the spring. However, a number of design changes in the design of the PSPS are required in order to incorporate the strain gauge. Figure 6.5 shows the proposed design. The modifications include:

- A new port in the PSPS Perspex case to connect the wires between the strain gauge mechanism and the signal recorder (amplifier plus voltage recorder). This is illustrated in figure 6.5(a).

- Redesign of the conical base holder attached to the base of the spring to hold a rigid support structure for the strain gauge and steel reed, as shown in figure 6.5(b). This modification is needed to ensure that only the steel reed is displaced when test sample is added to the spring.

- To prevent damage to the strain gauge, the air distributor used to feed the fluidisation air into the base of the spring should be removed. Instead, the spring used in the PSPS should be redesigned to include a metallic spring cap on the base of the spring through which the fluidising air would be fed in to the unit. Figure 6.6 shows a schematic representation of the proposed modified spring with the attached metallic spring cap. The base of the cap would be sealed with a thin 30 μm steel film with a contact node in the centre of the film. As mentioned in section 6.3, the steel reed would be positioned directly below the contact node to mirror the displacement of the steel film as test sample is added to the spring.

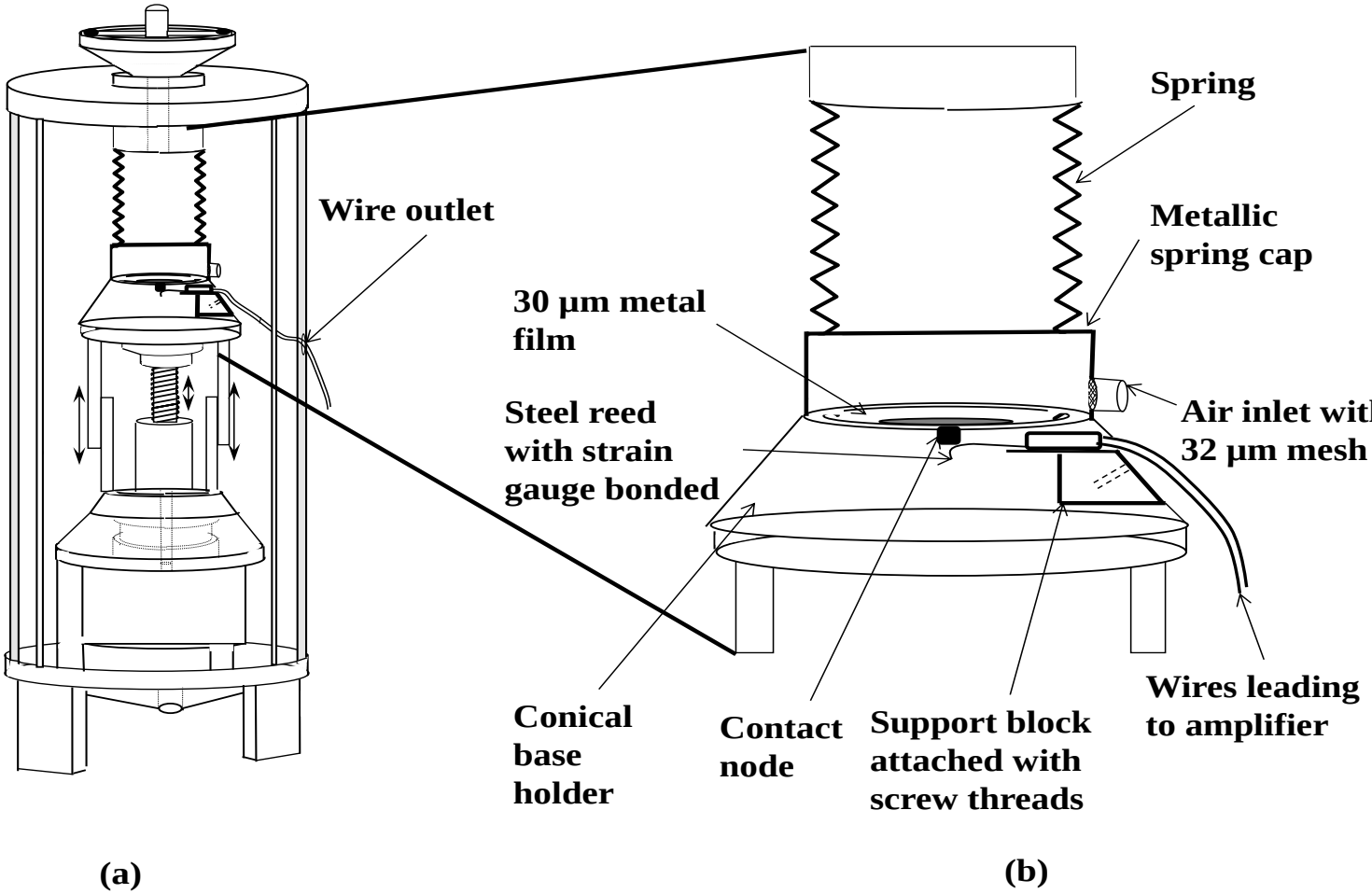

Figure 6.5: Schematic description for the proposed structural changes required for in-situ mass measurement in the PSPS using a strain gauge.

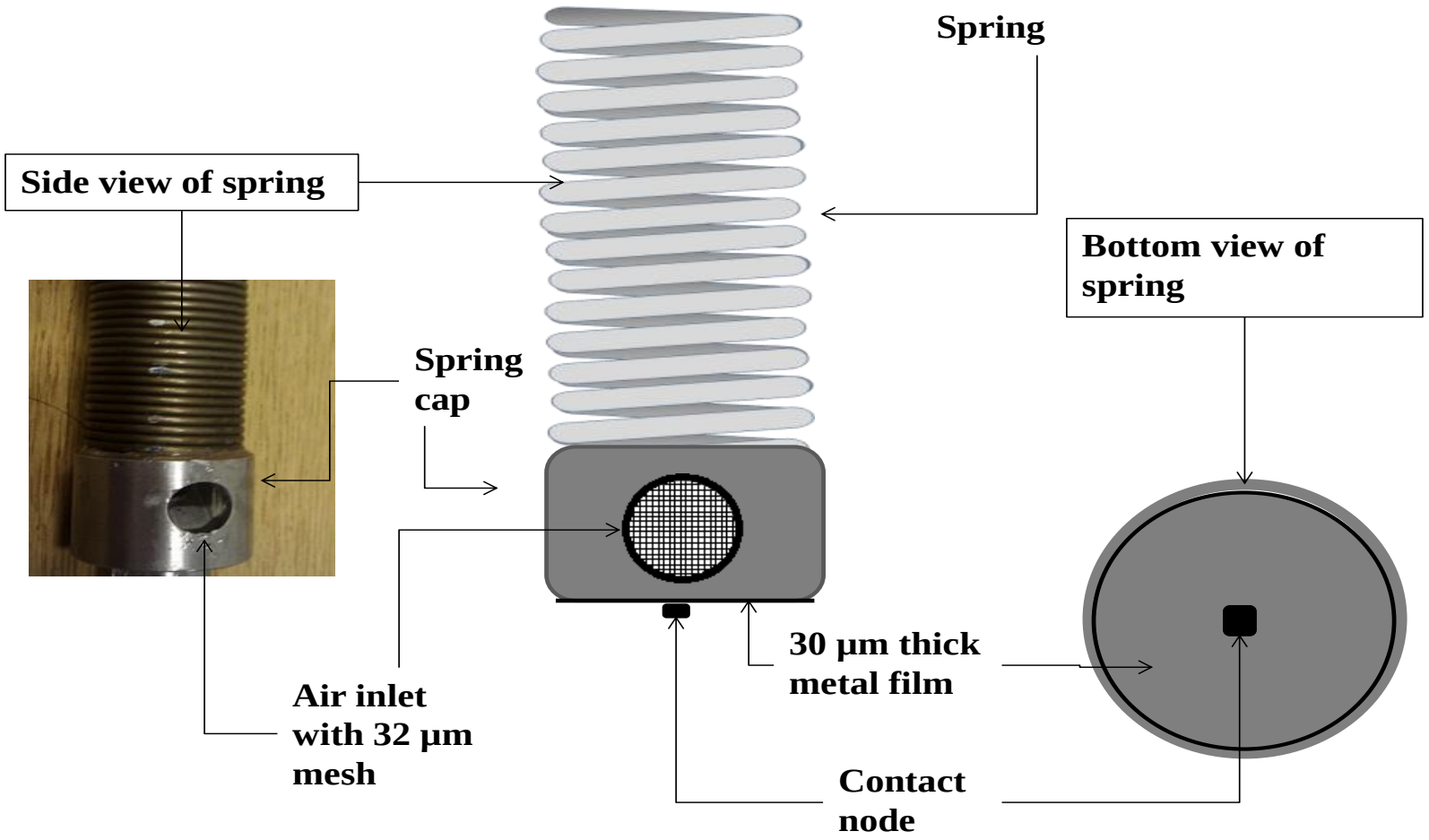

Figure 6.6: Diagrammatic description of structural changes required for PSPS for in-situ mass measurement using a strain gauge.

6.6 Application of Fluidisation Principles for Mass Measurement in the PSPS

The following presents the results of a series of experiments carried out using the Pneumatic Spring Particle Sizer (PSPS) with the aim of determining powder mass in-situ. The objective is to determine the correlation between the minimum fluidisation velocity and the mass of the particles within the spring which may subsequently be used for system calibration.

Figure 6.7 shows the variation of pressure drop with air flowrate for varying masses (5, 10, 20, 50 and 100 g) of glass Ballotini of size ranges 212 – 300 µm. The first test was conducted by feeding 5 g of test powder into the PSPS. The spring was opened to 50 µm aperture size, to allow its discharge through the spring coils but at the same time retain the particles within the spring. A constant air pressure of ca. 103.4 kPa was used. A Comark C9555 digital pressure meter (Comark Limited, 2011) connected to the unit to enable pressure drop measurement across the spring, with one port connected to the air inlet and the other port open. The air supply was slowly increased to a flowrate of 20 $dm^3 min^{-1}$ into the bed via a rotameter. The pressure drop across the bed was recorded using the digital pressure meter. The experiment was continued with a step wise increase in flowrate of 10 $dm^3 min^{-1}$ until 150 $dm^3 min^{-1}$ was attained. The procedure was then repeated for 10 g, 20 g, 50 g and 100 g each and for size ranges 300 – 425 µm, 425 – 500 µm, 500 – 600 µm, 710 – 850 µm and 850 – 1000 µm.

Returning to figure 6.7, as it may be observed, all the data demonstrate the same trends in terms of the variation of pressure drop with air flowrate. The following are the important features of the data:

i) For the same air flowrate, the pressure drop across the bed increases with sample mass. This is to be expected given the increase in the resistance to flow of air within the bed as the sample mass increases.

ii) In all cases for the same sample mass, there is a general increase in the pressure drop across the bed with increase in air flowrate. However, with the exception of 100 g sample, the data show an intermediate inflection point characterised by a small drop followed by a relatively rapid recovery in the pressure drop as the air flowrate increases. The observed discontinuity in the pressure is characteristic of the minimum fluidisation velocity for fluidised beds. This feature will be elaborated later. For the 100 g sample mass, a continuous increase in pressure drop is observed at all flow rates tested.

Figures 6.8 – 6.12 show the variation of pressure drop with air flowrate for varying masses (5, 10, 20, 50 and 100 g) of glass Ballotini for larger size ranges 300 – 425 µm, 425 – 500 µm, 500 – 600 µm, 710 – 850 µm and 850 – 1000 µm respectively. All figures exhibit the same trend where the pressure drop increases with air flowrate. However, it can be observed that for these larger size ranges, in contrast to the data in figure 6.7 for a smaller size range, in most cases, for samples below 50 g, the pressure drop is independent of the mass.

Returning to figures 6.7 – 6.12, all size ranges tested demonstrate the same characteristic fluidisation behaviour, known as slugging fluidisation (Holdich, 2002). The slugging fluidisation regime is experienced in the bed after the bubbling flow regime as the air flowrate increases. It is characterised by the bubble size approaching the bed's cross section and the bed surface rises and falls with regular frequency with corresponding pressure fluctuations which increase with an increase in flowrate. This trait of regular pressure fluctuations is also demonstrated by the PSPS. The slugging flow regime typically occurs in a bed which has a bed height to bed diameter ratio larger than 2. With a large aspect ratio, the bed provides enough time for bubbles to coalesce into bigger ones. When the bubbles grow to approximately two–thirds of the bed diameter, the bed enters the slugging regime with periodic passing of large bubbles and regular large fluctuation of bed pressure drop corresponding to the bubble frequency (Gibilaro, 2001; Holdich, 2002; Yang, 2003).

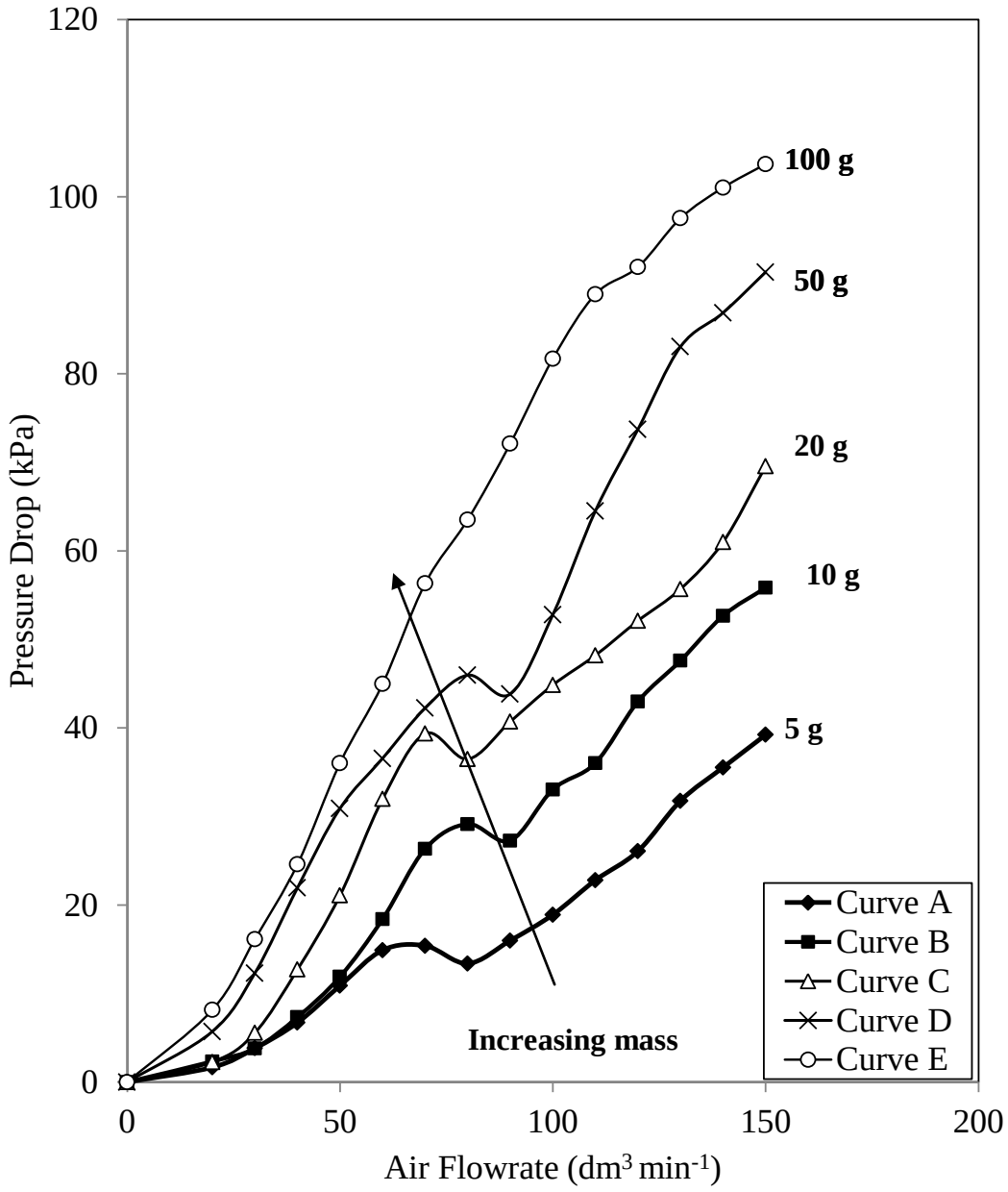

Figure 6.7: Variation of pressure drop with air flowrate for varying masses of glass Ballotini of size range 212 – 300 µm at 103.4 kPa air pressure.

Curve A: 5 g

Curve B: 10 g

Curve C: 20 g

Curve D: 50 g

Curve E: 100 g

In the case of the PSPS the spring height to diameter ratio is 7.83, indicating its characteristics as a slugging bed. Figure 6.13 is an illustration of slugging fluidisation and the variation of pressure drop with superficial gas velocity in this regime.

Returning to figures 6.7 and 6.8, the 100 g samples for 212 – 300 µm and 300 – 425 µm respectively, produce the same trend, where the pressure drop continuously increases with air flowrate. As the average particle size is increased (see figures 6.10 – 6.12), 100 g mass samples follow the characteristic slugging fluidisation trend. The 425 – 500 µm (refer to figure 6.9) is an exception, where the 100 g sample mass exhibits the characteristic trend for slugging fluidisation, however at 100 dm^3min^{-1}, there is a sudden decrease in pressure. The pressure then increases again beyond 100 dm^3min^{-1}.

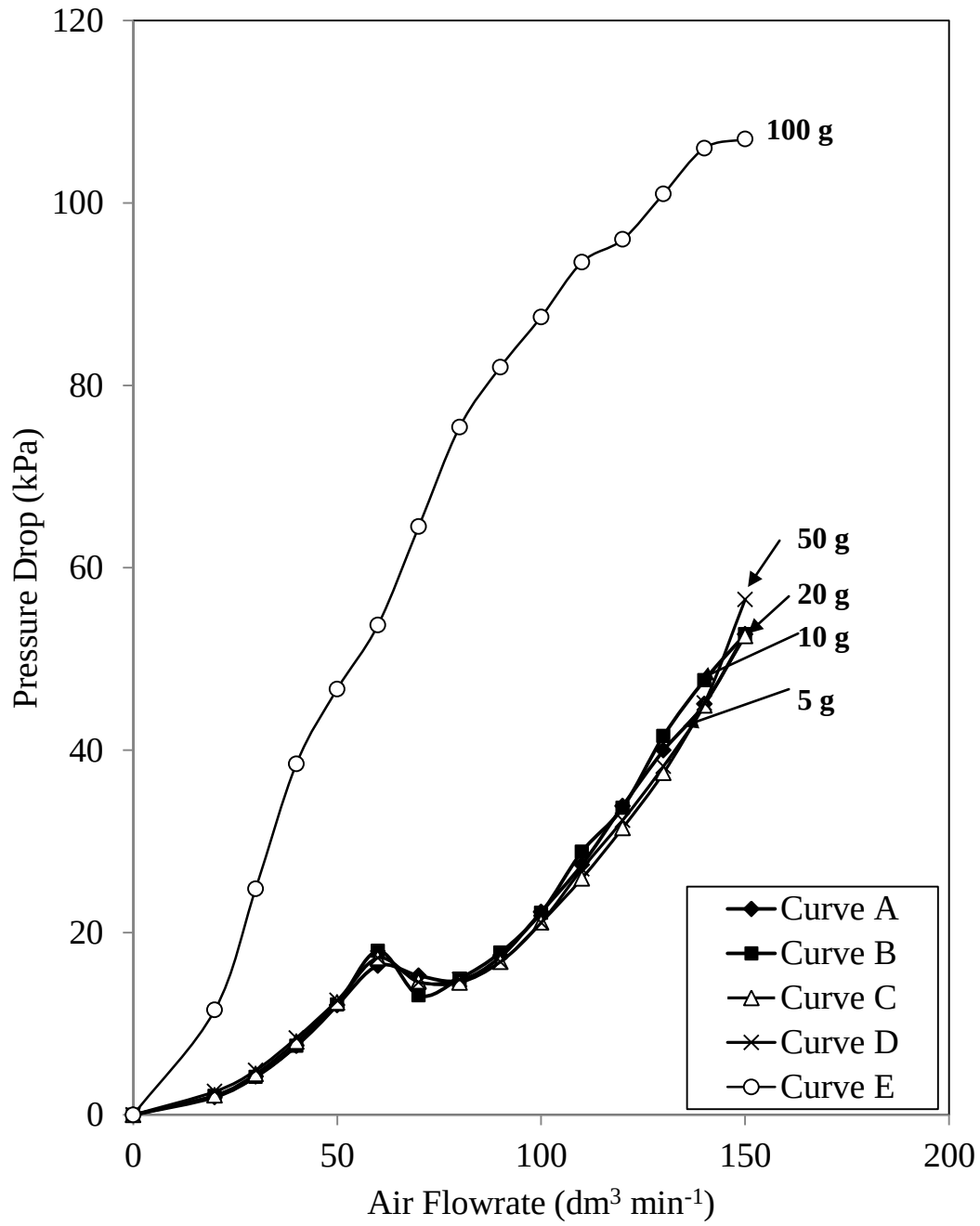

Figure 6.8: Variation of pressure drop with air flowrate for varying masses of glass Ballotini of size range 300 – 425 µm at 103.4 kPa air pressure.

Curve A: 5 g

Curve B: 10 g

Curve C: 20 g

Curve D: 50 g

Curve E: 100 g

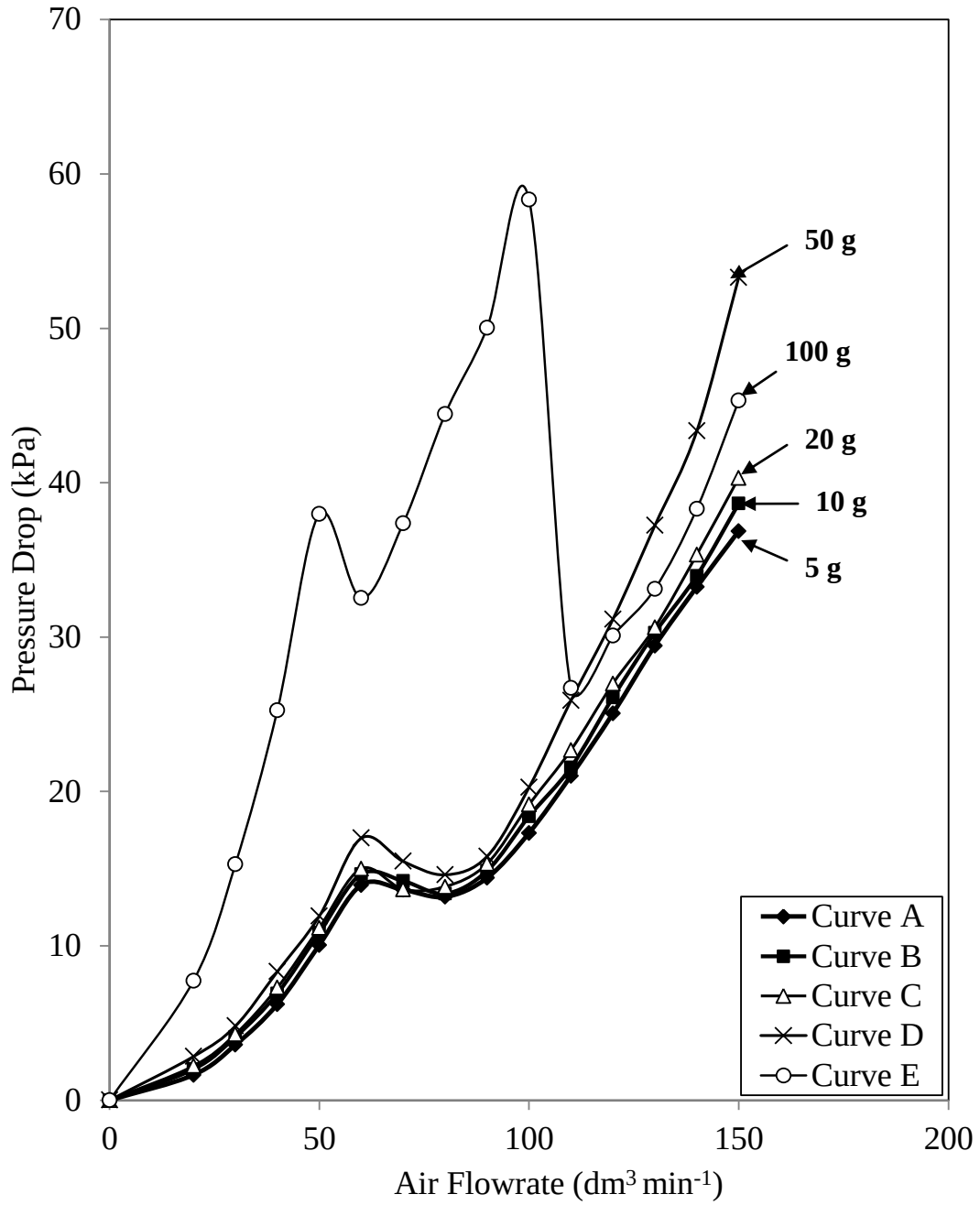

Figure 6.9: Variation of pressure drop with air flowrate for varying masses of glass Ballotini of size range 425 – 500 µm at 103.4 kPa air pressure.

Curve A: 5 g

Curve B: 10 g

Curve C: 20 g

Curve D: 50 g

Curve E: 100 g

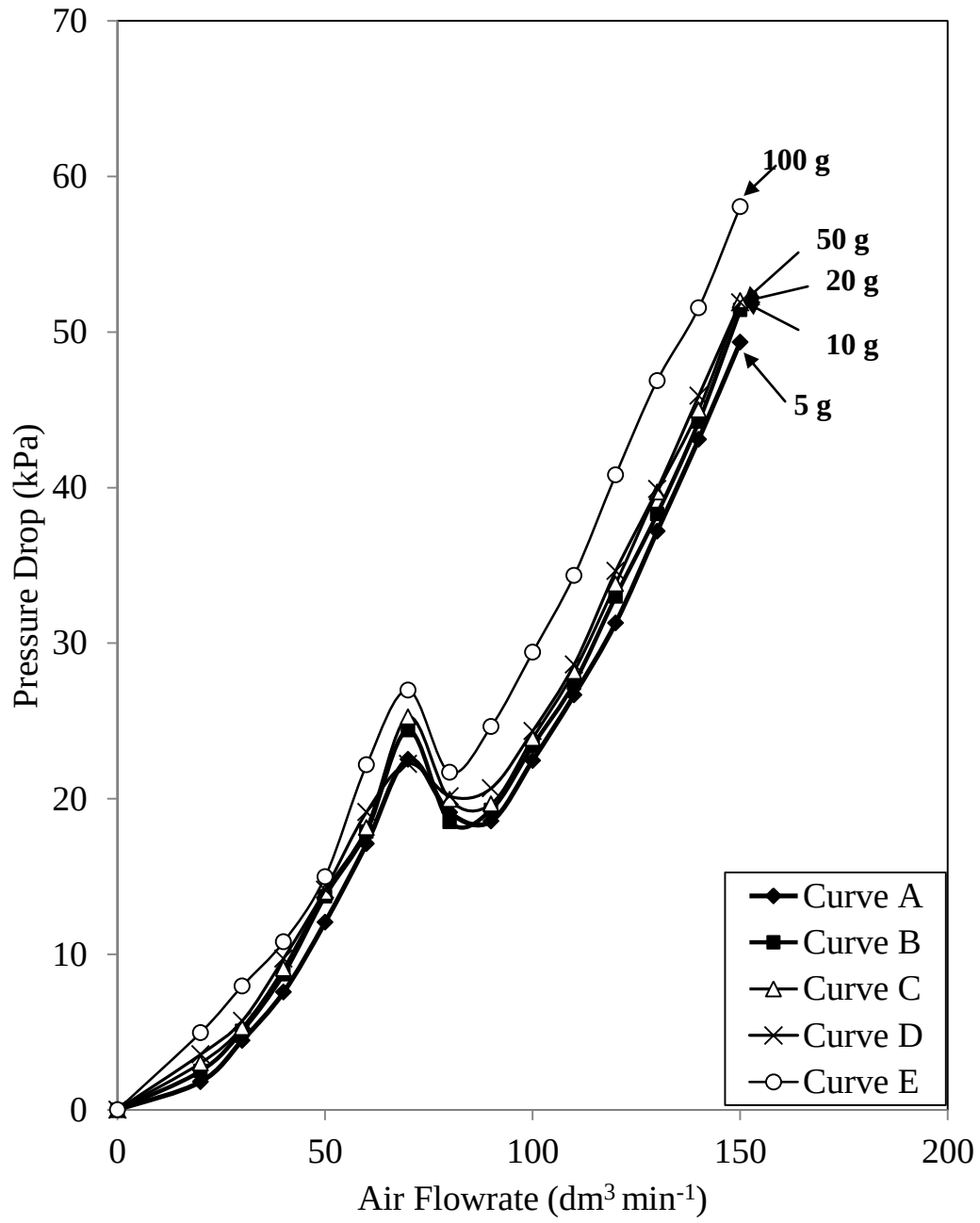

Figure 6.10: Variation of pressure drop with air flowrate for varying masses of glass Ballotini of size range 500 – 600 µm at 103.4 kPa air pressure.

Curve A: 5 g

Curve B: 10 g

Curve C: 20 g

Curve D: 50 g

Curve E: 100 g

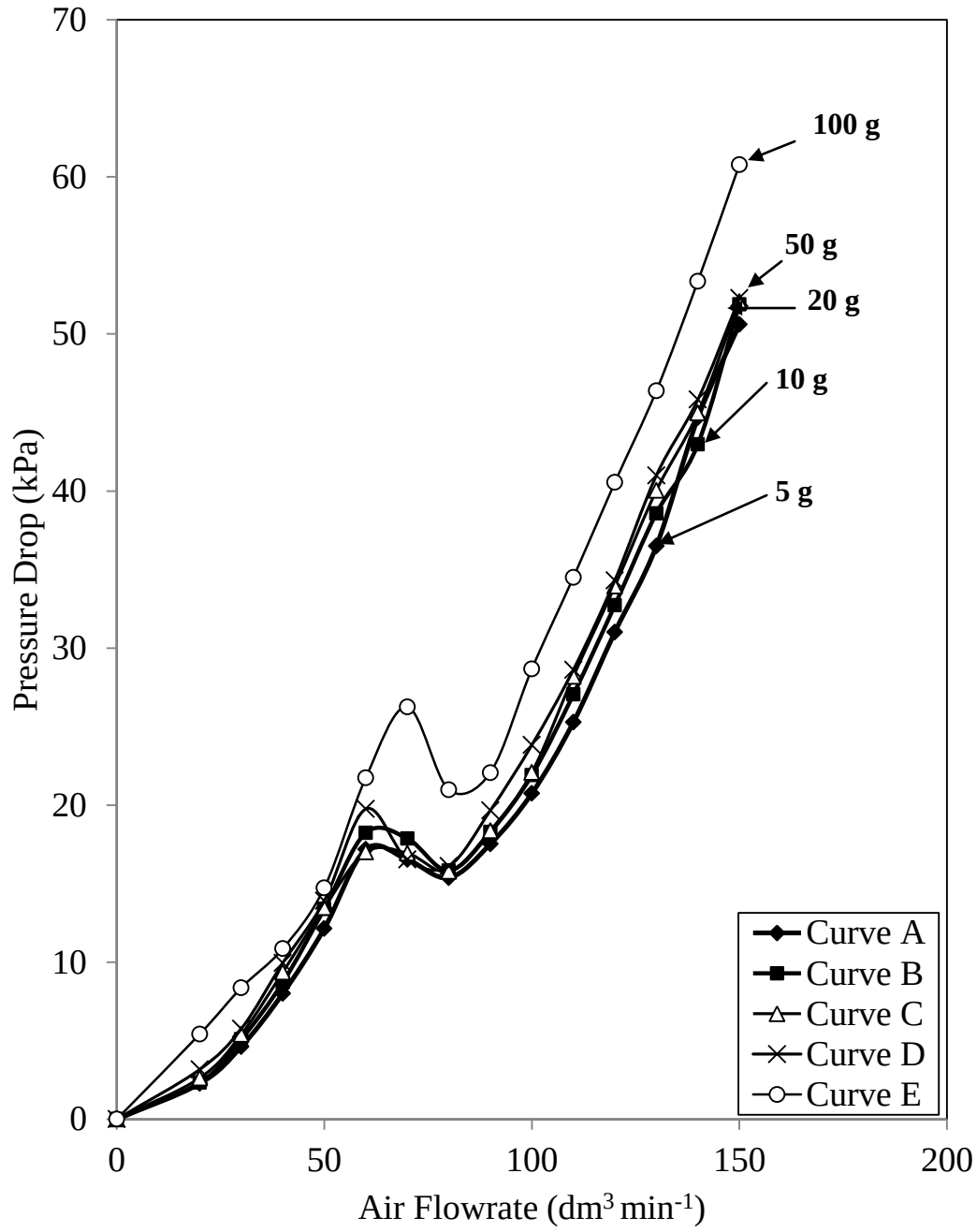

Figure 6.11: Variation of pressure drop with air flowrate for varying masses of glass Ballotini of size range 710 – 850 µm at 103.4 kPa air pressure.

Curve A: 5 g

Curve B: 10 g

Curve C: 20 g

Curve D: 50 g

Curve E: 100 g

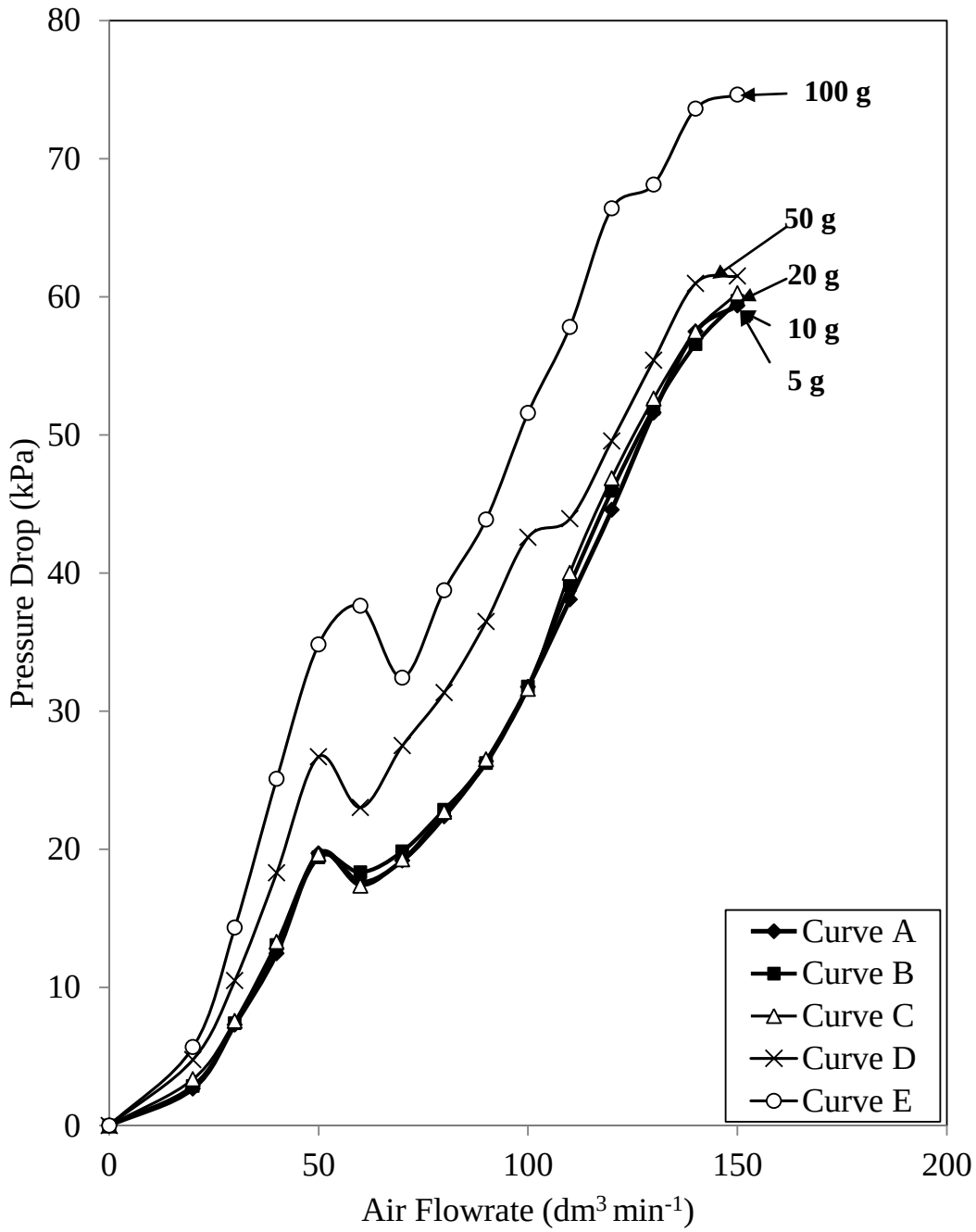

Figure 6.12: Variation of pressure drop with air flowrate for varying masses of glass Ballotini of size range 850 – 1000 µm at 103.4 kPa air pressure.

Curve A: 5 g

Curve B: 10 g

Curve C: 20 g

Curve D: 50 g

Curve E: 100 g

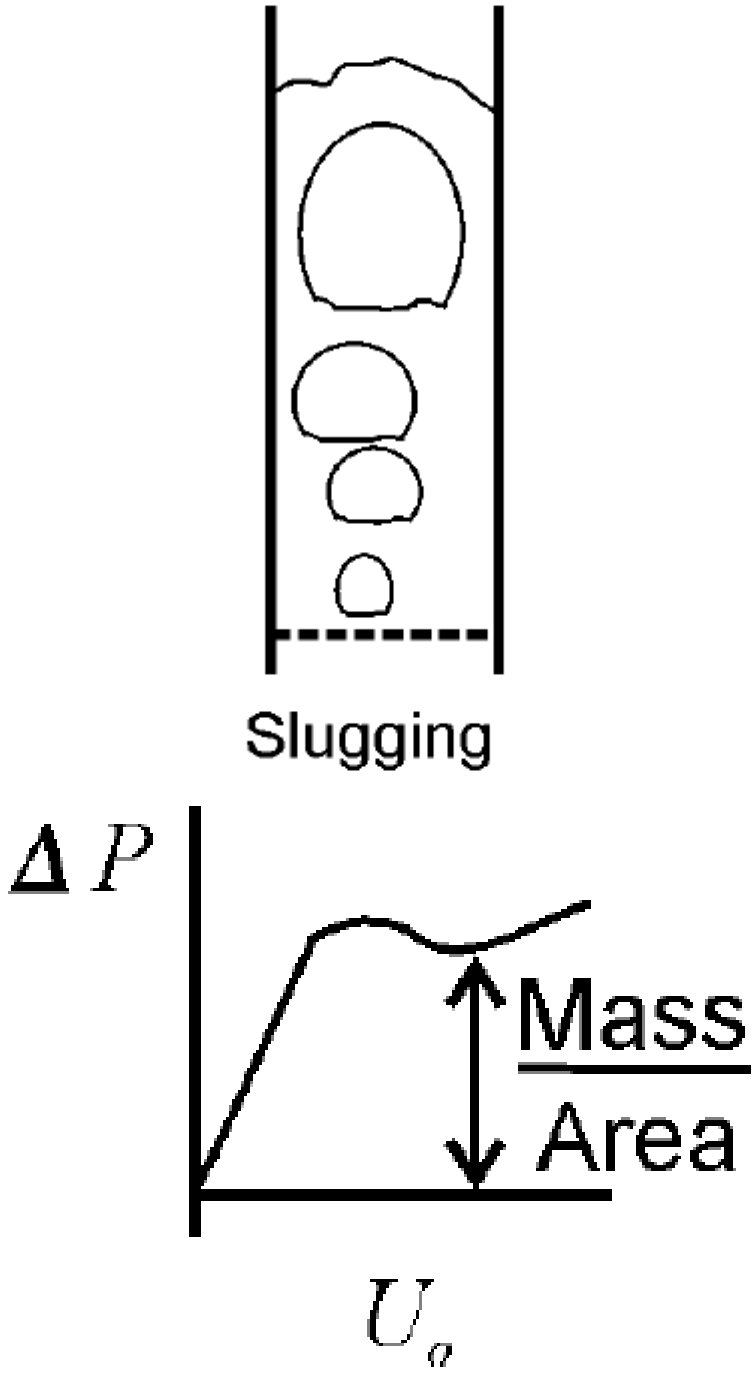

Figure 6.13: Slugging fluidisation regime and the variation of pressure drop with superficial gas velocity (Holdich, 2002).

The mathematical representation of the phenomenon described as the minimum fluidisation velocity (u_{mf}) is given by equation 6.2. The pressure drop, Delta P corresponding to the minimum fluidisation velocity, u_{mf} is given by:

$$\Delta P = \frac{m}{\rho_p A}\left(\rho_p - \rho_f\right)g \tag{6.2}$$

where,

ΔP = the pressure drop

m = the mass of particles

ρ_p and ρ_f = particle and fluid densities respectively

g = the acceleration due to gravity

Assuming particles are spherical, u_{mf} is given by 6.3 (Holdich, 2002):

$$u_{mf} = \frac{\left(\rho_p - \rho_f\right)g\varepsilon^3 x_{sv}^2}{180(1-\varepsilon)\mu} \tag{6.3}$$

where,

ε = the voidage

μ = the viscosity

x_{sv} = the surface volume diameter (see table 2.1)

The main purpose of this study was to determine if the PSPS will behave comparably to any established fluidisation flow regimes and to measure the residual mass of the test powder within the PSPS. Equations 6.2 and 6.3 may be used to develop a correlation between the minimum fluidisation velocity u_{mf}, with the mass of particles in the spring.

The height of the bed is required to determine the voidage in the fluidised bed and hence u_{mf} using equation 6.3. However it is extremely difficult to determine the height of the bed within the spring visually. As seen in figures 6.7 – 6.12, the inflection point (u_{mf}) in most cases does not change with mass and therefore cannot be used to develop a viable correlation.

6.7 Conclusions

In this chapter the suitability of using a full-bridge strain gauge circuit and fluidisation principles to measure the mass of sample in the PSPS in-situ were evaluated. The initial evaluation involved the development of a correlation for the mass of sample as a function of the strain gauge output voltage based on a linear regression of the voltage recorded as mass was added to the test spring. The coefficient of determination, R^2 obtained for the correlation was 0.9917. All experiments were found to be reproducible with 95 % confidence. The correlated data obtained was found to be a good predictive tool using the strain gauge for in-situ mass measurement in the spring with a mass resolution is of ± 2.6 g for a 280 g sample corresponding to a mass resolution of ca. ± 1 %.

Based on the results of the evaluation, a new PSPS design was proposed including the structural changes required to incorporate the strain gauge into the PSPS for mass measurement. These include:

- a change in the position of the air inlet from the base of the spring,
- fitting of a cap at the base of the spring to allow air to be passed through the side, and
- a support block attached to the hollow tube enclosing the extension mechanism which will hold the reed with adhered strain gauge in place.

The next part of the study involved the use of fluidisation principles to develop a correlation between minimum fluidisation velocity and sample mass within the PSPS. The data revealed that:

i) For the same air flowrate, the pressure drop across the bed increases with sample mass (only observed for the 212 – 300 μm size range). This is to be expected given the increase in the resistance to flow of air within the bed as the sample mass increases.

ii) In all cases for the same sample mass, there is a general increase in the pressure drop across the bed with increase in air flowrate. However, with the exception of 100 g for 212 – 300 µm and 300 – 425 µm the data show an intermediate inflection point characterised by a small drop followed by a relatively rapid recovery in the pressure drop as the air flowrate increases a characteristic of slugging fluidisation. The observed discontinuity in the pressure is characteristic of the minimum fluidisation velocity for fluidised beds.

iii) All size ranges tested exhibit the same characteristic slugging fluidisation behaviour, where the pressure drop increases with air flowrate. However, it can be observed that for these larger size ranges, in contrast to the data for 212 – 300 µm (a smaller size range), in most cases, masses below 50 g have no effect on the pressure drop.

iv) The slugging flow regime typically occurs in a bed which has a bed height to bed diameter ratio larger than 2, in the case of the PSPS the ratio is 7.83.

v) Minimum fluidisation velocity remains constant with mass in most cases.

vi) Based on the data presented, the variation of the pressure drop versus air flowrate cannot be used as a method for determining the sample mass within the spring.

CHAPTER 7 PARTICULATE BEHAVIOUR IN THE PNEUMATIC SPRING PARTICLE SIZER

7.1 Introduction

Two of the main factors affecting the efficacy of the Pneumatic Spring Particle Sizer (PSPS) as a practical unit for particle size analysis include the sample analysis time and the in-situ mass measurement capability.

The mass measurement aspect was dealt with in Chapter 6. This chapter presents the results of a series of experimental investigations aimed at understanding the processes governing the mass discharge rate from the spring and hence the sample analysis time by studying the particle migration behaviour. Given the practical difficulties in obtaining such data in a spring, a pulsating fluidised bed of similar dimensions to the spring is used for this purpose. The study of the impact of changing the pulsating air frequency on the discharge rate from the spring is dealt with first. As it will be shown, the results provide the incentive for the study of the particle migration behaviour.

7.2 Impact of Air Pulse Frequency on Discharge Rate

Figure 7.1 shows the variation of percentage cumulative discharged mass from the PSPS with time for 21 g of 212 – 300 μm glass Ballotini at various air pulse frequencies in the range 0 – 5 Hz. The spring gap opening corresponding to the upper particle size was 300 μm. A constant pulse air pressure of ca. 103 kPa was used as a higher pressure forced open the coil gaps, resulting in the discharge of particles larger than the spring coil opening. Lower operating pressures on the other hand resulted in insufficient fluidisation of the particles and hence slow discharge.

Returning to figure 7.1, it is clear that little change in the particle discharge rate occurs as the pulse frequency is increased. Also, with the exception of the data at 1 Hz (curve C), over 97 % of the test powder is discharged within 1 minute.

Figure 7.2 – 7.4 show the corresponding data for 300 – 425 µm, 600 – 710 µm and 850 – 1000 µm particles respectively. In each case the spring opening corresponds to the upper size range of each test sample. The pulse air pressure is ca. 103 kPa as before.

Referring to figure 7.2, the 300 – 425 µm test sample also shows similar behaviour to the 212 – 300 µm sample (figure 7.1) with the expectation of a marginally slower discharge rate. Although there are some differences in the data presented in the figure, no obvious dependency on the pulse frequency may be observed.

Similar observations may be made when examining the data presented in figures 7.3 (600 – 710 µm) and 7.4 (850 – 1000 µm) where no trend between the sample discharge rate and the pulse frequency may be observed. However, it is clear that the sample discharge rate decreases with increasing average particle size.

Having said this, it is interesting to note that with the exception of the 300 – 425 µm particles, the sample discharge rate decreases with increase in its poly-dispersity. For example in the case of the smallest particle size range of 212 – 300 µm, the maximum difference between the upper and lower size limit is 88 µm. This value increases to 150 µm for the 850 – 1000 µm. In essence the broader the size range or the greater the sample poly-dispersity is, the slower the discharge rate from the spring.

It appears that the discharge rate is a complex function of the pulse frequency and the degree of sample poly-dispersity.

The following investigates particle migration behaviour during pulsating fluidisation in order to elucidate the above important observation.

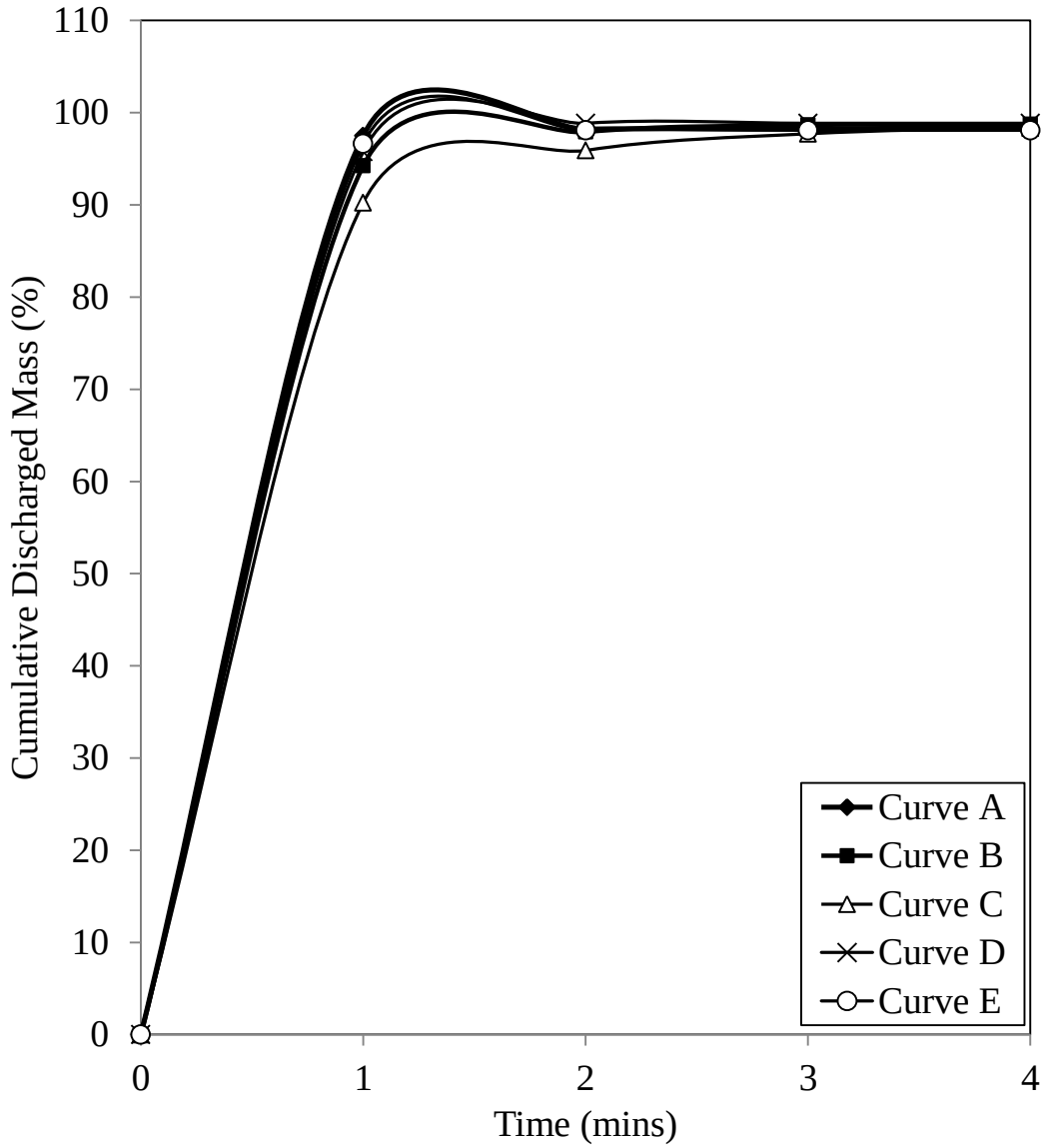

Figure 7.1: Cumulative discharged mass (%) against analysis time for 21 g of 212 – 300 µm glass Ballotini at various air pulse frequencies.

Curve A: 0 Hz (continuous air)

Curve B: 0.5 Hz

Curve C: 1 Hz

Curve D: 2 Hz

Curve E: 5 Hz

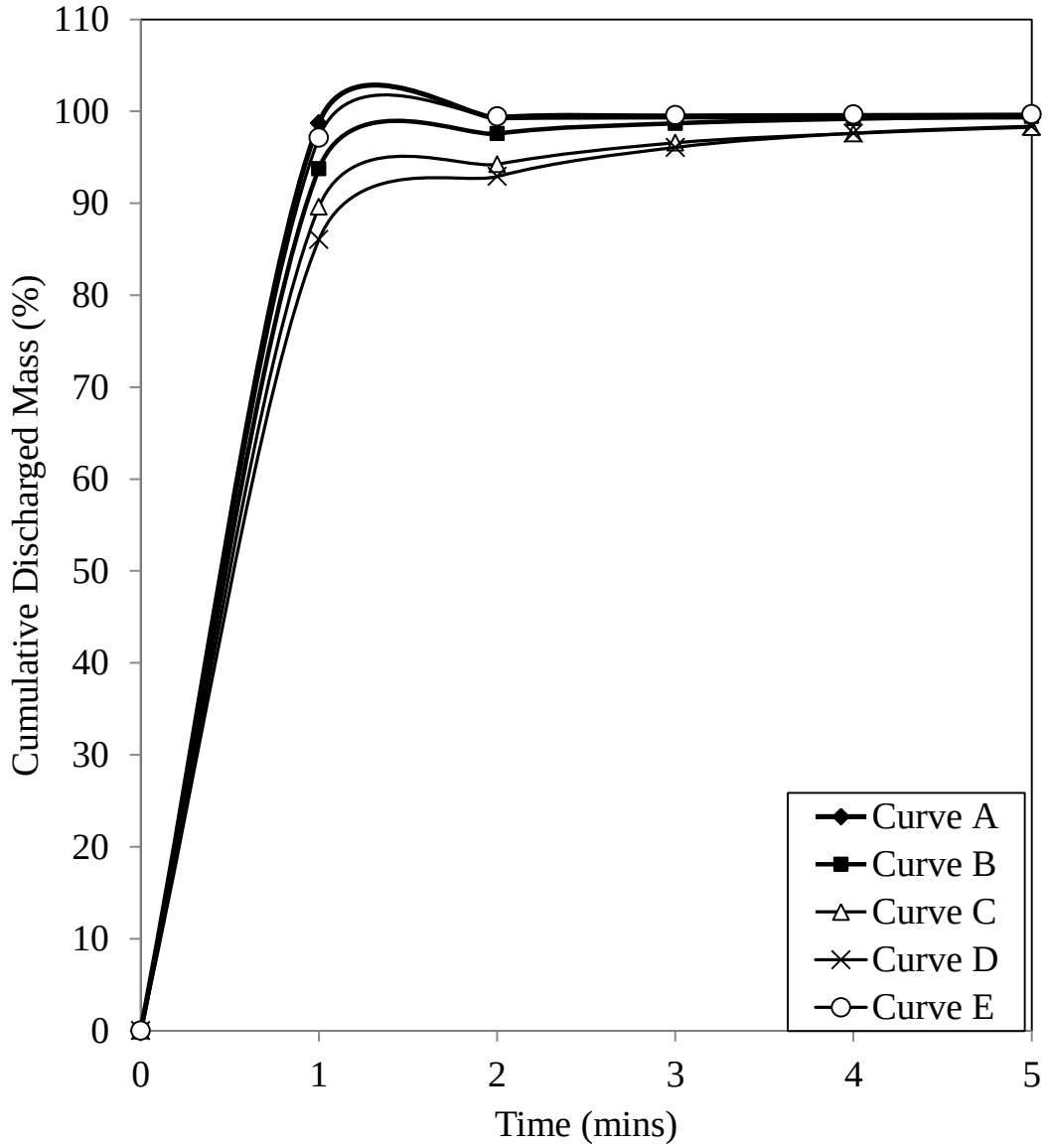

Figure 7.2: Cumulative discharged mass (%) against analysis time for 21 g of 300 – 425 µm glass Ballotini at various air pulse frequencies.

Curve A: 0 Hz (continuous air)

Curve B: 0.5 Hz

Curve C: 1 Hz

Curve D: 2 Hz

Curve E: 5 Hz

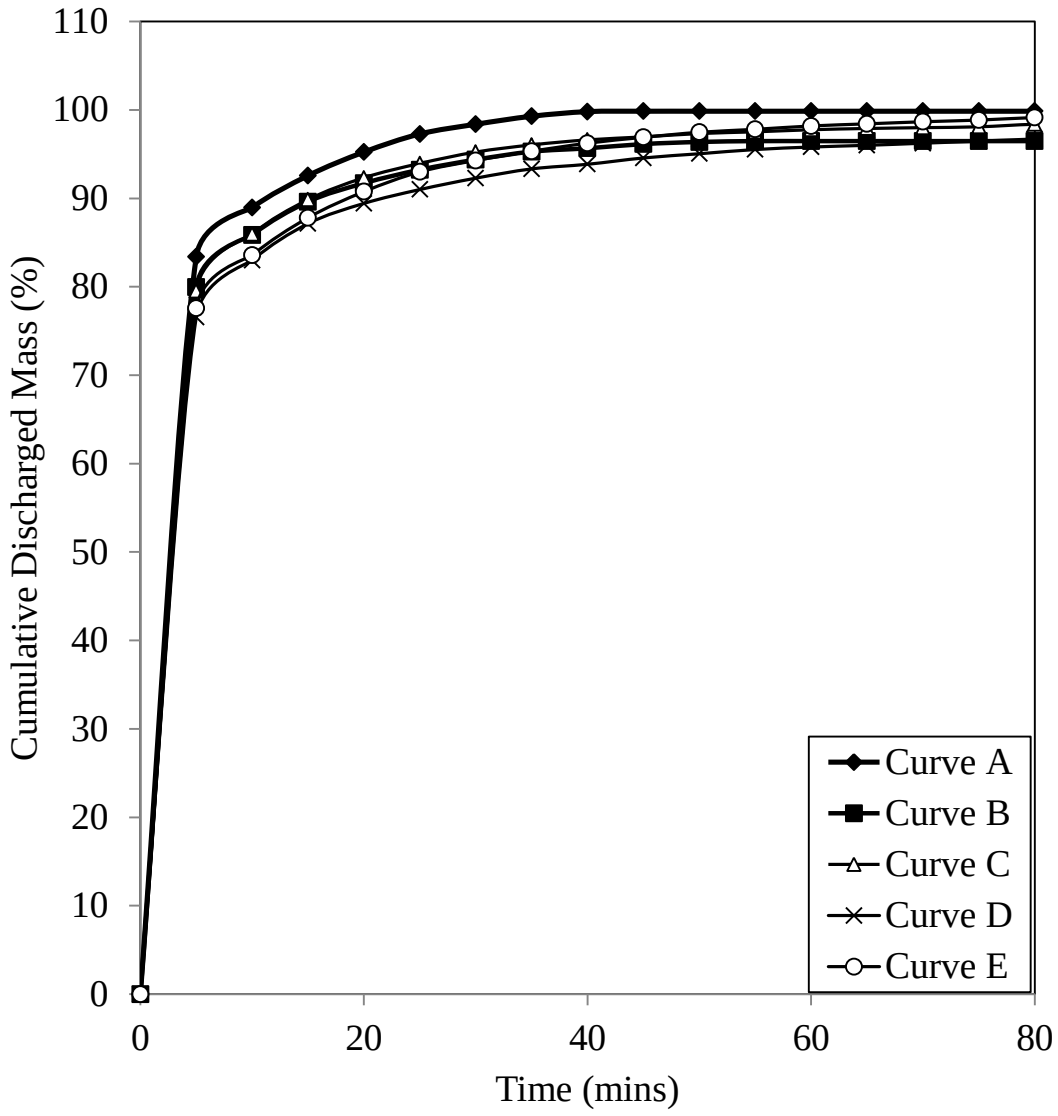

Figure 7.3: Cumulative discharged mass (%) against analysis time for 21 g of 600 – 710 µm glass Ballotini at various air pulse frequencies.

Curve A: 0 Hz (continuous air)

Curve B: 0.5 Hz

Curve C: 1 Hz

Curve D: 2 Hz

Curve E: 5 Hz

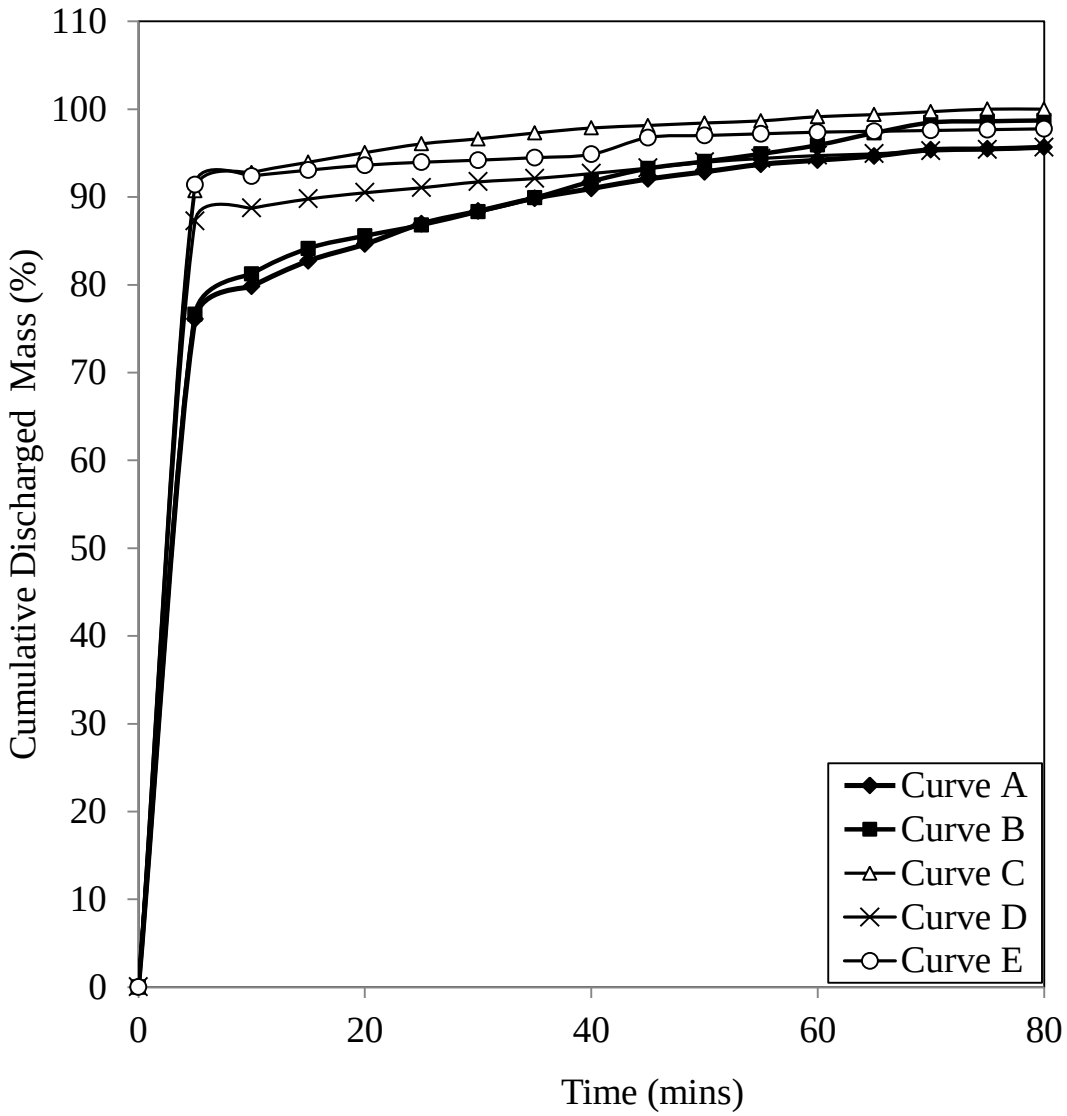

Figure 7.4: Cumulative discharged mass (%) against analysis time for 21 g of 850 – 1000 µm glass Ballotini at various air pulse frequencies.

Curve A: 0 Hz (continuous air)

Curve B: 0.5 Hz

Curve C: 1 Hz

Curve D: 2 Hz

Curve E: 5 Hz

7.3 Impact of Sample Poly-dispersity on Discharge Rate: Particle Segregation Studies

In this section the segregation behaviour of the test powder in the PSPS is investigated. As mentioned before, given the impracticality of obtaining such data in the spring, a cylindrical Perspex fluidised bed with similar overall dimensions to the spring is used. The experimental setup for this study is shown in figure 7.5.

The fluidised bed comprises a 36.5 mm i.d (6.8 mm thickness), 500 mm long Perspex cylinder. The corresponding i.d and length for the extended spring to provide a maximum coil opening of 500 μm are 23 mm and 210 mm respectively.

The test sample is supported on a 40 μm wire mesh distributor mounted near (85 mm from bottom) the base of the cylinder. The top of the cylinder is covered with a 30 μm filter cloth to prevent elutriation of the particles out of the bed during testing. A plenum chamber at the base air inlet ensures the uniform distribution of the pulsating compressed air inlet.

The unit is support by a retort stand. A graduation scale attached to the outer wall of the Perspex cylinder is used to read the bed height.

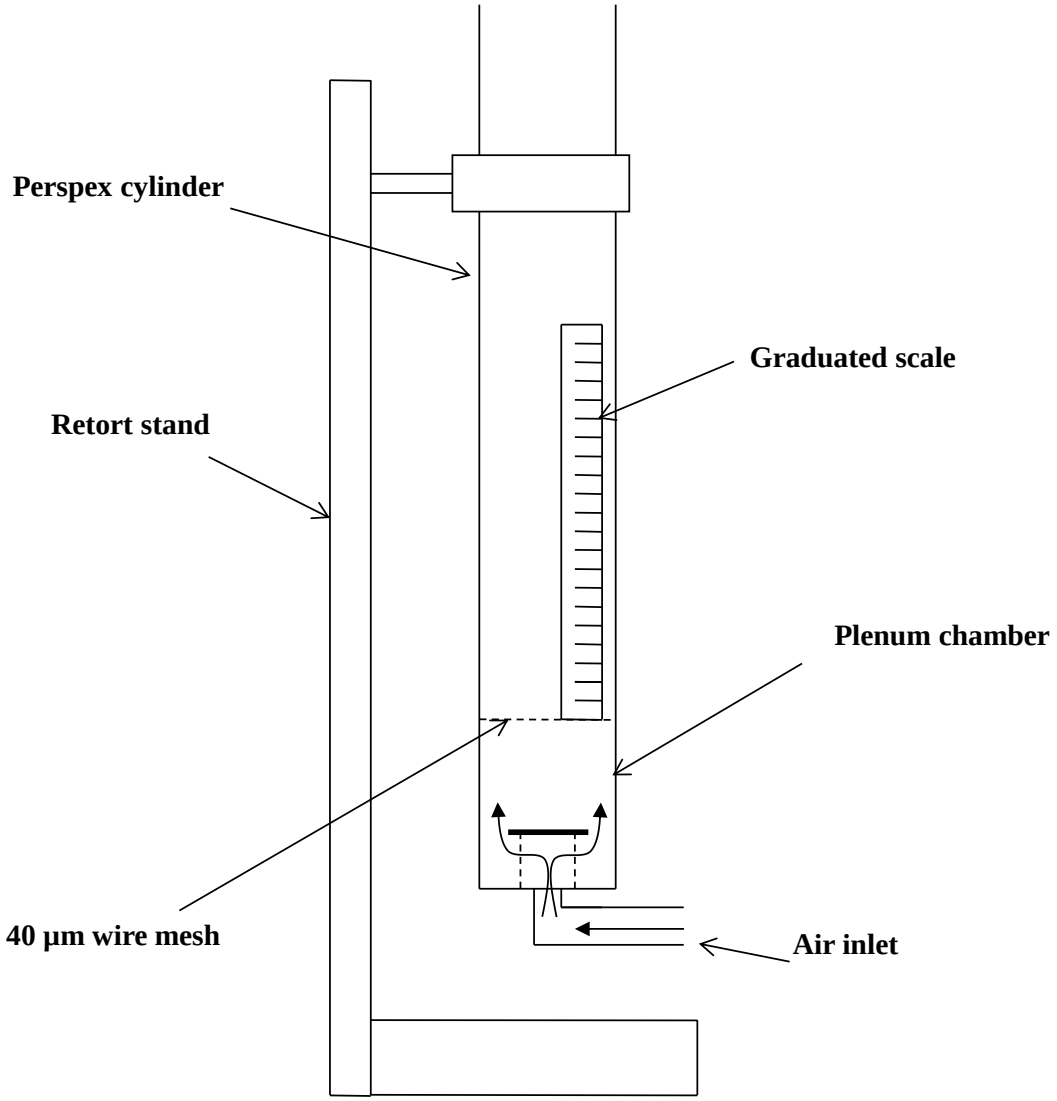

Figure 7.5: Schematic diagram illustrating the segregation experimental rig.

Each segregation experiment involved consecutive loading of the fluidised bed column with two samples of glass Ballotini test powders corresponding to small and large size ranges. The small size range is introduced first as it is expected to percolate to the top of the bed thus maximising particle migration (Rowe et al., 1972).

In order to ensure consistency, the height of each test powder loaded is fixed at 3 cm, resulting in a total bed height of 6 cm for two samples of different size ranges.

Figure 7.6 is a photograph of the sample collection equipment used for extracting representative samples from the fluidised bed following fluidisation for particle size distribution analysis using sieving. The unit comprises a 103 kPa vacuum pump (Telstar TD3, 2 stage, 2800 rpm), cylindrical sample collector and a 4.65 mm i.d steel probe used for extracting samples.

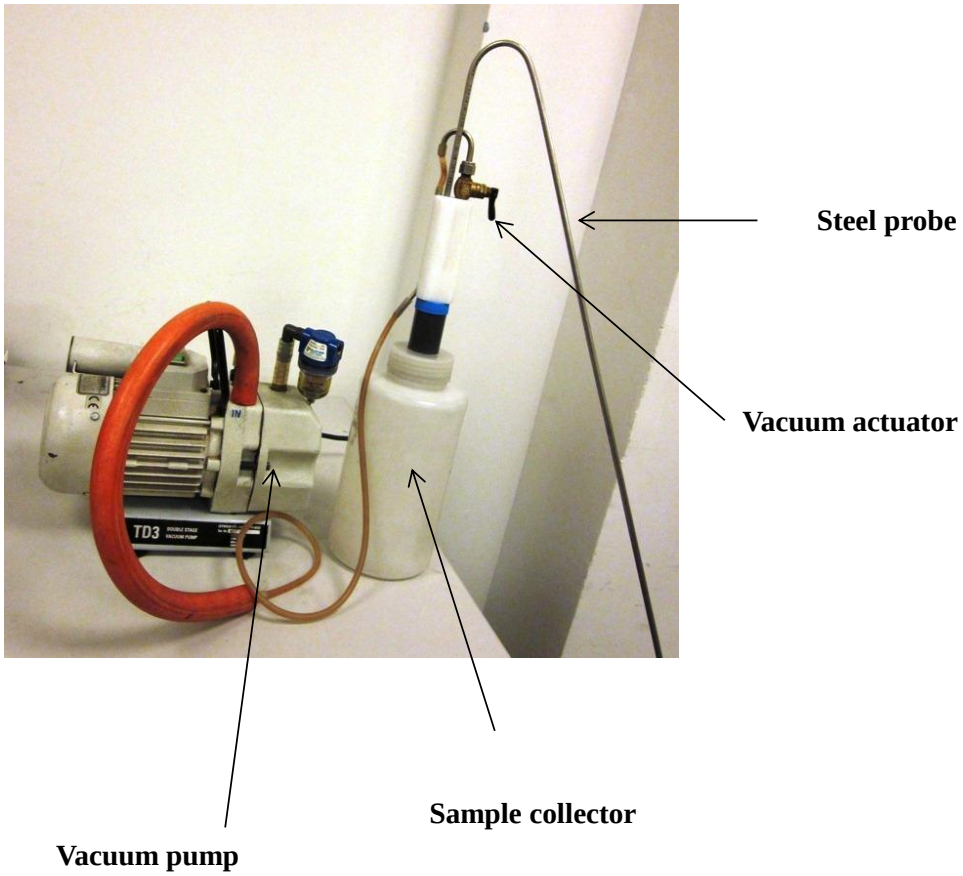

Figure 7.6: Photograph illustrating sample collection equipment used in segregation experiments.

The degree of segregation following pulsating fluidisation is determined by first nominally dividing the bed into three sections of equal heights (2 cm each). Starting from the top, these are referred to as ‘Top’, ‘Middle’ and ‘Bottom’ sections. The entire amount of powder in each section is then carefully extracted from the column

using the vacuum probe followed by analysis to determine the particle size distribution using sieving.

The degree of segregation within the poly-dispersed bed is determined by calculating the segregation coefficient, C_s as given by equation 7.1 (Williams, 1976):

$$C_s = \frac{X_{Lt} - X_{Lb}}{X_{Lt} + X_{Lb}} \tag{7.1}$$

where X_L is the mass fraction of the large particle size range within the test sample with subscripts *t* and *b* denoting the top and bottom of the bed respectively. X_L is calculated from:

$$X_{Li} = \frac{\text{Mass of large size range powder in section } i}{\text{Total mass of powder in section } i} \tag{7.2}$$

where *i* denotes Top, Middle or Bottom section.

When C_s is zero, no segregation is observed and perfect mixing occurs. On the other hand C_s equal to unity indicates complete segregation.

Two poly-dispersed samples namely A and B are used in these experiments. Sample A is made up of 150 – 300 µm and 425 – 600 µm sieve cuts. Sample B on the other hand comprises 180 – 355 µm with 850 – 1180 µm sieve cuts.

The segregation coefficient is determined as a function of pulse air frequency (0, 0.5, 1, 2 and 5 Hz) and fluidisation duration (1, 4, 7 and 10 minutes).

Given the very large number of possible test combinations, the segregation results relating to only a selected number of test conditions as indicated in table 7.1 are presented and discussed in the following. Segregation patterns presented in terms of the variation of mass fraction of the large powder with bed height for the poly-dispersed sample A for fluidisation durations of 4, 7 and 10 minutes at 0 – 5 Hz are

shown in the appendix. The corresponding segregation patterns for sample B for 4 minutes fluidisation duration at 0 – 5 Hz are also shown in the same appendix.

Table 7.1: Experimental conditions used for particle segregation studies.

	Powder A (150 – 300 µm and 425 – 600 µm)	**Powder B (180 – 355 µm and 850 – 1180 µm)**
Frequency (Hz)	0, 0.5, 1, 2, 5	0, 0.5, 1, 2, 5
Fluidisation duration (mins)	1, 4, 7, 10	1, 4
Fluidisation pressure (kPa)	103.4	41.4

Figures 7.7 – 7.11 illustrate the segregation patterns at various pulse frequencies of 5, 2, 1, 0.5 and 0 Hz respectively for the poly-dispersed sample A. The respective air pressure and total fluidisation time are 103.4 kPa and 1 minute.

X_{LP} shown in the figures corresponds to the mass fraction of the large powder size range in the entire sample when the bed is perfectly mixed.

The data in figure 7.7 is for two identical runs in order to demonstrate the degree of reproducibility of the results using the fluidised bed test arrangement. The good agreement between the two sets of measurements demonstrates the efficacy of the technique.

Returning to figures 7.7 – 7.11, as expected (Rowe et al., 1972) it is clear that in all cases, the mass fraction of the large particles (425 – 600 µm) decreases with bed height. This indicates the migration of the large particles towards the bed's base and the percolation of the smaller size range towards the top.

Interestingly, for the conditions tested, much the same as the spring data (figures 7.1 – 7.4), the pulsation frequency has a complex albeit small impact on the particle segregation behaviour.

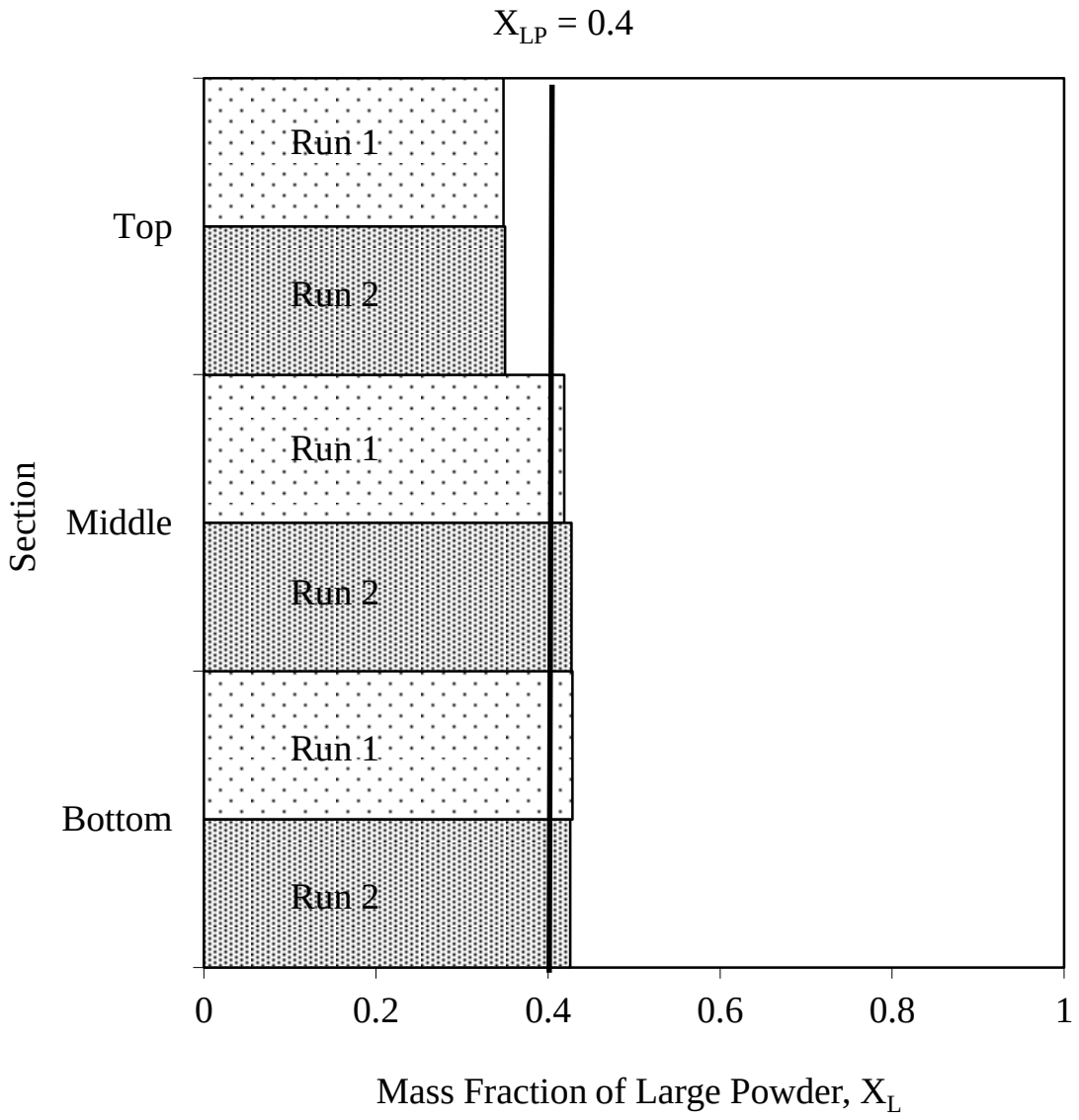

Figure 7.7: Segregation patterns for poly-dispersed sample A (150 – 300 µm and 425 – 600 µm). Run 1 and Run 2 correspond to two separate test runs using exactly the same conditions in order to demonstrate the degree of reproducibility in the data.

Pulse frequency = 5 Hz

Fluidisation duration = 1 min

Air pressure = 103.4 kPa

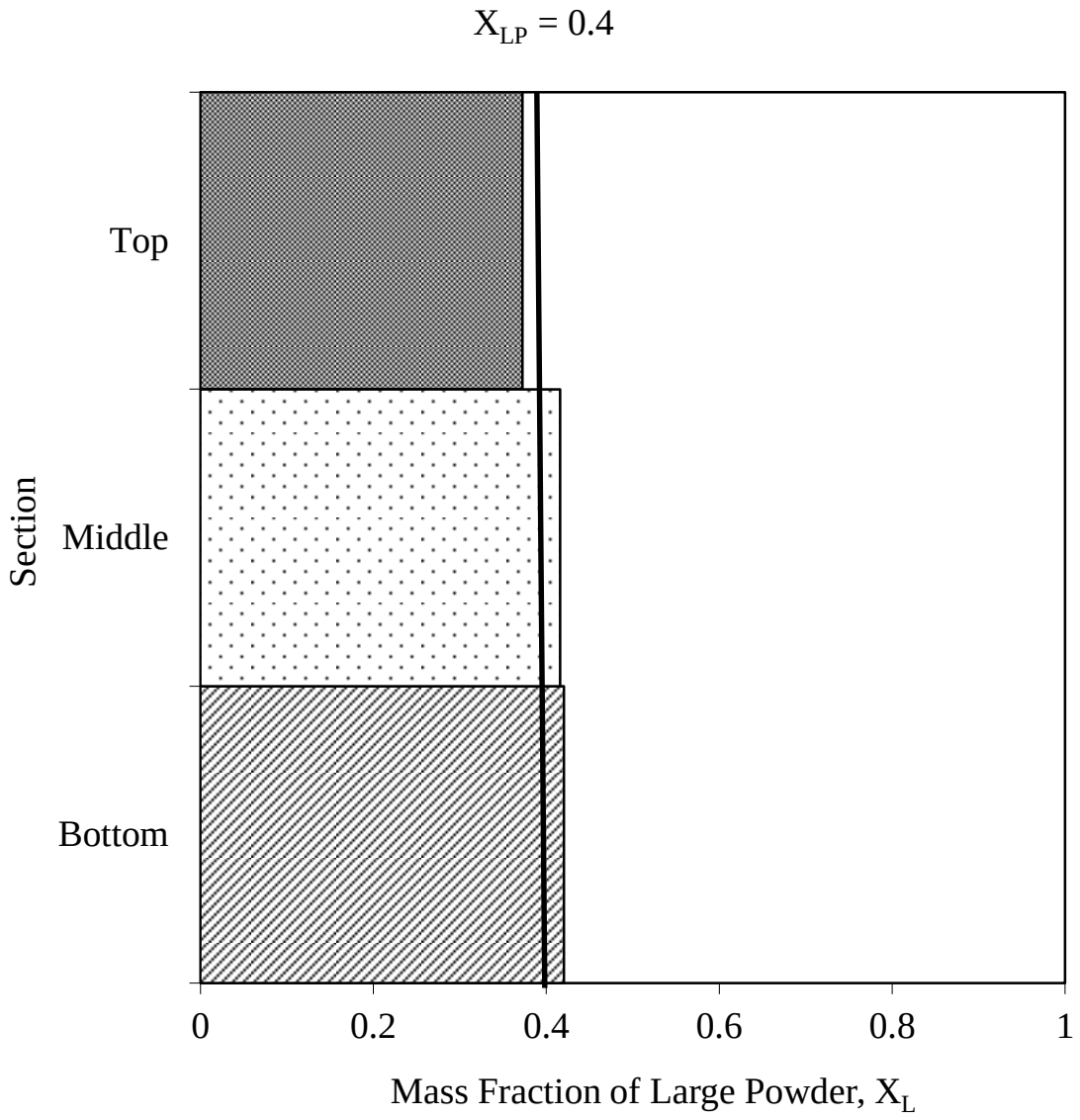

Figure 7.8: Segregation patterns for poly-dispersed sample A (150 – 300 µm and 425 – 600 µm).

Pulse frequency = 2 Hz

Fluidisation duration = 1 min

Air pressure = 103.4 kPa

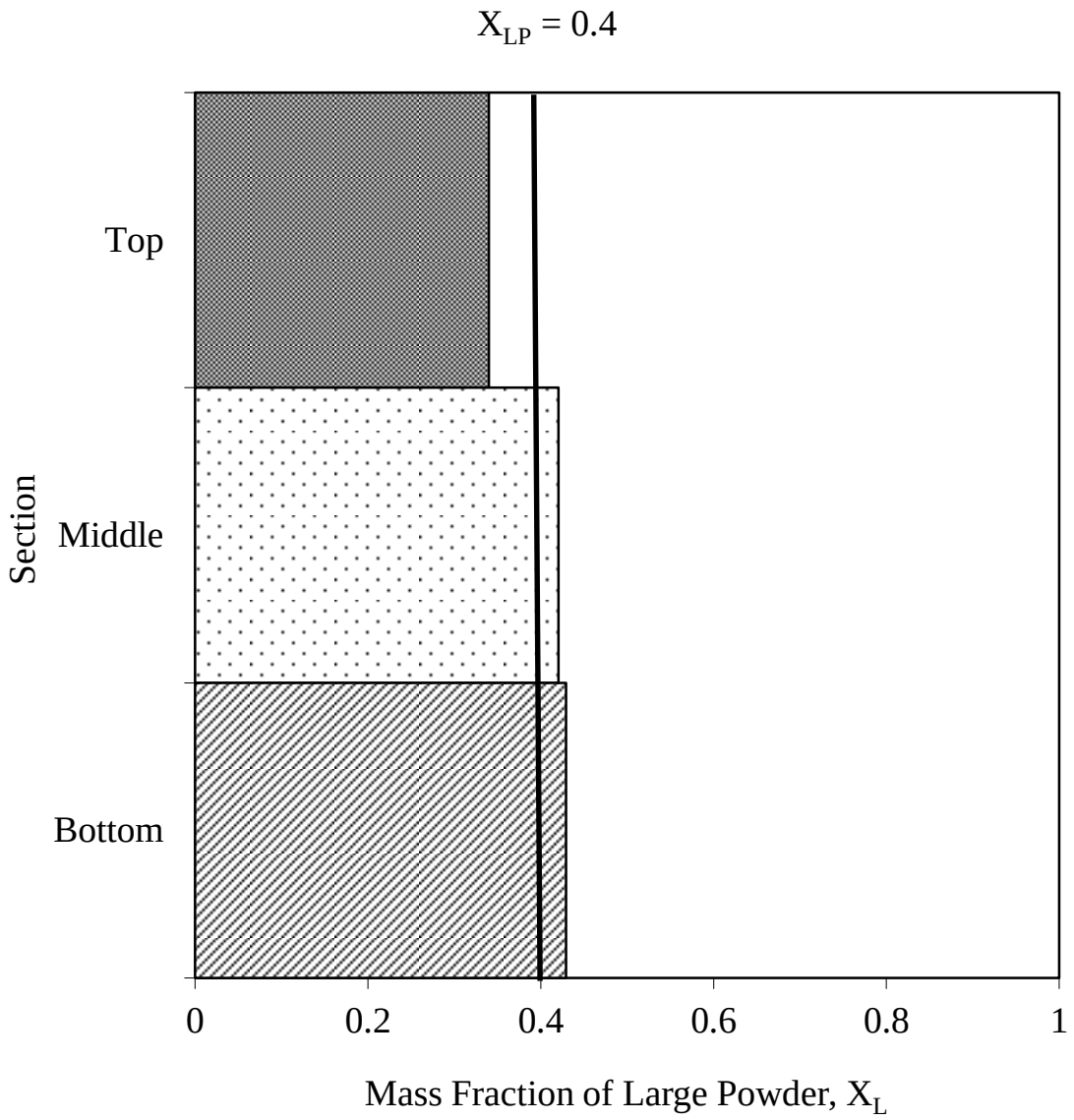

Figure 7.9: Segregation patterns for poly-dispersed sample A (150 – 300 µm and 425 – 600 µm).

Pulse frequency = 1 Hz

Fluidisation duration = 1 min

Air pressure = 103.4 kPa

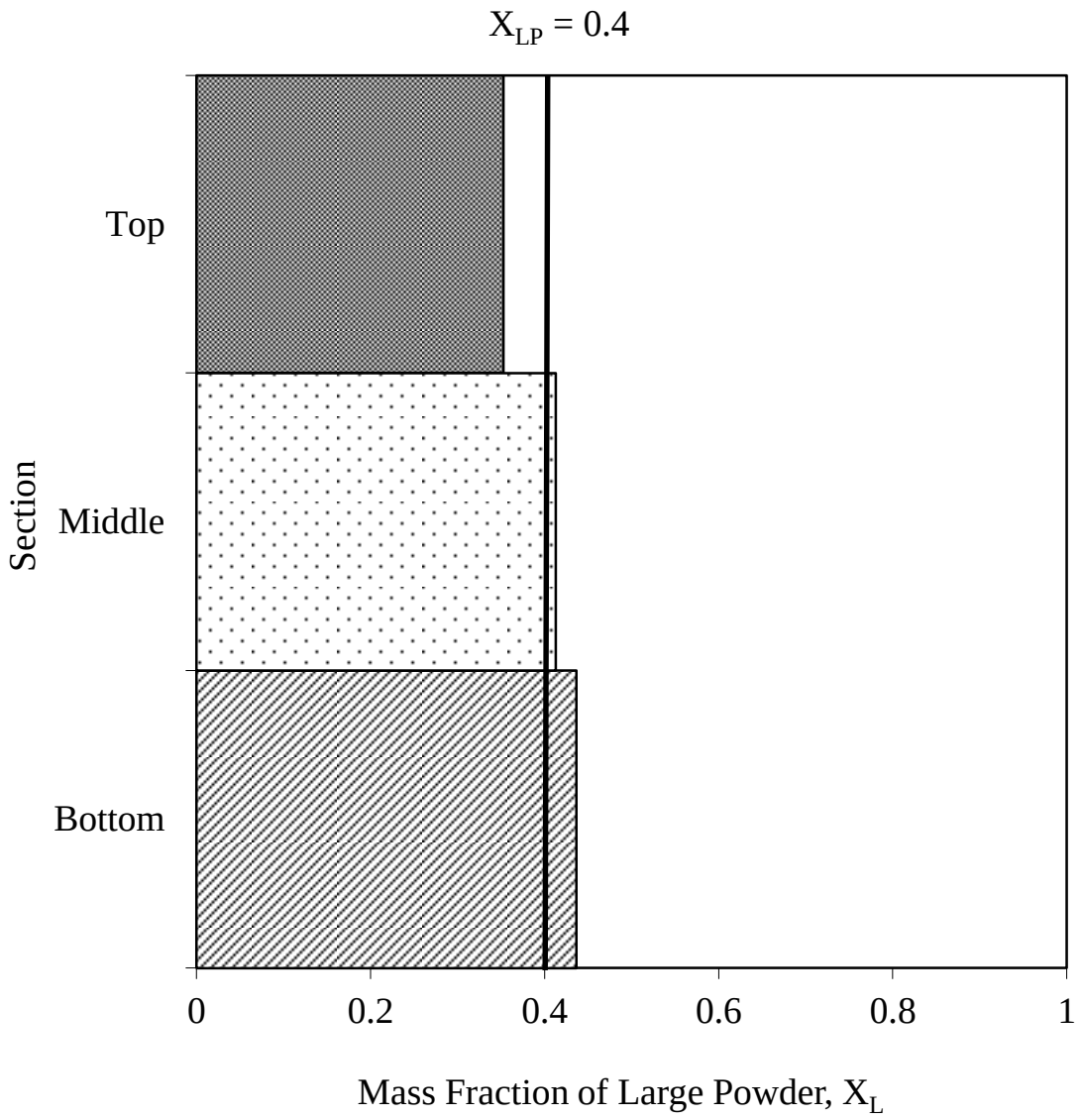

Figure 7.10: Segregation patterns for poly-dispersed sample A (150 – 300 µm and 425 – 600 µm).

Pulse frequency = 0.5 Hz

Fluidisation duration = 1 min

Air pressure = 103.4 kPa

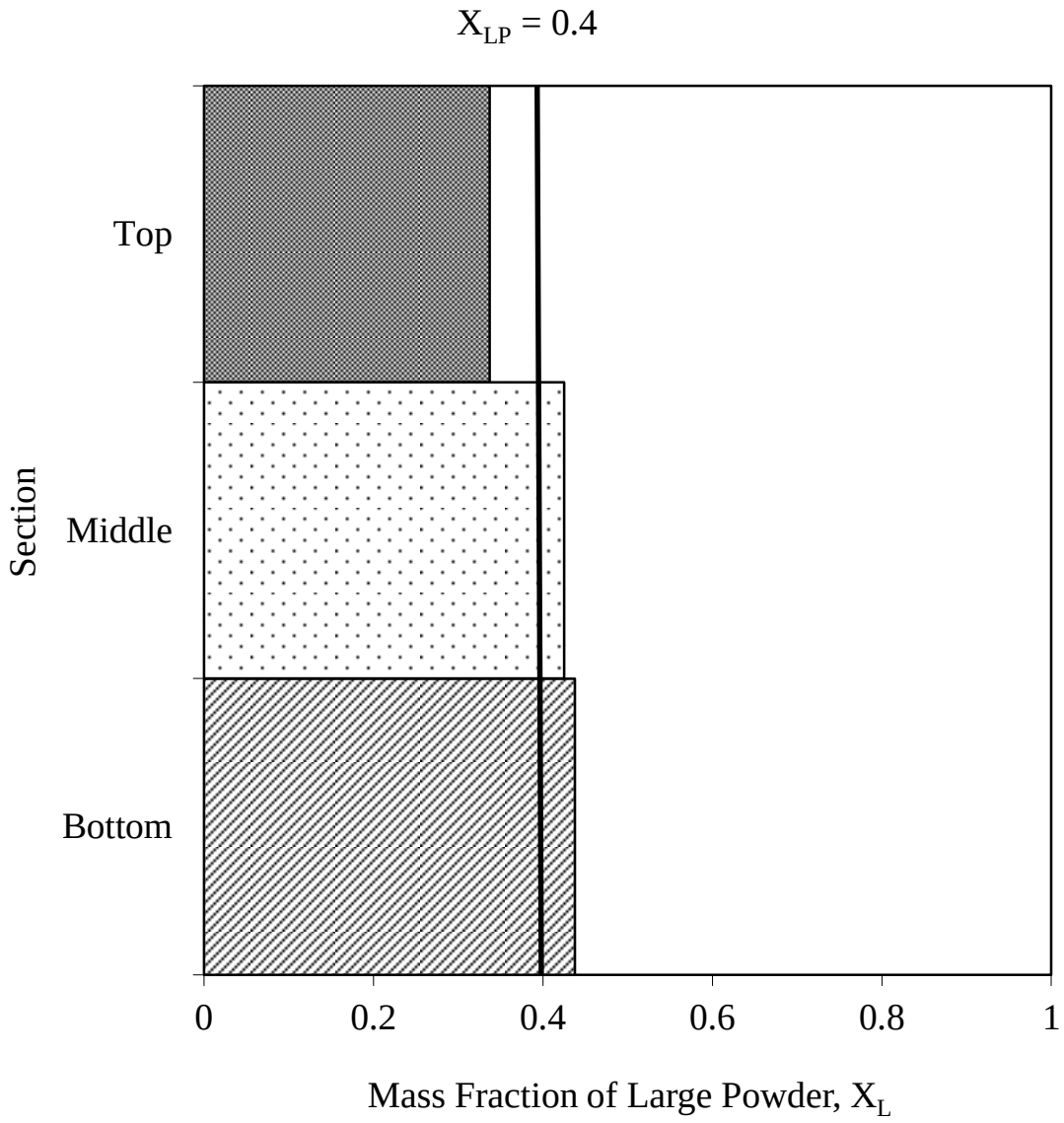

Figure 7.11: Segregation patterns for poly-dispersed sample A (150 – 300 µm and 425 – 600 µm).

Pulse frequency = 0 Hz (continuous air)

Fluidisation duration = 1 min

Air pressure = 103.4 kPa

Figures 7.12 – 7.16 show the corresponding segregation patterns at various pulse frequencies for the poly-dispersed sample B made up of 180 – 355 μm and 850 – 1180 μm particles. The respective air pressure and total fluidisation time are 41.4 kPa and 1 minute respectively.

As it may be observed with the exception of the data at 2 Hz, all cases indicate the migration of the large particles to the base of the bed, with the effect becoming significantly more pronounced as the vibration frequency is decreased. Also, as compared to sample A, the sample B data indicate a significantly higher degree of segregation.

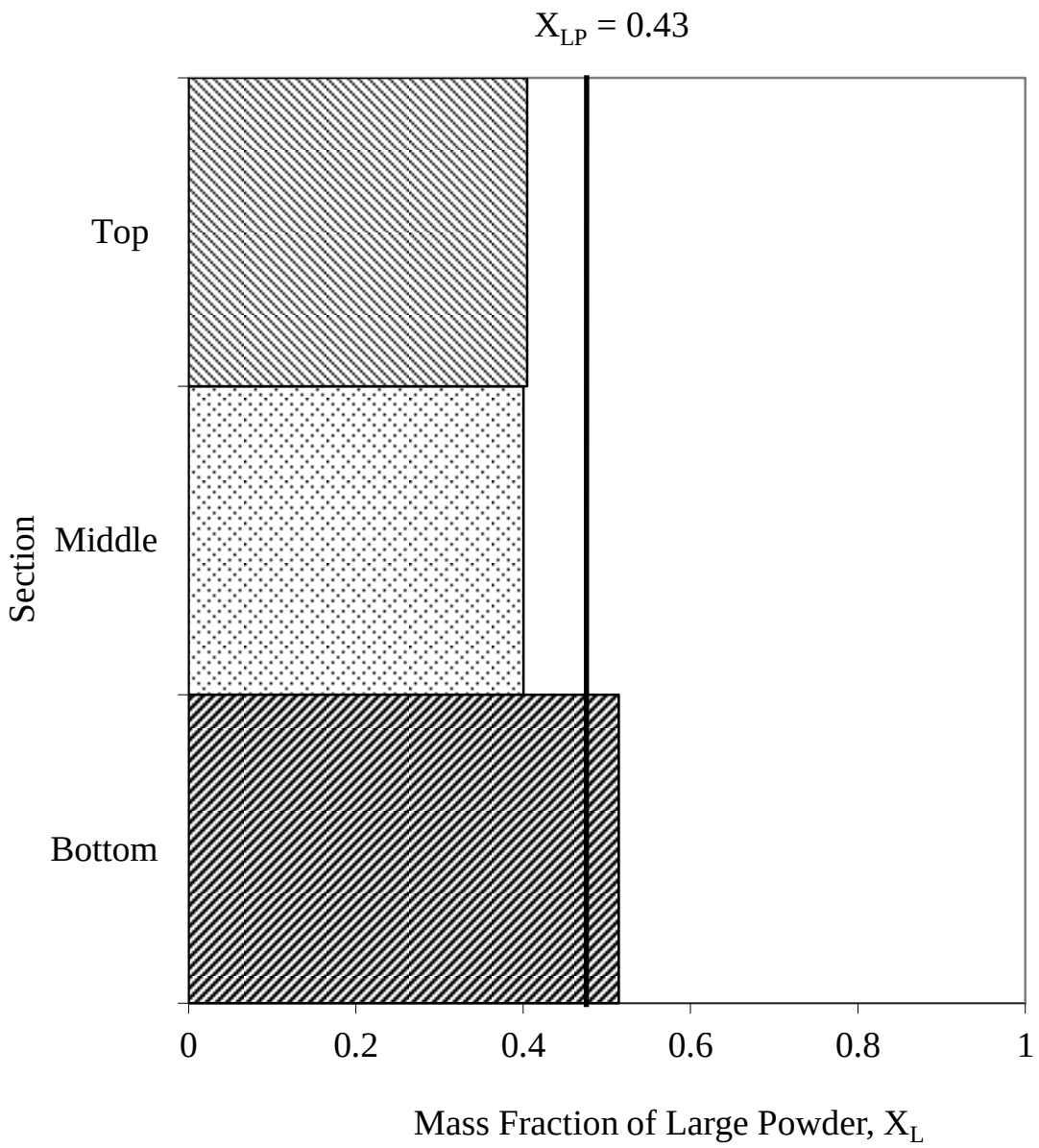

Figure 7.12: Segregation patterns for poly-dispersed sample B (180 – 355 µm and 850 – 1000 µm).

Pulse frequency = 5 Hz

Fluidisation duration = 1 min

Air pressure = 41.4 kPa

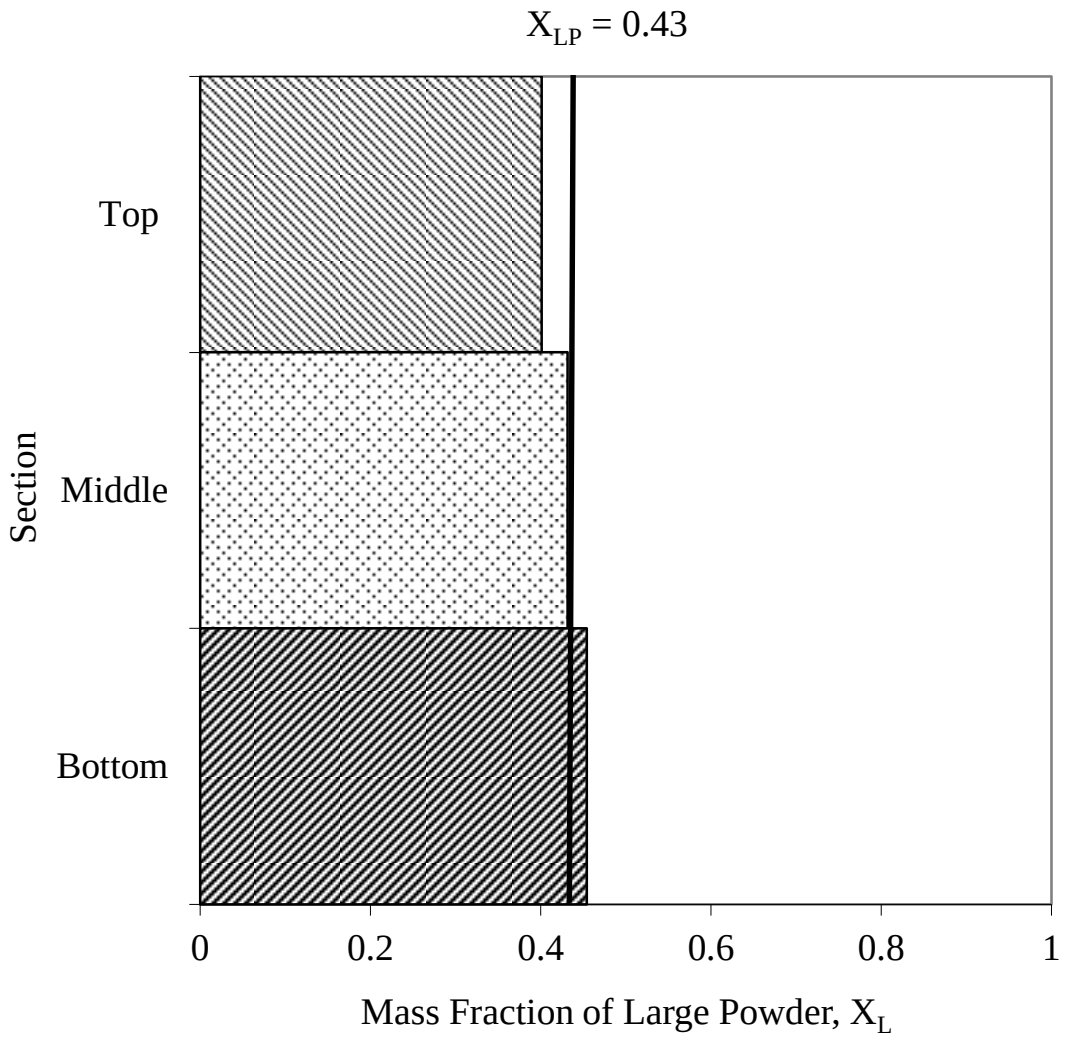

Figure 7.13: Segregation patterns for poly-dispersed sample B (180 – 355 µm and 850 – 1000 µm).

Pulse frequency = 2 Hz

Fluidisation duration = 1 min

Air pressure = 41.4 kPa

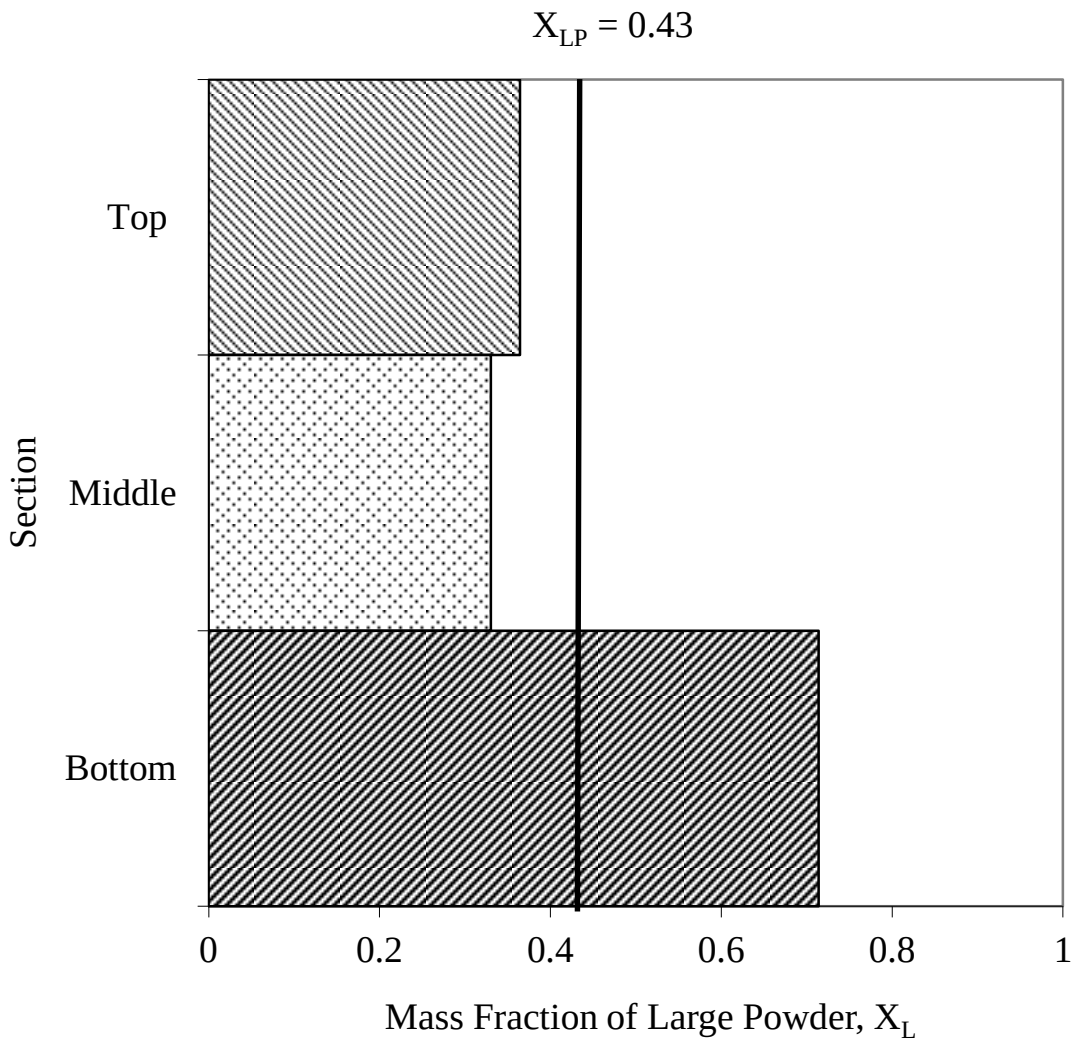

Figure 7.14: Segregation patterns for poly-dispersed sample B (180 – 355 µm and 850 – 1000 µm).

Pulse frequency = 1 Hz

Fluidisation duration = 1 min

Air pressure = 41.4 kPa

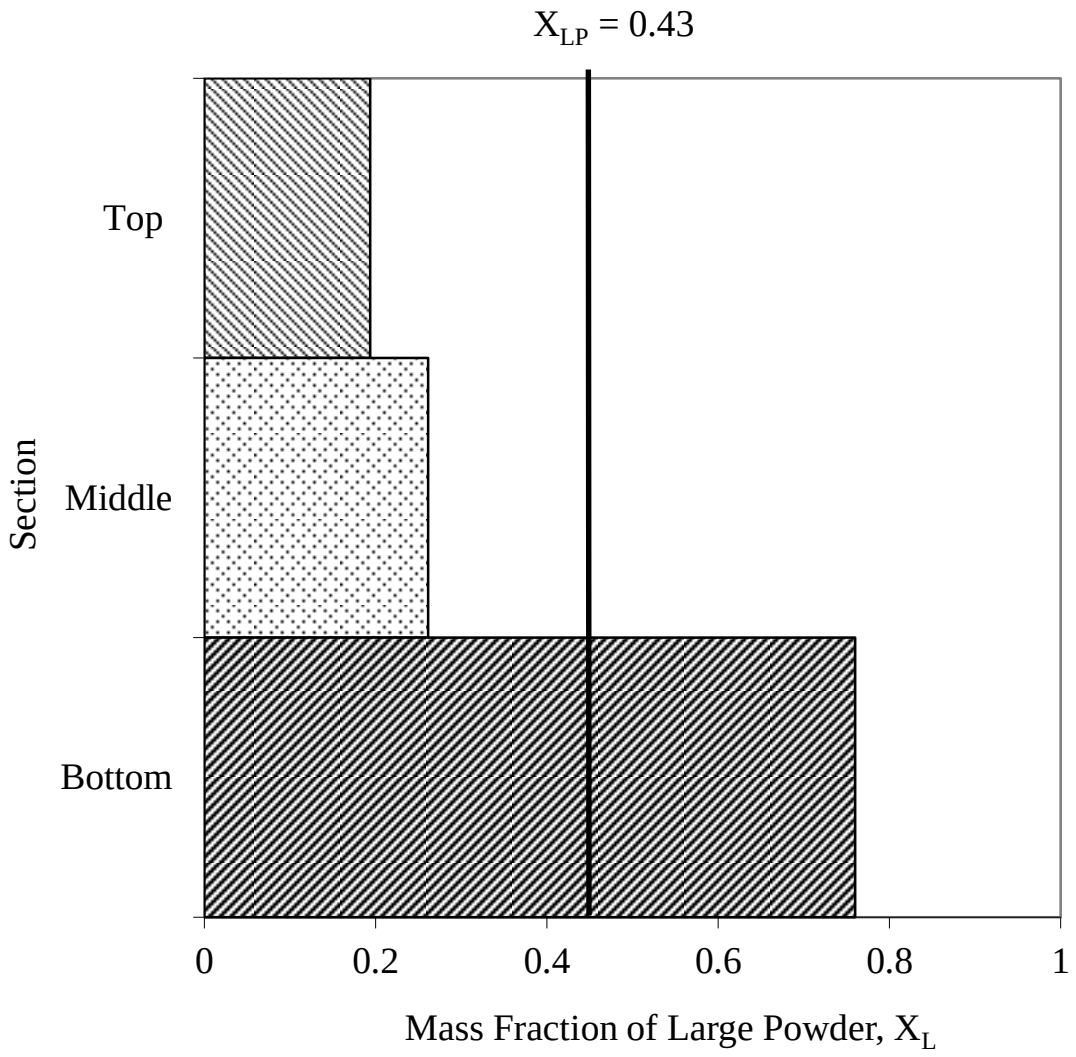

Figure 7.15: Segregation patterns for poly-dispersed sample B (180 – 355 µm and 850 – 1000 µm).

Pulse frequency = 0.5 Hz

Fluidisation duration = 1 min

Air pressure = 41.4 kPa

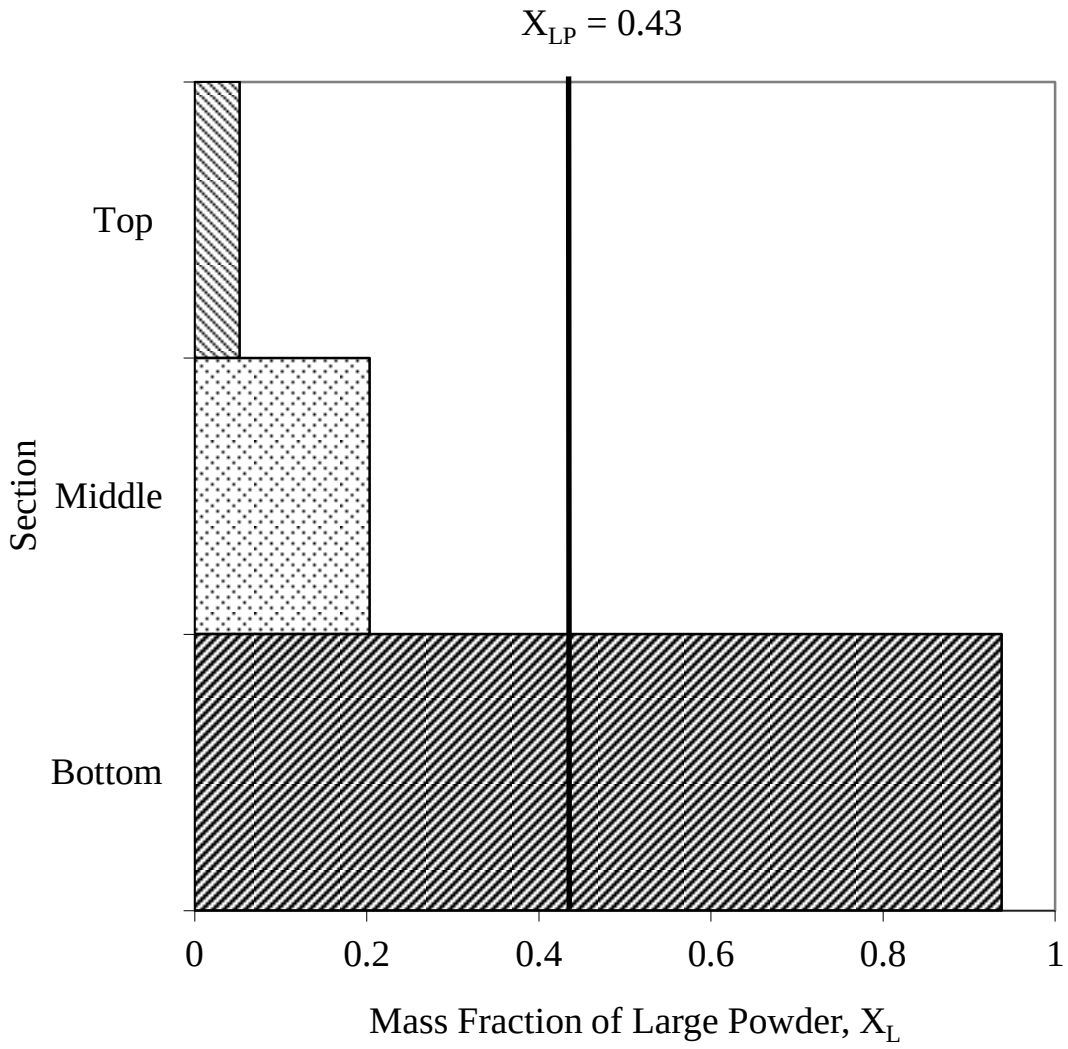

Figure 7.16: Segregation patterns for poly-dispersed sample B (180 – 355 µm and 850 – 1000 µm).

Pulse frequency = 0 Hz (continuous air)

Fluidisation duration = 1 min

Air pressure = 41.4 kPa

Figure 7.17 shows the variation of the segregation coefficient versus pulse frequency for the poly-dispersed sample A (150 – 600 μm). The data is obtained for various fluidisation durations of 1, 4, 7 and 10 minutes using a fixed air pressure of 103.4 kPa.

Close examination of the data reveals that with exception of the data at 4 minutes (curve B), in general the segregation coefficient initially decreases (hence more mixing) with vibration frequency up to 2 Hz before increasing again. Also, the fluidisation time has relatively little impact on the data. Interestingly, the data at 4 minutes fluidisation time indicate the largest degree of segregation as compared to the rest.

The curves do not provide a clear trend which can be used to analyse the results. However, 4 minutes of fluidisation produces the highest segregation coefficient for all pulse frequencies.

The highest segregation coefficient is ca. 0.17, achieved at four minutes of fluidisation duration with continuous air flow (0 Hz).

Figure 7.18 shows the variation of the segregation coefficient versus pulse frequency for the poly-dispersed sample B (180 – 1180 μm). The data is obtained for fluidisation durations of 1 and 4 minutes using a fixed air pressure of 41.4 kPa. The results show a considerably high segregation coefficient at 0.89 and 0.85 for 1 and 4 minute fluidisation durations respectively when using 0 Hz frequency. Figure 7.18 shows a general decrease in the segregation coefficient with frequency. In this case, the segregation coefficient increases again beyond 2 Hz as with sample A.

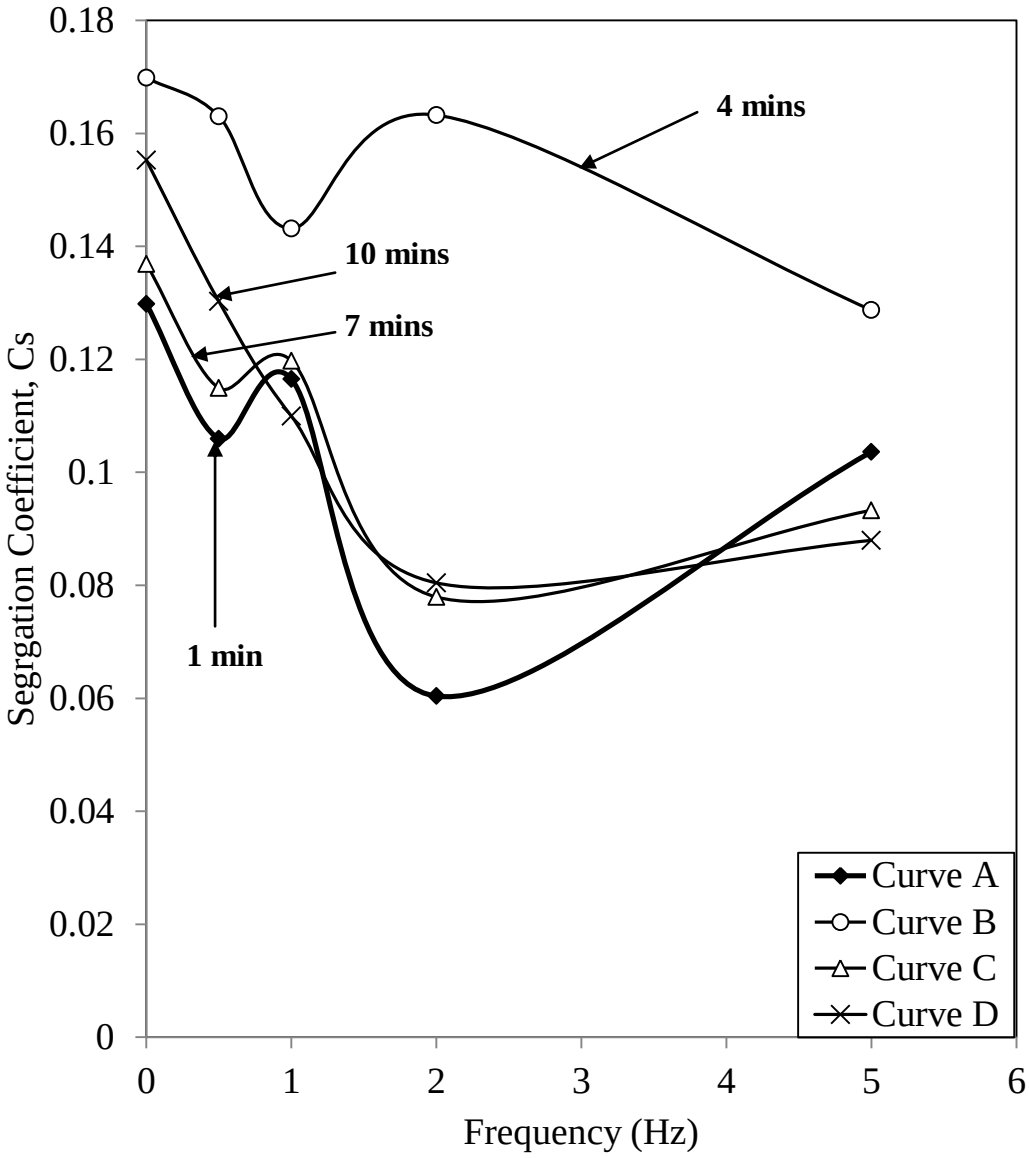

Figure 7.17: Variation of the segregation coefficient with air fluidisation frequency for 110 g poly-dispersed sample A (150 – 300 µm and 425 – 600 µm) at various fluidising durations using 103.4 kPa air pressure.

Curve A: 1 min

Curve B: 4 mins

Curve C: 7 mins

Curve D: 10 mins

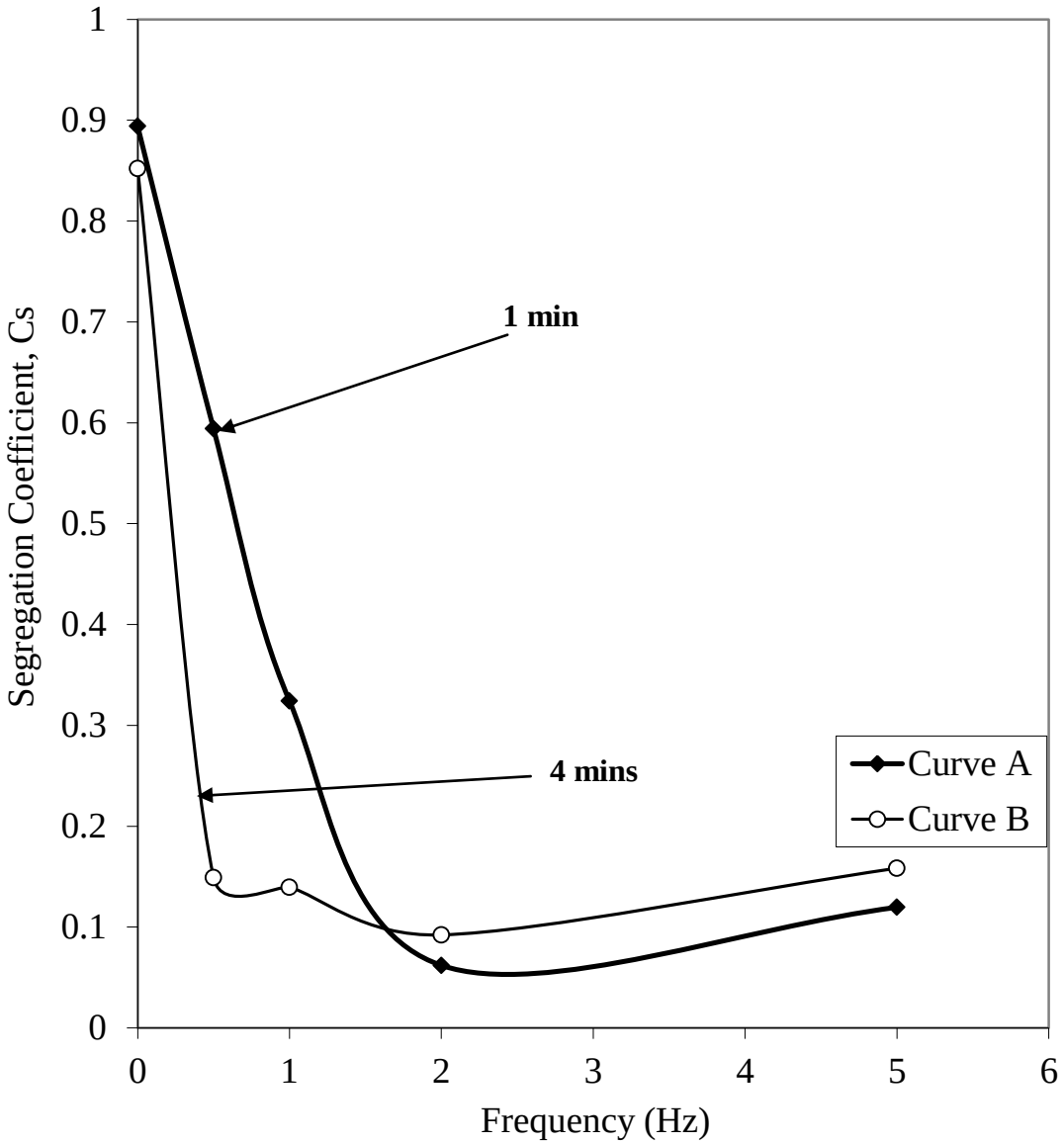

Figure 7.18: Variation of the segregation coefficient with air fluidisation frequency for 116 g poly-dispersed sample A (180 – 355 µm and 850 – 1180 µm) at various fluidising durations using 41.4 kPa air pressure.

Curve A: 1 min

Curve B: 4 mins

Clearly, the investigation of any correlation between the segregation behaviour shown in figure 7.17 and the sample discharge time from the spring is important. Since 41.4 kPa is too low a pressure to discharge sample B particles from the spring, sample A will be the main focus of the study.

Figure 7.19 shows the variation of the cumulative mass discharge from the spring against the discharge time at different pulse frequencies for the same sample A used in the above segregation fluidisation test (figure 7.17) using the same air pressure of 103.4 kPa.

Figure 7.20 on the other hand shows the corresponding variations of the segregation coefficient (extracted from figure 7.17) and the time for 95 % discharge (extracted from figure 7.19), chosen as an example, plotted vs. the fluidisation frequency. As it may be observed with the exception of the data at 1 Hz, there is a good correlation between the segregation coefficient and the sample discharge rate. In general as the degree of mixing increases (lower segregation coefficient) the duration for sample discharge decreases.

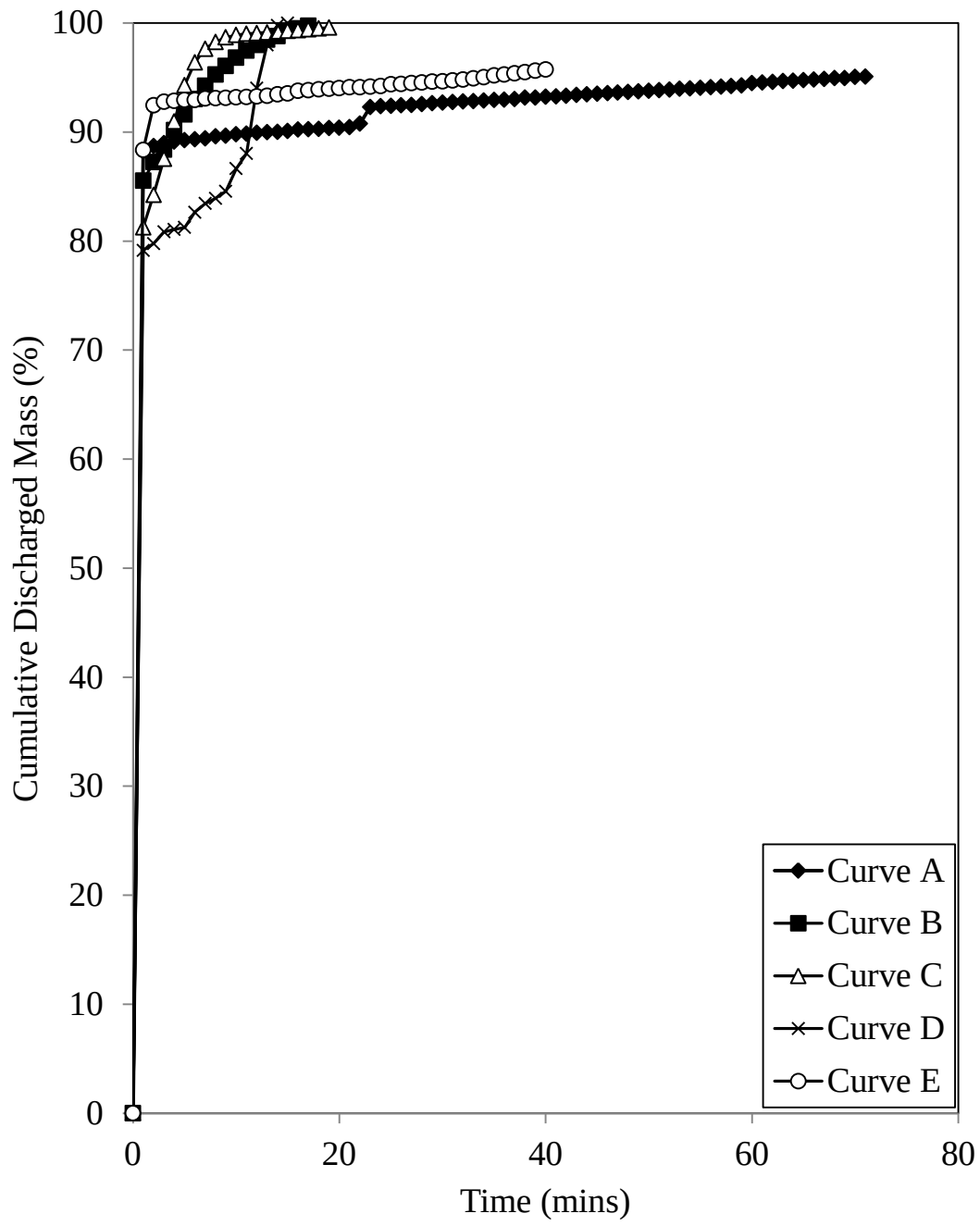

Figure 7.19: Cumulative discharged mass (%) from PSPS against analysis time for 110 g of sample A (150 – 300 µm and 425 – 600 µm) at various air pulse frequencies using 103.4 kPa air pressure.

Curve A: 0 Hz (continuous air)
Curve B: 0.5 Hz
Curve C: 1 Hz
Curve D: 2 Hz
Curve E: 5 Hz

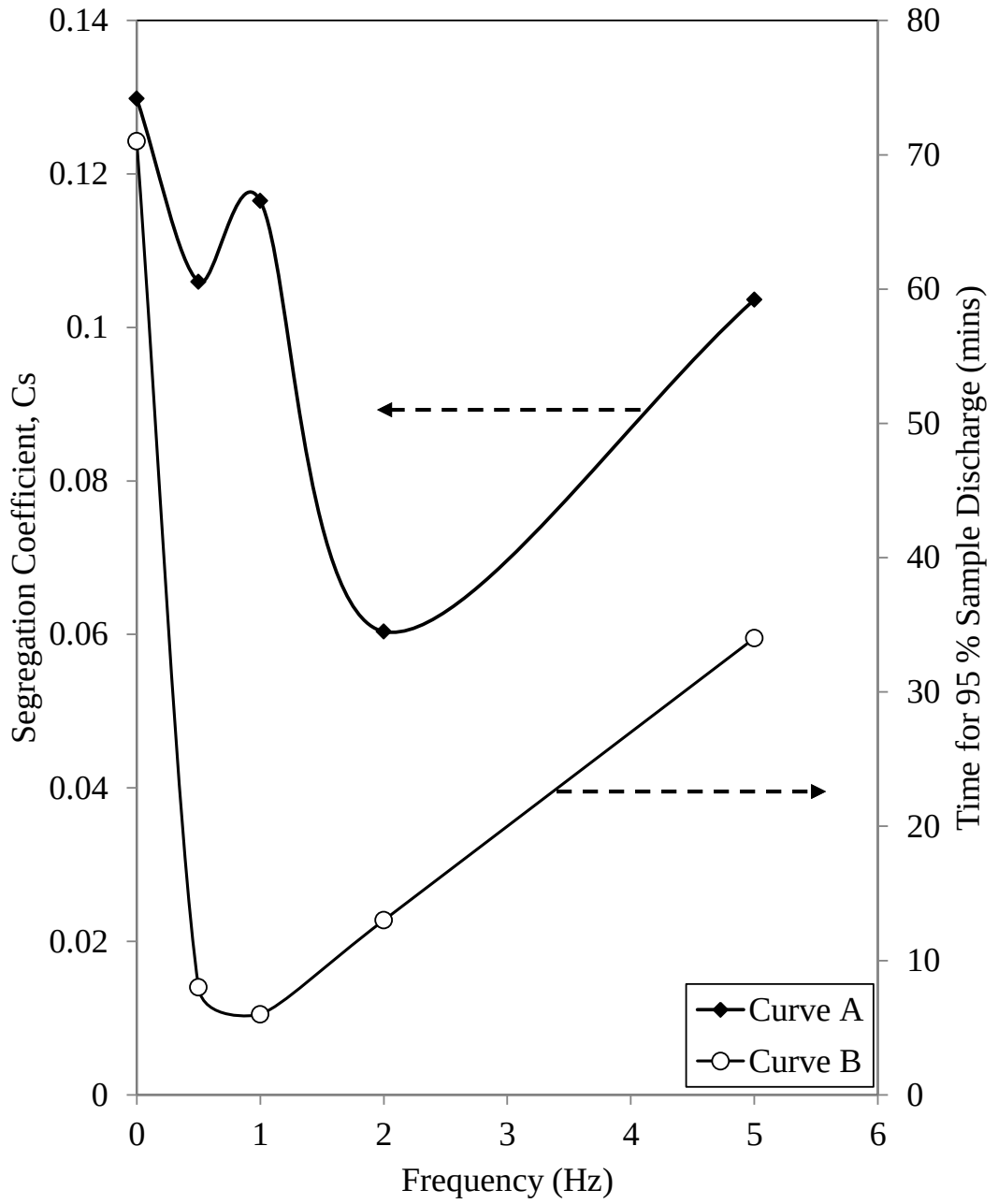

Figure 7.20: Variation of the segregation coefficient and time for 95 % discharge 110 of sample A (150 – 300 µm and 425 – 600 µm) with frequency at 103.4 kPa.

Curve A: Segregation coefficient, Cs

Curve B: Time required for 95 % sample discharge.

7.4 Conclusions

One of the important factors affecting the efficacy of the PSPS particularly for on-line operations is the sample analysis time, which in turn is directly governed by the rate of discharge of the particles from the spring.

This chapter initially investigated the impacts of the sample poly-dispersity and fluidisation pulse frequency on the sample discharge time. This was then followed by a study of the particle migration patterns using a pulsating fluidised bed system of similar overall dimensions as the spring in order to elucidate the mechanism responsible for the observed trends. In all cases Ballotini glass spheres of various size ranges at air pressures of 103.4 kPa and 41.4 kPa were employed.

The pulse frequency experiments using the PSPS revealed that

i) for the same sample size range, the discharge time was a complex function of the pulsation frequency where the dependency, albeit relatively small, became more significant with increase in the average particle size

ii) for the same air pulse frequency, in general, the sample discharge time increased with the degree of sample poly-dispersity and the average particle size.

The fluidised bed experiments were conducted to elucidate the mechanisms responsible for the above observed trends. These involved determining the particle migration profiles, expressed in terms of the segregation coefficient, following pulsation at the various frequencies. The results indicated

i) the expected migration of the large particles towards the bed's base and the percolation of the smaller size range towards the top

ii) much the same as the variation of the pulse frequency with sample discharge time, the pulsation frequency had a complex albeit small impact on the particle segregation behaviour

iii) a direct correlation between the sample discharge time and the degree of segregation within the fluidised bed existed. In general as the degree of mixing increased (lower segregation coefficient) the duration for sample discharge decreased.

Based on the above findings it is clear that any operating or design parameter that promotes the degree of mixing within the spring will improve the system's efficacy through a reduction in the sample analysis time. The analysis time also increases with increase in the sample's poly-dispersity.

CHAPTER 8 HANDHELD SPRING PARTICLE SIZER

The following chapter describes the performance evaluation of the handheld Spring Particle Sizer (handheld SPS). This includes the comparison of PSD measurement with standard sieves when using different test powders, as well as the development of volume to mass calibration curves for direct mass measurement from the unit. Finally, an investigation on the effect of agitation mode on system response is also presented. Section 4.4 gives a brief description of the handheld SPS design.

8.1 Spring Aperture Calibration

The following describes the results obtained for a series of tests conducted to calibrate the handheld SPS using glass Ballotini particles and three size ranges of calcium carbonate ($CaCO_3$) particles. The latter were supplied by Omya UK Limited (2011) hereby referred to as LG800, LG12 and L400 particles.

The standard test powder used was a 3 g sample of glass Ballotini. The size ranges tested were 212 – 300, 300 – 425, 425 – 500, 500 – 600, 600 – 710, 710 – 850 and 850 – 1000 μm.

The initial test involved loading the handheld SPS with 3 g of glass Ballotini with the size range 212 – 300 μm. The unit was held horizontally to ensure a uniform distribution of the test powder over the length of the spring. The screw cap was rotated by half a turn, to extend the spring. Based on the assumption of uniform spring extension, the above corresponded to a coil opening of 20 μm. The unit was hand shaken and manually tapped to enhance particle discharge. The discharged powder collected in the measuring cylinder attached to the base of the unit was weighed after 1 minute. The handheld SPS was shaken for a minute each time until the discharged powder mass remained unchanged by ± 1 % (0.03 g). The screw cap was rotated by further half turn intervals and the procedure was repeated until the test powder was fully discharged.

Figures 8.1 and 8.2 show PSDs for glass Ballotini in terms of the percentage cumulative discharged mass against the number of turns of the handheld SPS screw cap for seven

individual standard sieve size fractions (i.e. 212 – 300, 300 – 425, 425 – 500, 500 – 600, 600 – 710, 710 – 850 and 850 – 1000 μm). The results present seven sets of data. Each test was repeated to demonstrate reproducibility for all size fractions used. All tests showed good reproducibility with a maximum deviation between any two runs of ± 0.23 g.

Data extracted from figures 8.1 and 8.2 are plotted in figure 8.3 as the number of turns of the screw cap against the equivalent aperture size. Figure 8.3 shows the upper and lower size limits (curve A) and mean spring aperture data (curve B). The corresponding fitted curves based on polynomial regression are given by:

Upper & lower sizes (curve C)	$y = -1.3068x^2 + 73.887x$	(8.1)
Mean sizes (curve D)	$y = -1.3267x^2 + 73.95x$	(8.2)

Where, y is the spring aperture size and x is the number of turns of the handheld SPS screw cap. The above correlations gave coefficients of determination, R^2 of 0.9864 and 0.9949 respectively.

It can also be seen from figure 8.3 that both curves C and D are in very good agreement, with a maximum deviation of ± 0.24 turns for any two points between 212 – 1000 μm, this computes to ca. ± 10 μm. Therefore, either of the two calibration curves may be utilised.

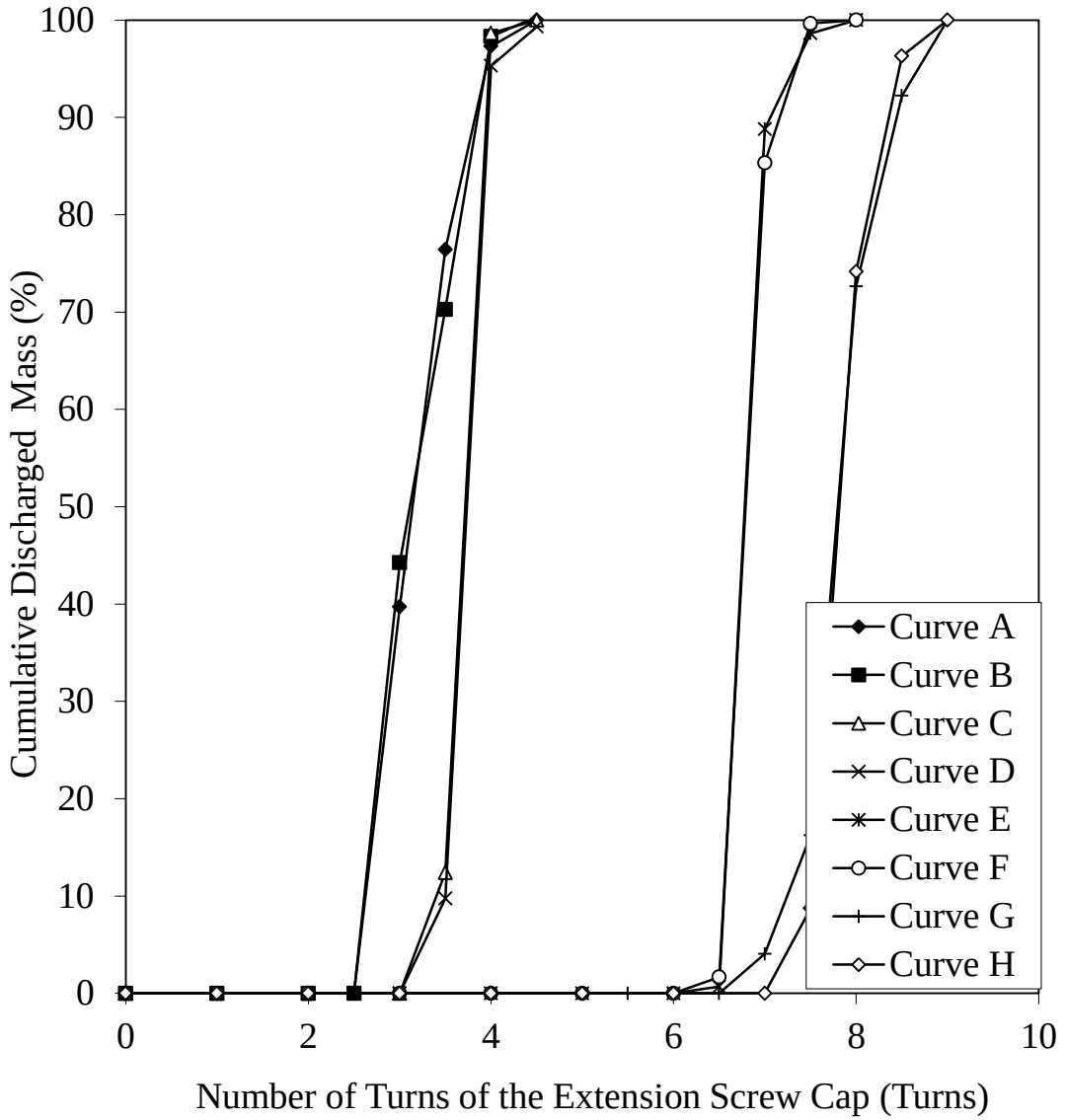

Figure 8.1: Calibration data handheld SPS using 3 g of glass Ballotini in size ranges 212 – 300, 300 – 425, 425 – 500 and 500 – 600 µm.

Curve A: 212 – 300 µm Run 1

Curve B: 212 – 300 µm Run 2

Curve C: 300 – 425 µm Run 1

Curve D: 300 – 425 µm Run 2

Curve E: 425 – 500 µm Run 1

Curve F: 425 – 500 µm Run 2

Curve G: 500 – 600 µm Run 1

Curve H: 500 – 600 µm Run 2

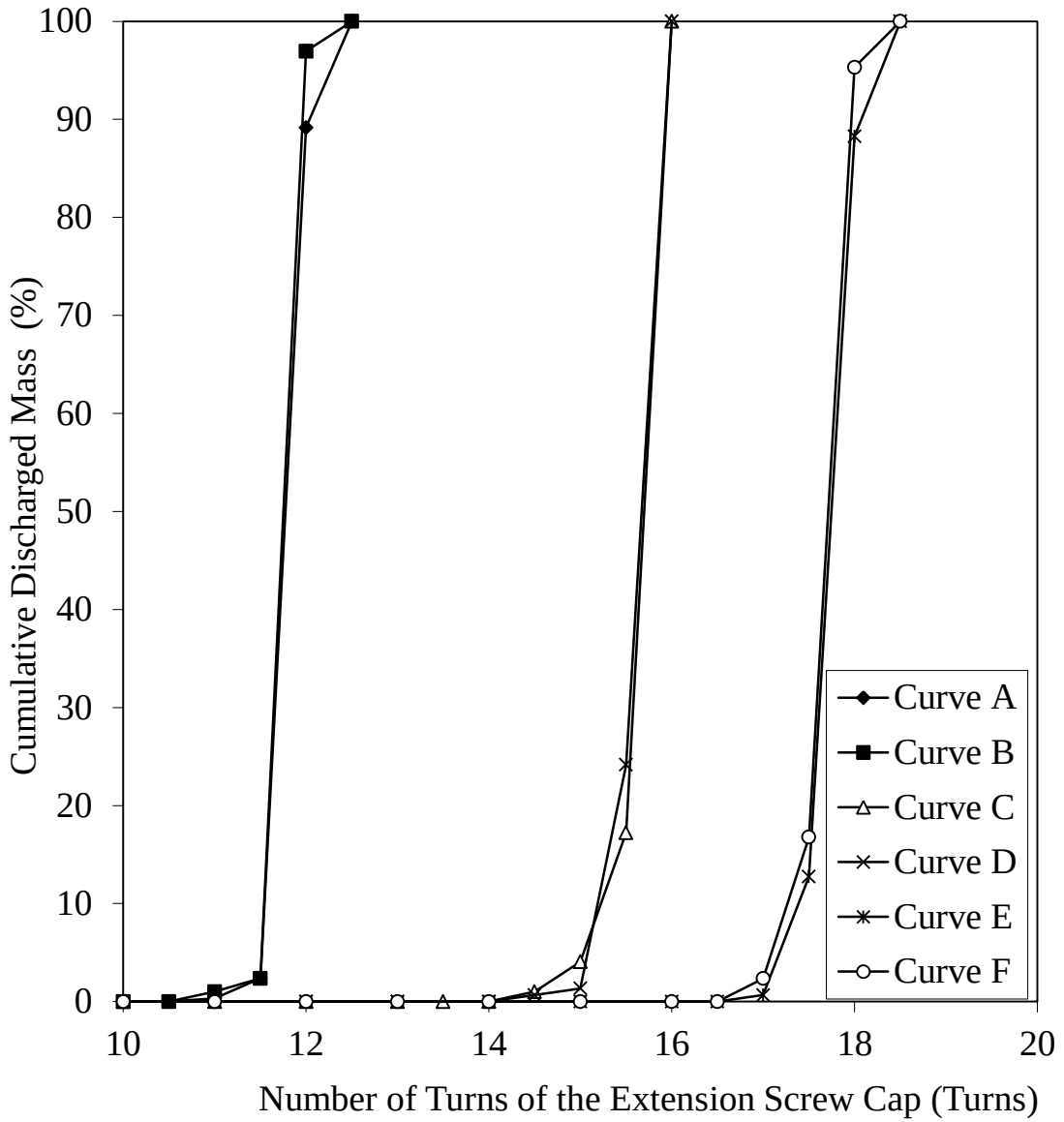

Figure 8.2: Calibration data handheld SPS using 3 g of glass Ballotini in size ranges 600 – 710, 710 – 850 and 850 – 1000 µm.

Curve A: 600 – 710 µm Run 1

Curve B: 600 – 710 µm Run 2

Curve C: 710 – 850 µm Run 1

Curve D: 710 – 850 µm Run 2

Curve E: 850 – 1000 µm Run 1

Curve F: 850 – 1000 µm Run 2

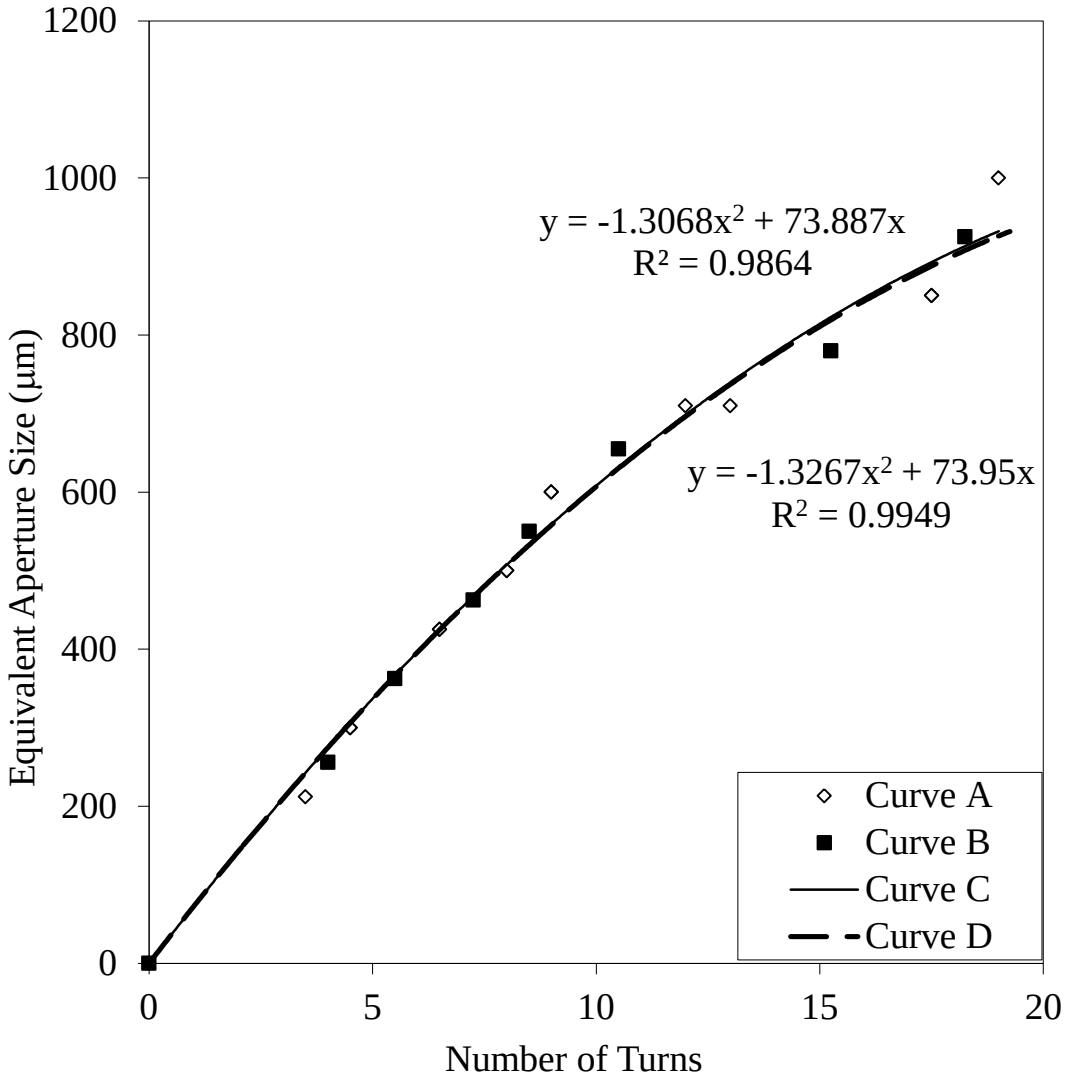

Figure 8.3: Handheld SPS calibration curve correlating number of turns of screw cap with aperture size using glass Ballotini of size range 212 – 1000 µm.

Curve A: Upper and lower size limits

Curve B: Mean sizes

Curve C: Correlated data using upper and lower size limits

Curve D: Correlated data using mean sizes

Figure 8.4 shows the performance evaluation of the handheld SPS using the correlated data obtained from equation 8.2. A 21 g glass Ballotini test powder with size range 212 – 1000 μm was placed into the handheld SPS for analysis. The correlation in equation 8.2 was used as a guide to separate the test powder into seven different size ranges. Each size range was weighed to produce a PSD as shown in figure 8.4. The figure shows the percentage cumulative discharged mass against aperture size. Curve A was obtained using the handheld unit. Curves B and C are repeat runs to demonstrate reproducibility. The corresponding data obtained using sieving is shown by curve D. As it may be observed the data show good agreement with the maximum deviation between the sieve and the spring data being ± 3.5 % of the total sample mass.

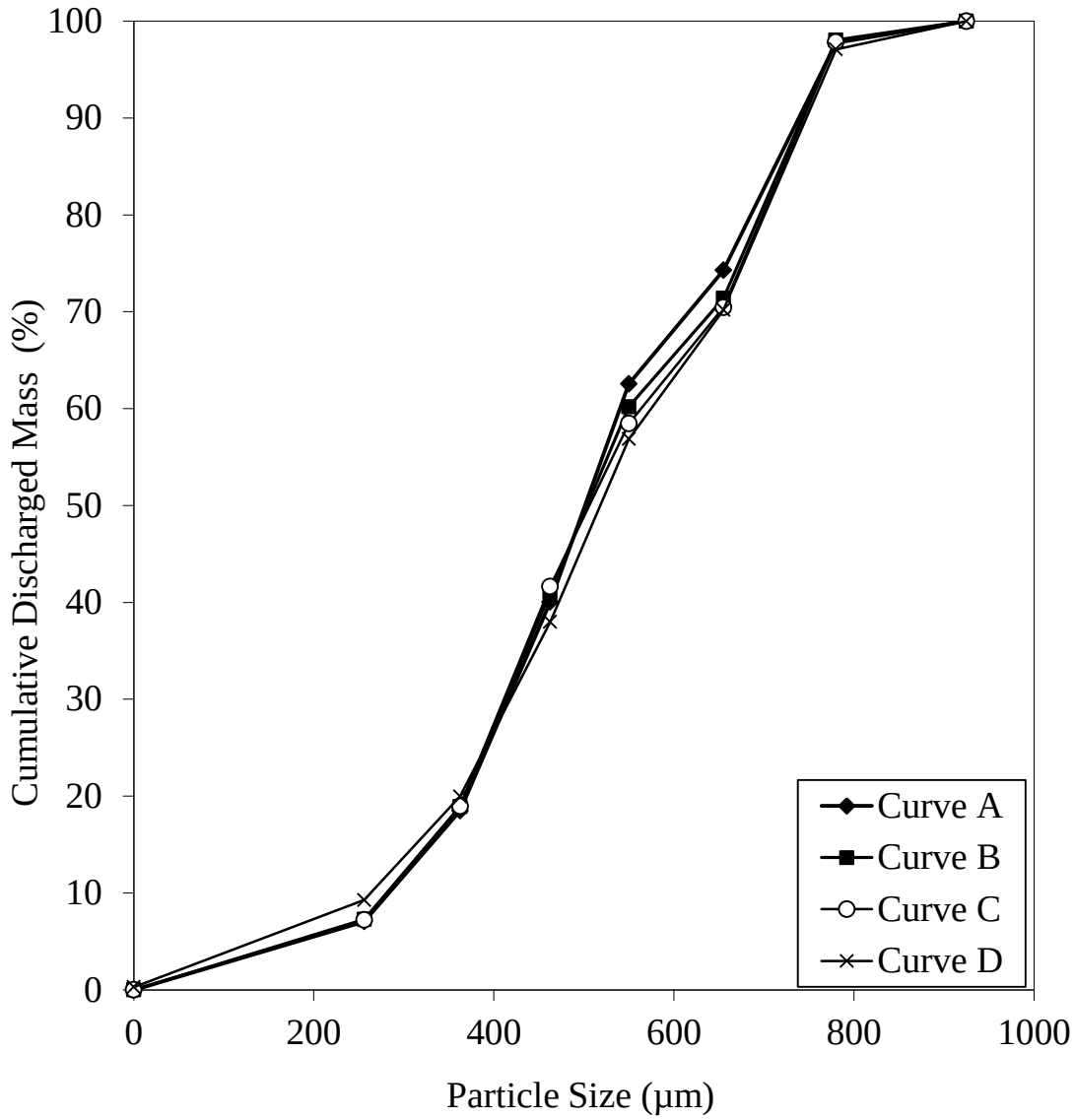

Figure 8.4: Performance evaluation using calibration curve obtained on the handheld SPS for glass Ballotini of size range 212 – 1000 µm.

Curve A: Run 1

Curve B: Run 2

Curve C: Run 3

Curve D: Sieve data

Figures 8.5 to 8.7 show the calibration curves obtained for the three $CaCO_3$ test powders namely LG800 (250 – 1000 µm), LG12 (250 – 1000 µm) and L400 (250 – 600 µm) respectively using the same procedure as described above for the glass Ballotini particles. The sample mass used for each size fraction was 3 g.

The correlations developed for the $CaCO_3$ test powders are given in table 8.1. The maximum deviations between the curves C and D in figures 8.5 to 8.7 are ± 11 µm, ± 5 µm, and ± 13 µm respectively. This therefore shows a very good agreement between the upper/lower size limit and mean size calibration curves in all cases. Hence, either correlation may be used in each case.

Table 8.1: Regression analysis results for calibration of handheld SPS using $CaCO_3$ test powders, LG800, LG12 and L400.

Material ($CaCO_3$)	**Upper & lower size limit correlation (curve C)**	**R^2**	**Mean size correlation (curve D)**	**R^2**
LG800	$y = -1.1479x^2 + 70.491x$	0.9867	$y = -1.1726x^2 + 70.741x$	0.9973
LG12	$y = -0.9042x^2 + 67.131x$	0.9816	$y = -0.8875x^2 + 66.972x$	0.9966
L400	$y = -2.3107x^2 + 76.608x$	0.9610	$y = -1.9763x^2 + 73.199x$	0.9915

Figures 8.8 to 8.10 show results of the performance evaluation for the $CaCO_3$ test powders using their respective mean size calibration curves. The results are shown in terms of percentage cumulative discharged mass from the unit against aperture size, all samples are also analysed using sieves and PSDs are generated to make a comparison. The experiments show a good reproducibility with a maximum deviation $\leq \pm 5$ % of the total mass in all three cases. The $CaCO_3$ particles do not exhibit a specific shape and do not readily flow like the spherically shaped glass Ballotini particles. The most brittle of the $CaCO_3$ samples was the L400 sample, it had the inclination to crumble and subsequently coagulate during agitation.

A maximum deviation of ± 21 %, between the sieve data and the handheld SPS is exhibited by sample L400 (250 – 600 µm). The corresponding deviations for samples LG800 (250 – 1000 µm) and LG12 (250 – 1000 µm) in terms of the total mass, are ± 8 % and ± 5 % respectively.

The main reason for the observed discrepancy between the sieve and the spring data is due to the irregular shape of the $CaCO_3$ particles as compared to the spherical glass Ballotini. Particle attrition during testing may be discounted as a cause given the very good reproducibility of the data. It is postulated that the L400 sample exhibits the maximum deviation against sieve data as compared to the LG800 and LG12 particles due to its highly irregular shape.

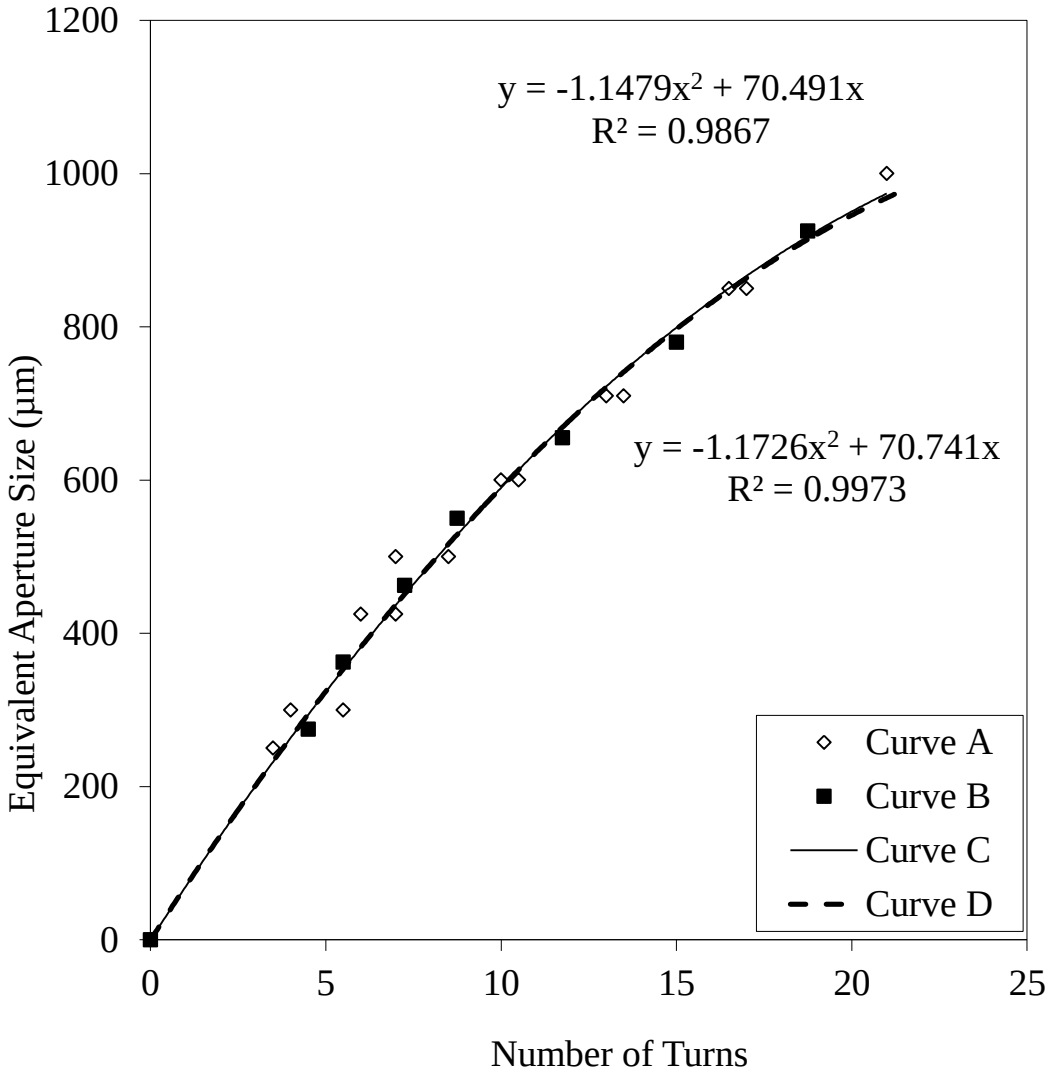

Figure 8.5: Handheld SPS calibration curve for $CaCO_3$ LG800 sample of size range 250 – 1000 µm.

Curve A: Upper and lower size limits

Curve B: Mean sizes

Curve C: Correlated data using upper and lower size limits

Curve D: Correlated data using mean sizes

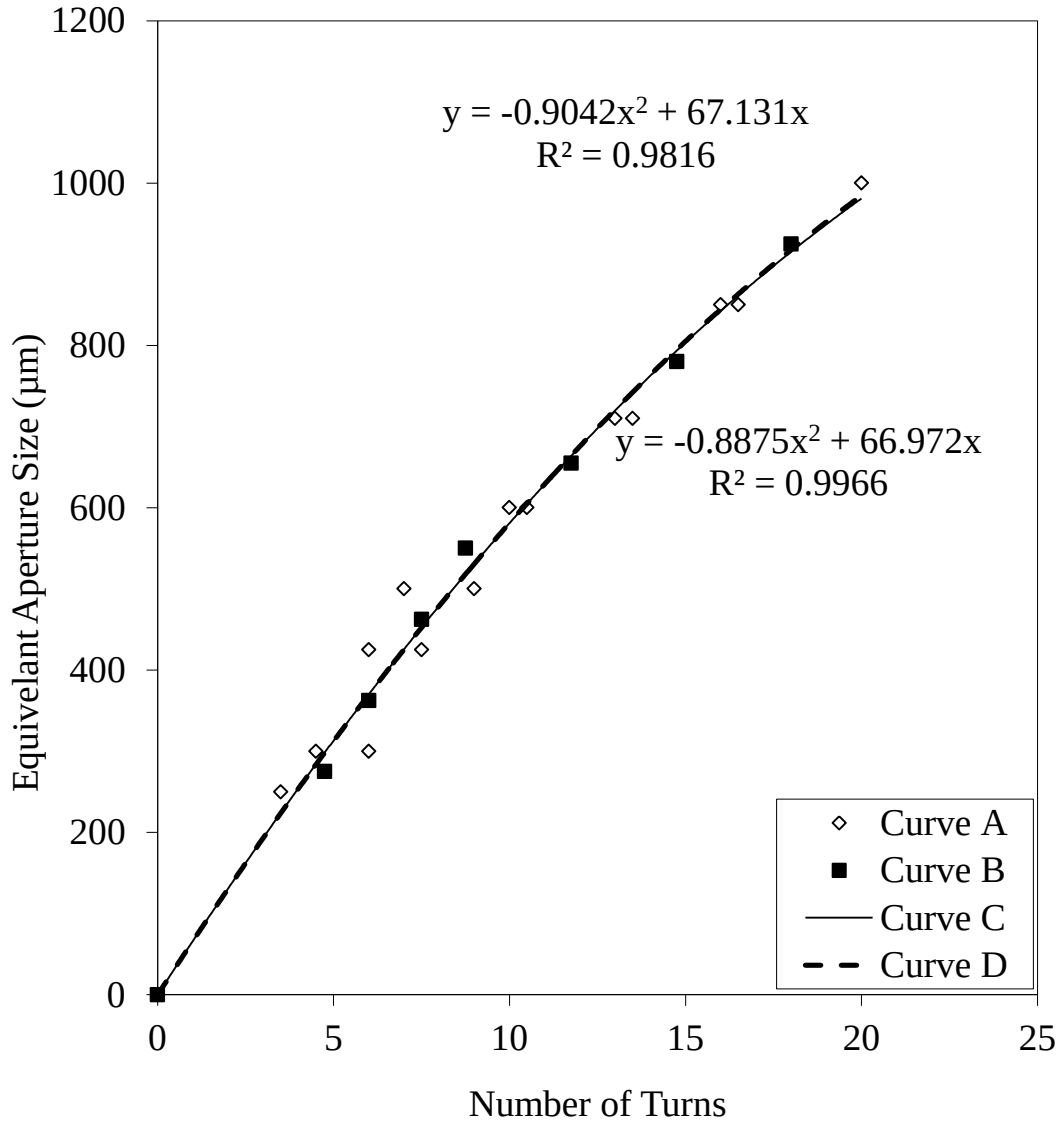

Figure 8.6: Handheld SPS calibration curve for $CaCO_3$ LG12 sample of size range 250 – 1000 µm.

Curve A: Upper and lower size limits

Curve B: Mean sizes

Curve C: Correlated data using upper and lower size limits

Curve D: Correlated data using mean sizes

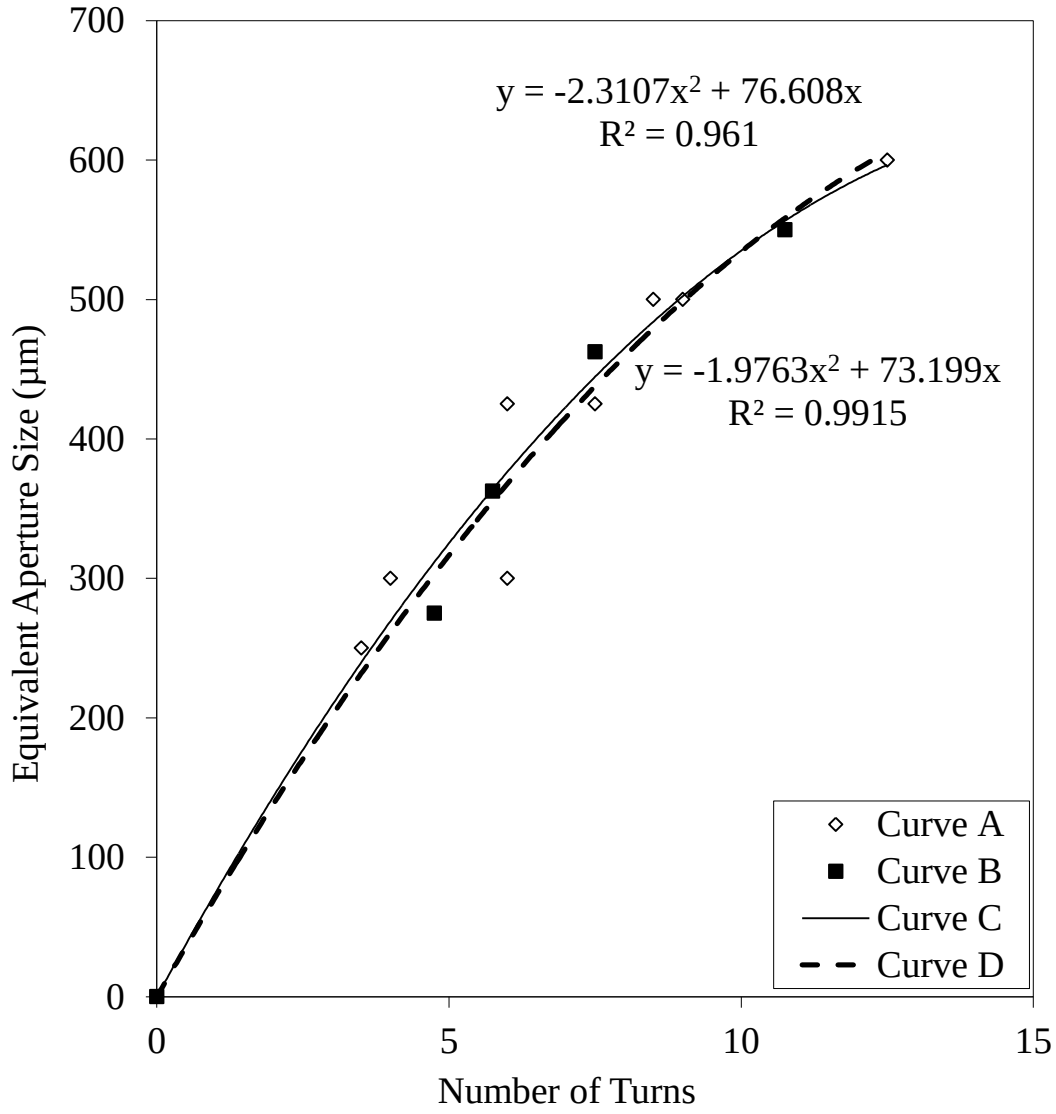

Figure 8.7 Handheld SPS calibration curve for $CaCO_3$ L400 sample of size range 250 – 600 µm.

Curve A: Upper and lower size limits

Curve B: Mean sizes

Curve C: Correlated data using upper and lower size limits

Curve D: Correlated data using mean sizes

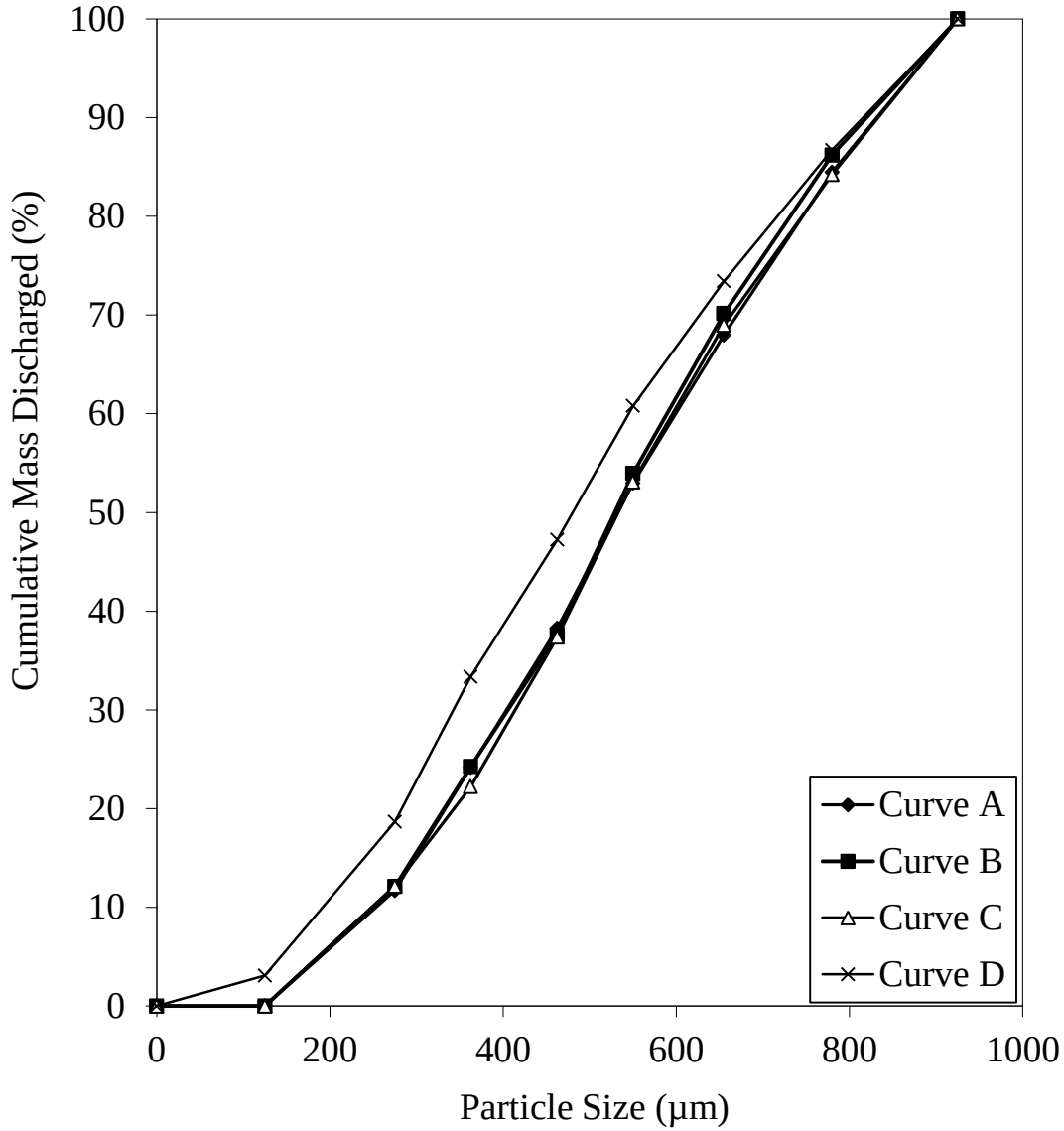

Figure 8.8: Handheld SPS performance evaluation for $CaCO_3$ sample LG800 for size range 212 – 1000 µm.

Curve A: Run 1

Curve B: Run 2

Curve C: Run 3

Curve D: Sieve data

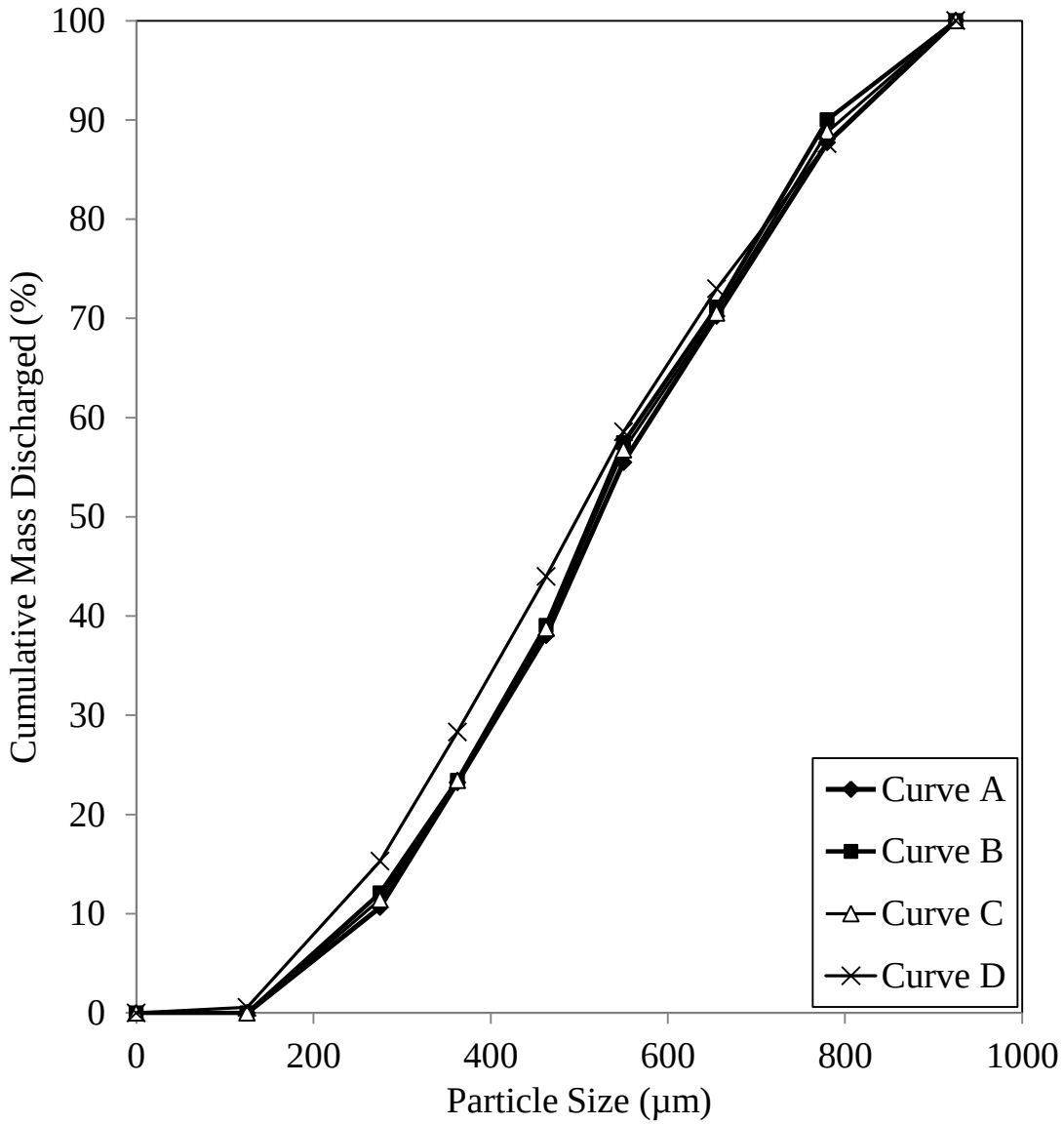

Figure 8.9: Handheld SPS Performance Evaluation for $CaCO_3$ Sample LG12 (212 – 1000µm).

Curve A: Run 1

Curve B: Run 2

Curve C: Run 3

Curve D: Sieve data

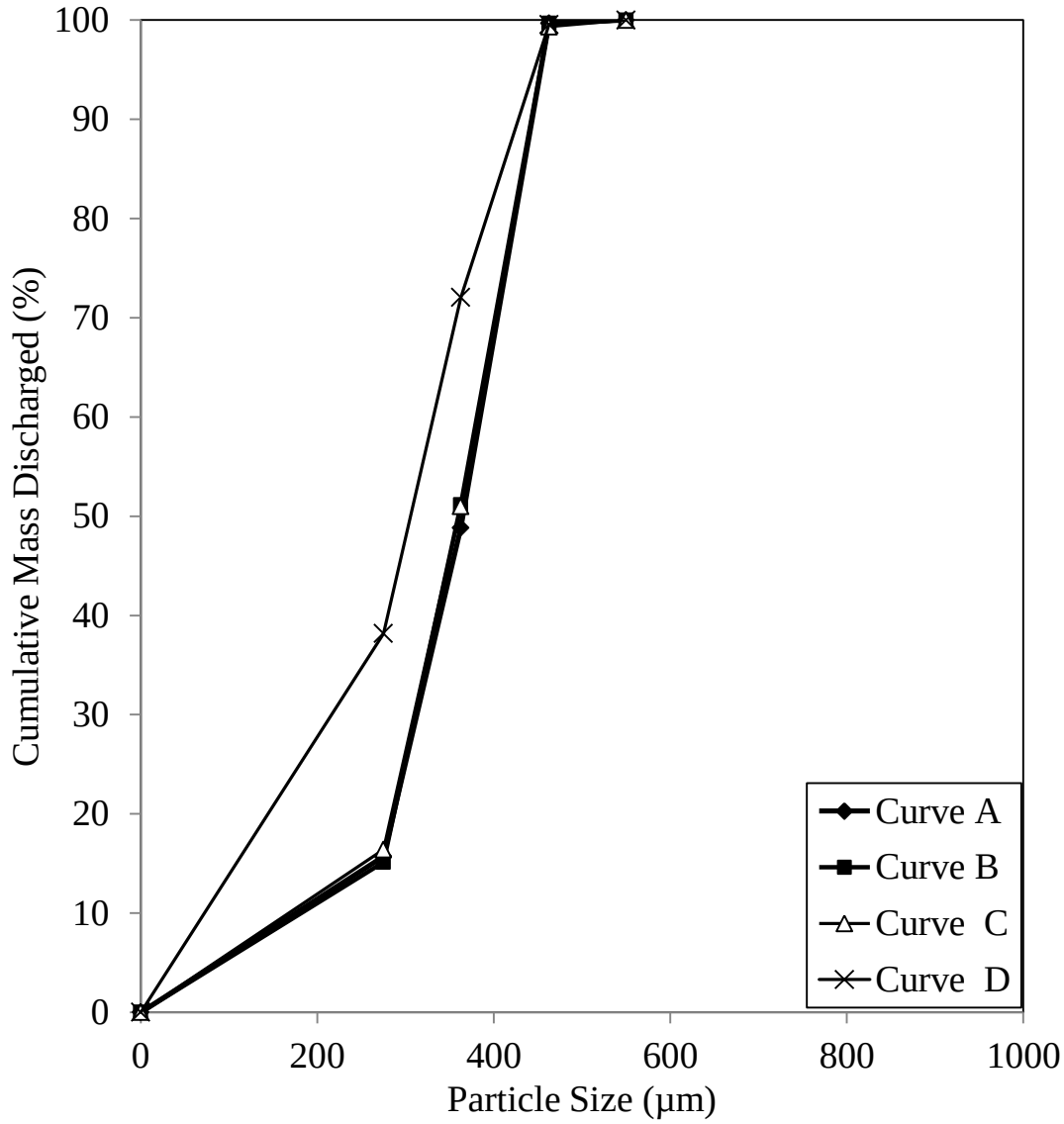

Figure 8.10: Handheld SPS Performance Evaluation for $CaCO_3$ Sample L400 (250 – 600 µm).

Curve A: Run 1

Curve B: Run 2

Curve C: Run 3

Curve D: Sieve data

8.2 Volume to Mass Calibration

The following describes the results of a series of experiments for directly determining the particle discharged mass from the handheld SPS, by recording the bed height or volume of the test powder collected in the graduated sample collector (see figure 4.7).

Glass Ballotini test powders of different size ranges, i.e. 212 – 300, 300 – 425, 425 – 500, 500 – 600, 600 – 710, 710 – 850 and 850 – 1000 μm are used in the study.

Figure 8.11 shows the variation of sample mass measured using a laboratory mass balance-(OHAUS Explorer E1RW60: with ±0.01g resolution), plotted against sample volume for 212 – 300 μm glass Ballotini using the handheld SPS. The test is repeated twice to verify its reproducibility as shown by curves A, B and C. Excellent agreement between the three sets of data is obtained producing a maximum mass irreproducibility of ± 0.24 g.

Curve D shows the correlated data obtained from the average of the three runs. The corresponding fitted line equation is given by:

$$y = 1.7095x \qquad (8.3)$$

Where, y is the mass of the test powder from the spring (g) and x is the volume of the test powder collected (cm^3). The corresponding correlation coefficient is 0.9998.

To verify the correlation obtained from figure 8.11, various masses of up to 15 g of powder discharged from the spring were weighed and the volumes were recorded. The test was repeated to confirm its reproducibility. Figure 8.12 shows the results obtained, illustrating the variation of volume with mass for glass Ballotini of size range 212 – 300 μm. Figure 8.13 shows the predicted data using the correlation obtained (i.e. equation 8.1) and the average of the actual data obtained for glass Ballotini (212 – 300 μm) extracted from figure 8.12. The maximum deviation between the predicted data and actual data is ± 0.1 g.

The same tests were carried out for other size ranges 300 – 425, 425 – 500, 500 – 600, 600 – 710, 710 – 850 and 850 – 1000 µm. Table 8.2 shows the correlations developed for all size ranges tested. Figures 8.14 to 8.19 show the comparison of predicted data and actual data for each size range mentioned above. It can be seen that there is a very small deviation between the predicted and actual data in all cases.

Table 8.2: Correlations for volume to mass conversions in handheld SPS for glass Ballotini of different size ranges

Size Range (µm)	Correlation	R^2
212 – 300	$y = 1.7095x$	0.9998
300 – 425	$y = 1.7206x$	0.9993
425 – 500	$y = 1.7394x$	0.9996
500 – 600	$y = 1.5999x$	0.9996
600 – 710	$y = 1.6162x$	0.9994
710 – 850	$y = 1.5897x$	0.9997
850 – 1000	$y = 1.6483x$	0.9985

Table 8.3 shows the average and maximum deviations between the predicted data obtained using the correlation developed for each size range and the actual observed data. It is clear that the correlated data is in close agreement to the observed data, the overall average deviation is ± 0.12 g, which is almost negligible in comparison to the overall mass used (15 g), ca. ± 0.8 %. The overall maximum deviation of ± 0.48 g was observed for 425 – 500 µm, which may be due to experimental errors, e.g. human errors, optical errors (e.g. incorrect reading of graduation on Perspex tube).

It is therefore clear that using the volume occupied in the sample collector is an excellent tool for direct mass determination in the handheld SPS.

Table 8.3: Deviations from the predicted data obtained from correlations and actual observed data for volume to mass conversions in handheld SPS using glass Ballotini.

Size Range (µm)	Average deviation between predicted and actual data (g)	Maximum deviation between predicted and actual data (g)
212 – 300	± 0.08	± 0.19
300 – 425	± 0.07	± 0.12
425 – 500	± 0.28	± 0.48
500 – 600	± 0.03	± 0.19
600 – 710	± 0.11	± 0.17
710 – 850	± 0.08	± 0.16
850 – 1000	± 0.22	± 0.41

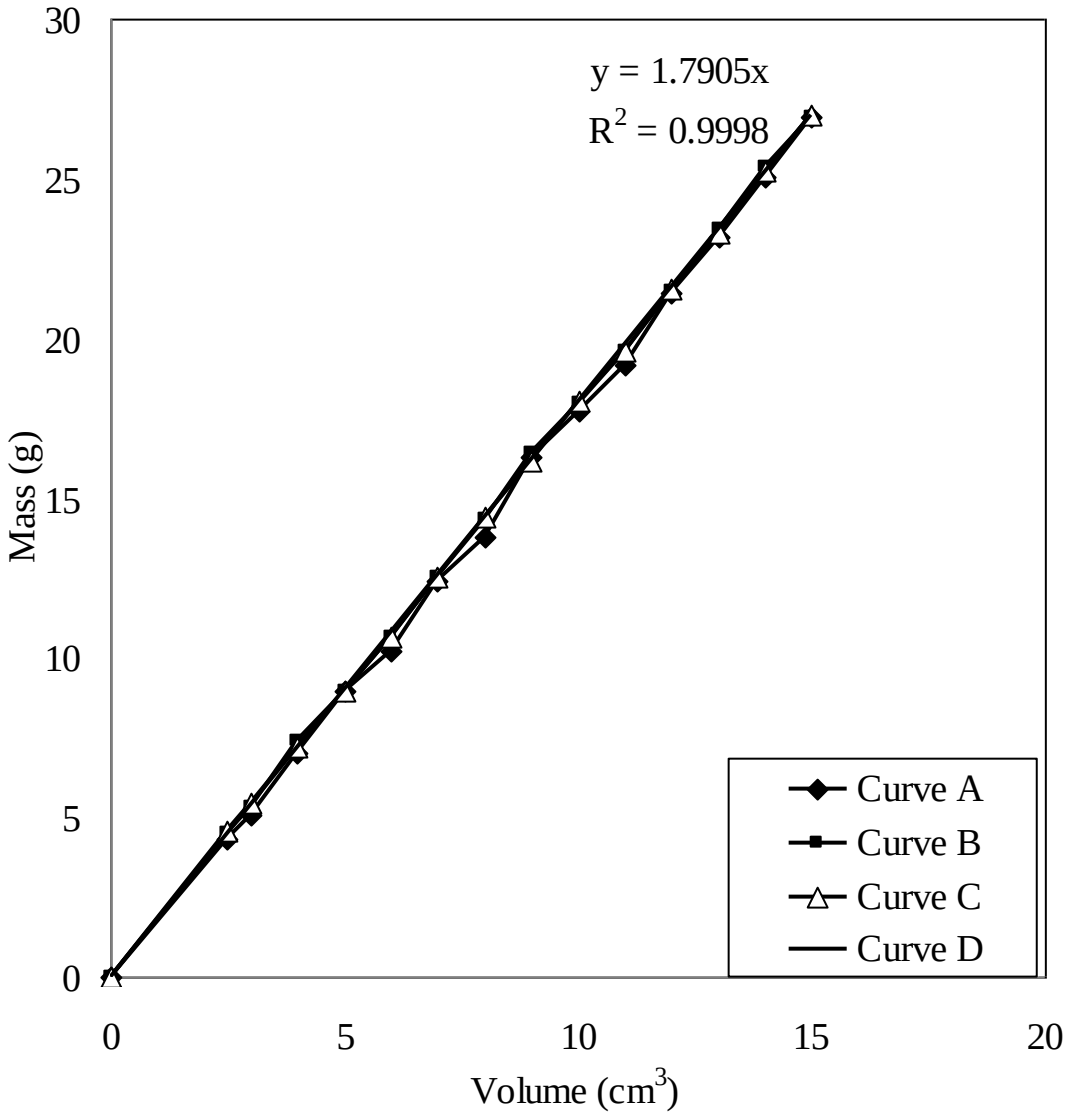

Figure 8.11: Variation of mass with volume for glass Ballotini of size range 212 – 300 µm in the handheld SPS.

Curve A: Run 1

Curve B: Run 2

Curve C: Run 3

Curve D: Correlated data obtained from the average of runs 1, 2 and 3

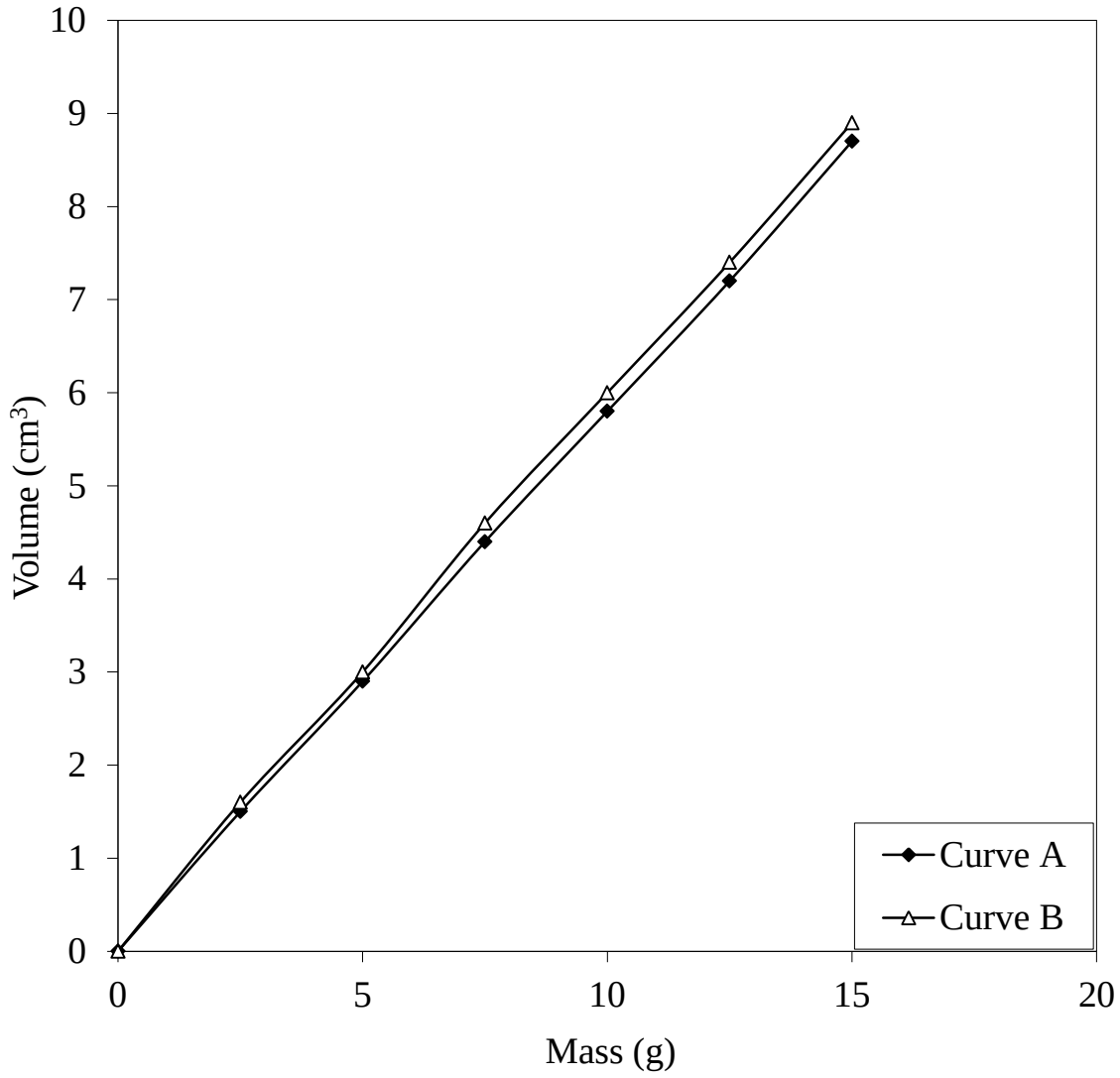

Figure 8.12: Variation of volume with mass for glass Ballotini of size range 212 – 300 μm in the handheld SPS.

Curve A: Run 1

Curve B: Run 2

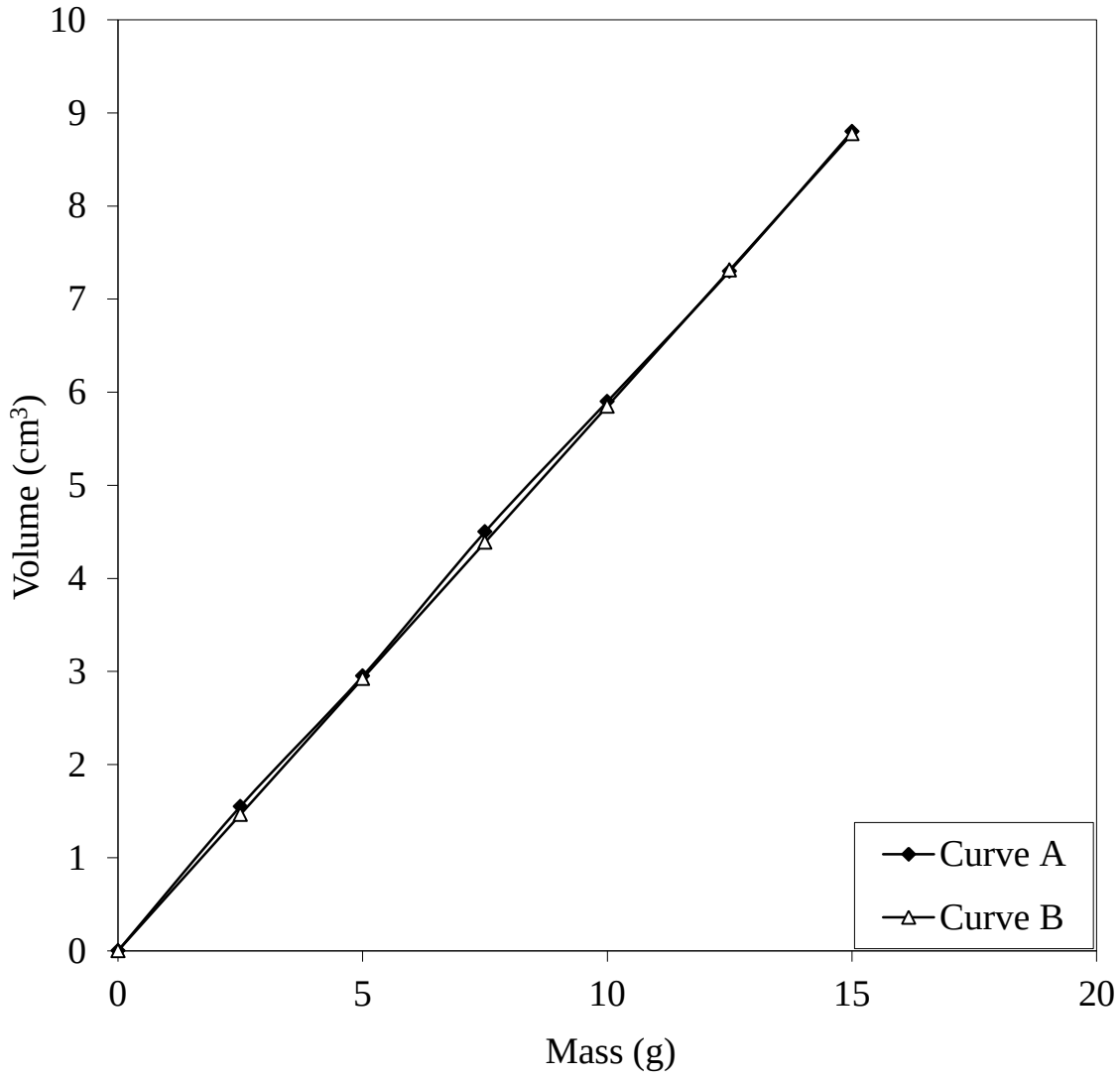

Figure 8.13: Variation of volume with mass in handheld SPS, a comparison of predicted data and actual data obtained for volume to mass calibration using glass Ballotini of size range 212 – 300 µm.

Curve A: Actual data

Curve B: Predicted data from correlation

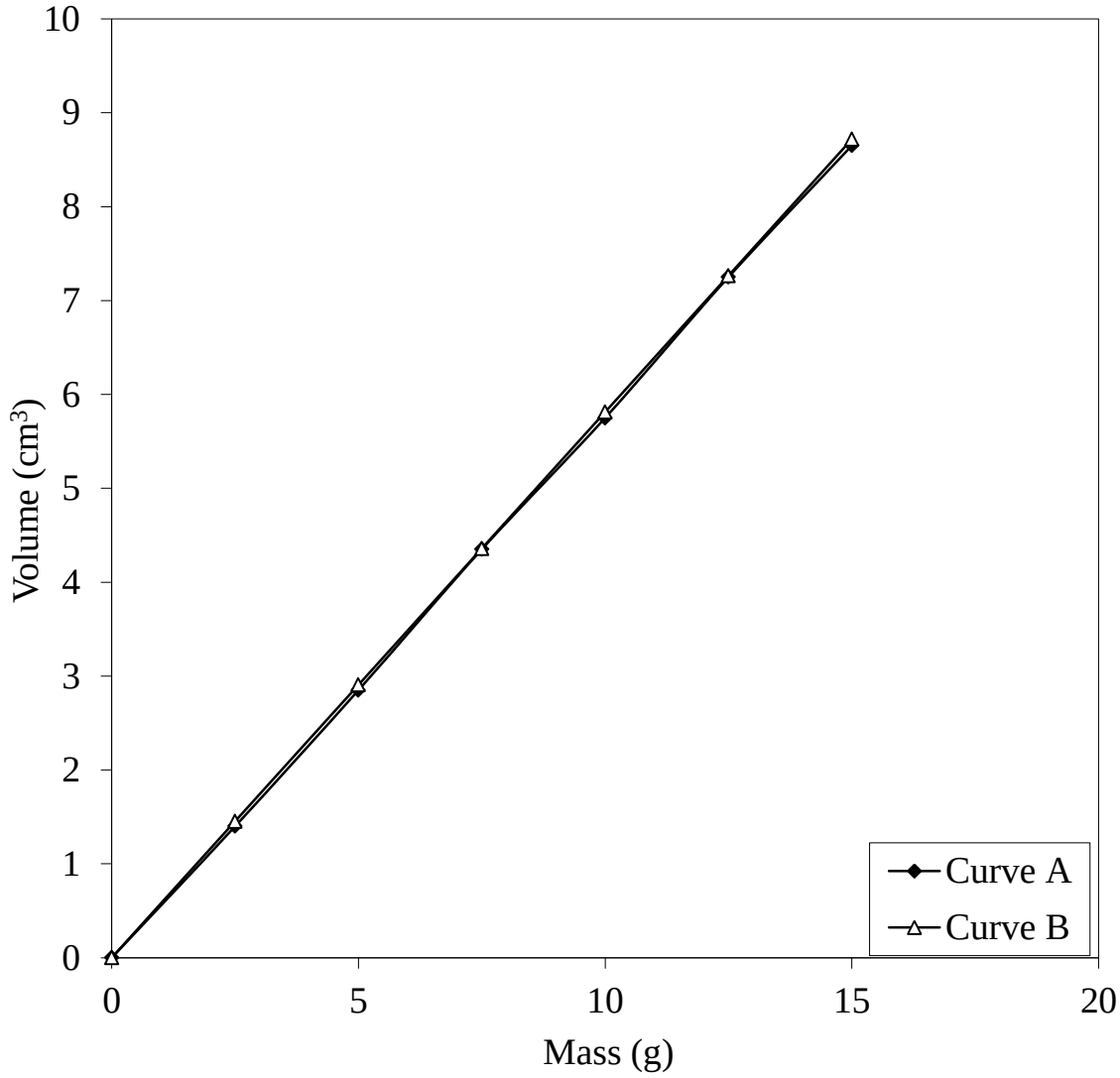

Figure 8.14: Variation of volume with mass in handheld SPS, a comparison of predicted data and actual data obtained for volume to mass calibration using glass Ballotini of size range 300 – 425 µm.

Curve A: Actual data

Curve B: Predicted data from correlation

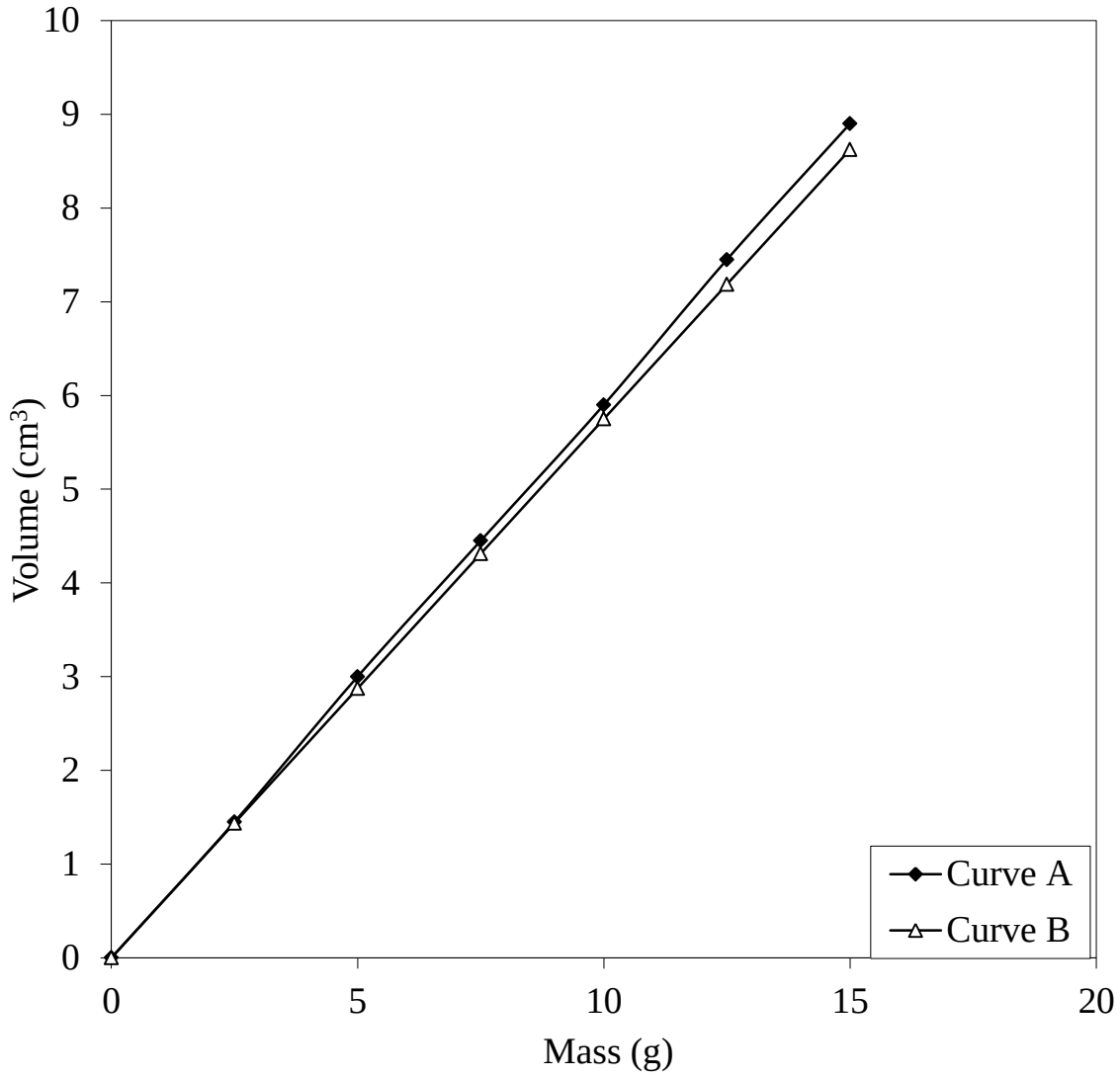

Figure 8.15: Variation of volume with mass in handheld SPS, a comparison of predicted data and actual data obtained for volume to mass calibration SPS using glass Ballotini of size range 425 – 500 µm.

Curve A: Actual data

Curve B: Predicted data from correlation

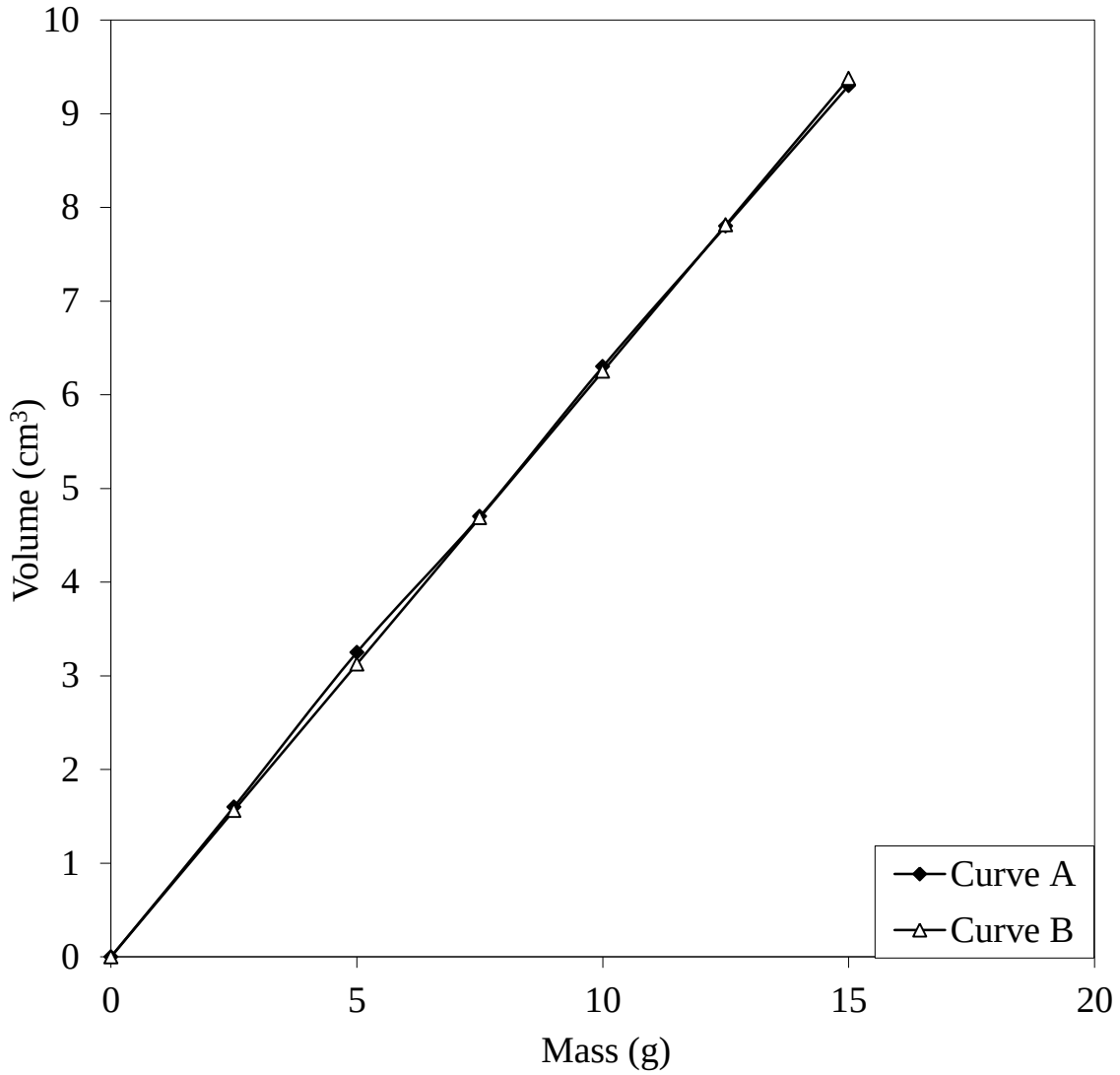

Figure 8.16: Variation of volume with mass in handheld SPS, a comparison of predicted data and actual data obtained for volume to mass calibration SPS using glass Ballotini of size range 500 – 600 µm.

Curve A: Actual data

Curve B: Predicted data from correlation

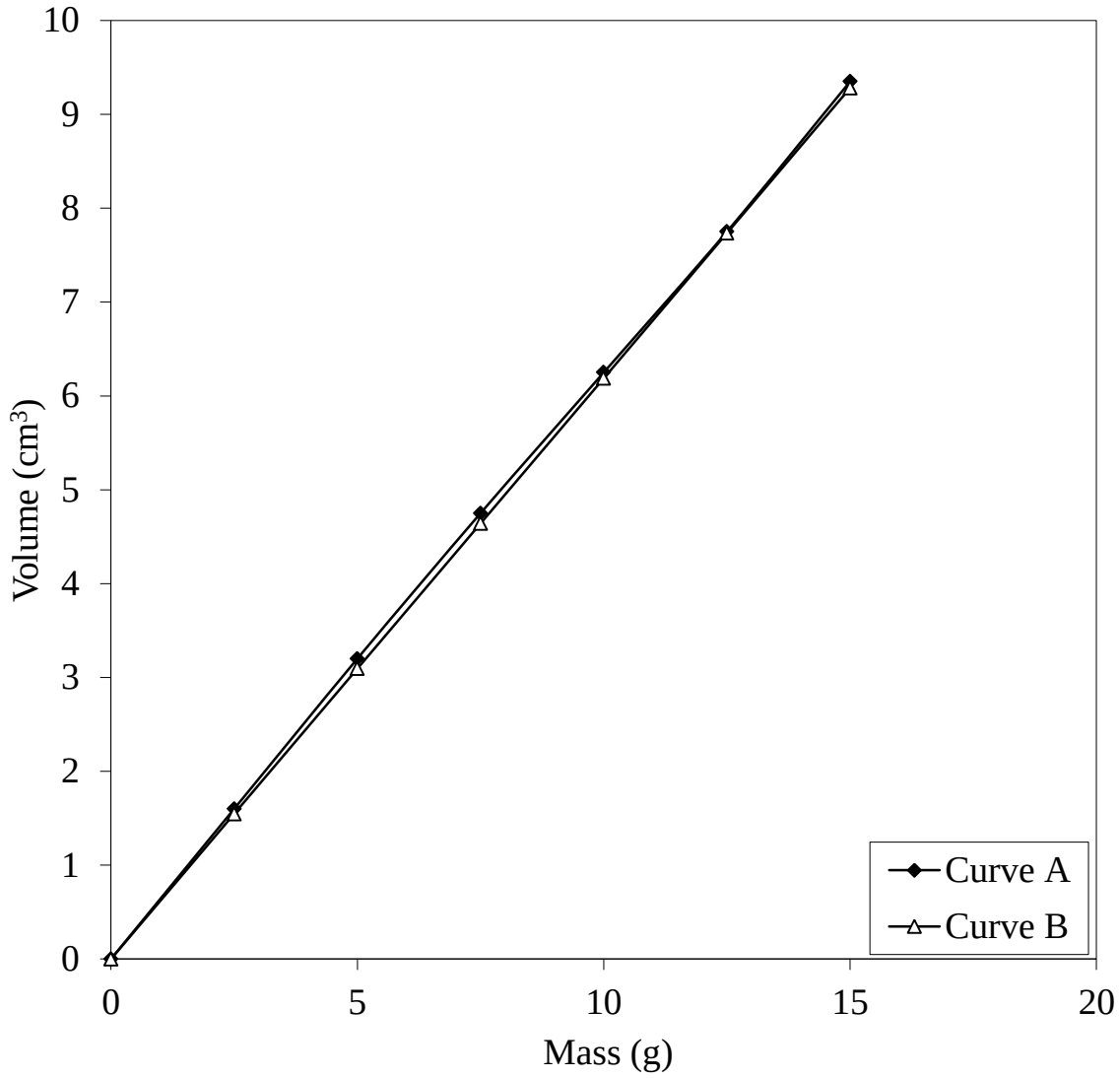

Figure 8.17: Variation of volume with mass in handheld SPS, a comparison of predicted data and actual data obtained for volume to mass calibration using glass Ballotini of size range 600 – 710 µm.

Curve A: Actual data

Curve B: Predicted data from correlation

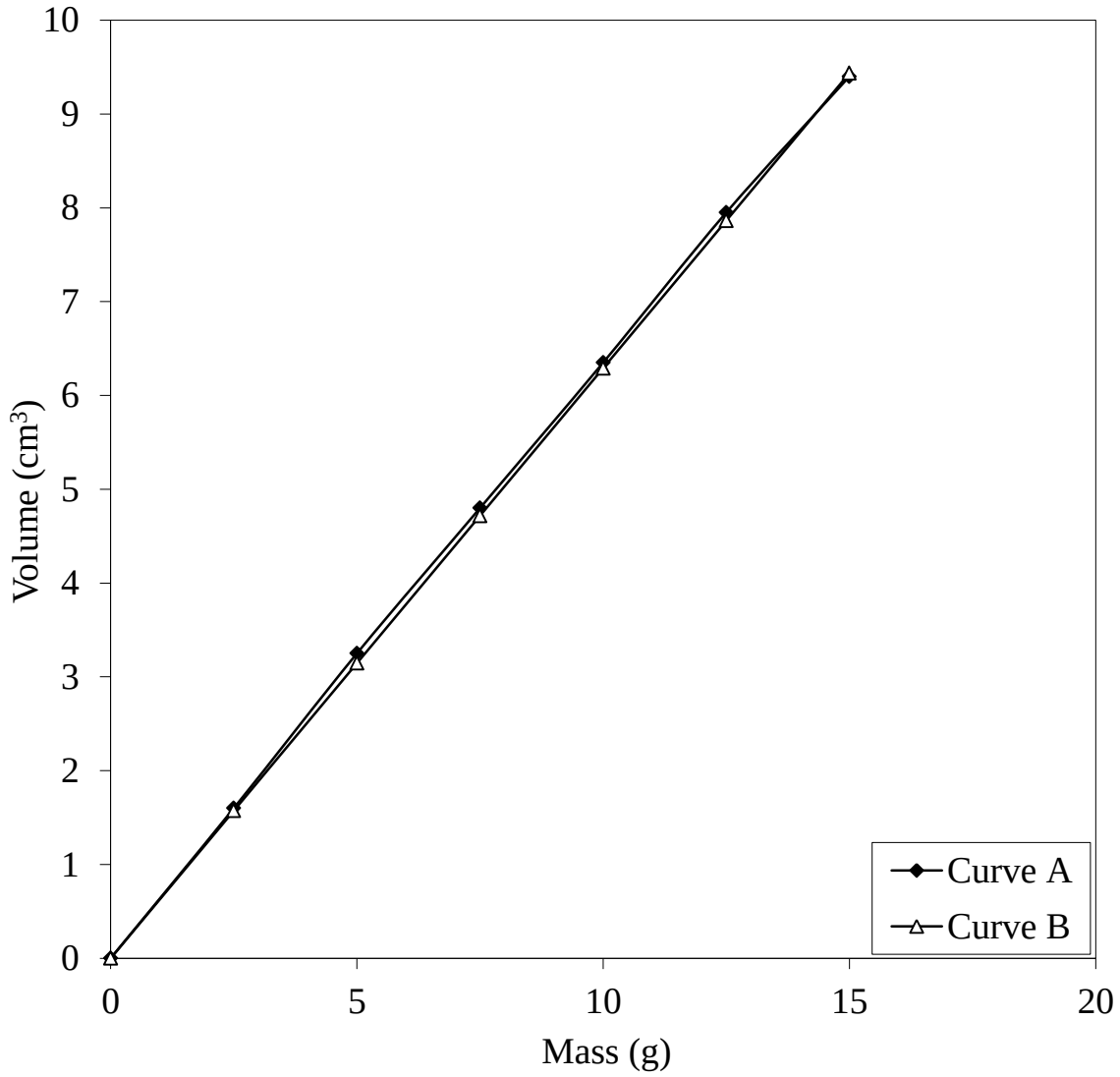

Figure 8.18: Variation of volume with mass in handheld SPS, a comparison of predicted data and actual data obtained for volume to mass calibration using glass Ballotini of size range 710 – 850 µm.

Curve A: Actual data

Curve B: Predicted data from correlation

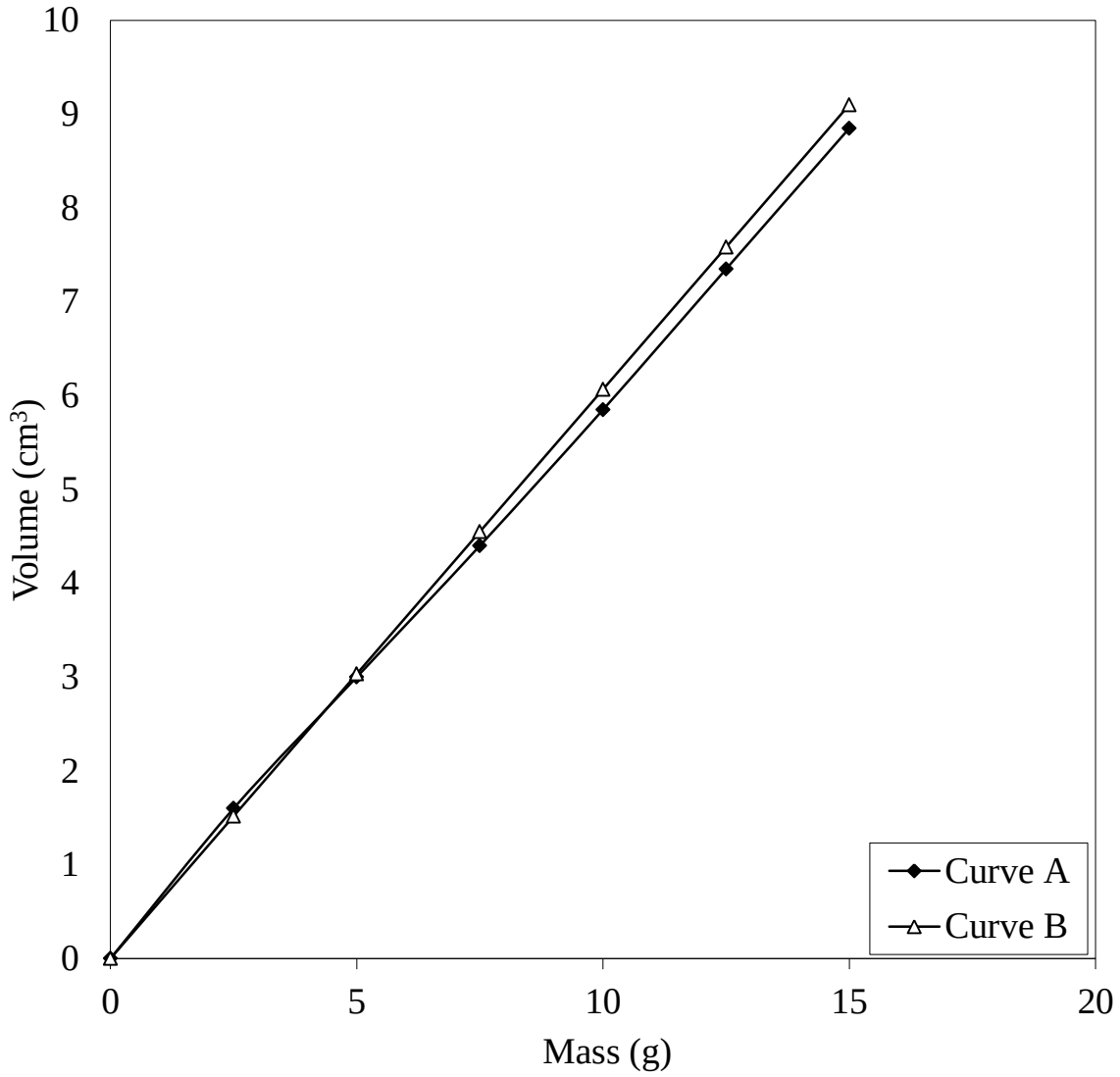

Figure 8.19: Variation of volume with mass in handheld SPS, a comparison of predicted data and actual data obtained for volume to mass calibration using glass Ballotini of size range 850 – 1000 µm.

Curve A: Actual data

Curve B: Predicted data from correlation

8.3 Effect of Agitation Mode on Analysis Time and PSD Accuracy

The following describes the results obtained from experiments aimed at studying the effect of agitation mode on analysis time and PSD accuracy using the handheld SPS. The agitation modes tested include hand shaking and the use of a specially designed variable speed tumbler as shown in figure 8.20. The tumbler consists of a 12 V geared DC motor (2947/GS38 supplied by RS Components Limited, 2011) producing an output speed of approx. 260 revolutions per minute (rpm), a driving wheel (87 mm o.d), and four idler wheels (75 mm o.d), on which the unit was placed upon. The test powder used in the investigation was a 10 g sample of glass Ballotini in the size range of 300 – 425 µm. To discharge the sample, the spring was stretched by 6.5 turns to create a spring aperture size of 425 µm. The handheld SPS was then placed on the variable speed tumbler between the idler wheels and driving wheel. A flange was placed on the handheld SPS to prevent the unit from sliding off the tumbler. The rotational speed was set to 100 rpm and the discharged sample mass was recorded every minute. The test was repeated for various rotational speeds of 200, 300, 400 and 500 rpm and using manual hand shaking.

Figure 8.21 shows the variation of percentage cumulative discharged mass from the handheld SPS with time for various rotational speeds. The data taken from 100 rpm and manual shaking give the slowest end-point at 27 and 16 minutes respectively. 500 rpm resulted in the fastest end-point of 3 minutes, while a constant time of 6 minutes was observed for 300 and 400 rpm. It is clear that the analysis time is dependent on the rotational speed employed, where the discharge rate increases with revolutions per minute.

The objective of the second test was to determine the effect of rotational speed on the PSD accuracy. The test involved the use of a 10 g sample of glass Ballotini test powder, containing 5 g of 300 – 425 µm and 425 – 500 µm each. The spring is extended to an equivalent aperture size of 425 µm and rotated at 100 rpm using the variable speed tumbler. In this case, the time taken to discharge 5 g of 300 – 425 µm was recorded. The test was again repeated for various voltage settings of 200, 300, 400 and 500 rpm and using manual hand shaking.

Figure 8.22 shows the variation of percentage cumulative discharged mass from the handheld SPS with time for various rotational speeds. The thick line at 100 % corresponds to when the particles ≤ 425 μm (the handheld SPS apertures at 6.5 turns of the screw cap) are expected to discharge. Based on the data, 400 rpm and 500 rpm discharge the test powder the quickest. However, rotating the handheld SPS at these settings for over 3 minutes, results in early discharge of particles (i.e. particles coming out at a smaller aperture size than they should), leading to PSD inaccuracy. Rotational speeds below 400 rpm and manual shaking exhibit no PSD inaccuracies due to early discharge, with 200 – 300 rpm reaching the target line in 3 – 5 minutes. On the other hand, 100 rpm and manual shaking demonstrate extended analysis times of 13 and 9 minutes respectively. Hence, it may be concluded that the analysis time and PSD accuracy is significantly dependent on the rotational speed employed. The fastest and easiest method without causing early discharge is the use of the variable speed tumbler at a speed setting between 200 – 300 rpm.

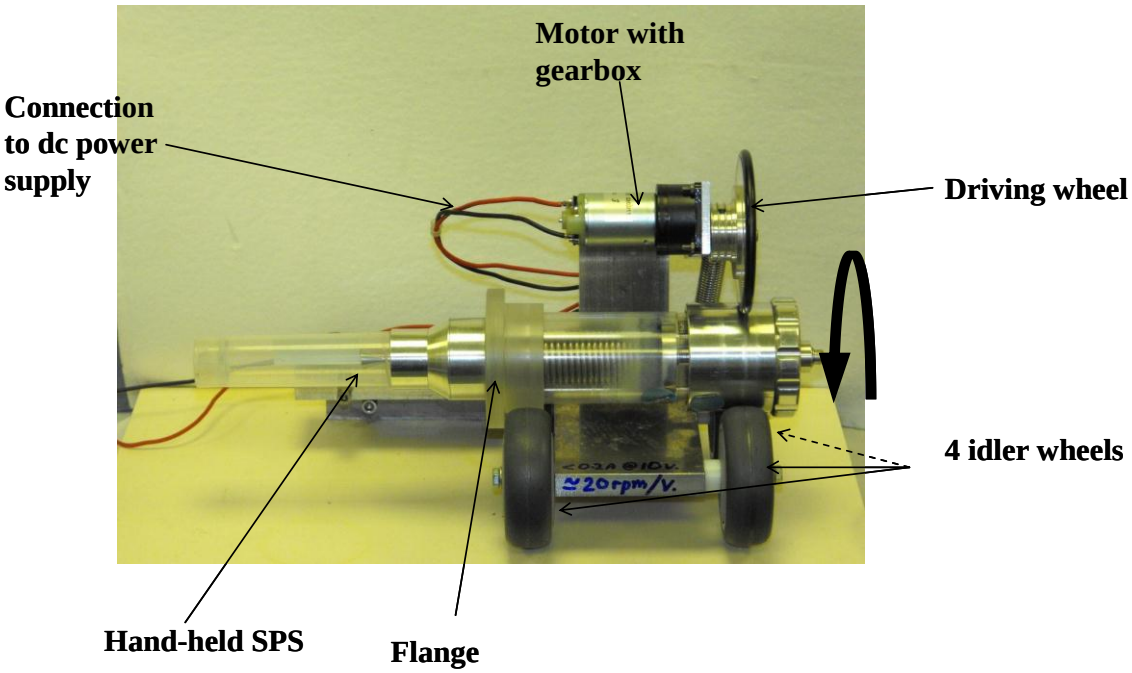

Figure 8.20: Photograph illustrating the tumbler unit used to rotate the handheld SPS for particle size analysis.

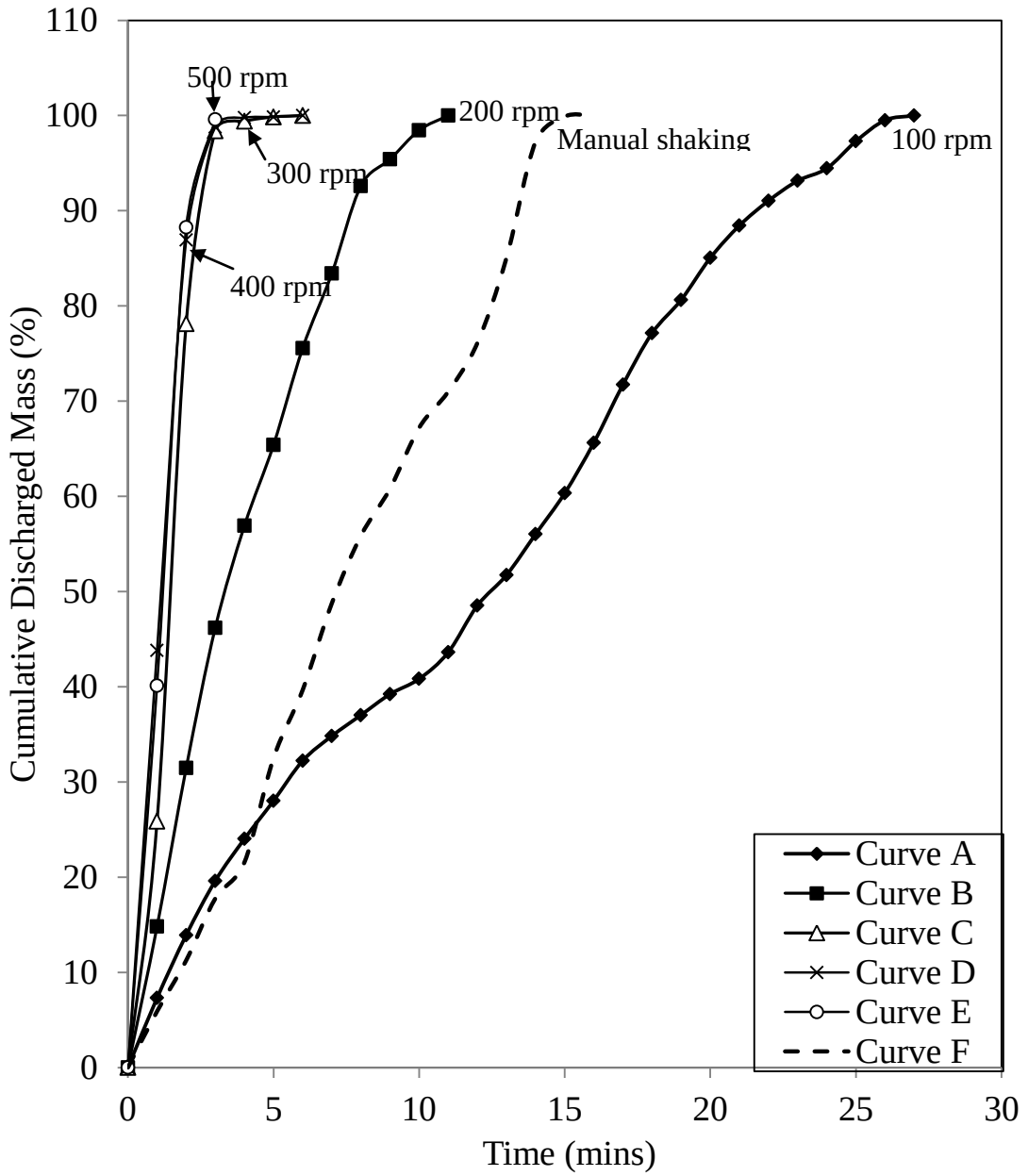

Figure 8.21: Variation of percentage discharged mass with time for different modes of agitating the handheld SPS using glass Ballotini of size range of 300 – 425 µm

Curve A: 100 rpm

Curve B: 200 rpm

Curve C: 300 rpm

Curve D: 400 rpm

Curve E: 500 rpm

Curve F: Manual shaking

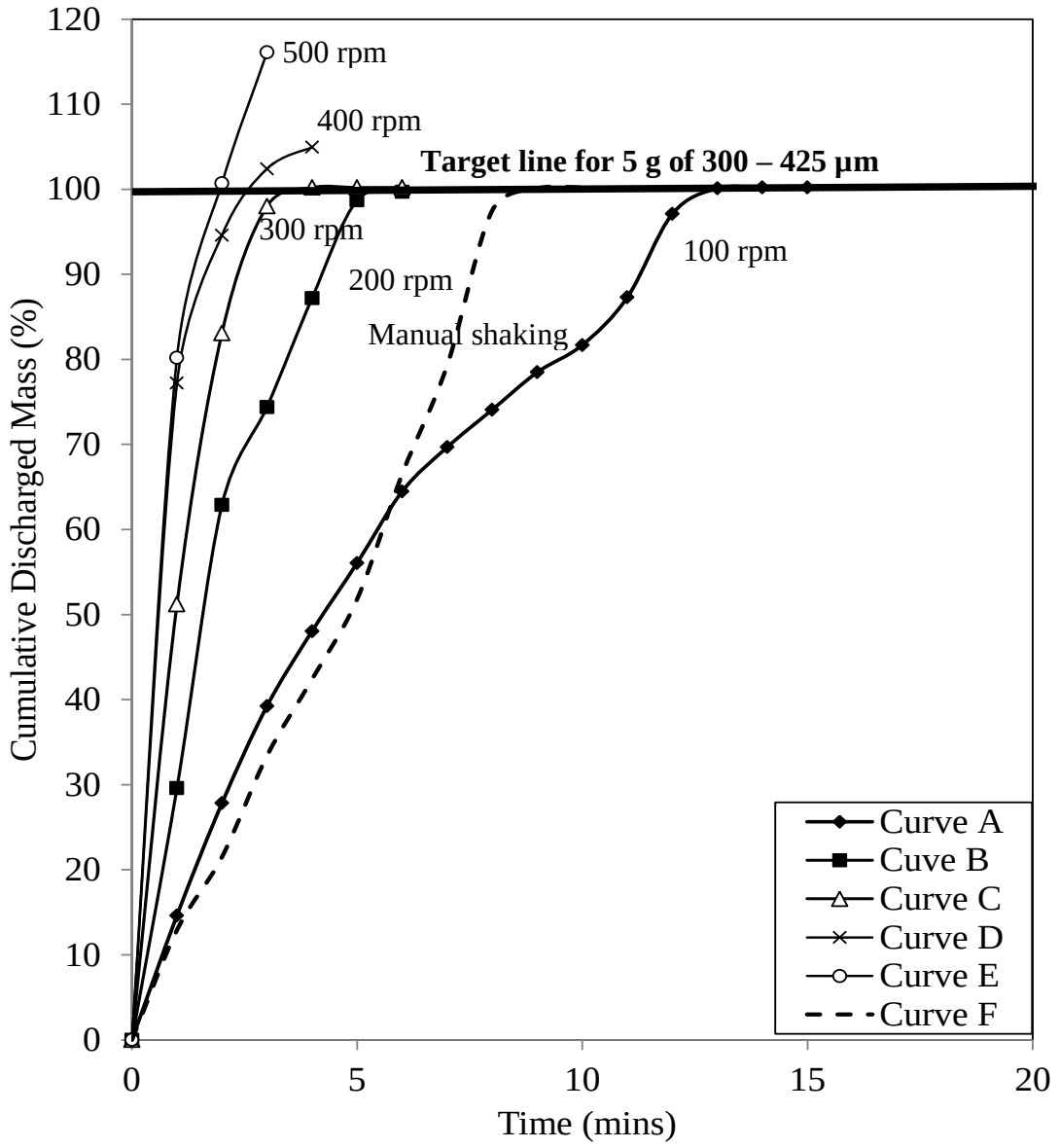

Figure 8.22: Variation of percentage discharged mass with time for different modes of agitating the handheld SPS to demonstrate PSD accuracy using glass Ballotini of size range of 300 – 500 µm.

Curve A: 100 rpm

Curve B: 200 rpm

Curve C: 300 rpm

Curve D: 400 rpm

Curve E: 500 rpm

Curve F: Manual shaking

8.4 Conclusions

The handheld SPS is primarily aimed for quality control applications where a relatively rapid manual PSD measurement is required during the powder production process.

In this chapter, an experimental evaluation of the handheld SPS was carried out using different size ranges of glass Ballotini and $CaCO_3$ samples. This involved the development of a correlation for the spring aperture size as a function of the number of turns of the handheld SPS screw cap. This was based on a polynomial regression of the cumulative mass of a certain size range discharged from the spring. Using the correlation developed a performance evaluation was carried out for each powder type and compared to sieve data. Results for glass Ballotini show an excellent reproducibility and good agreement with sieve data with a maximum deviation of ± 3.5 % in terms of the total mass. For the $CaCO_3$ powders, the largest deviation from sieve data is exhibited by L400 with a deviation of ± 21 %, while for LG800 and LG12 ± 8 % and ± 5 % respectively. In addition, all tests for the $CaCO_3$ powders show a reproducibility of $\leq$ ± 5 %.

To eliminate the need to weigh each discharged sample from the handheld SPS, a direct volumetric method of mass measurement is required from the Perspex collection tube. Volume to mass conversions were carried out to develop calibration curves for glass Ballotini powder of different size ranges. All predicted data obtained using calibration curves developed are in good agreement to actual observed data, with an average deviation of ± 0.12 g. Therefore, this method may be used for direct mass measurement in the handheld SPS.

The effect of rotational speed using a tumbler and manual shaking on sample analysis time and PSD accuracy were presented. Based on the data it was concluded that the analysis time and PSD accuracy are significantly dependent on the rotational speed employed. The fastest and easiest method, without causing early discharge, is the use of the variable speed tumbler at a speed between 200 – 300 rpm.

CHAPTER 9 CONCLUSIONS AND FUTURE WORK

9.1 Conclusions

The testing and optimisation of two analytical instruments, a pneumatic device and a handheld unit for Particle Size Distribution (PSD) analysis were presented. Both instruments share the same basic principle of operation involving the use of a spring for the PSD analysis of dry powders in the size range of 100 – 2000 μm.

During the past decade, Mahgerefteh and his co-workers at UCL developed the Pneumatic Spring Particle Sizer (PSPS) in response to a need for a simple to operate and robust inexpensive automated instrument primarily aimed at addressing some of the drawbacks of commonly used PSD instruments. The handheld SPS on the other hand is a portable device designed to provide on the spot analysis for quality control purposes.

The PSPS has encountered a number of fundamentally important design and operational limitations, which have hindered its commercial success. Major problems include sample retention primarily through static charge build up by the fluidising air stream in addition to accumulation of particles in crevices and joints along the structure of the PSPS. This consequently leads to errors in the PSD due to sample loss. The lack of an in-situ mass measurement system has limited its use for on-line applications. Other weaknesses include non-uniform spring coil openings, relatively low size resolution, inability to fabricate spring with the same extension characteristics thus requiring specific calibration and long analysis time.

This thesis presented the results of a series of experiments and fundamental design modifications aimed at addressing the above limitations.

Chapter 2 discussed a number of definitions used to characterise particles. The knowledge of particulate characteristics is essential for the manufacturing, handling and application of all particulate-based materials. Most particulate materials consist of irregular shaped particles thus, giving rise to complications in classifying individual particles into certain sizes. Several

methods are used to specify an equivalent diameter, based on volume, mass, surface or linear dimensions. As shown in chapter 2, for most practical applications, a particle size distribution can be used to characterise the range of particle sizes within a test powder.

Chapter 3 reviewed some of the most common techniques used for PSD analysis together with their advantages and limitations. It was concluded that none of the existing techniques are capable of on-line particle size analysis at low cost, while the rest are either non-robust, require complicated operating procedures or capable of handling only small amounts of sample which may not be representative of the bulk material. To address these issues, the Vibro-spring Particle Sizer (Mark I), was first developed by Mahgerefteh and Shaeri (2000). This was followed by its improved versions (next generation prototypes) including the Vibro-spring Particle Sizer (Mark II), the Pneumatic Spring Particle Sizer (Mark III) and finally the Handheld SPS as reviewed in chapter 4.

In order to test spring reproducibility, in chapter 5, two identically manufactured springs, A1 and A2 were evaluated by comparing the mean and the standard deviation of the spring coil apertures following extension. The coil apertures were measured from images of the extended springs obtained using digital photography for spring extensions ranging from 2 mm to 10 mm. Following analysis of the aperture data, both springs demonstrated a wide range of spring coil aperture sizes at any given extension in this range. The difference between the standard deviations of the apertures of the two equivalently extended springs was found to ± 2.2 μm. This difference decreases with aperture size and practically vanishes for apertures greater than 250 μm. In addition, the largest difference between the mean for both springs was 17.5 μm.

Comparisons of A1 and A2 at various extensions against sieve data showed that both springs exhibited standard deviations considerably greater than that for a sieve of the same aperture size. Thus, the results indicated that the springs were reproducible, due to the small difference in the between the means and standard deviations for both springs. It was however also found that that the precision of the apertures (in terms of their uniformity) at extensions between 2 mm to 10 mm was smaller compared to standard sieves.

Chapter 6 reviews two methods developed to address the sample loss issue in the PSPS. These included the use of a full-bridge strain gauge circuit and fluidisation principles to measure the mass of sample in the PSPS in-situ. The first method involved the development of a correlation for the mass of sample as a function of the strain gauge output voltage. This correlation was obtained using linear regression analysis of the voltage recorded as a function of the mass added to the test spring. The coefficient of determination, R^2 obtained for the correlation was 0.9917. The data show that the experiments were reproducible with 95 % confidence with a maximum deviation of ± 13.05 g, which was experienced for masses above 200 g. This may be as a result of hysteresis. The strain gauge was found to produce a mass resolution of ± 2.6 g for a 280 g sample corresponding to a mass resolution of ca. ± 1 %. The relatively high mass resolution coupled with the linear response established the principle of using the strain gauge as a promising method for in-situ mass measurement in the spring. A number of design modifications aimed at achieving the above were subsequently proposed.

The second part of the study involved the use of fluidisation principles for in-situ mass measurement capability by investigating the correlation between minimum fluidisation velocity and sample mass within the PSPS. The study using glass Ballotini of various size ranges was performed for a range of sample masses and air flowrates. The data showed that the bed followed a characteristic slugging flow regime, with a general increase in the pressure drop across the bed with increase in air flowrate. For the 212 – 300 μm size range, the pressure drop across the bed increased with sample mass, this relationship was not observed for other sizes tested. Based on the data, it was concluded that the variation of the pressure drop versus air flowrate could not be used as a method for determining sample mass within the spring.

Chapter 7 first investigated the impacts of the sample poly-dispersity and fluidisation pulse frequency on the sample discharge time. This was followed by a study of the particle migration patterns using a pulsating fluidised bed system of similar overall dimensions as the spring in order to elucidate the mechanism responsible for the observed trends. Ballotini glass spheres of various size ranges at air pressures of 103.4 kPa and 41.4 kPa were employed.

The pulse frequency experiments using the PSPS revealed that for the same sample size range, the discharge time was a complex function of the pulsation frequency, where the small

dependency, became more significant with average particle size. The data also revealed that for the same air pulse frequency, there was a general increase in sample discharge time with sample poly-dispersity and average particle size.

Fluidised bed experiments investigated the particle migration profiles at various frequencies to elucidate the mechanisms responsible for the above observed trends. The results indicated the expected migration of the large particles towards the bed's base and the percolation of the smaller size range towards the top. Additionally, the pulsation frequency also had a complex albeit small impact on the particle segregation behaviour. A direct correlation between the sample discharge time and the degree of segregation within the fluidised bed was established, where an increased degree of mixing reduced the sample discharge duration. Based on the above observations it was concluded that any operating or design parameter that promoted the degree of mixing (e.g. increasing the fluidising air pulse frequency) within the spring improved the system's efficacy through a reduction in the sample analysis time.

In chapter 8, an experimental evaluation of the handheld SPS using glass Ballotini and three $CaCO_3$ samples (namely LG800, LG12 and L400) of size range 250 – 1000 µm was presented. A correlation for the spring aperture size as a function of the number of turns of the handheld SPS screw cap was developed for each powder type. A performance evaluation was carried out for each powder using the correlation obtained, by comparing to sieve data. Results for glass Ballotini showed an excellent reproducibility and good agreement with sieve data with a maximum deviation of ± 3.5 % in terms of the total mass. For the $CaCO_3$ powders, the largest deviation from sieve data was exhibited by L400 with a deviation of ± 21 %, while for LG800 and LG12 ± 8 % and ± 5 % respectively. Additionally, all tests showed a reproducibility of $\leq \pm 5$ %. All data demonstrate the applicability of the handheld SPS for PSD analysis of various powders of size range 250 – 1000 µm. It was postulated that the L400 sample demonstrated the maximum deviation against sieve data due to its highly irregular shape.

A calibration was carried out to determine if sample mass discharged from the handheld SPS, could be directly related to the volume of the sample in the sample collection tube. Glass Ballotini particles of various size ranges were employed. A linear relationship between the discharged sample volume and its mass for all size ranges tested. All predicted data obtained

using calibration curves developed for each size range, were in good agreement to actual observed data, with an average deviation of ± 0.12 g. Therefore, the method may be used as a direct mass measurement method in the handheld SPS.

The effect of rotational speed when using a rotary tumbler on sample analysis time and PSD accuracy in comparison to manual shaking for the handheld SPS were presented. Based on the data it was concluded that the analysis time and PSD accuracy were significantly dependent on the rotational speed employed. From the study, it was concluded that the use of a rotary tumbler was an effective method to decrease analysis time. Additionally, the optimum range of rotational speeds between 200 – 300 rpm guaranteed a rapid analysis time without causing early discharge.

9.2 Future Work

9.2.1 Spring Design

It is commercially important that the springs in the PSPS demonstrate reproducible features to avoid individual calibrations, as mentioned in chapter 5. From the investigations in chapter 5 it was observed that attaining springs with uniform opening coils was challenging with springs made from stainless steel (a common spring material). Hence, springs with a unique material composition (i.e. a mixture of several spring materials) need to be specially fabricated to ideally optimise the uniformity of the spring openings. Another recommendation is the use of fiber-reinforced plastic springs, which are a recent development in spring engineering. They have several advantages over wire springs, which include being, lightweight, rustproof, non-conductive, and are fully recyclable and could be a solution to the uniformity problem (Advanex, 2009).

9.2.2 Control Software

Improvements on the computer program could be added to enhance the systems capability and reliability. Auto-calibration, data logging, mass and extension measurement inclusion would aid re-calibration of the system when operating conditions change, save results and

obtain size distributions via the computer. This will make data retrieval easier and improve efficiency.

9.2.3 Particle Segregation in the PSPS

Based on the studies carried out to determine the impact of particle segregation on sample discharge rate from the PSPS, further studies may be suggested to continue this investigation. The studies carried out as shown in chapter 7 are based on axial segregation within the spring. It would be advantageous to conduct further studies to determine the radial segregation within the PSPS. This would reveal whether larger particles are blocking smaller particles by adhering to the spring walls. Measurements may be taken at different radial positions in a bed.

9.2.4 In-Situ Mass Measurement in PSPS

One of the major problems associated with the PSPS is the loss of sample mass due to the particle retention inside the surface of the unit. Therefore, an in-situ mass measurement system needs to be employed in place of the current weighing mechanism, which consists of a large pan below the unit. Figures 6.5 and 6.6 illustrate a proposed design for the use of a strain gauge on the pneumatic SPS.

An alternative is to use a force sensitive resistor, which is a material that changes resistance following application of force to its surface (Crowder, 1998). This may be used in place of the metal film and strain gauge proposed in figures 6.5 and 6.6. A force-sensing resistor is made up of two parts, which include a resistive material applied to a film and a set of digitating contacts applied to another film. The resistive material serves to make an electrical path between the two sets of conductors on the second film. When a force is applied to this sensor, a better connection is made between the contacts; hence, the conductivity is increased and is approximately a linear function of force (Webster, 1999; Stilson, 1996).

REFERENCES

Advanex, 2009. *Plastic Springs.* [Online] Available at: http://www.advanex.co.jp/products_e/plastic_springs.php [Accessed 3 March 2009].

Airedale Springs Limited, 2008. *Airedale Springs Ltd - Spring manufacturers UK.* Ebor Works, Haworth, Keighley, Yorkshire BD22 8HT, UK

Allen, T., 1997. *Particle Size Measurement.* 5th ed. London: Chapman and Hall.

Allen, T., 2003. *Powder Sampling and Particle Size Determination.* Amsterdam: Elsevier Science Ltd.

Allen, T. and Khan, A., 1970. Critical evaluation of powder sampling procedures. *Chemical Engineer*, (238), pp. CE108-112.

Arai, Y., 1996. *Chemistry of Powder Production.* London: Chapman and Hall.

Barrett, P. and Glennon, B., 2002. Characterizing the Metastable Zone Width and Solubility Curve Using Lasentec FBRM and PVM. *Chemical Engineering Research and Design*, Issue 80, p. 799–805.

Beehag, G., 2000. *Sand Research Shaping Up.* [Online] Available at: http://www.agcsa.com.au/static/atm_articles/html/2_4f.html [Accessed 20 November 2009].

Bernhardt, C., 1994. *Particle size analysis: classification and sedimentation methods.* London: Chapman and Hall.

Bland, J. and Altman, D., 2009. *Statistical Methods for Assessing Agreement Between Two Methods Of Clinical Measurement.* [Online] Available at: http://www-users.york.ac.uk/~mb55/meas/ba.htm [Accessed 10 September 2010].

BS ISO 13317-1:2001. *Determination of particle size distributions by gravitational liquid sedimentation methods. General principles and guidelines.* International Organisation for Standardisation, Central Secretariat, Geneva, Switzerland.

BS ISO 13317-2:2001. *Determination of particle size distributions by gravitational liquid sedimentation methods. Fixed pipette method.* International Organisation for Standardisation, Central Secretariat, Geneva, Switzerland.

BS ISO 13319:2007. *Determination of particle size distributions. Electrical sensing zone method.* International Organisation for Standardisation, Central Secretariat, Geneva, Switzerland.

BS ISO 9276-1:1998 *Representation of results of particle size analysis. Graphical representation.* International Organisation for Standardisation, Central Secretariat, Geneva, Switzerland.

BS ISO 9276-2:2001 *Representation of results of particle size analysis. Calculation of average particle sizes/diameters and moments from particle size distributions*. International Organisation for Standardisation, Central Secretariat, Geneva, Switzerland.

BS ISO 9276-6:2008 *Representation of results of particle size analysis: Descriptive and quantitative representation of particle shape and morphology.* International Organisation for Standardisation, Central Secretariat, Geneva, Switzerland.

BS ISO 13320:2009. *Particle size analysis: Laser diffraction methods.* International Organisation for Standardisation, Central Secretariat, Geneva, Switzerland..

BS EN 933-3:1997. *Testing aggregates: Methods for determination of particle shape-Flakiness index*. British Standards Institute, 389 Chiswick High Road, London W4 4AL. UK.

BS 410-1:2000 *Test sieves-Technical requirements and testing: Test sieves of metal wire cloth.* British Standards Institute, 389 Chiswick High Road, London W4 4AL. UK.

BS 410-2:2000 *Test sieves-Technical requirements and testing: Test sieves of perforated metal plate*. British Standards Institute, 389 Chiswick High Road, London W4 4AL. UK.

Colloidal Dynamics, 1999. *Particle Size Distributions.* [Online] Available at: http://www.colloidal-dynamics.com/docs/CDElTut2.pdf [Accessed 15 January 2010].

Comark Limited, 2011. *Part Number C9555.* [Online] Available at: www.comarkltd.com/pdf/pressure-meter-datasheet.pdf [Accessed 9 July 2011].

Cooper, K., 2010. *Particle Size Analysis Applications For Agriculture.* [Online] Available at: http://www.articlesbase.com/agriculture-articles/particle-size-analysis-applications-for-agriculture-3833072.html [Accessed 12 January 2011].

Cornell, H. and Hoveling, A., 1998. *Wheat: Chemistry and Utilization.* Lancaster: Technomic Publishing Company Inc..

Crowder, R. M., 1998. *Automation and Robotics.* [Online] Available at: http://www.soton.ac.uk/~rmc1/robotics/artactile.htm [Accessed 08 July 2011].

Dukhin, A. S., Goetza, P. J. and Hackleyb, V., 1998. Modified log-normal particle size distribution in acoustic spectroscopy. *Colloids and Surfaces, Physicochemical and Engineering Aspects*, **138** (1) pp 1–9.

Earle, R. and Earle, M., 2004. Mechanical Separations: Sieving. In: *Unit Operations in Food Processing.* New Zealand:New Zealand Institute of Food Science & Technology Inc..

Eckhoff, R. K., 1969. A static investigation of Coulter principle of particle sizing. *Journal of Science and Instrumentation*, **2**(11), pp. 973-977.

Etzler, F. M. and Sanderson, M. S., 1995. Particle size analysis: A comparative study of various methods. *Particle and Particle Systems Characterization*. **12**, pp. 217-224.

European Council Directive 2008/50/EC of 21st May 2008 on ambient air quality and cleaner air for Europe. *Official Journal of the European Union.*

Figueiredo, M., 2000. *Encyclopedia of Analytical Chemistry: Applications, Theory, and Instrumentation.* R. Meyers, Ed. New York:John Wiley & Sons.

Gibilaro, L., 2001. *Fluidization Dynamics.* Oxford:Butterworth-Heinemann .

Gotoh, K., Masuda, H. and Higashitani, K., 1997. *Powder Technology Handbook.* New York: Marcel Dekker.

Helsel, R. (1998). *Visual Programming with HP VEE*. 3rd ed., Vol. 1. Upper Saddle River, N. J: Prentice Hall PTR.

Heyd, A. and Dhabbar, D., 1979. Particle shape effect on caking of coarse granulated antacid suspensions. *Drug and Cosmetic Industry*, **125**, pp. 42-45.

Holdich, R., 2002. *Fundamentals of Particle Technology*. Shepshed: Midland Information Technology and Publishing.

Horiba Jobin Yvon, 1996. *HORIBA Analysis Techniques.* [Online] Available at: http://www.horiba.com/scientific/products/particle-characterization/particle-size-analysis/laser-diffraction-techniques/ [Accessed 11 February 2009].

Huck, D., 2006. *Particle shape - an important parameter in pharmaceutical manufacturing.* [Online] Available at: http://www.chemie.de/articles/e/61206/ [Accessed 6 March 2009].

Jillavenkatesa, A., Dapkunas, J. S. and Lin-Sien, L., 2001. *Particle Size Characterization.* Gaithersburg: National Institute of Standards and Technology.

Kerdvibulvech, K., 2008. *Spring Particle Sizer, PhD Thesis.* London: University College London.

Khan, M., 2009. *Design and Development of a Spring Particle Size Analyser, MSc Thesis.* London: University College London.

Longo, W., Rigler, M. and Slade, J., 1995. Crocidolite Asbestos Fibers in Smoke from Original Kent Cigarettes. *American Cancer Research*, **55**(11), pp. 2232-2235 .

Mahgerefteh, H. and Kamugasha, R., 2004. *Particle size distribution analyser*. UK, Patent No. GB2356711, 2004.

Mahgerefteh, H. and Shaeri, A., 2000. *Particle size analyser*. UK, Patent No. GB2294772 (A).

Mahgerefteh, H. and Shaeri, A., 2001. Modelling of a Novel Vibro-Spring Particle Size Distribution Analyser. *American Institute of Chemical Engineers Journal*, **47**(3).

Malvern Instruments Limited, 2002. *On-line particle sizer,*. [Online] Available at: http://www.malvern.com/common/downloads/Malvern_Process_Systems_Brochure_2002.pdf [Accessed 25 March 2009].

Malvern Instruments Ltd, 2009. *Laser Diffraction Particle Sizing.* [Online] Available at: http://www.malvern.com/LabEng/technology/laser_diffraction/particle_sizing.htm[Accessed 3 May 2009].

Merkus, H. G., 2009. *Particle Size Measurements: Fundamentals, Practice, Quality (Particle Technology Series).* 1st ed. Dordrecht: Springer.

Mingzhong, L., Wilkinson, D. and Patchigolla, K., 2006. Obtaining Particle Size Distribution from Chord Length Measurements. *Particle & Particle Systems Characterization.* **23**(2), pp. 170-174.

Omega Engineering, 2009. *omega.co.uk*. [Online] Available at: http://omega.co.uk/ [Accessed 7 February 2009]. Omega Drive, River Bend Technology Centre, Northbank, Manchester M44 5BD, UK

Omya UK Limited, 2011. *Welcome to Omya UK and Ireland*. [Online] Available at: http://www.omya.co.uk/ [Accessed 12 March 2011]. 75 Station Road Steeple Morden Royston, Hertfordshire SG8 0NX, UK

OriginLab, 2009. *Statistical Graphs: Histogram Example.* [Online] Available at: http://www.originlab.com/index.aspx?go=Solutions/GraphGallery&pid=604 [Accessed 12 August 2009].

Patel, K., 2001. *Vibro-Spring Particle Size Distribution Analyser, PhD Thesis.* London: University College London.

Pugh, D., 2007. *Sizing Up Online Particle Size Analysis*. Chemical Engineering Progress. **103**(5).

Radecky, S., 2009. *Making Basic Strain Measurements: A Tutorial.* [Online] Available at: http://www.evaluationengineering.com/index.php/solutions/instrumentation/making-basic-strain-measurements-a-tutorial.html [Accessed 12 March 2011].

Rideal, G. R., 2000. *Quality control matters – The Best Laser Sizers Demand the Best Calibration Standards European Edition.* [Online] Available at: http://www.whitehousescientific.com/pdf%20reports/qualitycontrol.pdf [Accessed 10 December 2008].

Rowe, P., Nienow, A. and Agbim, A., 1972. The Mechanisms by which Particle Segregate in Gas Fluidised Beds- Binary Systems of Near-Spherical Particles. *Trans. Inst. Chem. Eng.*, **50**, p. 310-323.

RS Components Limited, 2011. *Geared DC motor, 12V 260rpm.* [Online] Available at: http://uk.rs-online.com/web/p/dc-geared-motors/3636589/[Accessed 8 January 2011].

Rumpf, H., 1990. *Particle Technology.* London: Chapman & Hall.

Seville, J., Tuzun, U. and Clift, R., 1998. *Processing of particulate solids.* London: Chapman & Hall.

Shaeri, A., 1997. *Vibro-Spring Particle Size Analyser, PhD Thesis.* London: University College London.

Škiljan, I., 2008. *IrfanView (Version 4.20).* Vienna (Republic of Austria): s.n.

Sommer, K., 2001. 40 Years of Presentation Particle Size Distribution- Yet Still Incorrect?. *Particle & Particle Systems Characterization,* **18**(1), pp. 22-25.

Stilson, T., 1996. *Force Sensing Resistors.* [Online] Available at: https://ccrma.stanford.edu/CCRMA/Courses/252/sensors/node8.html [Accessed 10 August 2011].

Strain gauges, 2011. *Strain gauges.* [Online] Available at: http://www.allaboutcircuits.com/vol_1/chpt_9/7.html [Accessed 5 May 2011].

Strategic Directions International Inc., 2001. Particle size analysis: growth in a fragmented market ($130 mn particle characterization instrument market). *Instrument Business Outlook*. [Online] Available at: http://www.allbusiness.com/specialty-businesses/838097-1.html [Accessed 8 April 2008].

Sympatec GmbH, 2010. *Laser Diffraction: Particle size analysis from 0.1 micron to 8.75 mm.* [Online] Available at: http://www.sympatec.com/EN/LaserDiffraction/LaserDiffraction.html [Accessed 12 October 2010].

Sysmex Corporation, 2009. *Particle Analyser.* [Online] Available at: http://particle.sysmex.co.jp/en/fpia/parameter.html [Accessed 5 March 2009].

Syvitski, J. P. M., 2007. *Principles, Methods and Application of Particle Size Analysis.*. Cambridge: Cambridge University Press.

United State of Pharmacopeia, 2000. *Optical Microscopy.* [Online] Available at: http://www.pharmacopeia.cn/v29240/usp29nf24s0_c776.html [Accessed 11 December 2010].

United States Pharmacopeia, 2007. *Particulate matter in injections and the USP particle count reference standard.* [Online] Available at: http://www.pharmacopeia.cn/v29240/usp29nf24s0_c788.html [Accessed 17 December 2010].

Van der Plaats, G., Herps, H. & William, L., 1981. *Size Determination of Conductive Particles with a Coulter Counter, Particle Size Analysis.* (N. Stanley-Wood, and T. Allen, Eds.). Chichester: John Wiley and Sons Ltd.

Wadell, H., 1933. Sphericity and roundness of rock particles. *Journal of Geology*, p. 41:310–331.

Webb, P. A. and Orr, C., 1997. *Analytical Methods in Fine Particle Technology,* Norcross: Micromeritics Instrument Corporation.

Webster, J. G., 1999. *The Measurement, Instrumentation, and Sensors Handbook.* Heidelberg: Springer-Verlag GmbH & Co.

Weiner, B. B., 2010. *A guide to choosing a particle sizer.* [Online] Available at: http://www.brookhaveninstruments.com/literature/lit_90Plus.html [Accessed 20 December 2010].

Williams, J., 1976. The Segregation of Particulate Materials: A Review. *Powder Technology,* **15**(2), pp. 245 - 251.

Wynn, E. J. and Hounslow, M. J., 1997. Coincidence Correction for Electrical-Zone (Coulter Counter) Particle Size Analysers. *Particle Technology,* **93**(2), pp. 163-175.

Yang, W.-C., 2003. *Handbook of Fluidization and Fluid-Particle Systems.* New York: Marcel Decker.

APPENDIX A

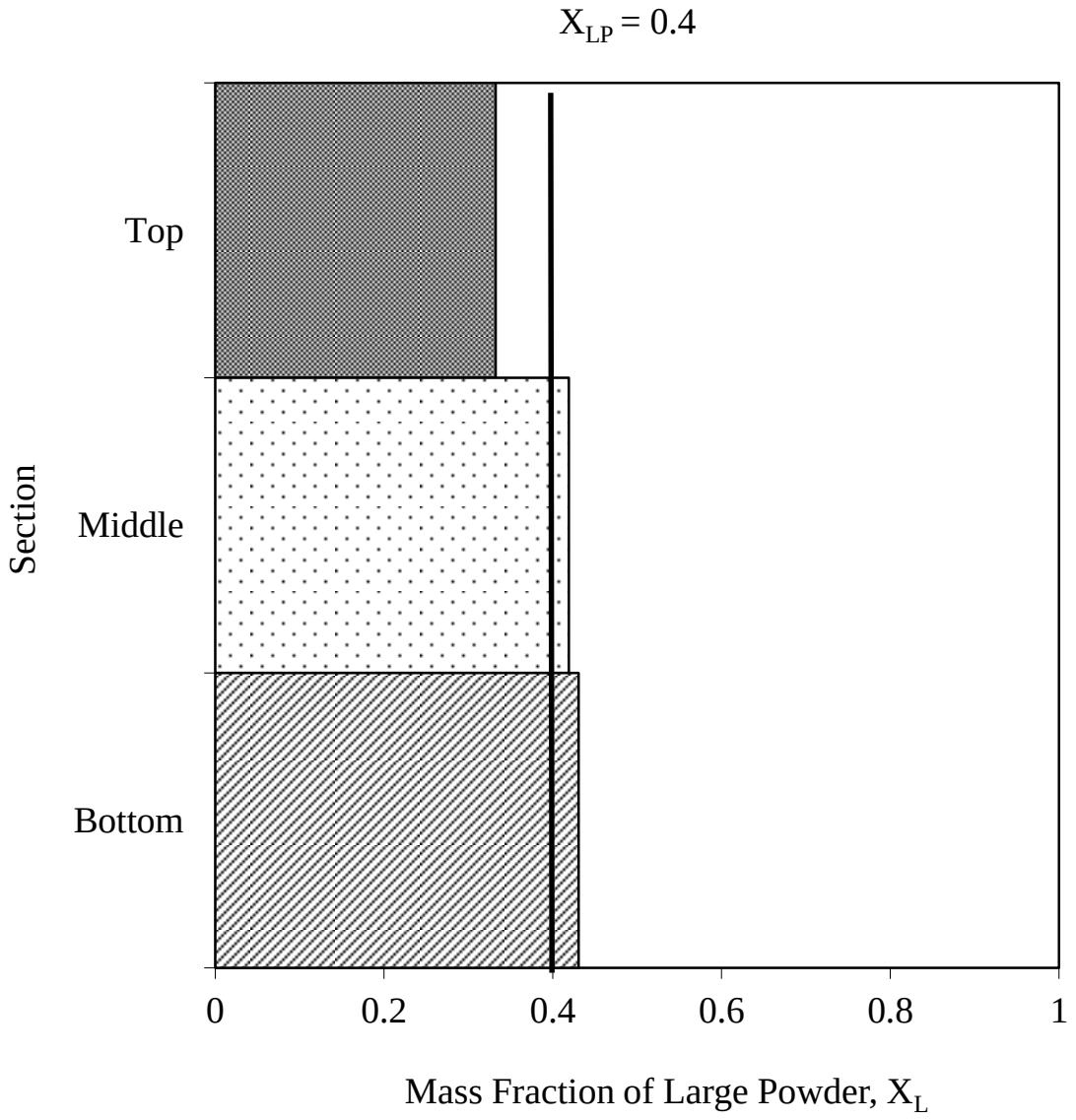

Figure A.1: Segregation patterns for poly-dispersed sample A (150 – 300 µm and 425 – 600 µm).

Pulse frequency = 5 Hz

Fluidisation duration = 4 min

Air pressure = 103.4 kPa

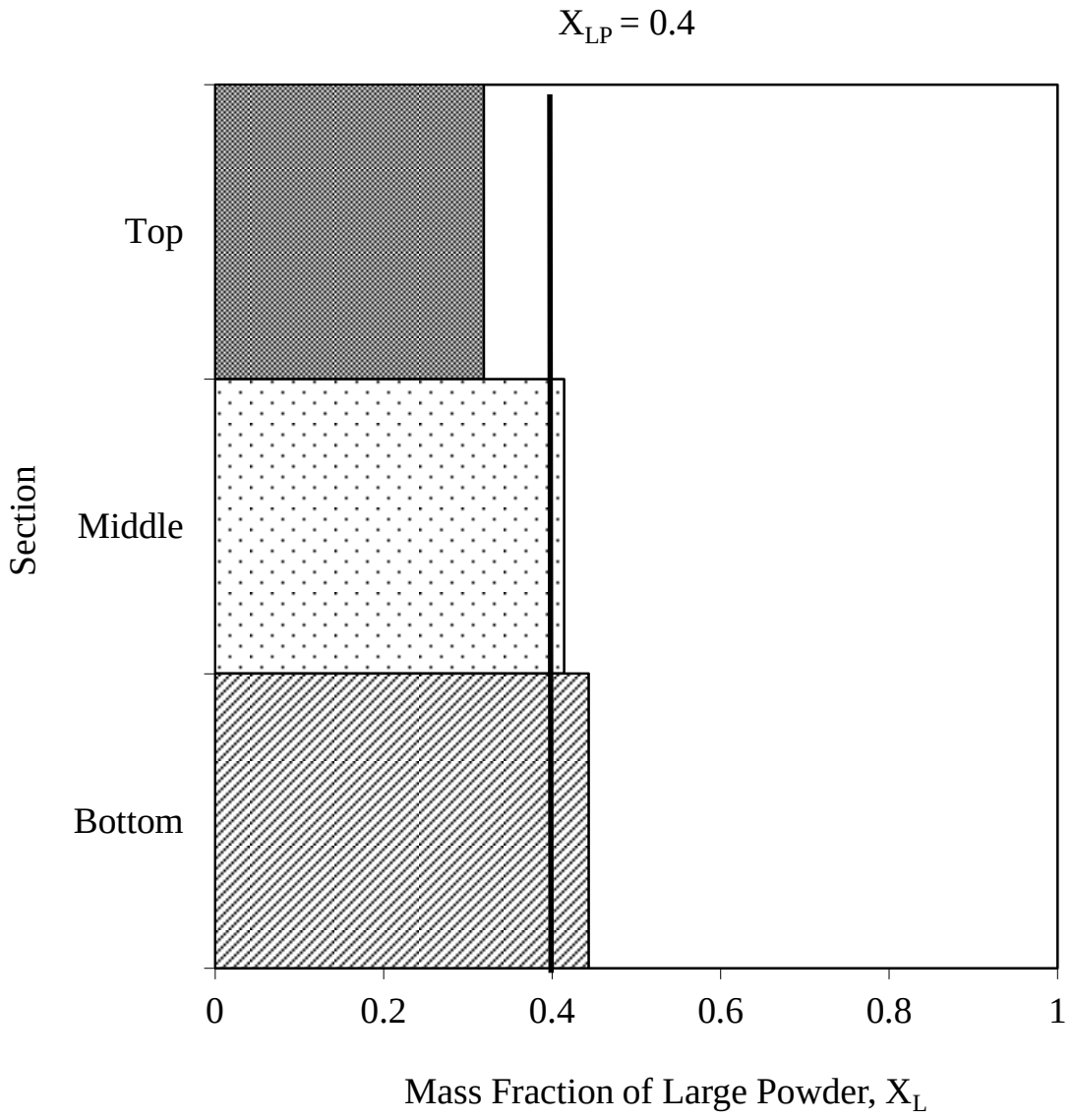

Figure A.2: Segregation patterns for poly-dispersed sample A (150 – 300 µm and 425 – 600 µm).

Pulse frequency = 2 Hz

Fluidisation duration = 4 min

Air pressure = 103.4 kPa

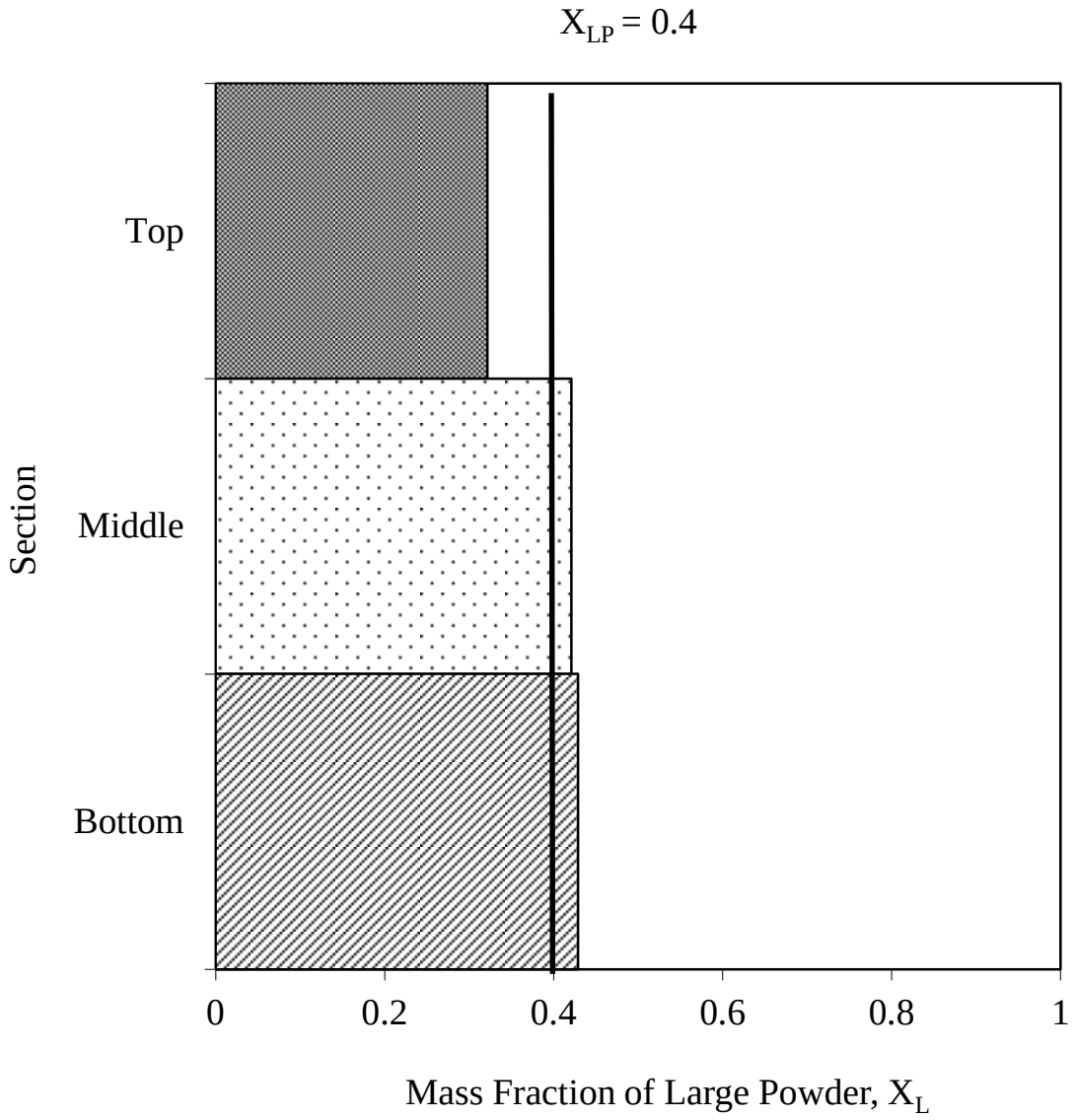

Figure A.3: Segregation patterns for poly-dispersed sample A (150 – 300 µm and 425 – 600 µm).

Pulse frequency = 1 Hz

Fluidisation duration = 4 min

Air pressure = 103.4 kPa

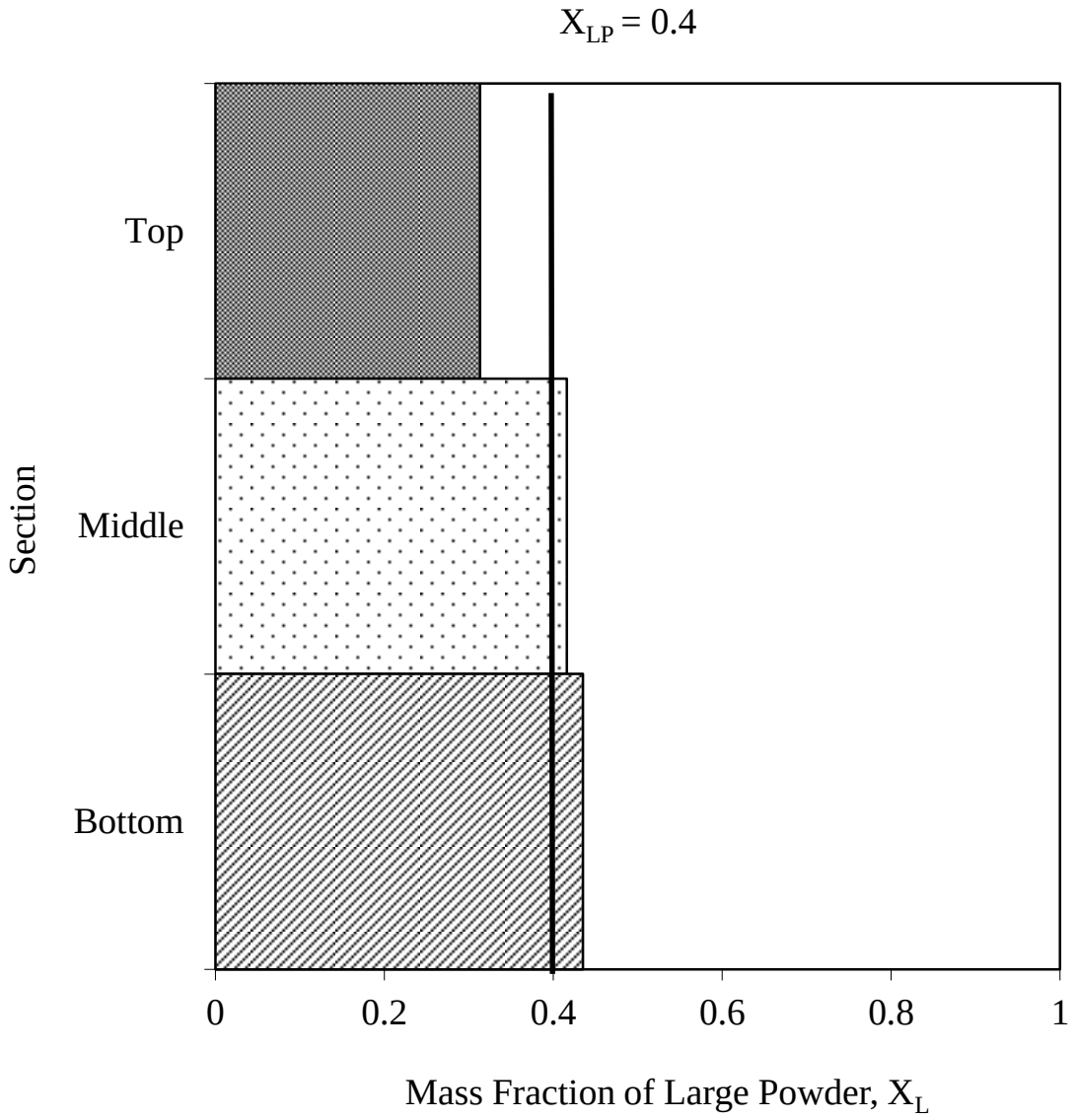

Figure A.4: Segregation patterns for poly-dispersed sample A (150 – 300 µm and 425 – 600 µm).

Pulse frequency = 0.5 Hz

Fluidisation duration = 4 min

Air pressure = 103.4 kPa

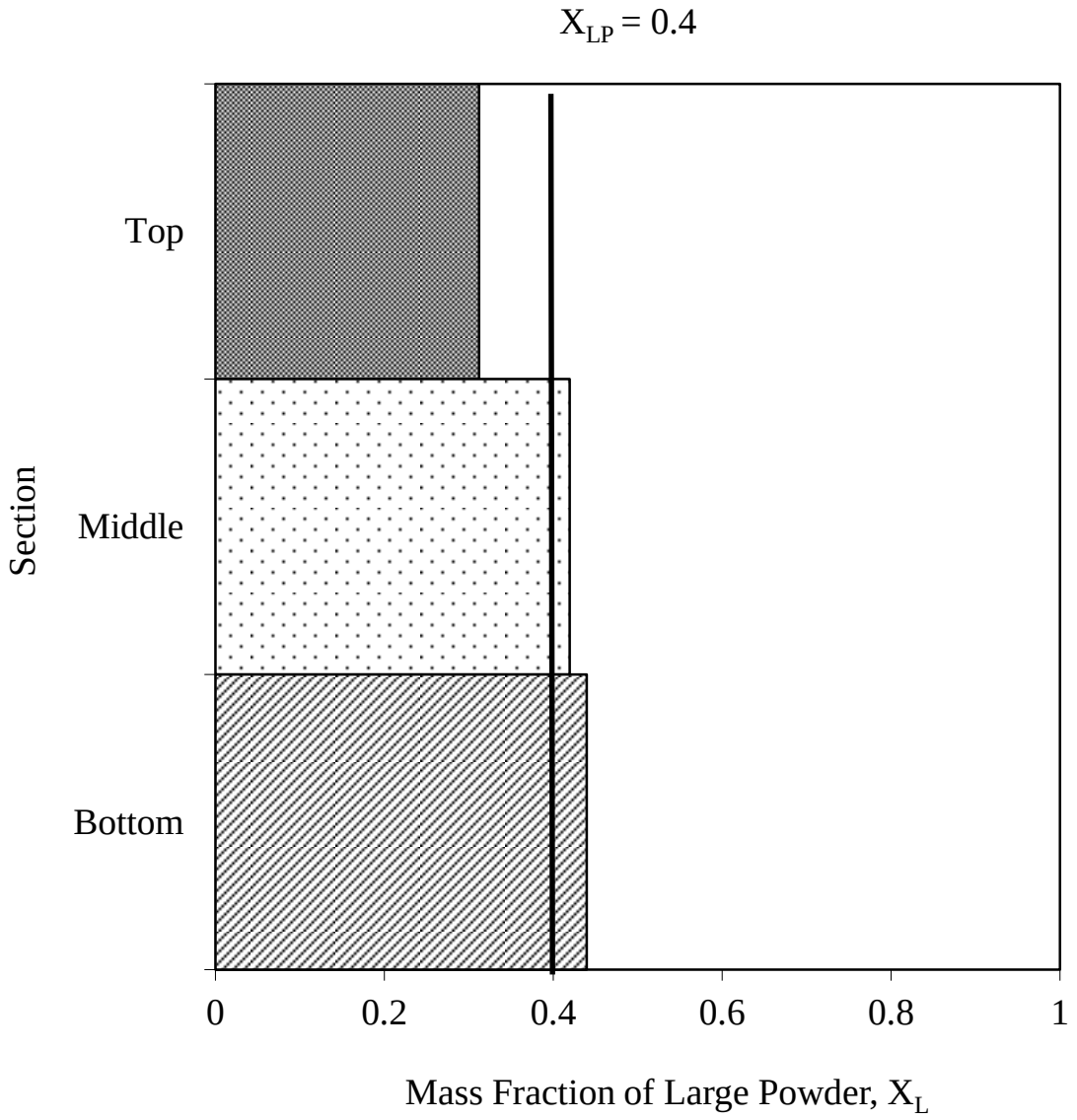

Figure A.5: Segregation patterns for poly-dispersed sample A (150 – 300 µm and 425 – 600 µm).

Pulse frequency = 0 Hz

Fluidisation duration = 4 min

Air pressure = 103.4 kPa

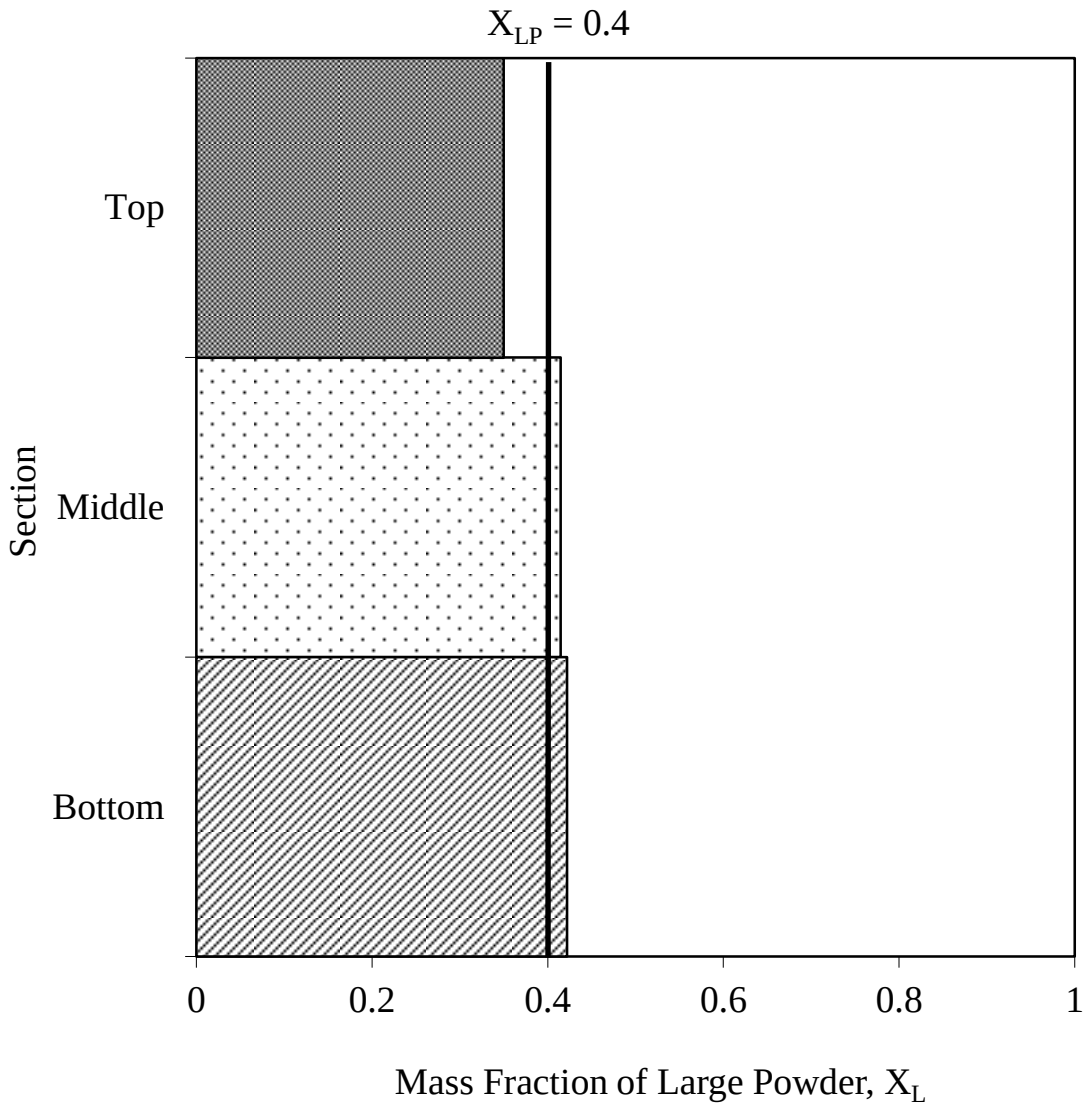

Figure A.6: Segregation patterns for poly-dispersed sample A (150 – 300 µm and 425 – 600 µm).

Pulse frequency = 5 Hz

Fluidisation duration = 7 min

Air pressure = 103.4 kPa

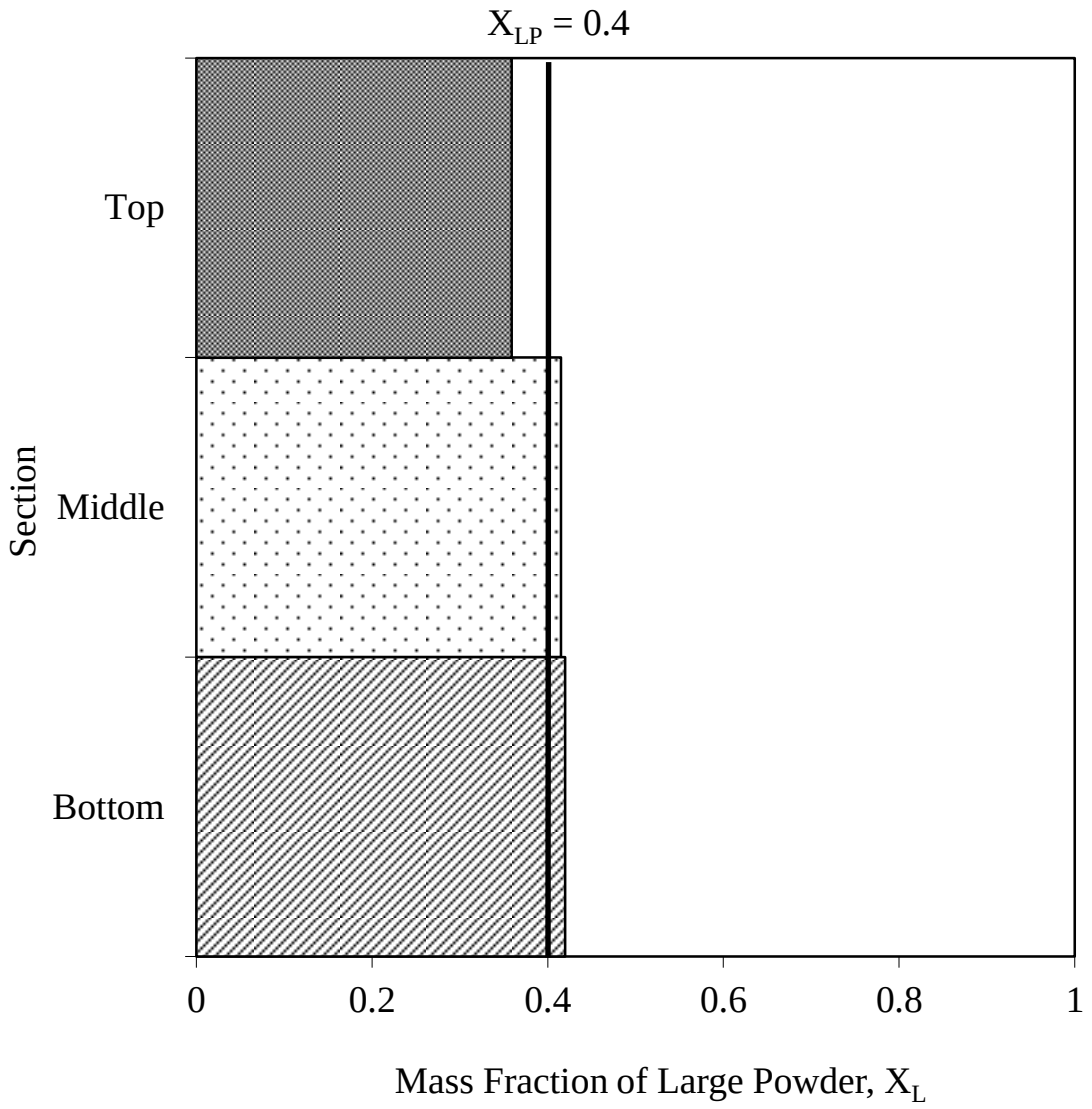

Figure A.7: Segregation patterns for poly-dispersed sample A (150 – 300 µm and 425 – 600 µm).

Pulse frequency = 2 Hz

Fluidisation duration = 7 min

Air pressure = 103.4 kPa

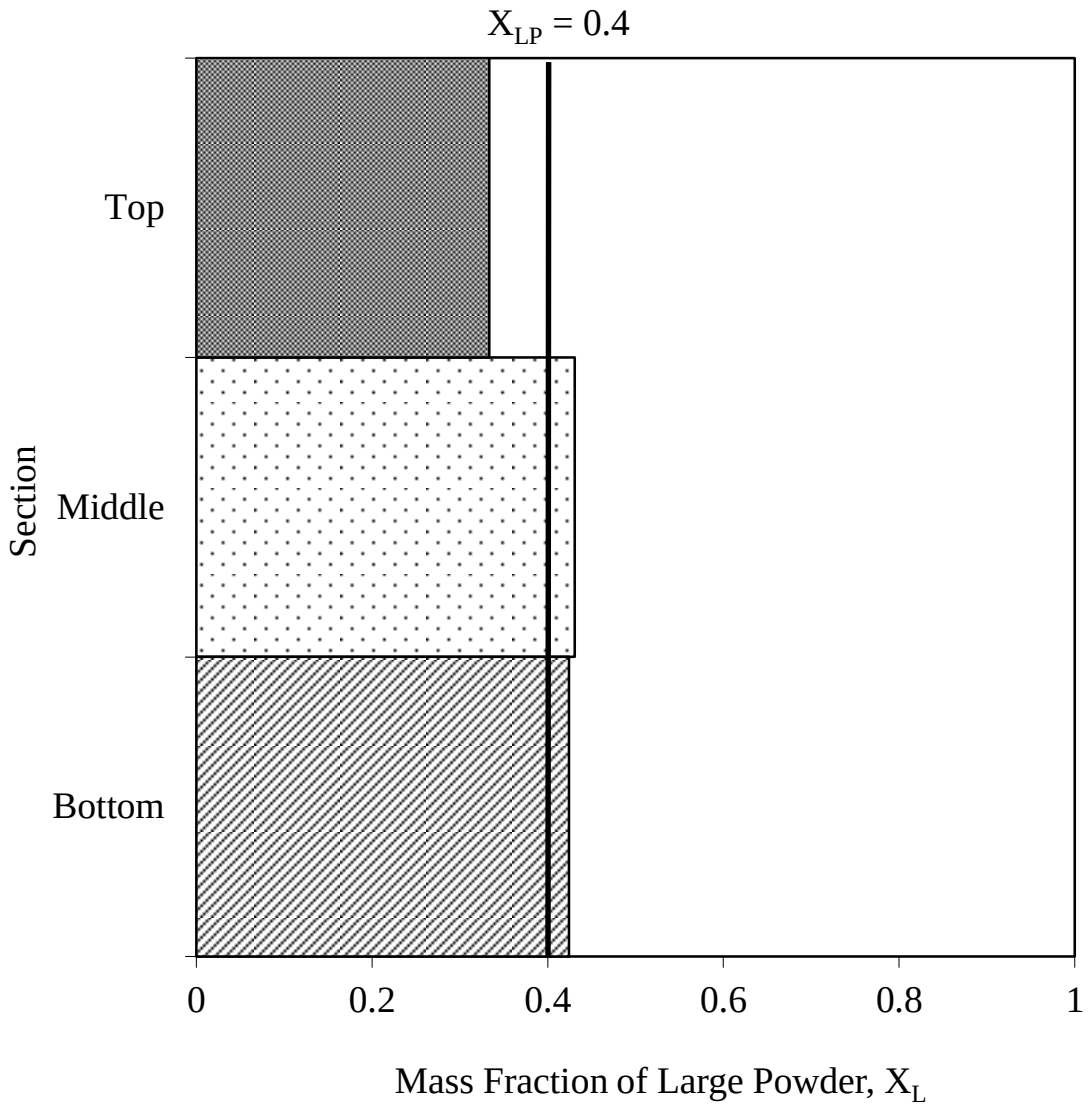

Figure A.8: Segregation patterns for poly-dispersed sample A (150 – 300 µm and 425 – 600 µm).

Pulse frequency = 1 Hz

Fluidisation duration = 7 min

Air pressure = 103.4 kPa

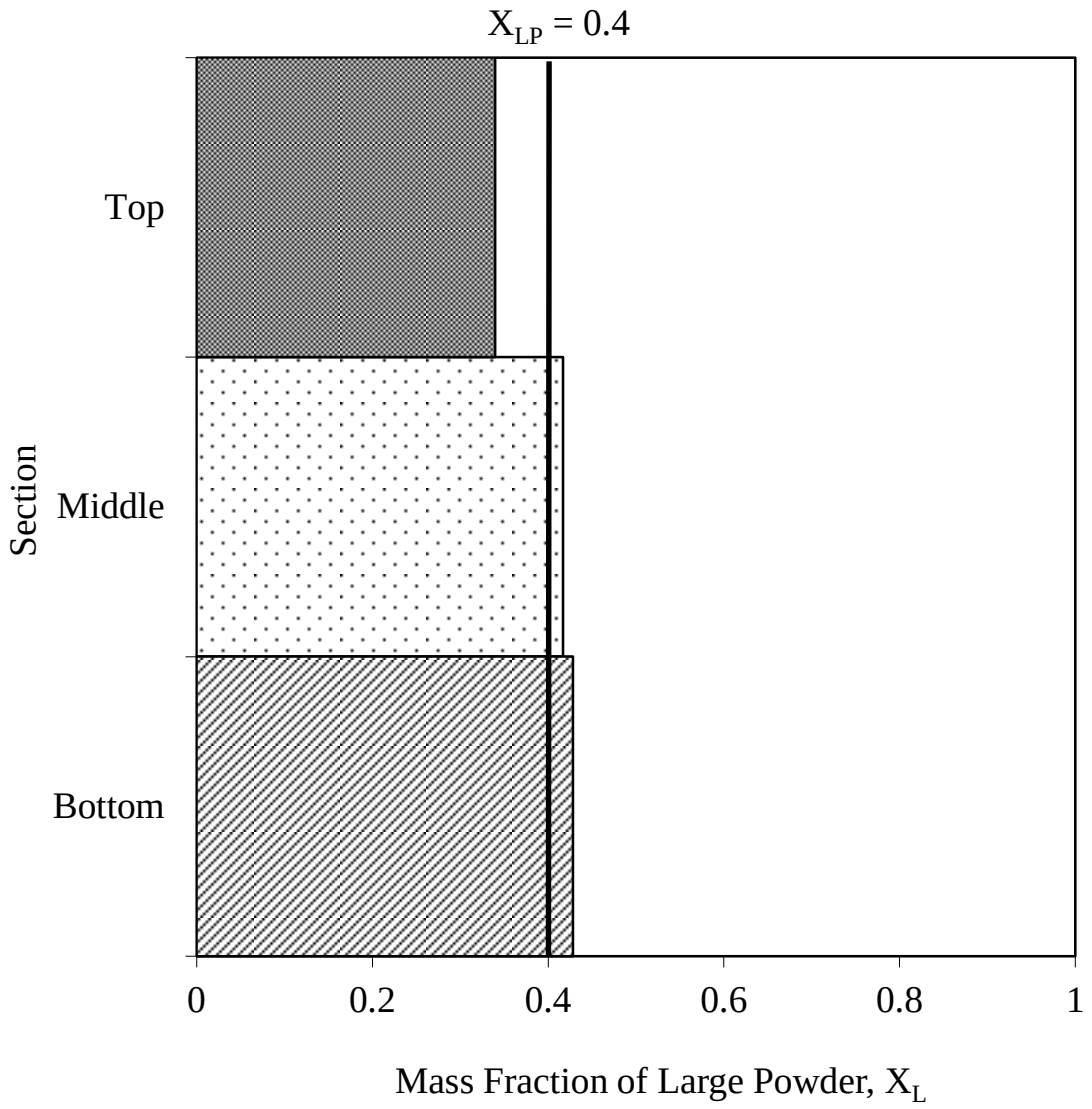

Figure A.9: Segregation patterns for poly-dispersed sample A (150 – 300 µm and 425 – 600 µm).

Pulse frequency = 0.5 Hz

Fluidisation duration = 7 min

Air pressure = 103.4 kPa

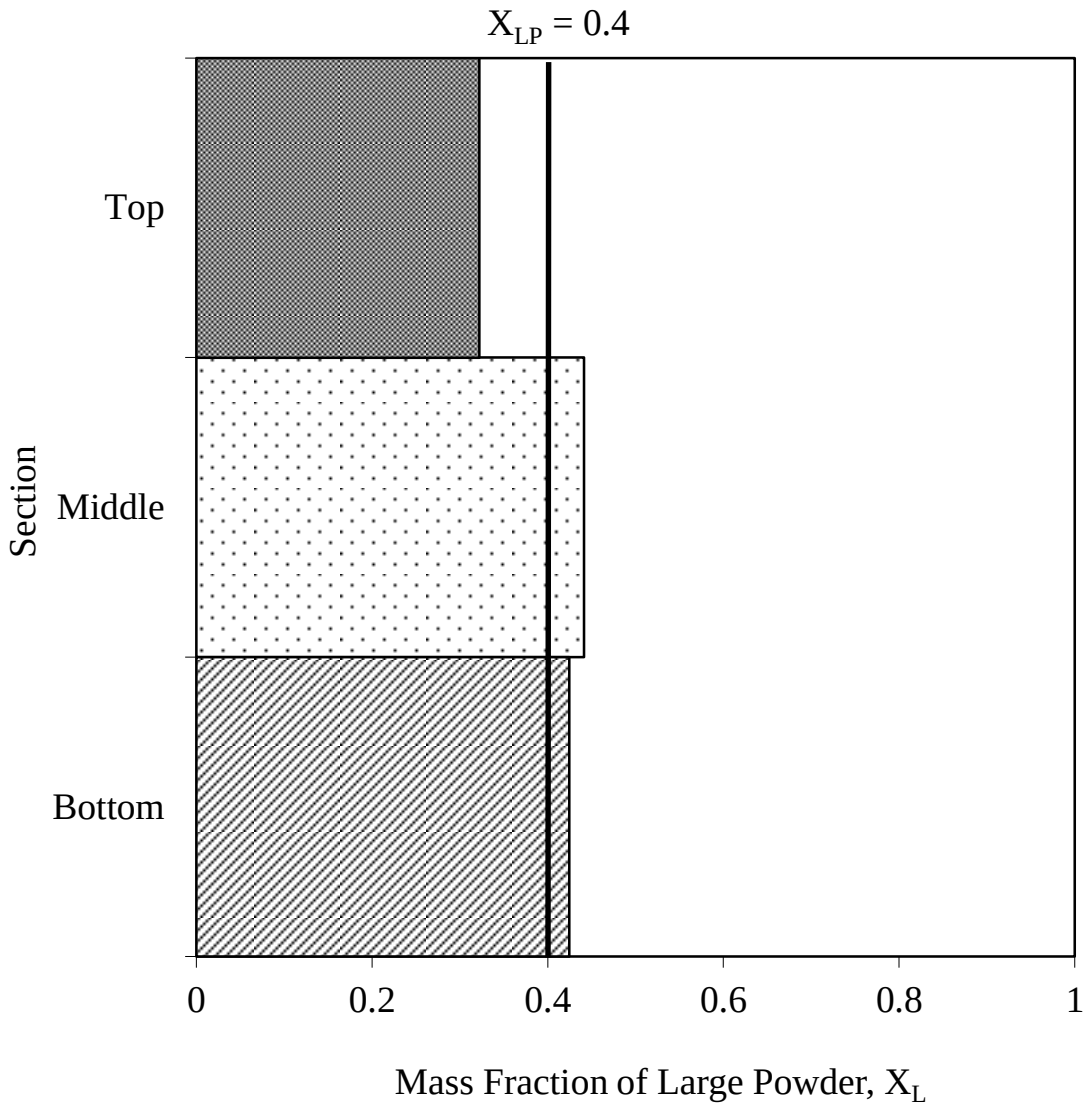

Figure A.10: Segregation patterns for poly-dispersed sample A (150 – 300 µm and 425 – 600 µm).

Pulse frequency = 0 Hz

Fluidisation duration = 7 min

Air pressure = 103.4 kPa

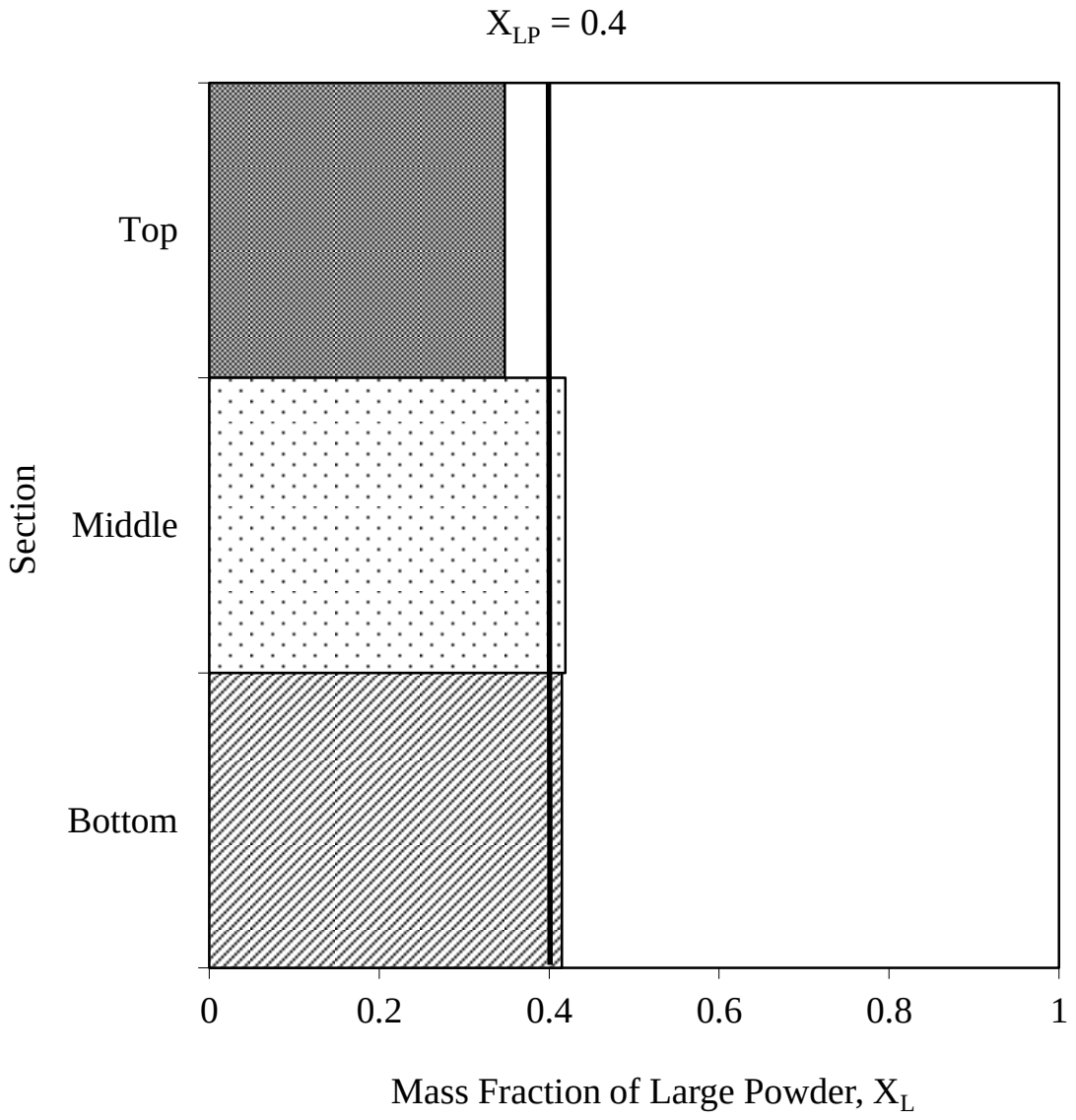

Figure A.11: Segregation patterns for poly-dispersed sample A (150 – 300 µm and 425 – 600 µm).

Pulse frequency = 5 Hz

Fluidisation duration = 10 min

Air pressure = 103.4 kPa

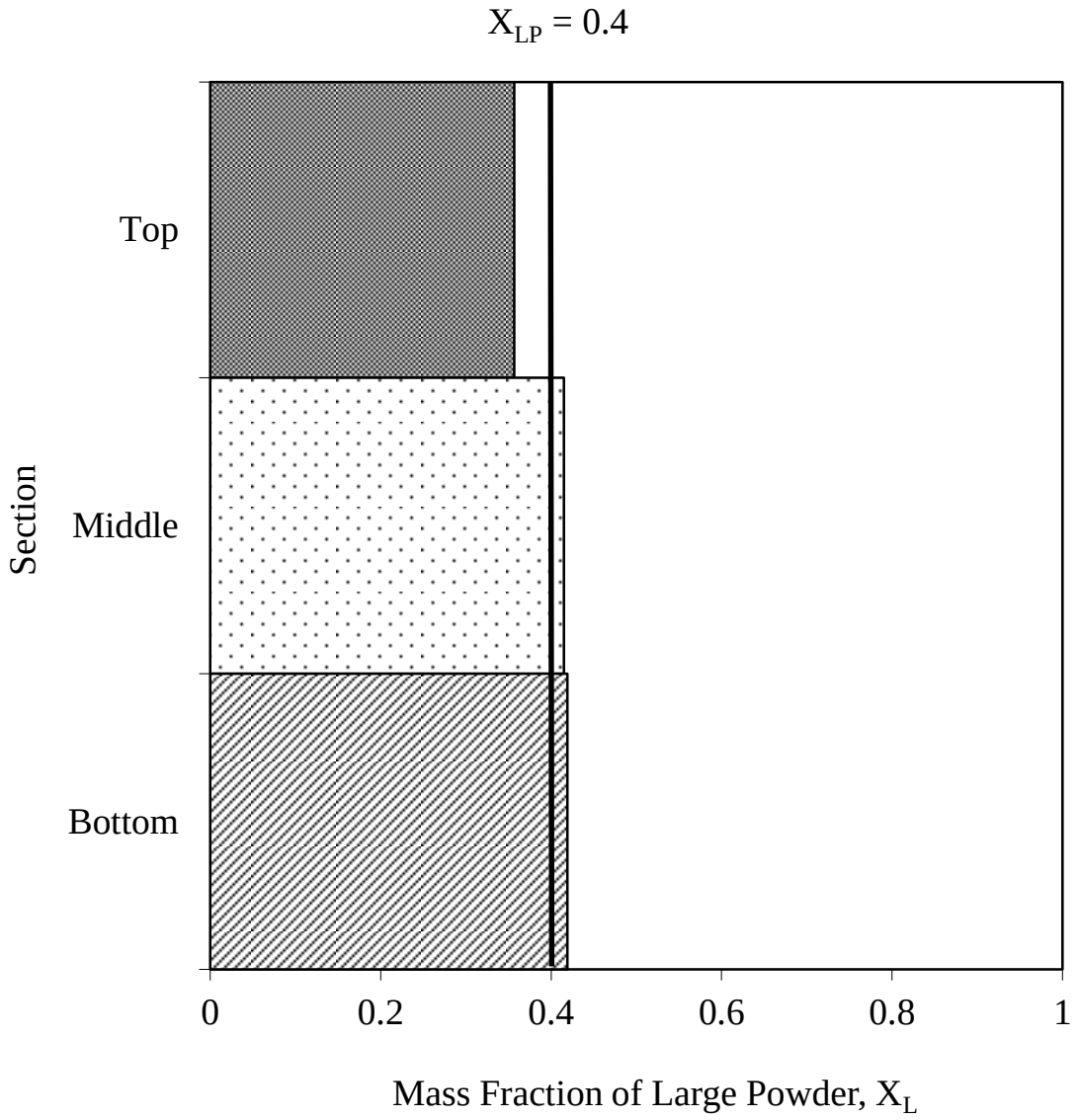

Figure A.12: Segregation patterns for poly-dispersed sample A (150 – 300 µm and 425 – 600 µm).

Pulse frequency = 2 Hz

Fluidisation duration = 10 min

Air pressure = 103.4 kPa

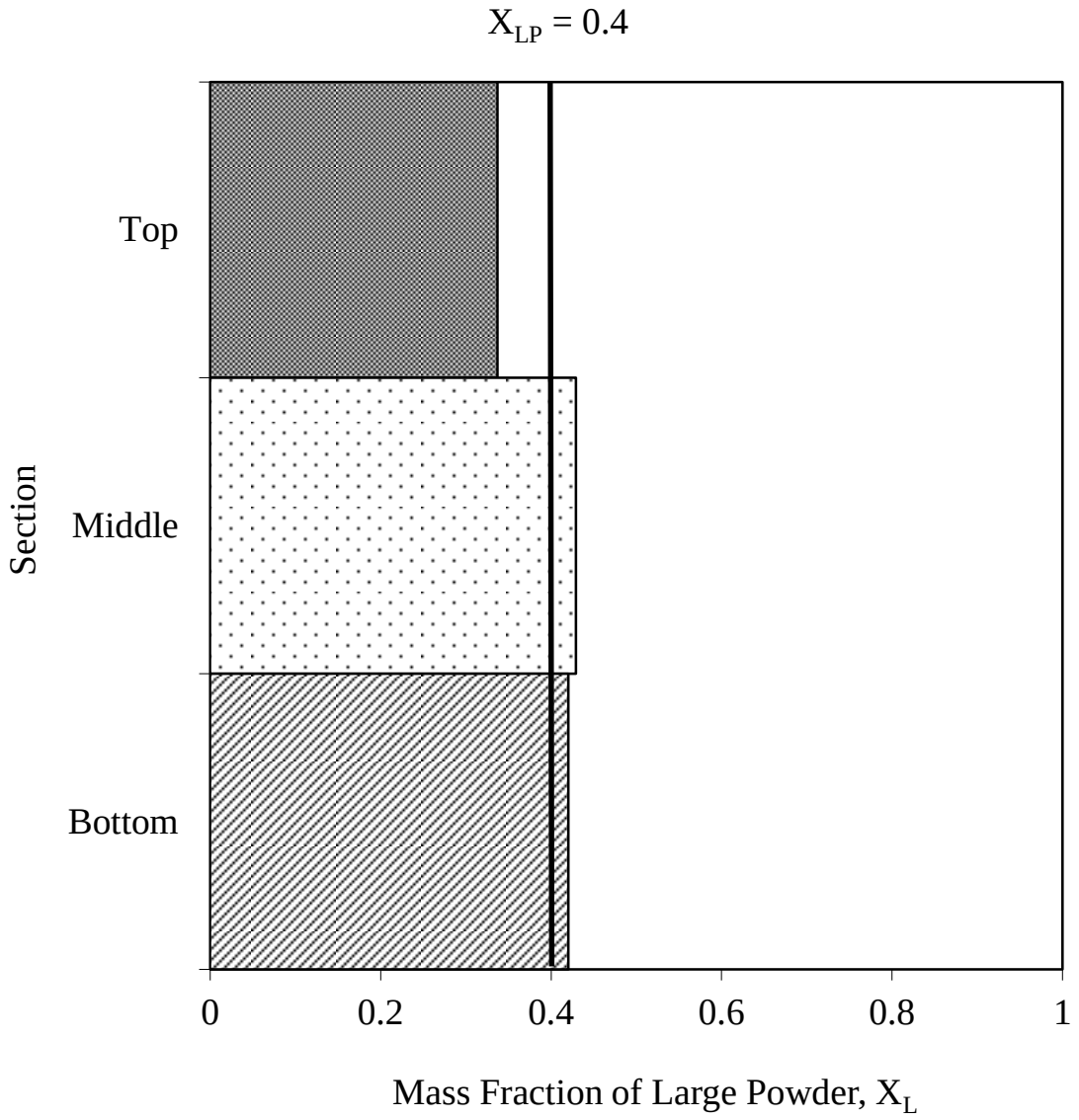

Figure A.13: Segregation patterns for poly-dispersed sample A (150 – 300 µm and 425 – 600 µm).

Pulse frequency = 1 Hz

Fluidisation duration = 10 min

Air pressure = 103.4 kPa

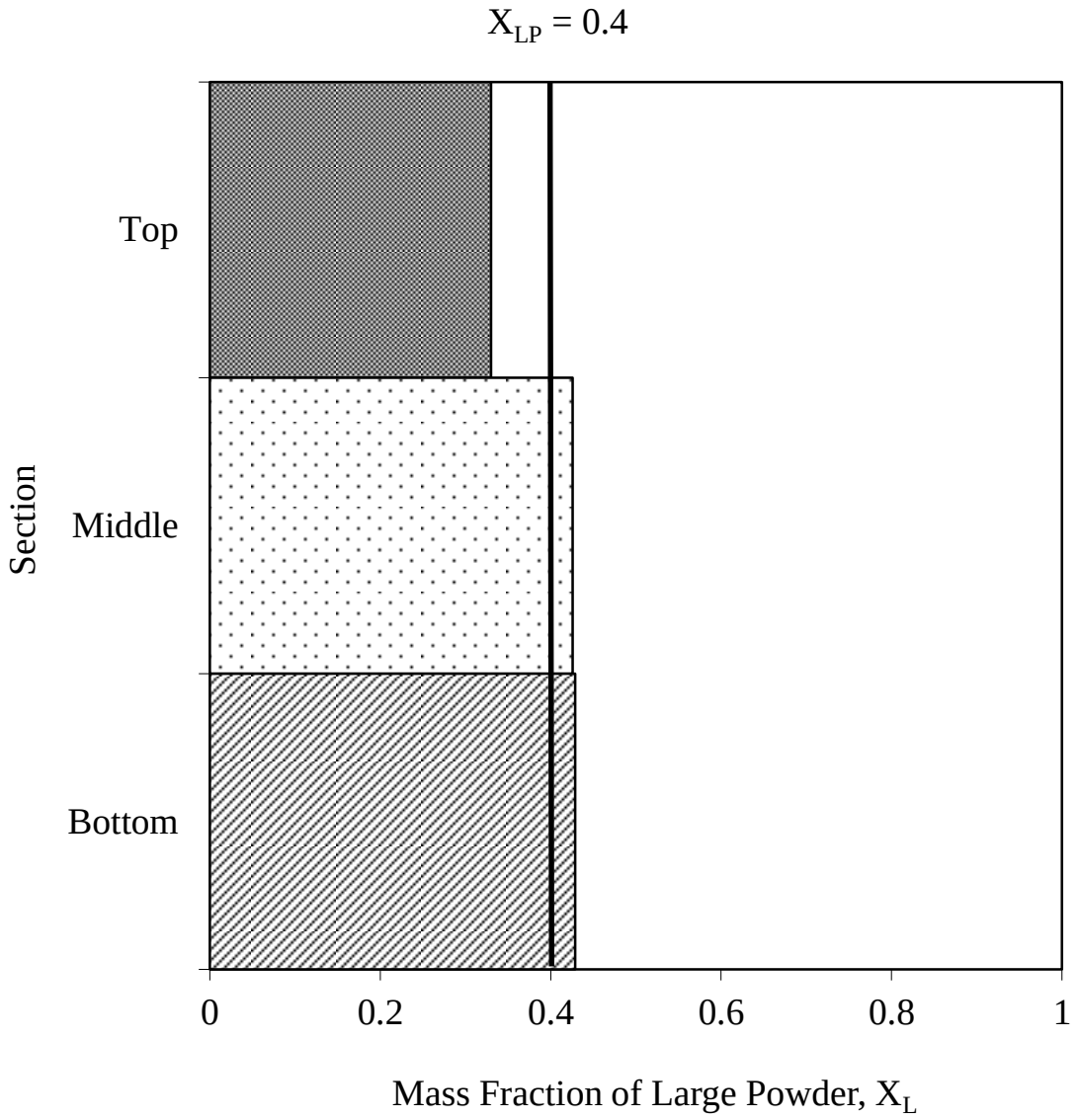

Figure A.14: Segregation patterns for poly-dispersed sample A (150 – 300 µm and 425 – 600 µm).

Pulse frequency = 0.5 Hz

Fluidisation duration = 10 min

Air pressure = 103.4 kPa

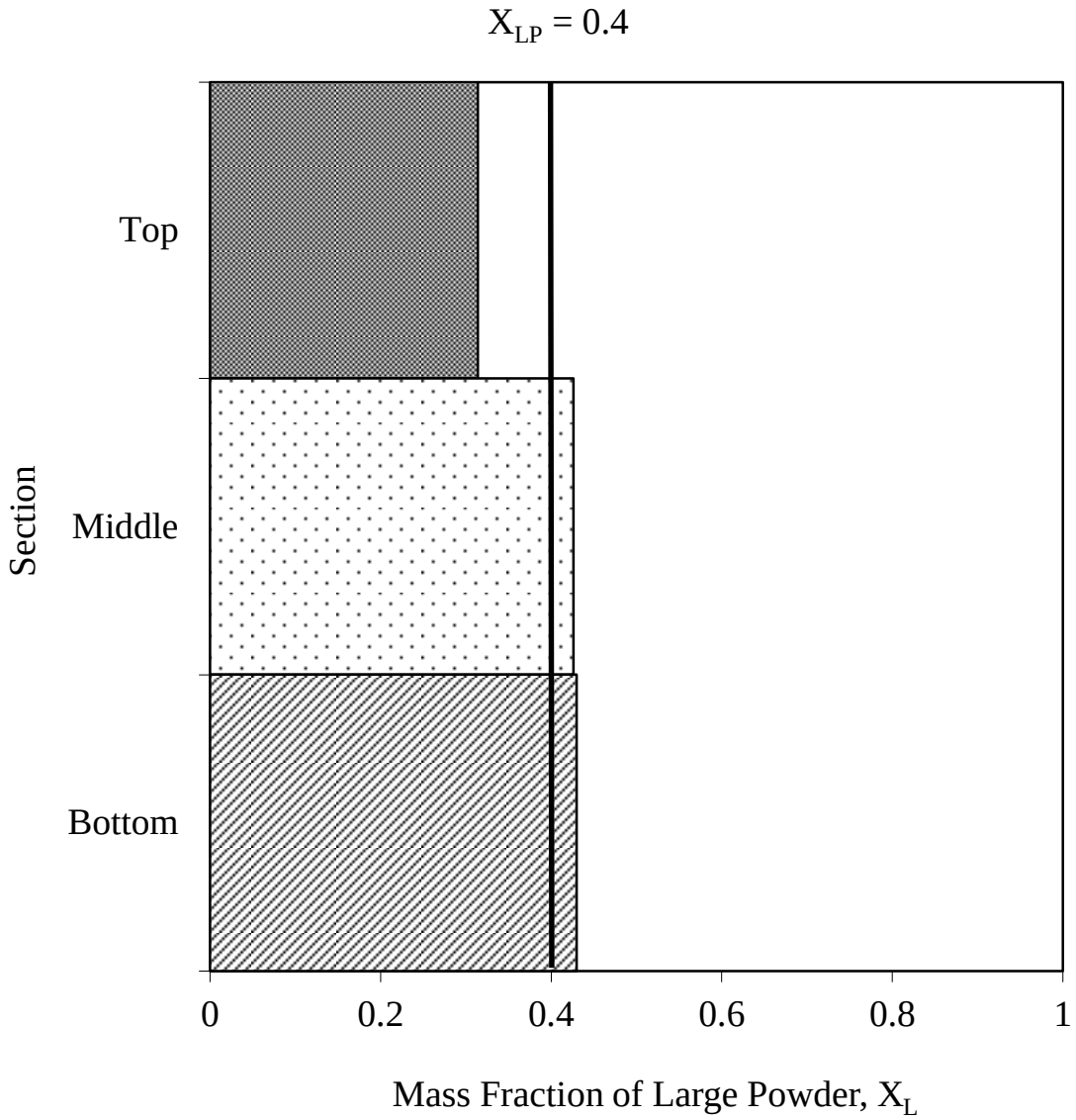

Figure A.15: Segregation patterns for poly-dispersed sample A (150 – 300 µm and 425 – 600 µm).

Pulse frequency = 0 Hz

Fluidisation duration = 10 min

Air pressure = 103.4 kPa

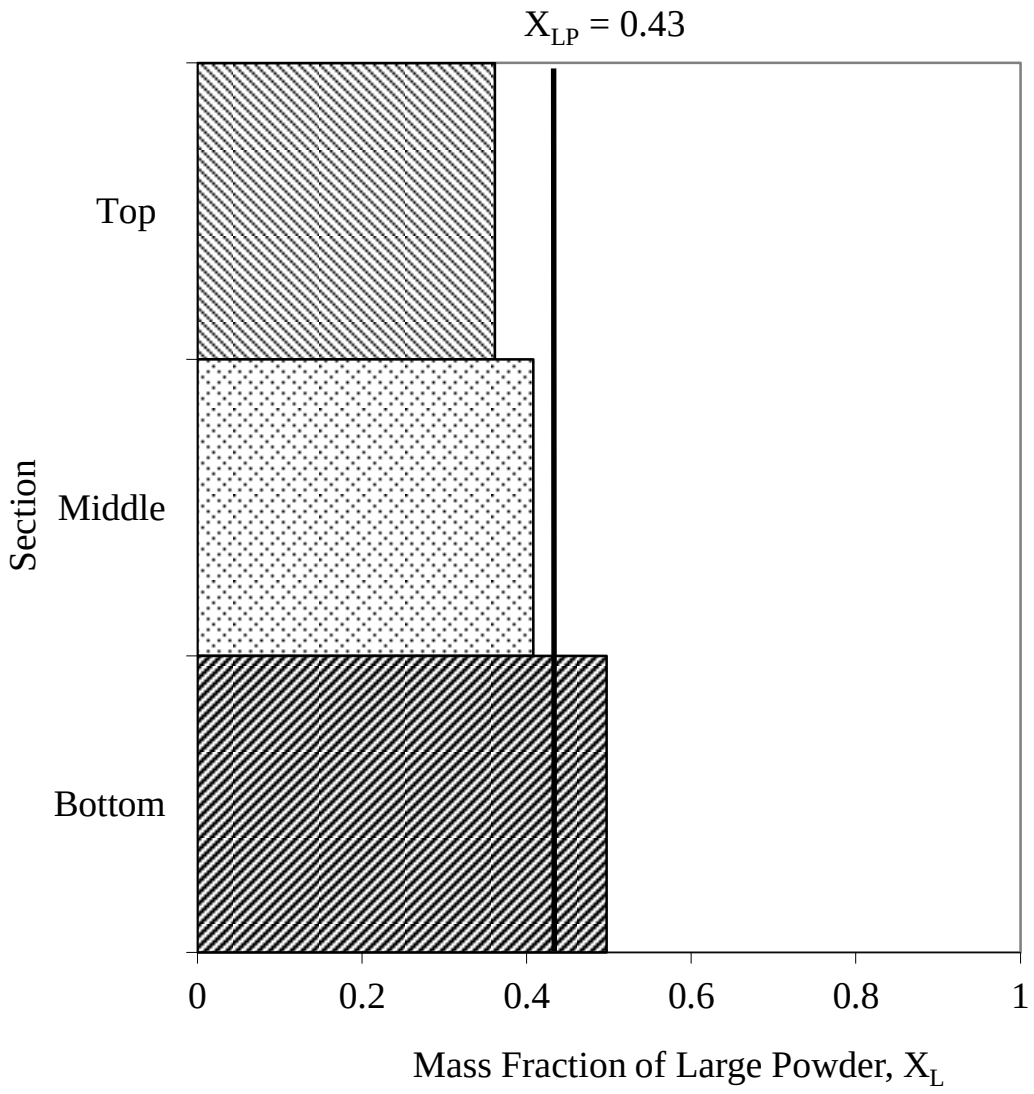

Figure A.16: Segregation patterns for poly-dispersed sample B (180 – 355 µm and 850 – 1000 µm).

Pulse frequency = 5 Hz

Fluidisation duration = 4 min

Air pressure = 41.4 kPa

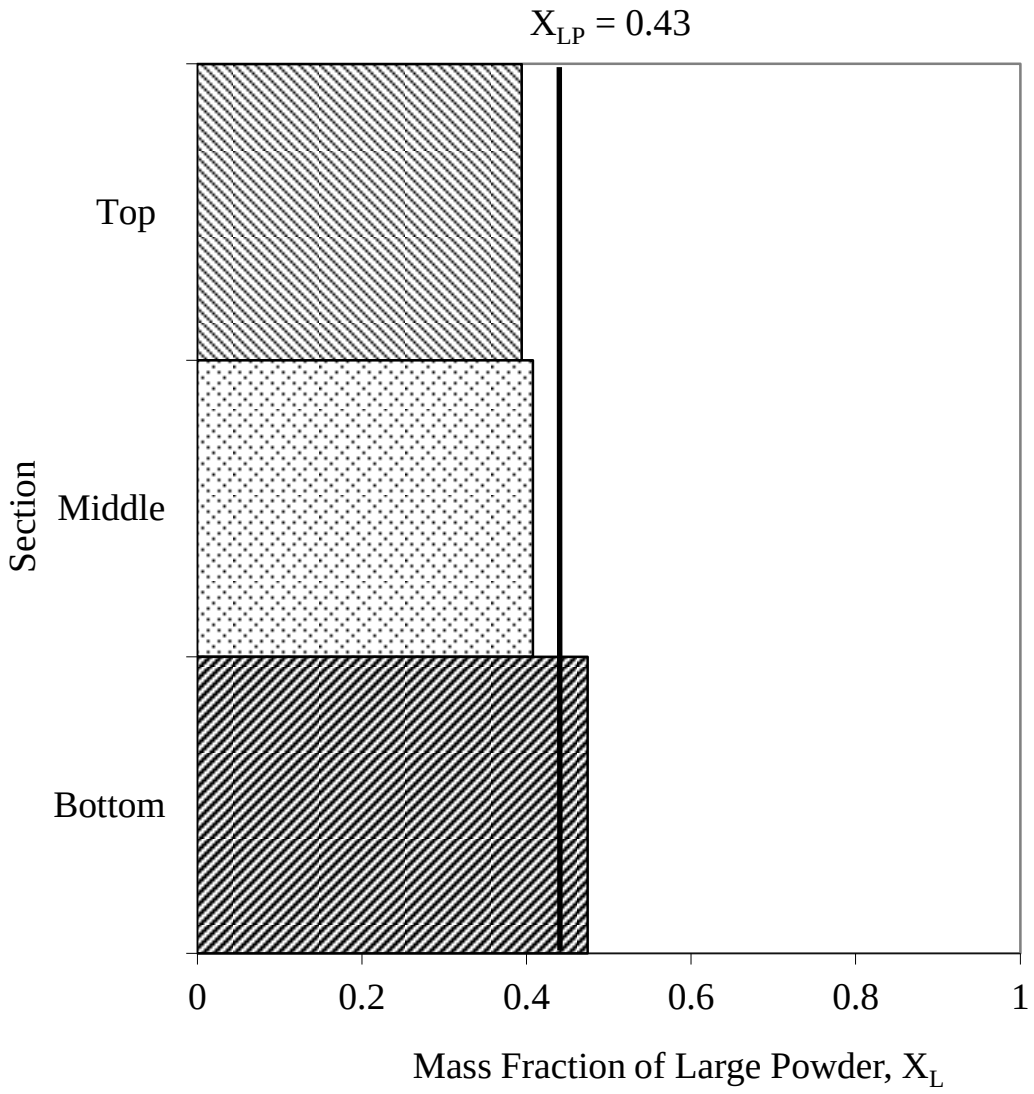

Figure A.17: Segregation patterns for poly-dispersed sample B (180 – 355 µm and 850 – 1000 µm).

Pulse frequency = 2 Hz

Fluidisation duration = 4 min

Air pressure = 41.4 kPa

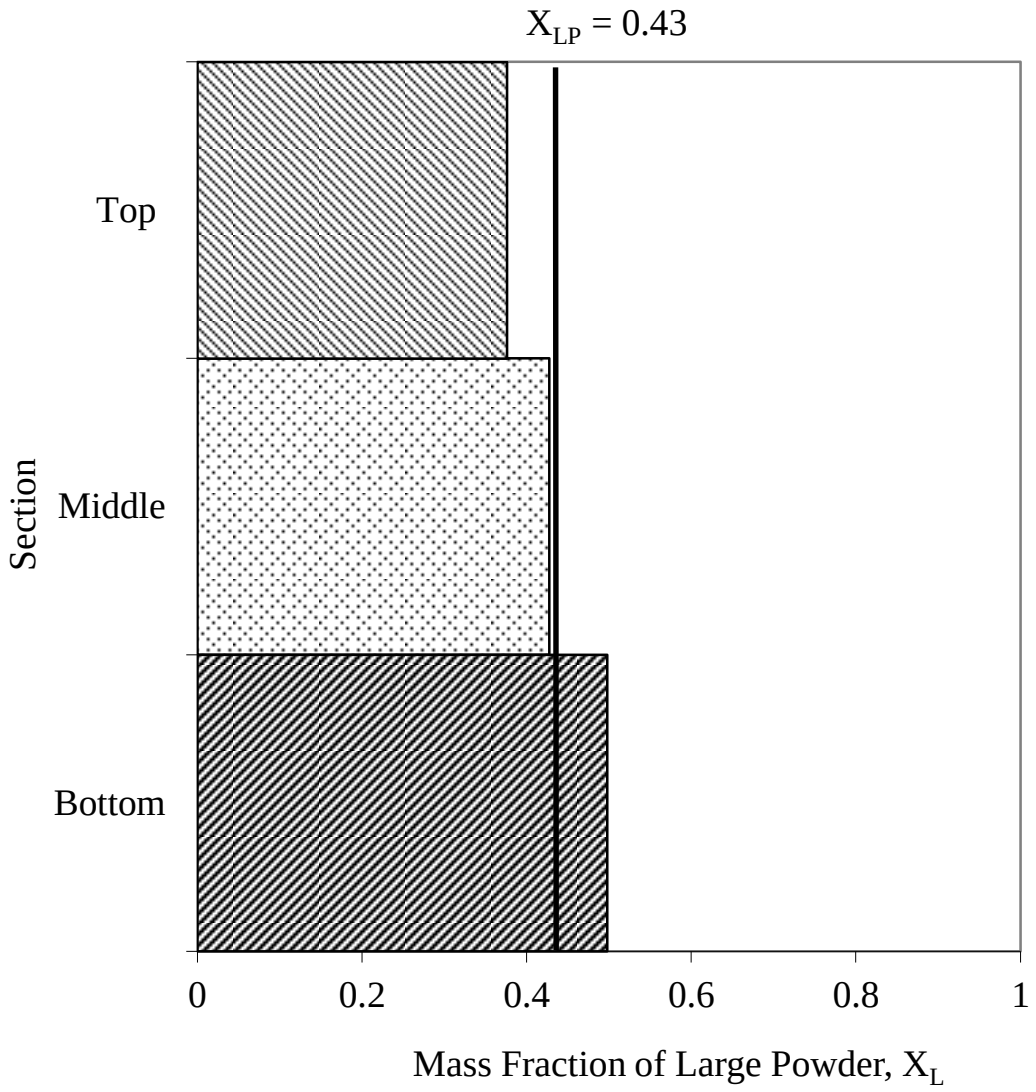

Figure A.18: Segregation patterns for poly-dispersed sample B (180 – 355 µm and 850 – 1000 µm).

Pulse frequency = 1 Hz

Fluidisation duration = 4 min

Air pressure = 41.4 kPa

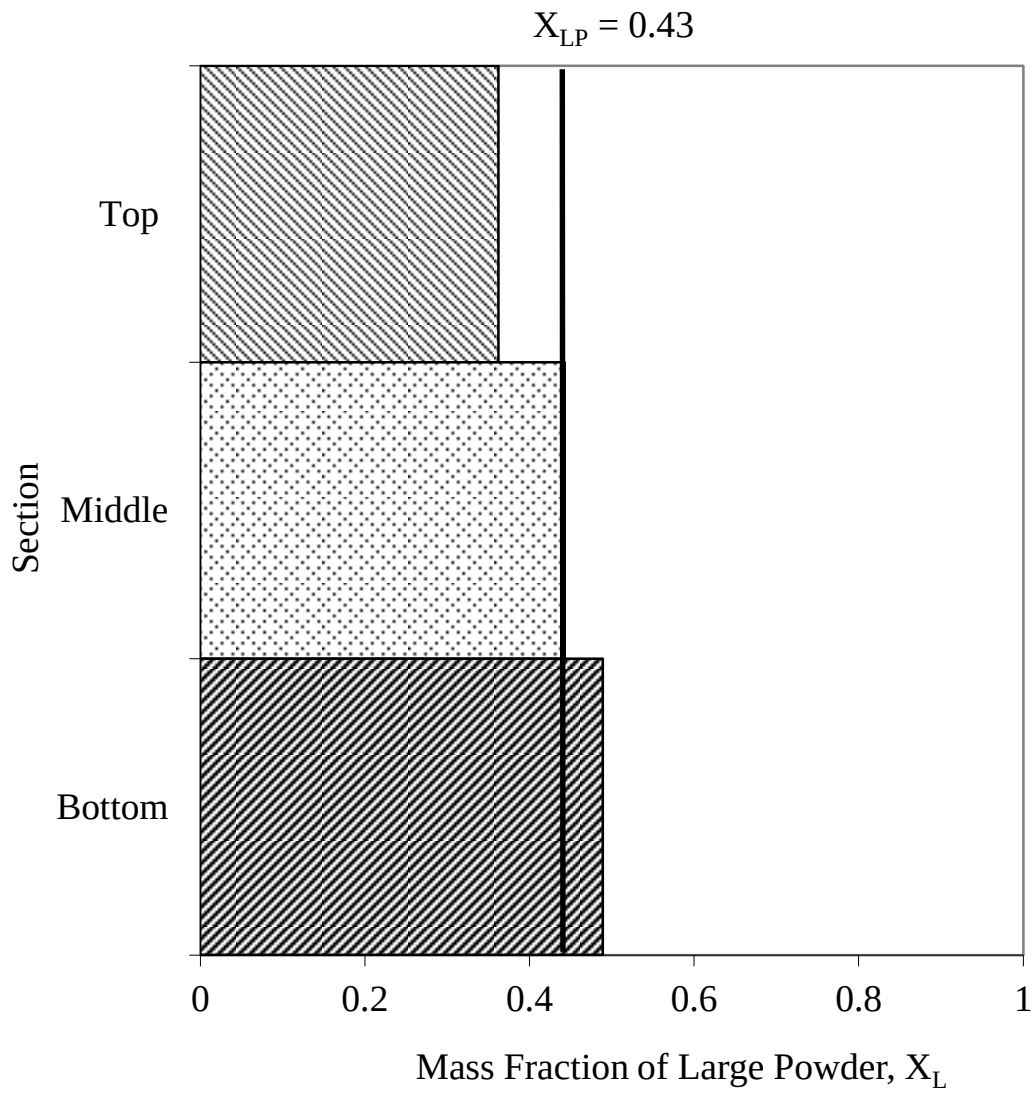

Figure A.19: Segregation patterns for poly-dispersed sample B (180 – 355 µm and 850 – 1000 µm).

Pulse frequency = 0.5 Hz

Fluidisation duration = 4 min

Air pressure = 41.4 kPa

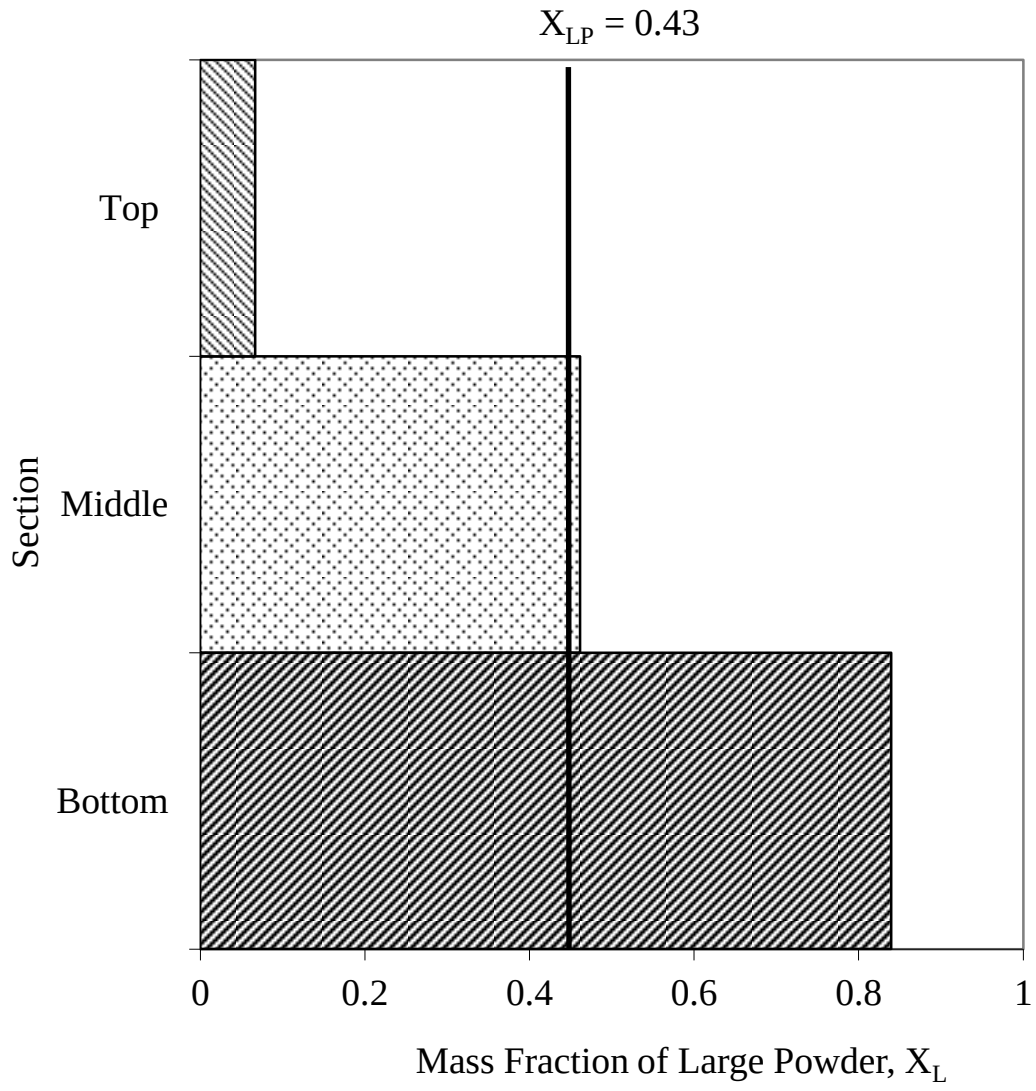

Figure A.20: Segregation patterns for poly-dispersed sample B (180 – 355 µm and 850 – 1000 µm).

Pulse frequency = 0 Hz (continuous air)

Fluidisation duration = 4 min

Air pressure = 41.4 kPa